UNIVERSITÉ DE MONTRÉAL

SEISMIC PERFORMANCE OF CONCENTRICALLY BRACED STEEL FRAMES OF THE CONVENTIONAL CONSTRUCTION CATEGORY

PIERRE XAVIER CASTONGUAY
DÉPARTEMENT DES GÉNIES CIVIL, GÉOLOGIQUE ET DES MINES
ÉCOLE POLYTECHNIQUE DE MONTRÉAL

MÉMOIRE PRÉSENTÉ EN VUE DE L'OBTENTION
DU DIPLÔME DE MAÎTRISE ÈS SCIENCES APPLIQUÉES
(GÉNIE CIVIL)
DÉCEMBRE 2009

UNIVERSITÉ DE MONTRÉAL

ÉCOLE POLYTECHNIQUE DE MONTRÉAL

Ce mémoire intitulé :

SEISMIC PERFORMANCE OF CONCENTRICALLY BRACED STEEL FRAMES OF THE CONVENTIONAL CONSTRUCTION CATEGORY

présenté par : CASTONGUAY Pierre Xavier
en vue de l'obtention du diplôme de : Maîtrise ès sciences appliquées
a été dûment accepté par le jury constitué de :

Mme KOBOEVIC Sanda, Ph.D., présidente
M. TREMBLAY Robert, Ph.D., membre et directeur de recherche
M. DUSSAULT Serge, M.Eng., membre

ACKNOWLEDGEMENTS

First and foremost I would like to thank my supervisor, Mr. Robert Tremblay, for his help, efforts, advice, patience, and financial support throughout this research project. I greatly enjoyed working with him and my time spent at École Polytechnique de Montréal under his supervision will greatly benefit my career.

Financial support for this project was provided by the *Fondation de recherche sur la nature et les technologies* (FQRNT). Their support was much appreciated.

I would also like to express my gratitude to the École Polytechnique structures' lab technical staff. Their help and patience made my time spent in the structures lab enjoyable and valuable.

I developed great friendships over these two years with my office colleagues. A special thank you goes to Kim Guilini-Charette, with whom I had the privilege of working with on this project, and Antoine Le Bec for their friendships, help, and advice. A big thank you as well goes to all the other students who created a friendly and enjoyable atmosphere in the office and made it a pleasure to come to school.

I would also like to thank my family, who constantly supported and encouraged me throughout these two years. Finally, I want to thank my girlfriend Paula who left her work in New Brunswick to be with me and support me for these two years in Montréal. You are a constant reminder of how fortunate I am.

RÉSUMÉ

Le principal objectif de ce projet de recherche était d'examiner la performance sismique de bâtiments de type de construction conventionnelle (CC Type). Ce principal objectif a été atteint avec les objectifs plus précis suivants :

- Évaluer la capacité en déformation des connexions couramment utilisées dans ces structures; et

- Réévaluer la pertinence de la limite de 15 m de hauteur imposée sur ces structures dans le code national du bâtiment (CNB). Cette limite a aussi été étudiée pour voir si elle pouvait être nuancée en fonction de certains paramètres, comme le type d'assemblages utilisé, la localisation au Canada (est versus ouest), le type de sol (C versus E) et le nombre d'étages, entre autres.

Des tests au laboratoire ont été effectués en deux phases expérimentales sur des assemblages typiques de diagonales de contreventement. Pour les deux phases, les spécimens consistaient de deux cornières dos-à-dos boulonnées à une plaque de gousset. Cette configuration est représentative d'une connexion couramment utilisée en pratique pour des contreventements.

La première phase expérimentale avait pour but d'évaluer la ductilité de cinq différents modes de rupture dans une connexion : rupture de soudures parallèles à l'effort, rupture sous pression diamétrale de boulons, rupture sur l'aire nette des cornières, rupture en cisaillement des boulons et le déchirement des cornières en traction et en cisaillement. Tous les spécimens ont été testés sous une charge monotonique en traction. Il a été déterminé que les ruptures sous pressions diamétrales de boulons offraient le meilleur potentiel comme connexions ductiles dans un bâtiment de type de construction conventionnelle.

La deuxième phase expérimentale avait pour but de maximiser la capacité en ductilité, ou déformation, d'un assemblage subissant une rupture sous pression diamétrale des

boulons contre le gousset d'assemblage. Plusieurs paramètres de connexion ont été examinés : distance au bord du boulon, espacement des boulons, types de trous (trous poinçonnés et forés, trous standards et oblongs). Tous les spécimens avaient une plaque de gousset d'épaisseur de 8 mm, sauf pour un sous-groupe de spécimens fabriqués avec une plaque de 13 mm pour vérifier le mode de rupture par écrasement sur une plaque plus épaisse. Tous les groupes de spécimens ont été soumis à des charges cycliques et monotoniques. Les résultats ont démontrés que ces connexions pouvaient atteindre jusqu'à 25 mm en déformation avant d'atteindre la rupture définie comme le point où la résistance diminue à 80% de la résistance maximum atteinte.

Dans la phase analytique du projet, vingt-quatre bâtiments ont été conçus et analysés dans le but d'évaluer leur performance sismique. Plusieurs paramètres pouvant influencer leur comportement ont été examinés : position du contreventement (sur travée intérieure ou extérieure), hauteur totale du bâtiment (8.1 m à 38.1 m) , hauteur des étages (3.0 m à 5.6 m), classification du site (C et E), configuration des contreventements (en Split-X et en chevron) et deux localités (Vancouver et Montréal).

La phase analytique a été séparée en trois séries d'analyses. La première consistait en des analyses dynamiques linéaires effectuées pour analyser le niveau de force sur les connexions non-ductiles. De ces analyses, on a trouvé, pour Montréal, des efforts excessifs par rapport à la force sismique de conception lorsque la limite de hauteur de 15 m est excédée ou pour les bâtiments construits sur un sol de classe E. Pour Vancouver, les efforts obtenus sont supérieurs à ceux prescrits dans le code, tant pour les sols de classes C que E. Les connexions des contreventements en chevron sont généralement soumises à des efforts moins élevés que les contreventements en X.

La deuxième phase consistait en des analyses dynamiques non linéaires sur les mêmes bâtiments. Dans les modèles numériques, on a inclus un fusible à l'extrémité inférieure des diagonales de contreventement pour représenter une connexion conçue pour subir une rupture ductile sous la pression diamétrale des boulons. Les déformations obtenues de ces fusibles ont été comparées à une déformation maximale acceptable déterminée

d'après les résultats expérimentaux. Pour Montréal, on a déterminé que les déformations dans les assemblages sont acceptables dans les bâtiments jusqu'à 38.1 m de hauteur, tant pour les sols de classes C que E. À Vancouver, les déformations sont acceptables pour les bâtiments de 15 m et moins sur un site de type C, mais elles sont excessives pour tous les bâtiments construits sur un site de type E, peu importe leur hauteur. Les connexions des contreventements en chevron ont subi de plus petites déformations que celles des contreventements en X. De plus, la distribution verticale des déformations inélastiques sur la hauteur des bâtiments est plus uniforme dans les contreventements en chevron.

La troisième phase analytique consistait en des analyses dynamiques incrémentales non linéaires sur deux des bâtiments localisés à Vancouver. Ces deux bâtiments avaient une hauteur totale de 15.6 m. Les modèles numériques utilisés étaient les mêmes que ceux de la deuxième phase, mais avec des connexions pouvant se briser puis maintenir une légère force résiduelle lorsque la déformation imposée dépassait leur capacité de déformation. On a trouvé que les deux bâtiments avaient une probabilité d'effondrement se situant entre 5 and 10%, ce qui est considéré acceptable.

Les résultats des trois séries d'analyse ont été compilés pour trois bâtiments afin d'étudier les efforts axiaux dans les poteaux. Ces résultats sont présentés sous la forme de rapports entre l'effort axial maximum à chaque étage et la résistance probable au flambement du poteau. Les résultats ont montrés que les poteaux sont surchargés dans les bâtiments avec connexions non-ductiles. Les efforts dans les poteaux des bâtiments conçus avec connexions ductiles sont jusqu'à 2.0 fois et 1.6 fois moins élevés que dans les mêmes bâtiments avec connexions non-ductiles, pour les bâtiments de 4 et 8 étages, respectivement.

ABSTRACT

The main objective of this research project was to study the seismic behaviour of regular conventional construction (CC Type) concentrically braced steel frames (CBFs). More specifically, this objective was achieved through the following objectives:

- Evaluate the deformation capacity of typical brace connections used in these structures; and
- Evaluate the suitability of the 15 m height limit imposed by the 2005 NBCC. This limit should also be studied to determine whether it can be made a function of several building parameters, such as the type of connections used (ductile versus non-ductile), the building location (eastern versus western Canada), the site class (C versus E), and the number of storeys, among others.

Two experimental phases were carried out in order to assess the ductility capacity of typical vertical bracing connections. For both phases, the specimens consisted of back-to-back angles bolted to a gusset plate. This configuration is representative of typical connections used in practice.

The first phase consisted of testing five different connection failure modes: failure of welds parallel to loads, bolt bearing failure on the gusset plate, net area rupture of the angles, bolt shear rupture, and shear and tension block failure of the angles. All specimens were tested under monotonic tensile loadings. It was found that bolt bearing failures offered the best potential for being used as a ductile connection failure mode in CC Type buildings.

The second phase consisted of performing further tests on bolt bearing failures in order to optimize their deformation capacities. Different connection parameters were studied: bolt end distance and bolt spacing, and types of holes (drilled and punched holes, standard and short-slotted holes). All specimens used 8 mm thick gusset plates, except for one sub-group of specimens where 13 mm plates were used to ensure bearing

failures can take place in thicker plates. All specimen sub-groups were subjected to both monotonic tensile loading and cyclic loading. The results showed that bolt bearing failures can reach up to 25 mm in deformation at their rupture, defined as the point where the load drops to 80% of the ultimate load.

An analytical phase was carried out to assess the seismic behaviour of CC Type CBFs. Twenty-four buildings, which covered different building plan layouts (external and internal bracing), building heights (between 8.1 and 38.1 m), storey heights (between 3.0 and 5.6 m), site classes (C and E), bracing configurations (Split-X versus chevron), and building locations (Montreal and Vancouver), were designed and analyzed. From the analyses, observations and conclusions were made based on the median statistics of connection force demands and deformations.

This phase was carried out in three phases. The first consisted of performing linear dynamic analyses to evaluate the connection force demands in non-ductile connections. From these analyses, it was found that Montreal had excessive connection force demands in structures with heights greater than 15 m or for structures located on a site class E. In Vancouver, it was found that force demands were excessive for all buildings, regardless of the building height and site class. The chevron-braced structures generally had connection force demands smaller than their Split-X equivalents.

The second phase consisted of performing nonlinear dynamic analyses of the same buildings, but with fuses located at the ends of brace members to evaluate the connection deformation demands. These deformations were compared to the maximum encountered deformation capacity in the second experimental phase: 31 mm. In Montreal, it was found that deformations were acceptable for building heights up to 38.1 m and for site classes C or E. In Vancouver, the connection deformations were acceptable for building heights up to 15 m on a site class C and were found excessive for buildings on site class E, regardless of their heights. Connections in chevron-braced structures underwent smaller deformations than their Split-X equivalents. Also, chevron structures had a more uniform distribution of deformations along the building height.

The third phase consisted of performing incremental nonlinear dynamic analyses on two buildings located in Vancouver. The buildings chosen had total heights of 15.6 m, just over the 15 m limit imposed by the NBCC. These models were the same as the ones from the second phase, except that connections were modeled with the ability to break off after reaching their deformation capacity and maintain a small residual force. It was found that both buildings had collapse probability of between 5% and 10%, which is considered acceptable.

Results from the three series were compiled for three buildings and the column axial force demand was studied in the form of ratios of the maximum axial force from the dynamic analyses to the column expected buckling capacity. It was found that columns are overloaded when non-ductile connections are used. The column axial load demands in buildings with ductile connections were found to be 0.5 to 0.6 times that of the demands in structures with non-ductile connections for 4- and 8-storey buildings, respectively.

CONDENSÉ EN FRANÇAIS

Le principal objectif de ce projet de recherche était d'examiner la performance sismique de bâtiments de type de construction conventionnelle (Type CC). Ce principal objectif a été atteint avec les sous-objectifs énumérés ci-dessous :

- Évaluer la capacité en déformation des connexions couramment utilisées dans ces structures; et

- Réévaluer la pertinence de la limite de 15 m de hauteur imposée sur ces structures dans le code national du bâtiment (CNB). Cette limite devrait aussi être étudiée pour voir si elle peut être nuancée en fonction de certains paramètres, comme le type d'assemblage utilisé, la localisation au Canada (est versus ouest), le type de sol (C versus E) et le nombre d'étages, entre autres.

Les bâtiments de Type CC sont de faible ductilité et sont conçus avec un facteur de modification de force sismique relié à la ductilité, R_d, de 1.5. La grande majorité de la recherche à été consacrée aux systèmes de résistance aux charges sismiques (SRCS) plus ductiles et ayant un facteur R_d plus grand ou égal à 2.0. Contrairement à ces systèmes, qui sont soumis à de strictes règles de conception sismiques, les bâtiments de Type CC n'ont qu'une restriction pour la conception du SRCS : les connexions pour diagonales doivent ou bien démontrer un mode de rupture ductile ou être conçues pour la charge sismique amplifiée par un facteur 1.5. Il n'existe pas présentement de critères ou directives permettant de déterminer si une connexion est ductile ou non et, par défaut, les assemblages sont souvent conçus comme des connexions non-ductiles avec la charge sismique amplifiée.

Le projet a été séparé en deux parties : une partie expérimentale et une partie analytique. La partie expérimentale avait pour objectif de quantifier la capacité en déformation d'un assemblage typiquement utilisé dans des bâtiments de Type CC. Cette partie a été séparée en deux phases : la première avait pour but d'évaluer la capacité en ductilité de cinq différents modes de rupture alors que la deuxième avait pour but d'optimiser cette

capacité pour le mode de rupture ayant été déterminé comme le plus prometteur dans la première phase. La partie analytique avait pour objectif d'évaluer la performance sismique des bâtiments de Type CC. Elle a été séparée en trois phases. La première phase consistait en une série d'analyses dynamiques linéaires visant à évaluer l'amplitude des efforts imposés aux connexions non-ductiles. La deuxième phase était une série d'analyses dynamiques non-linéaires servant à évaluer le niveau de ductilité anticipé dans les assemblages ductiles. La troisième phase comprenait une série d'analyses dynamiques incrémentales non-linéaires sur deux bâtiments localisés à Vancouver pour déterminer le niveau de confiance contre l'effondrement de bâtiments avec connections ductiles. Pour terminer, des résultats des trois séries d'analyses ont été rassemblés et examinés pour évaluer l'effet des connexions ductiles et non-ductiles sur les efforts axiaux imposés aux poteaux lors de séismes.

Les spécimens de la partie expérimentale consistaient en des assemblages de même configuration pour les deux phases. Ces spécimens étaient faits de deux cornières dos-à-dos boulonnées à une plaque de gousset. Ceci peut représenter l'assemblage de diagonales de contreventement faites de cornières dos-à-dos ou la demie d'une connexion souvent utilisée en pratique qui comprend des segments de cornières dos-à-dos qui sont soudées ou boulonnées à un profilé tubulaire formant la diagonale. Les spécimens avaient soit un ou deux boulons.

Pour la première phase expérimentale, des spécimens différents ont été conçus pour se briser selon cinq modes de rupture différents et ainsi permettre d'évaluer la ductilité associée à chacun de ces modes. Tous ces spécimens ont été testés sous des charges monotoniques en traction. Ces cinq modes de rupture, ainsi que les déformations à l'ultime qui ont été observés dans les essais, sont résumés ci-dessous :

- Rupture de soudures parallèles à l'effort de traction, avec une déformation moyenne à l'ultime de 7.3 mm.

- Rupture par pression diamétrale des boulons sur la plaque de gousset avec une déformation moyenne à l'ultime de 22.7 mm.
- Rupture sur l'aire nette des cornières avec une déformation moyenne à l'ultime de 16.0 mm.
- Rupture en cisaillement d'un boulon avec une déformation à l'ultime de 15.7 mm.
- Déchirement combinée en traction et en cisaillement des cornières, avec une déformation à l'ultime de 15.5 mm.

Le mode de rupture qui offrait la meilleure capacité en déformation était donc celui d'une rupture par pression diamétrale des boulons contre la plaque de gousset, suivi d'une cassure des cornières sur l'aire nette et d'une rupture en cisaillement des boulons. Il est important de souligner que ces déformations correspondent à la somme des déformations mesurées aux deux extrémités des spécimens, ce qui explique, par exemple, pourquoi la rupture du boulon en cisaillement a démontré une si grande capacité en déformation. En plus des déformations dans le boulon qui s'est brisé, ce mode de rupture a été caractérisé par des déformations sous forme d'ovalisation importante des trous dans les deux goussets et par des déformations considérables du boulon intact. En soustrayant ces autres déformations, on obtient une déformation approximative du boulon cassé de l'ordre de 6 mm, ce qui est proche des valeurs publiées dans la littérature.

Dans cette première phase, des trous poinçonnés ont été utilisés dans tous les spécimens. Des trous forés ont aussi été utilisés pour des spécimens qui se sont brisés par cassure des cornières sur l'aire nette. La cassure sur l'aire nette avec trous forés ne s'est pas produite de la même manière que dans le cas des spécimens avec trous poinçonnés. Dans le dernier cas, on a observé une cassure classique à travers l'aire nette, perpendiculaire à la direction de l'effort. La cassure sur l'aire nette avec trous forés a été caractérisée par une importante ovalisation des trous, ce qui a grandement contribué à

augmenter la déformation à la rupture de ces spécimens, ce qui laisse croire que les trous foré pourraient peut-être conduire à de plus grandes déformations dans une rupture sous pression diamétrale des boulons. Aussi, d'importantes fissures transversales ont été observées dans les spécimens se cassant sous pression diamétrale, ce qui a laissé croire que le processus de poinçonnage pouvait introduire des microfissures près du trou. Ces microfissures se seraient élargies durant l'essai et auraient causé ces fissures transversales.

Le mode de rupture par pression diamétrale des boulons sur la plaque de gousset a donc été choisi pour être étudié en détail dans la deuxième phase expérimentale. Les assemblages examinés comporteraient au moins deux boulons sur une file parallèle à l'effort à transmettre, comme cela est couramment utilisé en pratique. Avant de passer à la conception des spécimens, on a étudié l'effet possible de certains paramètres sur la ductilité associée à ce mode de rupture :

- Distance entre le bord de la plaque et le boulon, et espacement longitudinal des boulons. D'après la littérature, l'augmentation de la distance au bord du boulon mène à une augmentation de la capacité en déformation. Différentes combinaisons de distance de bord et d'espacement de boulons ont été sélectionnées: 2d5d, 4d5d et 5d6d (le premier est la distance au bord et le second est l'espacement). La première permettait d'observer l'effet d'avoir une déchirure sur les deux plans de cisaillement situés dans la plaque, de chaque côté du boulon, alors que les deux dernières devaient causer toutes les deux une rupture en écrasement des deux boulons sur la plaque de gousset.

- Trous forés et poinçonnés. D'après les résultats de la première phase expérimentale, les trous forés pourraient conduire à de plus grandes déformations. Ceci n'est pourtant pas toujours cohérent avec ce que l'on retrouve dans la littérature. On a tout de même décidé d'évaluer l'effet du mode de fabrication des trous.

- Trous ronds et trous oblongs courts. D'après la littérature, les trous oblongs ont les mêmes capacités de déformation qu'un trou rond standard mais sont moins rigides. On a tout de même juger important d'observer les différences entre les deux types de trous et de confirmer ce qui a été relevé dans la littérature.

- Tous les spécimens avaient des goussets d'épaisseur de 8 mm, sauf un sous-groupe qui avait une plaque de 13 mm pour observer la possibilité d'imposer une rupture sous pression diamétrale dans le cas de goussets plus épais. Pour ce spécimen, on a du spécifier des espacements de boulons plus faibles afin de réduire sa capacité en écrasement et pouvoir le tester dans la même presse d'essais que les autres spécimens.

La capacité des spécimens a été calculée avec l'équation du code qui limite la pression diamétrale à $3F_u$, où F_u est la contrainte ultime de l'acier. Cependant, la capacité attendue des spécimens à été calculée en utilisant $4F_u$, sur la base d'une étude menée en Alberta (Cai et al., 2008). Dans cette étude, comme dans celle décrite dans ce mémoire, on a utilisé des plaques de gousset confinées, c'est-à-dire se trouvant au centre d'un assemblage de pièces jumelles formant deux plans de cisaillement, conçus pour développer une rupture par pression diamétrale. Pour ces spécimens, les chercheurs d'Alberta ont trouvé que la capacité était mieux prédite en utilisant une contrainte diamétrale égale à $4F_u$. Chaque configuration de spécimens de notre étude comprenait trois spécimens identiques. Deux types de charges ont été considérés : charges cycliques et charges monotoniques. Les spécimens ont été évalués en termes de déformation à la rupture, définie comme le point où la résistance redescend à 80% de la charge ultime dans la région post-pic

Les conclusions suivantes ont été tirées de nos essais :

- Pour les goussets de 8 mm d'épaisseur, l'utilisation d'un configuration 5d6d a donné lieu à plus grandes déformations totales à la rupture, soit 47 mm sous une charge monotonique, et 34 mm sous une charge cyclique. On note ici qu'il s'agit

de la déformation d'un seul assemblage, et non de deux comme dans la phase I. Pour la configuration 4d5d, la déformation moyenne à l'ultime a été de 41 mm sous une charge monotonique et de 25 mm sous une charge cyclique. Pour les spécimens conçus avec une géométrie 2d5d, on a mesuré une déformation moyenne à la rupture de 42 mm sous une charge monotonique et de 23.5 mm sous une charge cyclique. Le spécimen 2d5d a développé une rupture par cisaillement sur les deux plans de cisaillement de chaque côté du trou du boulon extérieur tandis que le boulon intérieur a développé une rupture par pression diamétrale de boulon (écrasement). Les spécimens 4d5d et 5d6d ont développés une rupture par pression diamétrale des boulons (écrasement). En général, les spécimens qui ont développé une rupture en écrasement pur ont résisté à une contrainte considérablement plus élevée que ce que le code permet. Pour les essais cycliques, les quatre spécimens 4d5d ont repris une contrainte maximale de près de $4F_u$, tandis que la contrainte dans les spécimens 5d6d a atteint $4.7F_u$. Dû à ce comportement inattendu des spécimens 5d6d, il est recommandé d'utiliser des connexions de la configuration 4d5d lorsque l'on veut éviter d'induire des efforts trop importants dans les pièces adjacentes aux assemblages.

- Les différences observées en termes de déformation à la rupture entre les spécimens fabriqués avec des trous forés et poinçonnés sont minimes. Par contre, un des spécimens avec trous poinçonnés a développé, comme dans la première phase expérimentale, une fissure transversale au niveau du trou du boulon. Étant donné que ce genre de comportement n'est pas souhaitable dans le contexte d'un assemblage ductile, il est recommandé d'utiliser des trous forés.

- Les trous oblongs ont résisté à des charges ultimes légèrement moins élevées que les spécimens avec trous ronds standard. Ils ont cependant démontré plus de déformation par unité de charge dans la partie semi-élastique du comportement, au début de l'essai. Sur cette base, il est recommandé d'utiliser des trous ronds standards pour éviter d'affecter la rigidité de la structure.

- Malgré un espacement plus serré des boulons, les spécimens avec plaque de gousset de 13 mm ont tout de même développé des déformations importantes à leur rupture, soit 22 mm de déformations sous charge monotonique et 15 mm sous charges cycliques. Ces déformations sont toutefois moindres que celles observées pour le gousset de 8 mm d'épaisseur.

En résumé, la partie expérimentale permet de proposé une connexion ductile pouvant être utilisée dans les bâtiments de Type CC. Il est recommandé d'utilisé une distance de bord de 4d, un espacement de boulon de 5d, des trous forés et des trous ronds.

La partie analytique a été réalisée après avoir compléter la partie expérimentale. Vingt-quatre bâtiments ont été conçus avec le logiciel de conception automatisée Advanced Design America (ADA). Ce logiciel a la capacité de faire la conception de bâtiments suivant le code national de bâtiment du Canada (CNB) ainsi que la norme d'acier canadienne (CSA-S16). La méthode d'analyse dynamique spectrale a été utilisée pour déterminer les charges sismiques dans les membrures. Ces analyses ont été réalisées avec le spectre du CNB 2005 spécifique à chaque site. Les effets P-Δ ont été pris en compte en amplifiant les effets dus aux charges latérales par le facteur U_2 de la norme CSA-S16. Une excentricité horizontale accidentelle de 10% de la dimension du bâtiment a été considérée par ADA. Pour les diagonales des contreventements, on a utilisé des profilés tubulaires ASTM A500, nuance C, tandis que les poutres et les colonnes étaient des profilés de type W faits d'acier CSA-G40.21-350W. Dans le modèle ADA, les colonnes ont été conçues avec un coefficient de longueur effective égal à 1.0, tandis qu'une valeur de 0.9 a été retenue pour les diagonales, ceci pour tenir compte de la rigidité et de la taille des assemblages. Les 24 bâtiments englobaient différentes configurations: de 2 à 10 étages en hauteur, trois différentes hauteurs d'étages pour le bâtiment de 15.6 m de hauteur, deux types de sol porteur différents (sites de classes C et E), deux différentes configurations de contreventements (en chevron et contreventement en X sur deux étages, aussi désigné Split-X), et deux positions du cadre contreventé dans les bâtiments (sur un axe intérieur et sur le

périmètre du bâtiment). Cinq bâtiments ont été choisis comme « standard » et comme points de référence pour comparer les paramètres des bâtiments énumérés. Les bâtiments standards étaient ceux avec une hauteur d'étage normale, des contreventements de type Split-X localisés sur le périmètre du bâtiment et localisés sur un sol de classe C. Tous les bâtiments étudiés avaient la même géométrie en plan, soit une structure régulière et carrée, avec une dimension de 45 m divisée en 5 travées égales de 9 m dans les deux directions principales.

Une façon de quantifier la partie de la sur-résistance aux charges sismiques des bâtiments induite par la méthode de calcul des charges sismiques du CNB est de calculer le ratio V_e/V_{de}, où V_e est la charge sismique élastique totale à la base obtenue de l'analyse spectrale et V_{de} est le cisaillement à la base de conception multiplié par R_dR_o , soit le cisaillement élastique de conception. Cette sur-résistance provient surtout des limites imposées sur la période de la structure à utiliser dans la conception, l'obligation de normaliser les résultats par rapport à la charge sismique statique, etc. Les ratios V_e/V_{de} pour les bâtiments de Montréal sont inférieurs à 1.0, et ces structures possèdent une plus grande sur-résistance que les bâtiments de Vancouver, ces derniers ayant généralement des ratios égaux à 1.0. On peut donc s'attendre à ce que les bâtiments de Montréal soient moins sollicités que ceux de Vancouver au niveau des forces dans les assemblages obtenus des analyses temporelles dynamiques linéaires, ceci relativement aux forces de conception.

Après la conception des bâtiments, des modèles numériques non-linéaires ont été réalisées avec le logiciel OpenSees. Une seule travée contreventée de la structure à été modélisée mais les poteaux de gravité tributaires de ce contreventement ont été regroupées et inclus dans le modèle pour bien reproduire les effets P-Delta. Les colonnes et les contreventements ont été modélisés par des éléments de type poteau-poutre dont la section était discrétisées à l'aide de fibres. Les défauts de rectitude de ces pièces ont été incorporés pour initier le flambement en compression. Les épissures de poteaux contreventés ont été supposées capables de développer la pleine capacité en

flexion des poteaux, tandis que les poteaux de gravité ont été modélisés avec des épissures plus souples et moins résistantes aux deux étages. Un amortissement égal à 3% de la valeur critique dans les deux premiers modes de vibration a été considéré dans les analyses.

Le même modèle est donc utilisé pour les trois analyses. Cependant, pour évaluer les efforts imposés aux connexions, on a assigné une limite élastique élevée aux matériaux, de telle sorte que la structure demeure élastique durant l'analyse. Les effets P-Delta ont d'ailleurs été omis pour ces analyses linéaires pour permettre une comparison directe avec les forces de dimensionnement obtenues à partir du CNB. De même, il a été trouvé que les effets P-Delta sont négligeables pour une structure élastique soumise à une sollicitation sismique (Bernal 1987; Humar et al., 2006). Pour les analyses dynamiques non-linéaires, des analyses en grandes déformations ont été effectuées (P-Delta par représentation co-rotationelle) et toutes les résistance réelle de l'acier étaient assignées aux membrures, de telle sorte qu'elles pouvaient atteindre et même dépasser leur point de plastification ou de flambement. Dans les analyses non linéaires, les connexions ont été modélisé par un élément de type ressort présentant un comportement bi-linéaire, avec une résistance égale à R_oC_f, où C_f est l'effort de conception en compression des diagonales. La loi hystérétique utilisée pour les connexions présentait aussi un pincement pour reproduire la résistance réduite des connexions qui se déforment à l'intérieur de la plage de déformation atteinte préalablement durant un séisme. Ce même modèle a été utilisé pour les analyses dynamiques incrémentales, mais avec des connexions pouvant se briser lorsque la capacité en déformation déterminée dans la partie expérimentale du projet était atteinte.

Pour les deux premières séries d'analyses, soit les analyses linéaires et non-linéaires, un ensemble de 10 mouvements sismiques synthétiques a été utilisé pour les sites de classes C et E à Montréal. Pour Vancouver, 10 mouvements sismiques synthétiques et 10 enregistrements lors de séismes historiques ont été utilisés pour le site de classe C alors que 10 mouvements sismiques synthétiques et 12 enregistrements lors de séismes

historiques ont été utilisés pour le site de classe E. Au total, 748 analyses dynamiques (linéaires + non-linéaires) ont été effectuées. Pour les analyses dynamiques incrémentales, un ensemble de 20 enregistrements lors de séismes historiques a été utilisé pour Vancouver. Par la suite, pour fins de comparaisons avec les résultats obtenus de ces mouvements sismiques, les analyses ont été reprises pour un bâtiment avec 10 mouvements sismiques synthétiques. Ceci a permis d'observer des différences entre les résultats d'analyses incrémentales effectuées avec séismes synthétiques et historiques.

Le comportement sismique des bâtiments a été étudié en examinant les valeurs de pointe des paramètres d'intérêt obtenues pendant les séismes. Ces paramètres de réponse comprenaient la force et la déformation dans les éléments représentant les assemblages des diagonales, ceci pour les analyses linéaires et non-linéaires, respectivement. Les efforts ont été exprimés sous la forme du ratio P/P_{de}, où P est la valeur obtenue des analyses et P_{de} est l'effort sismique de conception amplifiée par R_oR_d. Les résultats d'analyses non-linéaires ont été comparés à une déformation maximale obtenue dans la phase expérimentale, soit 31 mm. Ce 31 mm fait l'hypothèse que la déformation totale de l'ensemble contreventement – assemblages est concentrée à 80% d'un côté et de 20% de l'autre. Pour les analyses incrémentales, un déplacement inter-étage de 10% à n'importe quel instant et n'importe quel étage a été considéré comme l'effondrement de la structure. En plus de ces paramètres de réponse, l'effort axial dans les poteaux à été étudié à chaque étage de trois des bâtiments examinés. Deux de ces bâtiments se trouvaient dans les trois séries d'analyses et un se trouvait dans les analyses linéaires et non-linéaires. Ceci a permis d'évaluer les efforts dans les poteaux pour des bâtiments conçus avec des connexions ductiles ou non-ductiles.

Les observations et conclusions suivantes ont été tirés des analyses linéaires (connexions non-ductiles) et d'après les statistiques médianes sur les ratios P/P_{de} :

- Les bâtiments standards à Montréal ont démontrés que l'amplitude de la force sur les connexions est plus élevée que 1.0 pour les bâtiments plus hauts que 15

m. À Vancouver, tous les bâtiments standards ont été soumis à des amplitudes plus élevée que 1.0 et ont en moyenne des ratios P/P_{de} de 1.3 à 1.5 fois plus élevé que les bâtiments à Montréal. Il est donc recommandé, pour les connexions non-ductiles, de limiter la hauteur du bâtiment à 15 m à Montréal et d'augmenter les efforts de dimensionnement de ceux-ci avant de permettre leur usage à Vancouver. Pour permettre une hauteur de 38.1 m, il faudrait dimensionner les connexions avec des forces sismiques correspondant à R_oR_d de 0.80 à Montréal et 0.65 à Vancouver.

- Pour les chevrons à Montréal, les ratios P/P_{de} étaient moins élevés que 1.0 pour tous les bâtiments à cause de leur sur-résistance sismique (V_e/V_{de} plus petit). À Vancouver, les chevrons avec connexions non-ductiles n'étaient pas adéquats et devraient avoir des efforts de dimensionnement correspondant à R_oR_d de 0.65 pour pouvoir être utilisés jusqu'à 30.1 m de hauteur.

- À Montréal et Vancouver, les bâtiments situés sur un sol de type E ont été soumis à des ratios plus élevés que 1.0. Pour permettre que leur usage soit permis avec aucune limite de hauteur à Montréal et une limite de 15 m à Vancouver, les efforts de dimensionnement des connexions devraient être calculés avec R_oR_d égale à 0.76 à Montréal et 0.65 à Vancouver.

- Pour les différentes hauteurs d'étages et pour les différentes localisations de contreventement (intérieure versus extérieure), aucune tendance n'a été observés. Cependant, les analyses sur les bâtiments de même hauteur (15.6 m) mais comprenant un nombre d'étages différents n'ont démontré aucune tendance où différences significatives, ce qui suggère que la hauteur totale du bâtiment peut être utilisée comme paramètre de référence lorsque l'on limite l'applicabilité des bâtiments de la construction conventionnelle.

Les observations et conclusions suivantes ont été faites par rapport aux analyses non-linéaires (connexions ductiles) et d'après les statistiques médianes sur les déformations des assemblages :

- À Montréal, les déformations obtenues étaient inférieures à 31 mm. À Vancouver, les déformations étaient de 2.0 à 3.6 fois plus élevées qu'à Montréal. Pour les bâtiments plus élevées que 15 m à Vancouver, les déformations étaient supérieures à 31 mm. Les assemblages devraient être conçus pour accommoder des déformations d'environ 40 mm si la limite de 15 m est dépassée à Vancouver.

- Comparés aux Split-X, les chevrons ont généralement subit moins de déformations. À Montréal, leurs déformations étaient inférieures à 31 mm. À Vancouver, la déformation moyenne sur la hauteur du bâtiment de 8 étages en chevrons était 19% moins élevée que le Split-X. Les chevrons ont atteints des déformations médianes de 28 mm dans le 4-étages et 35 mm dans le 8-étages à Vancouver. Cependant, les déformations maximales dans les connexions des chevrons se retrouvaient généralement à l'étage supérieur.

- Sur les sols de type E à Montréal, les déformations ont montés jusqu'à 14 mm pour le bâtiment de 8 étages qui dépasse la limite de hauteur prescrite par le CNB. À Vancouver, les déformations ont atteintes 42 mm et 65 mm dans le bâtiment de 4 étages et 8 étages, respectivement. En moyenne, les déformations sur un sol de type E étaient 1.5 fois plus élevées à Montréal et 2.0 fois plus élevées à Vancouver que sur un sol de type C. À moins que les bâtiments à Vancouver puissent accommoder ces déformations importantes dans leurs assemblages, la construction conventionnelle avec connexions ductiles n'est pas adéquate à Vancouver.

- Les déformations ne semble pas varier selon la hauteur d'étage pour un bâtiment d'une hauteur donnée, ni selon l'emplacement de la travée contreventée (intérieur ou extérieur).

Les analyses dynamiques incrémentales de deux bâtiments localisés à Vancouver ont révélé une probabilité d'effondrement entre 5 à 10%, ce qui est considéré comme acceptable. Ces deux bâtiments avaient une hauteur totale de 15.6 m, tout juste au-dessus de la limite actuelle du CNB. Ce résultat suggère que les bâtiments ayant une hauteur égale ou inférieure à la limite de 15 m peuvent offrir une protection adéquate contre l'effondrement, à la condition d'avoir des assemblages ductiles, d'être sur un sol C et d'avoir des contreventements en Split-X ou chevrons. Il serait important de vérifier, dans le futur, la performance de bâtiments semblables mais avec des différents paramètres : assemblages non-ductiles, sol de type E et des hauteurs plus élevées.

L'étude des efforts axiaux dans les poteaux a démontré que l'utilisation de connexions ductiles a pour effet de réduire grandement les efforts axiaux dans les poteaux par rapport au cas des bâtiments avec connexions non-ductiles. Basé sur les statistiques médianes des efforts axiaux, la réduction moyenne à Vancouver est d'un facteur 2.0, 1.6 et 1.6 pour les bâtiments de 4, 5 et 8 étages, respectivement.

Suite à ces conclusions, les recommandations suivantes ont été faites :

- Des études additionnelles seront nécessaires pour comprendre davantage le comportement des connexions dont la rupture se produit par pression diamétrale des boulons. En particulier, Il est important de connaître la vraie résistance ultime de l'acier à une pression diamétrale. Il serait aussi intéressant de déterminer l'effet d'avoir plus d'acier avoisinant au boulon sur les côtés car cet acier pourrait offrir un confinement à l'acier situé à proximité du boulon et ainsi augmenter sa résistance.

- Dû à la nature ductile des ruptures sous pression diamétrale des boulons, il serait intéressant d'observer les effets de concevoir un assemblage pour $4F_u$ pour la

résistance pondérée aux charges sismiques et de vents. Si le vent contrôle le dimensionnement, le bâtiment pourrait être soumis à des déformations excessives dû aux déformations élevées correspondantes à une contrainte en écrasement de $4F_u$. Ceci pourrait avoir des effets néfastes sur la serviceabilité de la structure.

- L'étude a démontré que les sols de classe E ont pour effets d'augmenter l'amplitude de force sur les connexions non-ductiles et l'amplitude des déformations sur les connexions ductiles. Limitée à des connexions ductiles sur des bâtiments de moins de 15 m à Montréal pour les sols E, la construction conventionnelle est grandement restreinte. L'effet des sols E mérite d'être étudié davantage, particulièrement en tenant compte de l'interaction sol-structure.

- Les analyses ont montré que les bâtiments situés sur un site C à Montréal offrent un comportement adéquat, qu'ils soient conçus avec des assemblages ductiles ou non. La hauteur des bâtiments étudiés était de 38.1 m au maximum pour un bâtiment « standard » et de 30.8 m lorsque des différents paramètres étaient utilisés. Il serait recommandé d'étudier des bâtiments avec des hauteurs plus élevées afin de déterminer si d'autres limites devraient exister.

TABLE OF CONTENTS

LIST OF FIGURES

LIST OF TABLES

LIST OF SYMBOLS

b_w Whitmore's effective gusset plate width (mm).

C_f Factored compressive design force (kN).

C_u Expected buckling load (kN). Calculated with $\phi = 1$ and $R_y = 1.1$.

d Nominal bolt diameter (mm).

F_u Specified minimum tensile strength of the connection material (MPa).

h_n Building height (m).

K Structural member's effective length factor.

L_c Clear distance, in the direction of the force, between the edge of the hole and the edge of the adjacent hole or edge of the material (mm).

L Distance from the center of the bolt hole to the edge of the material (mm).

M_w Seismic moment magnitude

n Number of bolts.

P Load transmitted by the bolt, or load encountered in the connection rigid link from the time history analysis (kN).

P_a Anticipated capacity of the connection, calculated using F_y and F_u from coupon tensile tests (kN).

P_{de} Brace axial load coming from response spectrum analysis amplified by R_oR_d (kN).

P_e Expected capacity of the connection, calculated using R_y and R_t factors (kN).

ϕP_n Factored capacity of the connection (kN).

P_n Nominal capacity of the connection (kN).

$P_{u,exp}$ Ultimate load as found in experimental testing. Any load past this point is smaller (kN).

$P_{1/4"}$ Load at ¼" (6.35 mm) deformation. Used only for bearing specimens (kN).

R_d Seismic force reduction factor accounting for system ductility.

R_o Seismic force reduction factor accounting for system overstrength.

R_t Ratio of expected tensile strength to the specified minimum tensile strength, F_u.

R_y Ratio of expected yield strength to the specified minimum yield strength, F_y

s Spacing between bolts in connection (mm)

$\hat{S}_{CT}$ Median value of collapse level earthquake (g).

S_{MT} Design level ground acceleration (g).

SF Scaling factor used to scale historical earthquakes to respective NBCC uniform hazard spectrum.

$SF_{col.}$ Incremental scaling factor applied to a suite of ground motions.

t Thickness of connection material, or plate (mm)

t_g Thickness of gusset plate (mm).

T Structural fundamental period based on NBCC formula (s).

T_1 Structural period as calculated by eigenvalue analysis (s).

V Seismic base shear based on the NBCC equivalent static force procedure (kN)

V_d Elastic seismic base shear coming from the response spectrum analyses, Ve,

multiplied by I_e/R_dR_o (kN).

V_e Elastic seismic base shear coming from the response spectrum analysis (kN)

V_{Chosen} Design base shear (kN).

V_s Slip resistance (kN).

τ_u^p Ultimate shear capacity of the connected material (MPa).

σ_b Shear stress on the bolt (MPa).

σ_u^p Ultimate tensile capacity of the connected material (MPa).

ε Strain

δ_P Connection deformation as determined by the nonlinear analyses series (mm).

$\sigma_{u,exp}$ Bearing stress at the ultimate load. Normalized w.r.t. the steel's F_u.

δ_u Deformation at ultimate (mm).

δ_{rupt} Deformation at the rupture point, defined as the deformation corresponding to a force equal to 80% of $P_{u,exp}$ (mm).

$\delta_{Int.}$ Average bearing deformation found in the gusset plate which did not undergo a bearing failure (intact end) (mm).

δ_{Br} Bearing deformation capacity of the failed end (mm).

LIST OF APPENDICES

INTRODUCTION

Introduction. In the National Building Code of Canada (NBCC) (NBCC 2005), the design earthquake lateral loads are obtained by dividing the equivalent lateral load, representing the elastic seismic response, by a ductility-related force modification factor, R_d. Different R_d values are assigned to different types of seismic force resisting systems (SFRS) and range between 1.0 for very brittle systems (e.g. unreinforced masonry) to 5.0 for very ductile systems (moment-resisting steel frames). The most ductile systems can withstand strong ground motions by going through large cyclic inelastic deformations in selected members.

CSA-S16-01 (CSA 2001) includes detailing provisions to achieve ductile response for different SFRSs for which large inelastic behaviour is expected. Generally, detailing provisions for systems which are expected to go through the most inelastic demand (high R_d) are more demanding, or stringent. Capacity design principles must be used when using R_d values between 2.0 and 5.0 to ensure the hierarchy of yielding during strong ground motions. This, coupled with the numerous detailing provisions, requires considerable additional design checks and significantly lengthens and complicates the design process. On the other hand, structures of the conventional construction category (CC Type) are designed with R_d equal to 1.5 and do not require any capacity design checks. They are deemed to possess sufficient inherent ductility arising from traditional construction practices to sustain their anticipated limited inelastic demand. The only requirement for CC Type structures is that they use primary framing member connections (brace connections) that exhibit ductile failure modes. If connections do not exhibit a ductile failure mode, they must be designed for the seismic load amplified by R_d, 1.5. The design process therefore remains relatively simple and quick, as member forces from elastic analysis using commercially available computer programs can be used by practicing engineers.

Because of their limited ductility, the use of CC Type SFRSs has been limited to certain uses in the 2005 NBCC. CC Type structures cannot be used for post-disaster buildings

such as hospitals or power-generating stations. Currently, CC Type structures cannot be used for buildings taller than 15 m where the specified short-period spectral acceleration ratio, $I_E F_a S_a(0.2)$, is equal to or greater than 0.35, or where the one-second spectral acceleration ratio, $I_E F_v S_a(1.0)$, is greater than 0.30. These two ratios give a measure of the ground motion intensity at the building's site for firm soil site conditions.

Due to its simplicity and cost-efficiency during the design phase, the concentrically braced frame (CBF) system is by far the most popular for resisting lateral loads in steel structures in Canada. It is used for all building applications, including residential and commercial buildings as well as for industrial facilities. For CBF, case studies have shown that designs using an R_d greater than 2 typically require heavier sections and connections, leading to more costly structures (Tremblay 2005). This is true even though these structures are designed for lower seismic loads than CC Type structures. This increase in cost has a negative impact on the competitiveness of braced steel frames for all multi-storey buildings, when the use of CC Type systems in certain locations is prohibited because of the prescribed height limits. It will also affect tall single-storey structures used in industrial settings (aircraft hangars, steel mills or processing plants), as these often exceed 15 m in height. CC Type structures are also not permitted for power houses or other electrical generating facilities as these qualify as post-disaster buildings. In heavy industrial structures, the structures typically have a complex geometry with non uniform stiffness and mass distributions. Performing capacity design checks for these structures can be a challenging task, adding cost and creating an obstacle to practical design and construction.

In the past, studies have mostly focused on systems with R_d greater than or equal to 2.0, with little attention given to low-ductility systems (CC Type). Therefore, very limited scientific data exists to support any relaxations to the NBCC height limits for CC Type buildings. Of special interest are the differences in connection ductility demand between structures located in eastern and western Canada. Practicing engineers also have very few examples of ductile bracing connections and there is, to some degree, confusion as

to what qualifies as a ductile connection. To avoid this problem, connections are often designed using the amplified seismic loads.

Analysis of an 8-storey CC Type braced steel frame in Victoria, BC, showed extensive brace buckling and tensile yielding, as well as overloading of beams and columns (Redwood et al., 1991). The system was considered unacceptable for severe seismic regions. For the same building in Montreal, only limited inelastic straining was seen in the framing members. Earthquake ground motions in eastern North America have their energy concentrated at higher frequencies and are therefore less critical for structures having longer periods of vibration. Another study was performed on braced frames up to 4 storeys in western Canada, where the inelasticity was assumed to be concentrated in the gusset plates (Mullin et al., 2004). Peak inelastic deformations varied between 30 and 40 mm and were found to generally increase with the number of storeys. No such data exists for eastern Canada. Other studies (Gupta et al., 1999; Lacerte et al., 2006; Tremblay 2005; Tremblay et al., 2002; Tremblay et al., 2001) confirm that structures built in eastern North America experience significantly less seismic damage compared to those on the west coast, suggesting that there may be a potential to extend the range of application of CC Type structures in eastern Canada. This research project will serve to complement these findings and better assess the variation in connection inelastic deformation demand resulting from the two different ground motion types.

Objectives. The principal objectives of this study are to generate scientific data to 1) increase our current knowledge of the inelastic seismic response of CC Type braced steel frames and 2) propose typical connection details aiming to improve their performance under strong ground shaking. These two objectives will enable us to evaluate the relevance of the 15 m height limit imposed by the NBCC and whether or not this limit can be made a function of different building parameters, such as the building's location (eastern versus western Canada), the site class, the number of storeys, or the type of bracing connection used (ductile versus non-ductile), among others. More specifically, the study will focus on the following objectives:

- Assessment of the ductility capacity of typical vertical bracing connections.
- Evaluation of the seismic performance of regular CC Type concentrically braced steel frames located in eastern and western Canada to revisit the height limits imposed by the NBCC, based on scientific evidence.

Methodology. To attain the latter objectives, the study is separated into two sections: an experimental one and an analytical one, respectively.

The experimental phase serves to determine the ductility capacity of typical vertical bracing connections. A typical bracing connection consists of two pairs of back-to-back angles attached to either sides of a tubular brace. A single pair of the back-to-back angles bolted to a gusset plate is studied in two phases. The first phase consists of identifying a ductile failure mode. Five different connection limit states are examined: parallel weld failures, bolt bearing failure, bolt shear rupture, net area rupture, and shear and tension block failure. The second phase consists of further studying the effects of different connection parameters on the force-deformation behaviour of bolt bearing failures, which was found to be the most ductile failure mode in the first phase.

The analytical phase is divided into three series. The first series consists of linear time history dynamic analyses to determine the force demand on brace connections. The second series consists of nonlinear time history dynamic analyses with fuses at the ends of bracing members to determine the expected ductility demand on bracing connections. The third series consists of incremental nonlinear dynamic analyses to determine a level of confidence against collapse. The first two series are performed on 24 different buildings while the third series is performed on two buildings. The buildings encompass different building geometries and parameters such as the building height, different storey heights, two different types of bracing systems, the soil properties (site classes), and the location of the bracing bents in the structure. The third series is performed on two buildings with total heights of 15.6 m. Information is taken from all three analysis

series to evaluate the benefits of using ductile connections, with regards to the axial loads encountered by the columns.

Organization of thesis. The thesis is organized into five different chapters:

- Chapter 1 gives a literature review on bolt bearing connection failures and low-ductility seismic force resisting systems.
- Chapter 2 presents the first experimental phase performed to find a ductile connection failure mode.
- Chapter 3 reports on the second experimental phase performed to optimize the deformation capacity of the connection failure mode established in chapter 2.
- The analytical phase is described in Chapter 4. The buildings studied are presented along with their design. The analytical models used for analysis are presented and explained. Results are then provided for all three series of analyses in addition to a quick look at the benefits of using ductile connections.
- Chapter 5 provides the conclusions drawn from the research project, preliminary recommendations to enhance the use and design of CC Type concentrically braced steel frames, and recommendations for future studies.

Chapter 1. LITERATURE REVIEW

A literature review of research pertaining to both the experimental and the analytical phase of this research project is given in this section. The literature review for the experimental phase deals with bolted steel connections failing under bolt bearing, while the literature review for the analytical phase deals with previous studies performed on low ductility steel braced frames as well as gives a review of the Canadian seismic design provisions for these structures, otherwise known as structures of the conventional construction category (CC Type).

1.1. Literature Review of Bolt Bearing Failures

Section 1.1 gives a literature review of connections failing under bolt bearing on plates. This connection failure mechanism is expected to provide sufficient ductility capacity to accommodate the inelastic deformations anticipated in connections of braced steel frames designed as CC Type SFRS.

1.1.1. Theoretical Background

Shear splice connections can be classified as either a slip-resistant or bearing type. A slip-resistant connection has pre-tensioned bolts which introduce friction forces between different components of the connection (for example, between clip angles and a beam web). The distribution of frictional forces is shown schematically in Figure 1.1. The load is initially carried by friction forces at the ends of the joints and this zone of friction forces extends toward the center of the joint when the load increases (Kulak et al., 1987). The frictional resistance will be exceeded at the ends first, and small relative displacements between contact points on the faying surfaces take place. As the load continues to increase, the slip zone moves inward from the ends and major slip happens once the friction resistance over the entire faying surface is exceeded. Major slip may be equal to twice the hole clearance but has been observed to be less than half the hole clearance (Kulak et al. 1987). The bearing stresses will appear after major slip has occurred in the connection. However, only the end bolts may come into contact with the

plate material (Kulak et al. 1987). Increasing the load will cause these bolts and the plate material to deform and the succeeding bolts with then come into bearing.

At first, the bearing stress is concentrated at the point of contact between the bolt and plate material. An increase in load causes the plate material to yield and further embedment of the bolt into the plate. At this point the bearing stresses become more uniform and a uniform stress distribution can be assumed. Figure 1.2 illustrates this concept.

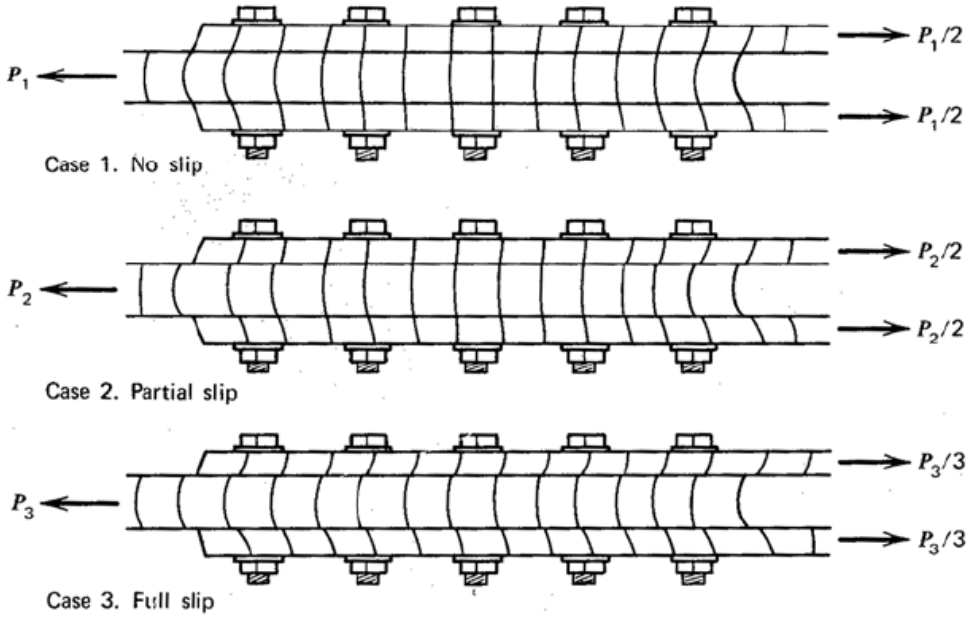

Figure 1.1: Distribution of friction forces (Kulak et al. 1987)

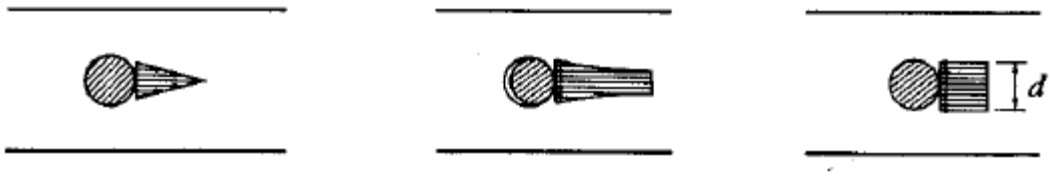

Figure 1.2: Bearing stresses (Kulak et al. 1987)

The uniform bearing stress is defined as:

$$\sigma_b = \frac{P}{dt} \tag{1.1}$$

where d is the bolt diameter and t is the plate thickness. Although the bolt is subjected to the same bearing stresses, tests have always shown that the fastener is not critical (Kulak et al. 1987).

Several factors influence the manner in which the material fails under bearing pressure: the bolt end distance, the bolt diameter, and the thickness of the connection material. The three failure mechanisms are:

- The fastener splits out through the end zone (a tear-out failure).
- Excessive deformations develop in the vicinity of the bolt hole (material pile-up).
- A combination of the first two mechanisms.

Failure mechanisms 1 and 2 are shown in Figure 1.3 a) and b), respectively.

One can estimate the end distance required to prevent the plate from splitting by equating the force transmitted by the end bolt to the force that corresponds to shear failure of the plate along the dotted lines shown in Figure 1.3c.

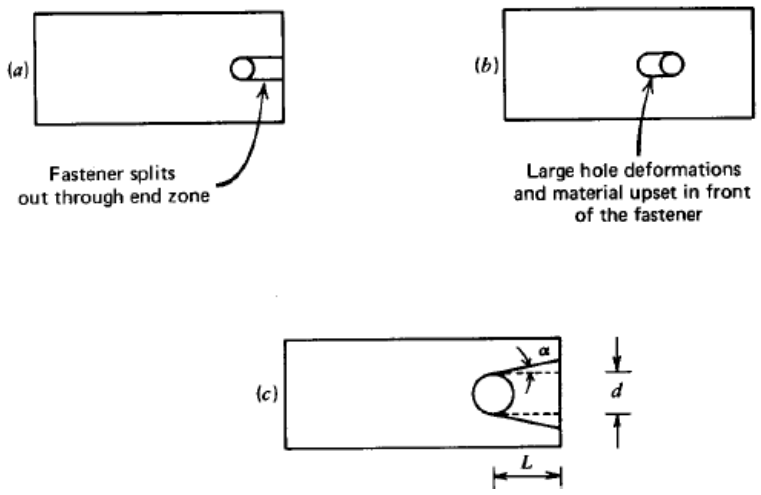

Figure 1.3: Bearing failure mechanisms (Kulak et al. 1987)

It is important to note that, in Figure 1.3c, L is the distance from the center of the hole to the end of the plate, not to be confused with the clear distance used in AISC 360-05. The clear distance, L_c, is equal to this L minus half the bolt hole diameter.

Kulak et al. (1987) developed an equation to relate the bearing ratio σ_b / σ_u^P to the end distance represented by the L/d ratio assuming that the bolt capacity is lower bound by the shear capacity of the plate along the dotted lines shown in Figure 1.3c.

$$P_s^{\,b} = 2t(L - \frac{d}{2})\tau_u^p \qquad 1.2$$

where t is the plate thickness and τ_u^p is the ultimate shear strength of steel, which Kulak et al. state is generally 70% that of the tensile strength. Equation 1.2 becomes:

$$P_s^b = 2t(L - \frac{d}{2})(0.7\sigma_u^{\,p}) \qquad 1.3$$

Equating equations 1.2 and 1.3 yields:

$$\frac{L}{d} \geq 0.5 + 0.715\frac{\sigma_b}{\sigma_u^{\,p}} \qquad 1.4$$

Equation 1.4 relates the end distance, expressed as a ratio to the bolt diameter, to the bearing ratio. Figure 1.4 compares the analytical results of this last equation with experimental data (Kulak et al. 1987). One, two, and three-bolted, mostly symmetric butt splices are included in these tests. An example of a symmetric butt splice is given in Figure 1.5. All specimens were critical on the main pull plate (enclosed plate), but some were critical in the outer plies; these are shown by symbols with a dash. Some specimens had finger tightened bolts and others had pre-tensioned bolts, introducing friction forces between plates.

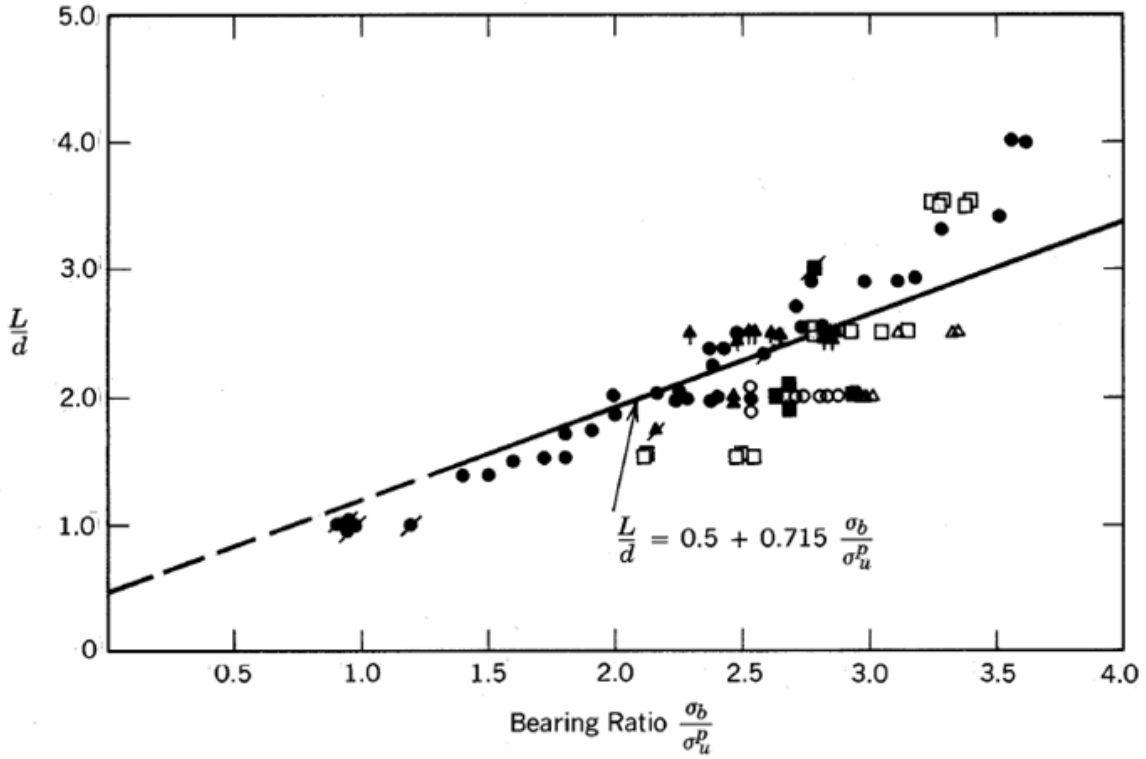

Figure 1.4: Influence of type of specimen on the bearing strength. ● One-bolt specimen (non-tightened); ○ one-bolt specimen (tightened); ▲ two-bolt specimen (non-tightened); Δtwo-bolt specimen (tightened); ■ three-bolt specimen (non-tightened); □ three-bolt specimen (tightened). Note: All specimens were critical on enclosed ply except those symbolized with a dash symbol. Those specimens had outside plates critical (Kulak et al. 1987).

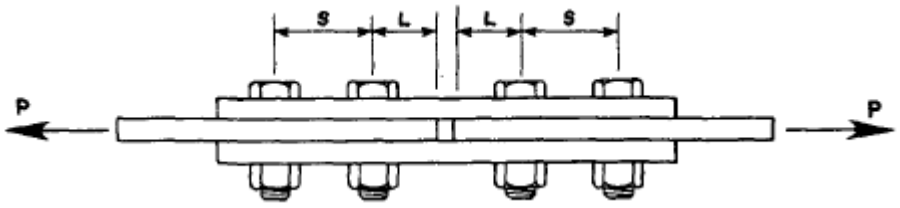

Figure 1.5: A symmetric butt splice (Frank et al., 1981).

There is reasonably good agreement between the analytical equation and the test results. However, they seem to diverge at a larger L/d ratio, which is expected since the equation assumes a failure in the plate in the form of a tearout. At larger L/d ratios (or larger end distances), failure is likely to occur in the form of a material pile-up, as

shown in Figure 1.3b. The design equation associated with a pile-up failure mode is explained in sections 1.1.2.

Providing a clamping force in the bolt leads to an increase in the ultimate bearing ratio, indicating part of the load is transmitted by frictional forces on the faying surfaces (Kulak et al. 1987). The equation for the shear capacity of the connection material, equation 1.2, applies to multiple in-line bolts (Frank et al. 1981) as shown in Figure 1.6. In this figure, the plate's capacity would be calculated by finding, for bolts 1, 2, and 3, the plate resistance in tear-out and bolt bearing. Under the applied load P, the length of the shear planes when calculating the tear-out capacity would be equal to L for bolt 1 and s for bolts 1 and 2. Depending on the standard used for design, as explained in sections 1.1.2 and 1.1.3, the bolt hole diameters would be excluded from these distances. The total resistance of this resistance would be the sum of the plate's resistance at every bolt hole.

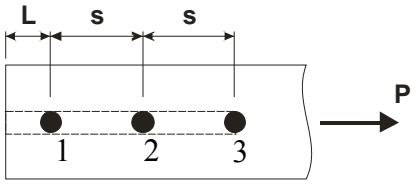

Figure 1.6: Multiple in-line bolts joint

Both Canadian and American design standards (AISC 2005; CSA 2001) include design specifications and requirements when dealing with bolted connections. More specifically, they give similar guidelines in preventing the tearout failure modes. They prevent large deformations at bolt holes (material pile-up) by limiting the bearing stresses to $\sigma_b = C \times \sigma_u$. C is a factor that can vary from 2.0 to 3.0, depending on the situation. Hole deformations are currently limited to ¼", or 6.35 mm, in most cases. This is covered in sections 1.1.2 and 1.1.3 of this document.

1.1.2. Canadian Steel Design Standard: CSA S16-01

In CSA-S16-01, the factored resistance associated to bolt tear-out is given in Clause 13.11 that deals with tension and shear block failure in gusset plates, framing angles, etc. The capacity is expressed as the sum of the factored tension resistance, T_r, along the net section loaded in tension and the factored shear resistance, Vr, along either the gross or the net section loaded in shear along the bolt lines. That resistance is therefore given by the lesser of:

$$T_r + V_r = \phi A_{nt} F_u + 0.60 \phi A_{gv} F_y \qquad 1.5$$

$$T_r + V_r = \phi A_{nt} F_u + 0.60 \phi A_{nv} F_u \qquad 1.6$$

where A_{nt} is the net area subjected to tension, and A_{gv} and A_{nt} are, respectively, the gross and net area loaded in shear. These areas are defined in Figure 1.7 for the cases of single bolt line and multiple bolt line joints. It is noted that the shear capacity of steel in CSA-S16 is taken equal to $0.6F_u$ (F_u is the steel tensile strength of the connection plate), rather than the $0.7F_u$ as assumed by Kulak et al. (1987) and discussed in section 1.1.1. As shown, failure for multiple bolt line joints can occur by either bolt tear-out along the individual bolt lines or block shear, depending upon the geometry of the connections. In all cases, it is assumed in CSA-S16-01 that the contribution of the shear resistance to the connection capacity is given by the shear strength available along the entire connection length, not just over the length L, as discussed previously. The ϕ factor in the two above S16-01 equations is equal to 0.9.

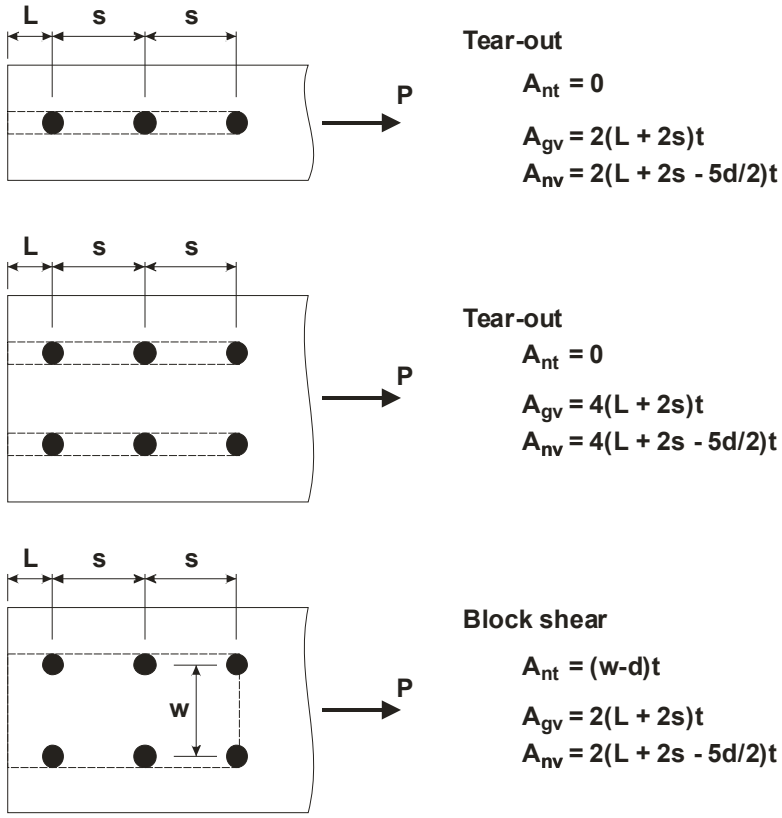

Figure 1.7: Failure of single and multiple bolt line joints

Clause 13.10(c) of S16-01 (CSA 2001) specifies the maximum factored bearing resistance of a connection, B_r:

$$B_r = 3\phi_{br} tdnF_u \qquad 1.7$$

where ϕ_{br} is 0.67. From equation 1.7, one can deduce S16-01 is simply limiting the bearing stress on the plate material to three (3) times the ultimate tensile resistance of the material, F_u. However, the CSA-S16 commentary clarifies that this limit is based on previous studies which showed that the ratio of the bearing stress (B_r / dt) to the ultimate tensile strength of the plate (Fu) is in the same ratio as the end distance of the bolt (e) to its diameter (d) as shown in equation 1.8 (CSA 2001). Because these test studies did not provide data for L/D greater than 3, an upper limit of L = 3d was imposed and yielded

equation 1.7 as the bolt bearing capacity, where n is the number of bolts in the connection. Frank and Yura (1981) state that using equation 1.7 as an upper bound anticipates bearing deformations, or hole ovalization, greater than ¼", or 6 mm.

$$\frac{B_r}{\phi dt} = \frac{L}{d} F_u \qquad 1.8$$

In Clause 27.1.6 of S16-01, which is part of the seismic design provisions for steel structures, the end distance L should be equal to a minimum of two times the bolt diameter when the factored bearing force due to seismic load exceeds 75% of B_r from equation 1.7. This minimum requirement is set to ensure minimum deformation capacity (or prevent non-ductile bearing or tear-out failure modes) in bolted connections of seismic force resisting systems (SFRSs). It is noted that these requirements apply to a SFRS for which a ductile failure mode is expected, i.e. systems for which an R_d factor greater than 1.5 is used in design (see section 1.2.1), and would therefore not apply to braced steel frames of the conventional construction category (R_d = 1.5). However, CSA-S16-09 draft standard suggests Clause 27.1.6 should also apply to conventional construction structures of 15 m or more in height.

Clause 27.1.6 also contains additional requirements for bolted connections that are relevant to this research. For instance, bolts must be pre-tensioned and the contact surfaces of the connected parts must be Class A surface (or surfaces with a minimum coefficient of friction of 0.33). The intent is to minimize slip and damage in small or moderate earthquakes and prevent bolts from loosening under strong seismic motions. Short slotted holes parallel to loading and long slotted holes either parallel or perpendicular to loading are not permitted to prevent excessive deformations of the connection material. These requirements are based on the AISC 2005 seismic provisions (2005) and are explained in the commentary.

1.1.3. AISC Specifications: AISC 360-05

Clause J3.10 of the 2005 AISC Specifications uses the same bearing resistance but has added several more stringent requirements (AISC 2005). When deformation at the bolt hole under service loads is a design consideration, the available nominal bearing strength, R_n, is determined as:

$$R_n = 1.2L_c tF_u \leq 2.4dtF_u \qquad 1.9$$

where ϕ, the resistance factor, would be 0.75 and L_c is the clear distance between the edge of the hole in question and the edge of the adjacent hole or edge of the material. This equation is therefore used at all bolt hole locations to find their resistances and the connection's capacity is therefore calculated as the sum of the latter. The $1.2L_ctF_u$ component of the equation is the force needed to cause a bolt to tear out of the plate. Equation J4.4 of AISC 360-05 shows the nominal shear strength of a connecting element rupturing in shear to be $0.6F_uA_{nv}$ (AISC 2005). Taking account for both shear planes extending from either side of the hole to the edge of the connected material, the shear resistance of a bolt shearing through a plate is $2 \times (0.6F_uA_{nv}) = 1.2F_uA_{nv}$. Note the bolt end distance, L_c, in equation 1.9 is the clear end distance and not the distance shown in Figure 1.3c. Hence, except for the difference in the ϕ factors, the equation for tear-out in AISC Specifications corresponds to the CSA-S16-01 block shear equation with net shear area. Yielding along the areas loaded in shear is not considered in the AISC Specifications.

The $2.4dtF_u$ component of equation 1.9 is the sum of the permissible bearing stress of all bolts bearing on a connected material. Since deformations are restricted, this equation limits the bearing stress to 2.4 times F_u instead of 3.0, as was the case in S16-01.

In AISC Specifications, when deformation at the bolt hole is not a design consideration equation 1.9 becomes:

$$R_n = 1.5L_c tF_u \leq 3.0dtF_u \qquad 1.10$$

The equation relies on an increased shear capacity from 0.6 F_u to 0.75 F_u. The upper limit corresponds to the value adopted in S16-01.

Equations 1.9 and 1.10 apply for standard, oversized, short-slotted holes, each independent of the direction of loading, and long-slotted holes with the slot parallel to the direction of the bearing force. Table 1.1 shows a definition of bolt hole types relative to bolt diameters as given in the AISC Specifications. The AISC allows the use of slotted holes in only one of the connected parts of either slip-critical of bearing-type connections at an individual faying surface. Long-slotted holes are permitted without regard to the direction of loading in slip-critical joints, but must be normal to the loading in bearing-type joints. Like the CSA S16-05 requirements, a washer or a continuous bar must be used to cover the slot after installation.

Table 1.1: Bolt hole dimensions according to its type

Bolt Diameter	Hole Dimensions			
	Standard	Oversize	Short-Slot (Width x Length)	Long-Slot (Width x Length)
M16	18	20	18 x 22	18 x 40
M20	22	24	22 x 26	22 x 50
M22	24	28	24 x 30	24 x 55
M24	27	30	27 x 32	27 x 60
M27	30	35	33 x 37	30 x 67
M30	33	38	33 x 40	33 x 75
≥M36	d + 3	d + 8	(d + 3) x (d + 10)	(d + 3) x 2.5d

When using long-slotted holes perpendicular to the direction of the force, the following applies:

$$R_n = 1.0L_c tF_u \leq 2.0dtF_u \qquad 1.11$$

These reduced capacities result from the work of Frank and Yura (1981), who found that slotted holes gave larger deformations than a round standard holes for the same bearing stresses. This is discussed in section 1.1.7.

In order to prevent excessive deformations of the connected material under earthquake loading, the bearing capacity of bolts is limited to $2.4dtF_u$ in clause 7.2 of the 2005 AISC seismic provisions (2005), i.e., the "deformation-considered" option of Clause J3.10 in the AISC specifications (equation 1.9). As in CSA-S16-01 Clause 27.1.6, only standard circular and short-slotted holes perpendicular to loading are permitted in bolted connections, the bolts must be pre-tensioned, and the connected parts must have Class A or better contact surfaces.

1.1.4. Effect of Hole Type

Holes in structural connections may be punched, punched and reamed, or drilled. The effects of the type of hole can be important when looking at the behaviour of connections in bearing. It was found through experiments that punching caused a reduction in strength of about 10%, and a reduction in ductility of about 40% (Vasarhelyi et al., 1959). However, other research has shown that punched holes show no decrease in the ultimate strength (Iwankiw et al., 1982).

The report of an experimental research performed by L. Wallin showed that punched holes have about 90% of the bearing strength displayed by drilled holes and that the punched hole elongation was generally between 50 and 90% that of the drilled (Wallin 1975).

Owens et al. (1981) performed a series of tests which demonstrated that drilled holes were much more ductile than punched ones, sometimes undergoing twice the amount of deformation. These results are shown in Table 1.2. The one-bolt specimens consisted of two different types of steel (300 MPa and 450 MPa yield strengths) and of 20 mm bolts located two bolt diameters from the edge of the plate. The deformations shown are the average of the three specimens tested for each test series. Failures in punched hole

specimens initiated with tears developing from the bolt hole, oriented at 30 degrees. This type of failure would be more brittle than a failure caused by the piling of plate material.

Owens et al. (1981) drew the following conclusions:

- Punching does not significantly alter the bearing strength of a connection.
- Deformations of punched hole at service loads are likely to be slightly less than drilled holes, meaning punched holes are stiffer than drilled ones under a given bearing stress.

Table 1.2: Comparison of punched and drilled hole connections at ultimate load (Owens et al. 1981)

	Deformation at failure (mm)	
Specimen series	Drilled holes	Punched holes
43.1.1	12.0	9.7
43.1.2	13.3	6.9
43.1.3	18.0	11.2
43.1.5	9.2	7.6
43.1.6	24.3	9.3
50.1.1	10.0	11.8
50.1.4	15.0	11.7

1.1.5. Effect of End Distance

As discussed, the bearing strength of a connection is calculated using two equations: one for a tear-out failure mode and another for a bearing failure mode. The end distance of a bolt, found to have a major influence on the bearing stress distribution, is the principal factor in calculating the tearout capacity. Kim (1996) reports that the ductility is directly affected by the end distance when this distance is short and as long as the free end of the plate failing in bearing is restrained against warping out-of-plane. This warping is caused by a lack of lateral confinement in single lap splices. Typical gusset plates in conventional construction would be restricted against any out-of-plane warping. Longer end distances translate into the capability of having greater deformations, as the failure

modes changes from a tearout to a bolt bearing failure of the end bolt. As can be expected, shorter end distances translate into less stiff connections (Perry 1981).

1.1.6. Effect of Bolt Pre-Tension

A connection with pre-tensioned bolts will transfer forces through friction between connection elements. It will continue to pick up load without any additional displacements until major slip occurs. After slippage, the load quickly peaks, the connection fails, and the connection force is then transferred through bolts bearing on the connected parts. Frank and Yura (1981) found that the difference between snug-tight bolts and pre-tensioned bolts on bearing failures is insignificant in terms of the ultimate load. Geometrically identical symmetric butt splices in which the outside, unconfined plates were critical were tested with snug-tight and pre-tensioned bolts: the results were virtually identical in terms of ultimate loads and displacements. The significant difference between the two is the difference in initial stiffness in the load vs. displacement curve; untorqued bolts offer much less initial stiffness because slippage occurs much earlier.

1.1.7. Effect of Slotted Holes

Slotted holes parallel to the loading in bearing-type shear splices have the same capacity as round holes. However, slotted holes perpendicular to the direction of the loading behave differently. Frank and Yura (1981) found that slotted holes in bearing show considerably more displacement per load in the early stages of loading than the round hole specimens with only slightly different ultimate loads. This is due to the increase in bending deformation between the edge of a hole and another hole or edge of material.

However, slotted holes have much less capacity when deflection limits are used as failure criteria. This is shown in equation J3-6c of AISC 2005, where clause J3.10b states that, for long-slotted holes with the slot perpendicular to the direction of the force, the bearing stress is limited to $2.0F_u$. This was based on the work of Frank and Yura (1981), who tested long-slotted hole specimens failing in bearing and found that these

specimens underwent more deformations than standard round holes under a given bearing stress.

1.1.8. Effect of Ultimate Stress to Yield Stress Ratio

A material with a high ratio of ultimate stress to yield stress (F_u/F_y) ratio is said to be a ductile material, as opposed to one having a small F_u/F_y ratio. Kim (1996) determined that this ratio does not affect the strength in bearing at ¼ inch displacement when greater than 1.13 and confirmed that the bearing strength is proportional to the ultimate stress. Kim and Yura (1999) showed through experimental testing that the F_u/F_y ratio has a negligible effect on the deformations at ultimate in tear-out and bearing failures, as shown in Table 1.3. The two columns of specimens correspond to two different types of steel used. The second letter indicates whether One or Two bolts were used. The following two pairs of numbers indicate the end distance and bolt pitch, respectively, normalized with respect to the bolt diameter.

Table 1.3: Test results from Kim (1996) showing effect of F_u/F_y

Specimen	$P_{u,exp}$ (mm)	Specimen	$P_{u,exp}$ (mm)
AO050	5	BO050	6
AO100	7	BO100	8
AO150	13	BO150	12
AT0510	6	BT0510	9
AT0520	8	BT0520	12
AT0530	5	BT0530	11
AT1510	10	BT1510	10
AT1520	14	BT1520	13
AT1530	9	BT1530	13

1.1.9. Effect of Connection Geometry

Perry (1981) reports the best manner by which different connection configurations can be compared is by the bearing ratio. The bearing ratio is defined as the bearing stress divided by the net tensile stress across the plate's cross-section and is given by equation

1.12. Since the load term is present in each of the stresses, the load cancels out and only the net area and bearing area are left. Perry reports that his testing showed specimens having a higher bearing ratio underwent more bearing deformations. It was also reported that geometrically different connections with similar bearing ratios behaved similarly. No equations were found that relate the connection deformation to the bearing ratio.

$$BR = \frac{Bearing\ Stress}{Net\ Section\ Stress} = \frac{\frac{P}{A_{Br}}}{\frac{P}{A_n}} = \frac{A_n}{A_{Br}} \qquad 1.12$$

1.1.10. End Tear-Out Failures of Bolted Tension Members, Cai and Driver (2008)

Fifty tests were conducted on wide-flange shapes in three series. Attention was given to the strength prediction of these specimens based on available standards, with little attention given to a connection deformation capacity under different connection parameters. This section first presents Cai and Driver's findings on the connection strength prediction aspect followed by a presentation of the connection deformations encountered in their testing.

Series A had 12 specimens connected through their webs by four to six bolts in two lines, while Series C had 32 specimens also connected through their webs by six bolts in two lines. Series B had six specimens connected through both the web and the flanges and are not included in this review because of the combined failure modes in the web and flanges taking place. Specimens in Series A failed by bolt tear-out along each of the individual bolt lines. Specimens with the thicker web in Series C failed in a combination of shear failure of the inner bolts and either tear-out, bolt bearing, or bolt shear of the two end bolts. The failure mode of the end bolts depended on the end bolt distance. Specimens with the thinner web in series C failed in a combination of bearing at the four

inner bolts and tear-out or bearing failure at the two end bolts. Test series A used A490 ¾" bolts while series C used A325 ¾" bolts.

In test series C, all specimens had two bolt lines of three bolts each and the only variable was the bolt end distance. For this series, specimens C1 through C16 and specimens C17 through C32 had, respectively, web thicknesses of 9 mm and 6 mm. The authors observed different failure mechanisms for the two halves as the series with thicker webs experienced bolt shear ruptures. The authors show traditional failure modes in Figure 1.8 while "combined" failure modes are shown in Figure 1.9. The failure modes shown in Figure 1.8 are based on the assumption that the ductility of the connection is sufficient to develop the full capacity at each individual bolt or that it would fail in a global connection failure mode. The first three modes of Figure 1.9, like those of Figure 1.8, are considered ductile enough to develop the full capacity at each bolt, while the last two failure modes are considered non-ductile (Cai et al. 2008).

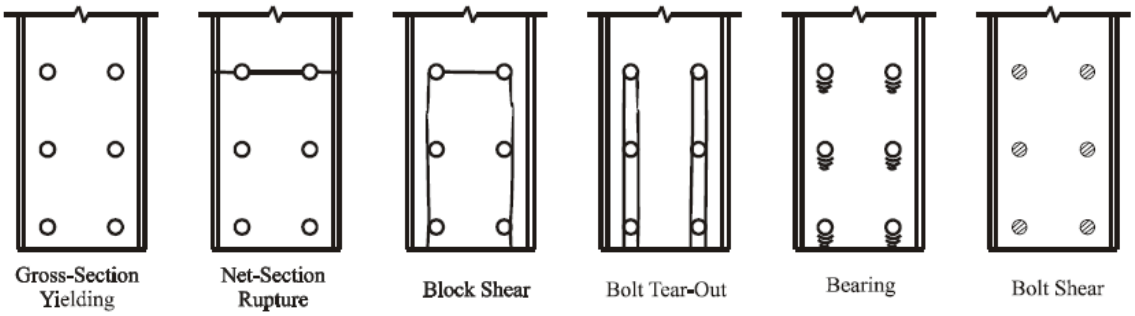

Figure 1.8: Conventional connection failure modes (Cai et al. 2008).

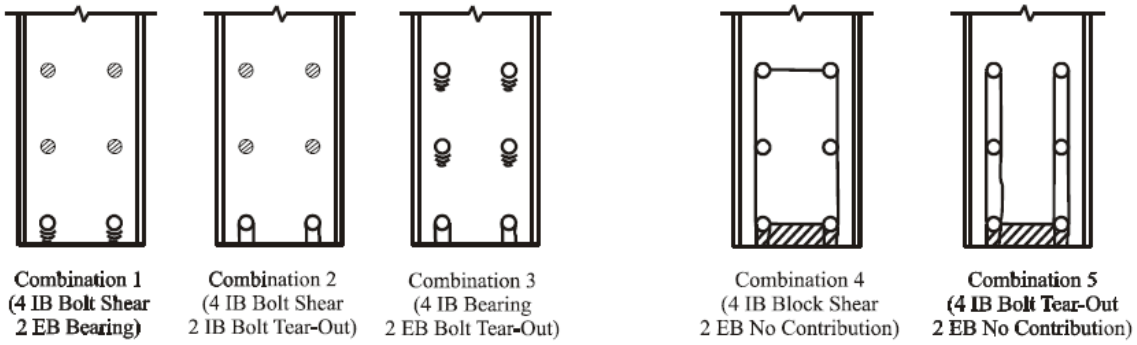

Figure 1.9: Combined ductile and non-ductile failure modes (Cai et al. 2008).

The authors proposed using the second term of the "unified" equation, shown in equation 1.13 and proposed by Driver et al. (2006), when calculating tear-out capacities. The current draft of the CSA-S16-09 uses the slightly modified equation 1.14 (CSA 2009) to calculate the shear and tension block failure of connections.

$$T_r + V_r = \phi A_{nt} F_u + \phi A_{gv}\left(\frac{F_y + F_u}{2\sqrt{3}}\right) \qquad 1.13$$

$$T_r + V_r = \phi A_{nt} F_u + \phi 0.6 A_{gv}\left(\frac{F_y + F_u}{2}\right) \qquad 1.14$$

where the resistance factor, ϕ, is equal to 0.75 in both equations.

For the thicker webs, or specimens C1 through C16, the authors found that the non-ductile combination failure modes of Figure 1.9 did not accurately predict the connection capacities, implying the connections have sufficient ductility to develop the full capacity of each individual bolt or develop a global connection failure mode, such as the ones shown in Figure 1.8 or the first three modes of Figure 1.9. The authors found the governing capacity for the Series C specimens with thicker webs to be the sum of four fully developed inner bolt shear capacities and the strength of either the end material (lesser of bolt tear-out using unified equation or bolt bearing) or two additional bolts failing in shear. Table 1.4 shows the governing failure modes for these specimens; a failure mode combination refers to the numbers shown in Figure 1.9, while 6-V_{Bolt}

corresponds to the shear failure of the 6 bolts. The authors reported both the CSA-S16-01 and AISC 2005 expected capacities using 1.13 for bolt tear-out. CSA-S16-01 gives a mean test-to-predicted ratio of 0.97 and AISC 2005 has a mean of 1.02. These capacities are reported as very acceptable and, again, the authors recommend the use of the unified equation when calculating the bolt tearout capacity.

Table 1.4: Connection test-to-predicted ratios for specimens with thick webs (Cai et al. 2008)

		CSA-S16-01 & Equation 1.13		AISC 2005 & Equation 1.13		$P_{u,exp}$ / P_e	
Specimen	$P_{u,exp}$ (kN)	P_e (kN)	Fail. Mode Comb.	P_e (kN)	Fail. Mode Comb.	CSA	AISC
C1E1a	1082.1	1114.7	2	1042.5	1	0.97	1.04
C2E1b	1111.8	1118.0	2	1046.0	1	0.99	1.06
C3E1c	1112.8	1118.2	2	1045.3	1	1.00	1.06
C4E2a	1244.6	1176.7	2	1131.6	1	1.06	1.10
C5E2b	1190.4	1182.4	2	1138.4	1	1.01	1.05
C6E2c	1152.3	1177.1	2	1133.7	1	0.98	1.02
C7E3a	1211.7	1235.9	2	1194.3	2	0.98	1.01
C8E3b	1155.4	1236.4	2	1198.9	2	0.93	0.97
C9E3c	1215.3	1240.5	2	1247.7	2	0.98	1.01
C10E4a	1215.0	1298.9	2	1247.7	6-V_{Bolt}	0.94	0.97
C11E4b	1249.1	1299.8	2	1247.7	6-V_{Bolt}	0.96	1.00
C12E4c	1182.8	1299.9	2	1247.7	6-V_{Bolt}	0.91	0.95
C13E5a	1293.1	1310.1	6-V_{Bolt}	1247.7	6-V_{Bolt}	0.99	1.04
C14E5b	1187.8	1310.0	6-V_{Bolt}	1247.7	6-V_{Bolt}	0.91	0.95
C15E5c	1279.8	1310.1	6-V_{Bolt}	1247.7	6-V_{Bolt}	0.98	1.03
C16E6	1323.3	1310.1	6-V_{Bolt}	1247.7	6-V_{Bolt}	1.01	1.06

For the thinner webs, or specimens C17 through C32, the authors concluded that the connections had sufficient ductility to develop the full capacity at each individual bolt or develop a global connection failure mode, as mentioned in the above paragraph. The governing capacity for the thinner web specimens was the sum of the bearing capacity at the four inner bolts and the strength of the end material (as explained above). Table 1.5 shows the governing failure modes for these specimens; the failure mode combination refers to the numbers shown in Figure 1.9, while 6-B_r corresponds to a bolt bearing failure of the plate adjacent to the bolts. Again, the authors reported both the CSA-S16-01 and AISC 2005 expected capacities using equation 1.13 for bolt tear-out. CSA-S16-01 and AISC 2005 give mean test-to-predicted ratios of 1.22 and 1.23, respectively.

Table 1.5: Connection test-to-predicted ratios for specimens with thin webs (Cai et al. 2008)

		CSA-S16-01 & Equation 1.13		AISC 2005 & Equation 1.13		$P_{u,exp}$ / P_e	
Specimen	$P_{u,exp}$ (kN)	P_e (kN)	Fail. Mode Comb.	P_e (kN)	Fail. Mode Comb.	CSA	AISC
C17E1a	967.4	760.8	3	740.1	6-B_r	1.27	1.31
C18E1b	984.6	755.0	3	734.0	6-B_r	1.30	1.34
C19E1c	1013.6	760.7	3	739.9	6-B_r	1.33	1.37
C20E2a	1014.9	798.0	3	792.5	6-B_r	1.27	1.28
C21E2b	961.6	795.2	3	789.8	6-B_r	1.21	1.22
C22E2c	976.2	796.7	3	791.3	6-B_r	1.23	1.23
C23E3a	1033.2	850.9	3	850.9	3	1.21	1.21
C24E3b	1072.1	740.7	3	840.7	3	1.28	1.28
C25E3c	1015.3	730.7	3	830.7	3	1.22	1.22
C26E4a	1023.9	889.7	3	889.7	3	1.15	1.15
C27E4b	1031.0	882.6	3	882.6	3	1.17	1.17
C28E4c	1018.6	873.7	3	873.7	3	1.17	1.17
C29E5a	1043.8	899.7	3	899.7	3	1.16	1.16
C30E5b	1037.2	902.9	3	902.9	3	1.15	1.15
C31E5c	1043.8	905.5	3	905.5	3	1.15	1.15
C32E6	1243.3	938.7	6-B_r	938.7	6-B_r	1.32	1.32

From the thin web specimens, the authors conclude that existing bearing equations from CSA-S16-01 and AISC 2005 are conservative in predicting the bearing capacity of a connection undergoing large deformations. Specimen C32E6, which failed purely in bearing (design governed by equation 1.7 for CSA and the right part of equation 1.10 for AISC at all bolt locations), had a test-to-predicted capacity ratio of 1.32. The authors point out that if the bearing capacity would be changed from $3dtF_u$ to $4dtF_u$ (33% greater, based on results from specimen C32E6) and the right part of equation 1.13 (unified equation) is used for bolt tearout the test-to-predicted ratios would have an average ratio of 1.00. They do point out that more research on bearing strength is required before recommending increasing the allowable bearing stress on plates and that current design standards provide conservative bearing capacity estimates.

An aspect that was not talked about by the authors is the effect of confining the plate undergoing bolt bearing failure. Frank and Yura (1981) stated that bearing failures are highly dependent of the amount of lateral confinement provided to the plate and stated that fully restrained, or confined, surfaces such as the inside splice plate of symmetrical splice plates reached ultimate loads at bearing stresses of 3.0 to $3.5F_u$. Since bearing failures involve the material around the bolt hole "bulging" outwards, as shown in Figure 1.3.b), having these plates laterally confined will increase their resistance. Since Cai and Driver tested W-section webs that were confined between two clevis plates, it is likely that their elevated bearing stresses are due to plate confinement.

The focus of Cai's research was on the strength capacity of connections failing in bolt tear-out and bearing. Little attention was given to the displacement capacity, or the tendency of the latter under different connection parameters. However, displacements at peak ultimate loads were given.

Series A had several specimens that were identical except for their bolt end distances. These specimens consisted of two bolt lines containing two bolts each. Their respective end distances, L, and deformations at ultimate, $\delta_{u,exp}$, are shown in Table 1.6 and graphically in Figure 1.10. Specimens A5E1 and A6E2 were unloaded right after their peak load (after a drop of about 5 kN) and specimens A11E1 and A12E2 were unloaded after a 5% drop in load. The authors explained specimen A6E3 experienced a premature drop in load because of hairline fractures forming in the weld line holding an LVDT reference tab. The 5.90 mm deformation for A6E3 is therefore given as a lower bound by the authors. As can be seen by the following table and figure, there is no clear conclusion from these tests on the effect of end distances on these six bolt connections. With specimen A6E2 providing lower bound values, there does not exist a large difference in deformations at the peak loads between specimens A11E1 and A12E2. Because the specimens were not loaded to complete failure, deformations at rupture were not reported.

Table 1.6: Partial results from test series A of Cai and Driver (2008)

Specimen	F_y (MPa)	F_u (MPa)	L	s	$\delta_{u,exp}$ (mm)
A5E1	343	487	1.62d	2.83d	8.60
A11E1	397	511	1.48d	2.83d	12.70
A6E2	343	487	2.50d	2.92d	5.90
A12E2	397	511	2.30d	2.92d	13.00

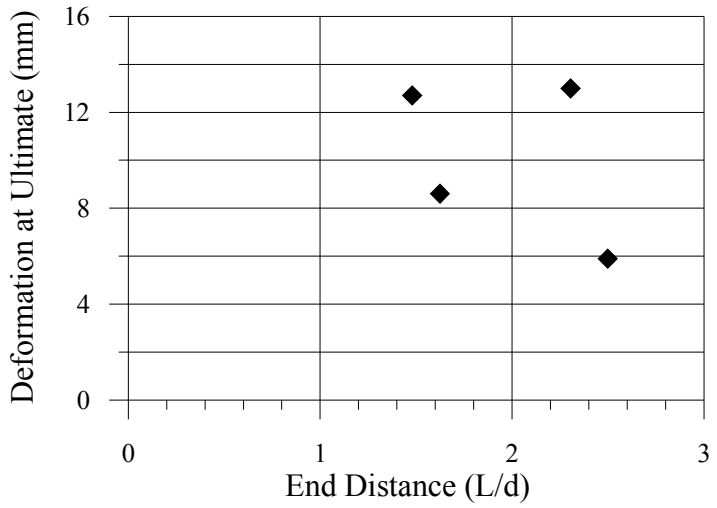

Figure 1.10: Effect of end distance (Cai et al. 2008).

Figure 1.11 shows two series of connections where the variable was the bolt end distance: one series has a thin web (6 mm) while the other has a thicker web (9 mm). The thin webs had a bolt gauge (w in Figure 1.7) of 9.3 bolt diameters while the thick webs had a bolt gauge of 7.3 bolt diameters. The pitch (s in Figure 1.7) was held constant for both web thicknesses at 8 bolt diameters. The bolts used were 19.1 mm in diameter. All specimens had two lines of three bolts. The thinner webs had a F_y of 397 MPa and a F_u of 511 MPa, while the thicker webs had 372 MPa and 457 MPa as their F_y and F_u values, respectively.

From Figure 1.11 the thin web specimens showed a tendency towards greater deformations at the ultimate load with greater end distances. The same cannot be said for the thick web specimens, mostly because the failure mode involved bolt failures as

shown in the figure the peak load sometimes corresponded to a failed bolt. The authors either unloaded their specimens immediately after the peak load or loaded their specimens all the way to failure.

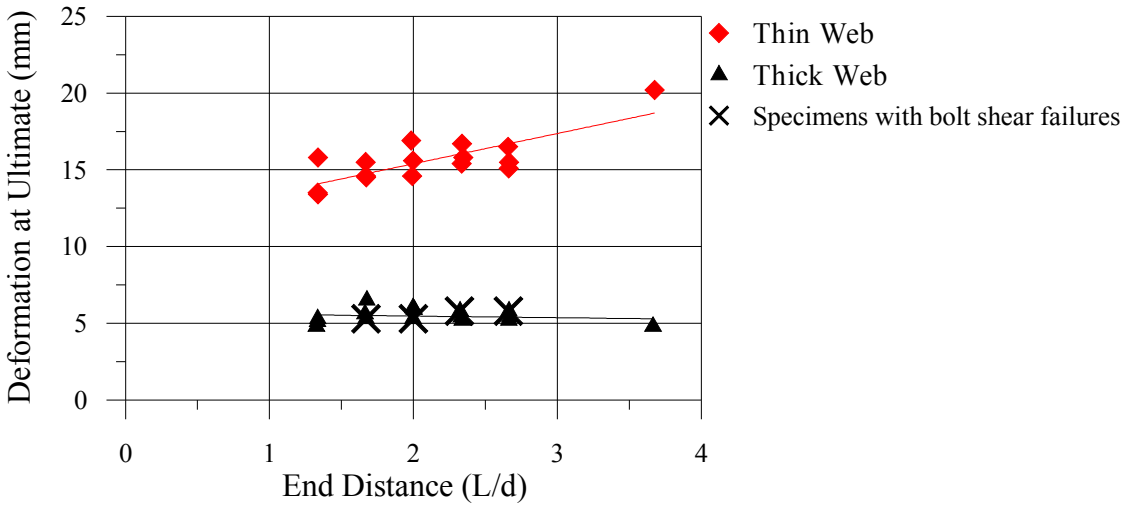

Figure 1.11: Effect of end distance on 6 bolt connection (Cai et al. 2008).

1.1.11. The Effect of End Distance on the Bearing Strength of Bolted Connections, Kim (1996)

Kim (1996) performed a study on the effects of end distances on the bearing strength of bolted connections. One-bolt and two-bolt specimens with punched holes were tested. A490 ¾" bolts were used in all specimens. Two heats of steel were used: Heat A has a high ultimate-to-yield ratio while Heat B has a low ratio. Two series of tests existed for one- and two-bolt specimens: one for each heats of steel. In the latter two series the end distances were varied along with different bolt spacing.

Figure 1.12 shows the influence of bolt pitch, s. Larger end distances have the effect of increasing the ultimate displacement capacity within each heats of steel. This effect is more pronounced, however, in the steel which has a high ultimate-to-yield ratio. The author used splice plates which were not confined. Despite the fact that a percentage of the deformations shown for specimens D03X can be attributed to the intact connection

end, it can be concluded that confinement has a positive impact on the connection ductility.

Figure 1.13 shows the effect of bolt clear end distance, L_c, on the ultimate displacement of one-bolt connections undergoing bearing deformations (Kim 1996). From Figures 1.12 and 1.13, it can be seen that bolt end distances have significantly more effect on the connection ductility than bolt spacings. In Figure 1.13, the slope of the line joining the three deformations is positive, even up to the last point. This leads to believe that bolt end distances greater than 2.5 bolt diameters could provide even greater deformation capacity. This is to be expected because small spacings are controlled by tear-out while larger spacings are controlled by bolt bearing (piling up). A bearing failure undergoes more deformation than a tear-out failure.

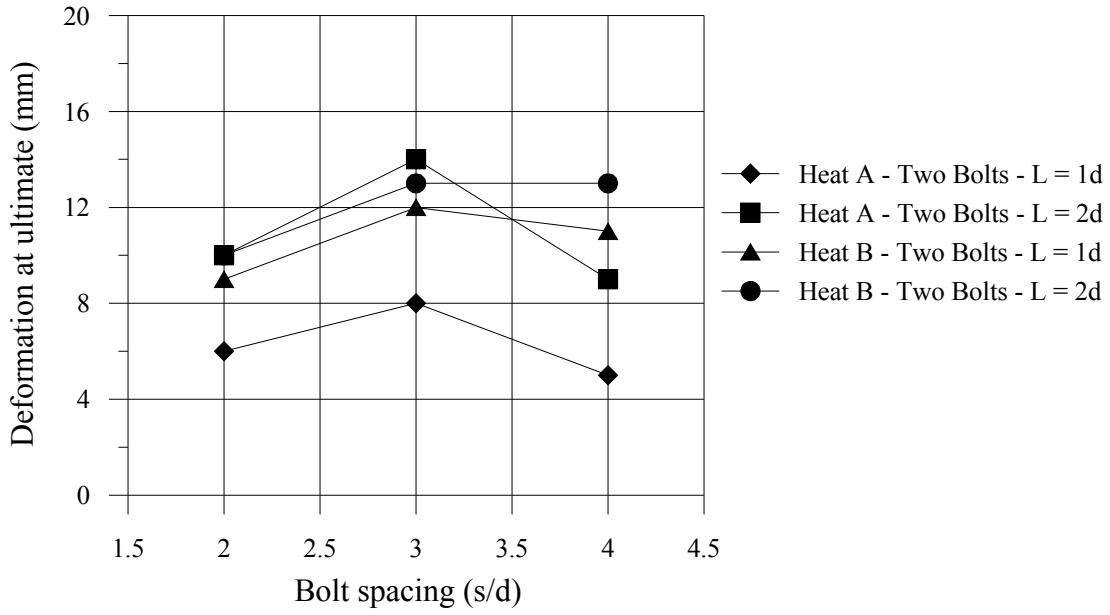

Figure 1.12: Influence of bolt pitch in two-bolt specimens (Kim 1996)

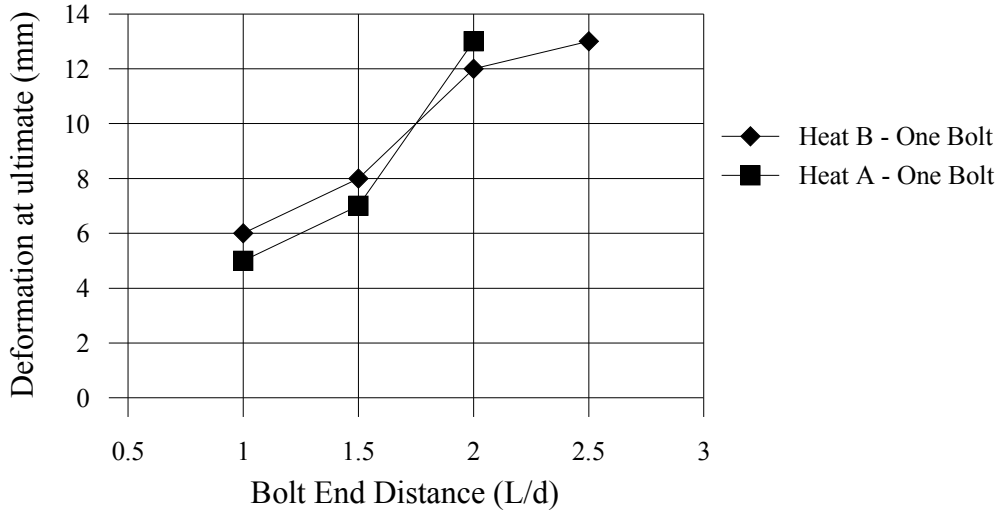

Figure 1.13: Influence of bolt end distance in one-bolt specimens (Kim 1996)

1.1.12. The effect of steel strength and ductility on bearing failure of bolted connections, Aalberg and Larsen (2002)

The authors performed an experimental study on the bearing strength of bolted connections in steels of normal, high, and very high ultimate strength. The specimens included one and two bolts in a single bolt line. All bolts were M20 in 21 mm holes. The bolt end distance, L, and pitch, s, were the variables examined, and the connection geometry of Kim and Yura (1996) was duplicated as best as possible.

The one-bolt connections involved bolt clear end distances, L_c, varying from 1d to 2.5d in steps of 0.5d. The width of the specimen was chosen as 89 mm to avoid net section failure. For the two-bolt specimens, the bolt end distance was either 1d or 2d, with the pitch, s, varied between 2.0d, 3.0d, and 4.0d. The authors looked at three different heats of steel, having yield values of 387 MPa, 830 MPa, and 1340 MPa. Only the 387 MPa steel results are reported herein as it corresponds to common structural steel. For that steel, the ultimate tensile strength was 539 MPa.

For the one-bolt specimens, the authors reported that the deformation at peak load clearly increased with L. The same could not explicitly be said about the two-bolt connections, as shown in Figure 1.14. A graph is shown for every different pitch used.

Within each graph, two different end distances were examined. There does not seem to be a clear relation between the deformations at the peak load and the bolt end distance.

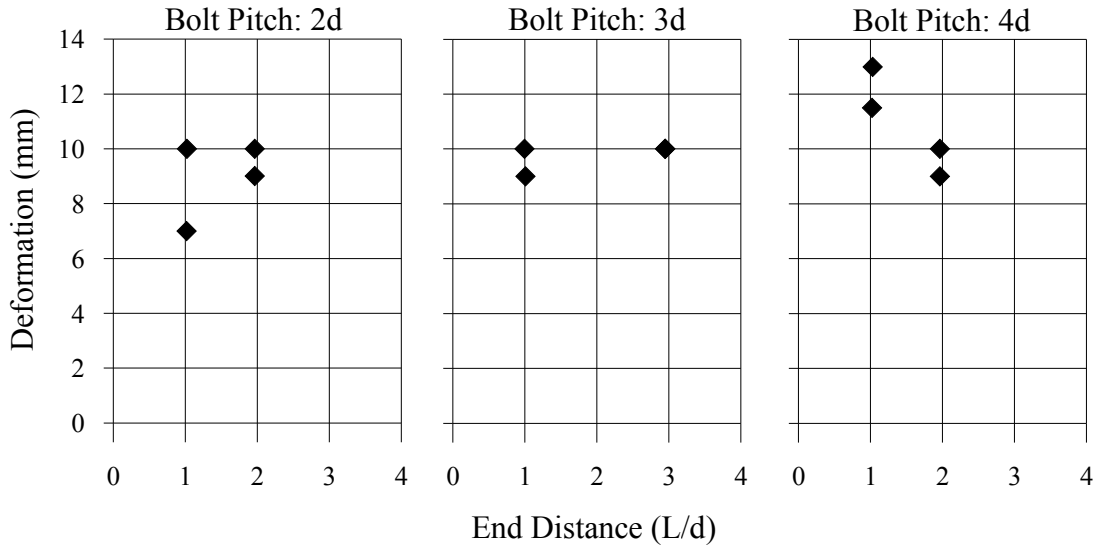

Figure 1.14: Effect of end distance and bolt pitch (Aalberg et al. 2002).

The authors put a strong emphasis on investigating the effects of different grades of steel. They concluded that two-bolt specimens with higher grade steel underwent smaller deformations at ultimate load. They stated that, at final failure (when the material in front of the inner bolts fails – past the ultimate deformation), higher grade steel specimens underwent a deformation of 15 to 20 mm, while lower grade steel (measured F_y = 387 MPa) underwent up to 25 mm of deformation.

Figure 1.15 shows the effect of bolt pitch on specimens with mild steel (F_y = 387 MPa). Two different end distances were used. This figure shows that deformations at ultimate tend to increase with the bolt pitch for both end distances used. Note that the minimum bolt spacing in CSA-S16-01 is 2.7 times the bolt diameter. The authors investigated connections with bolt spacing up to four times the bolt diameter.

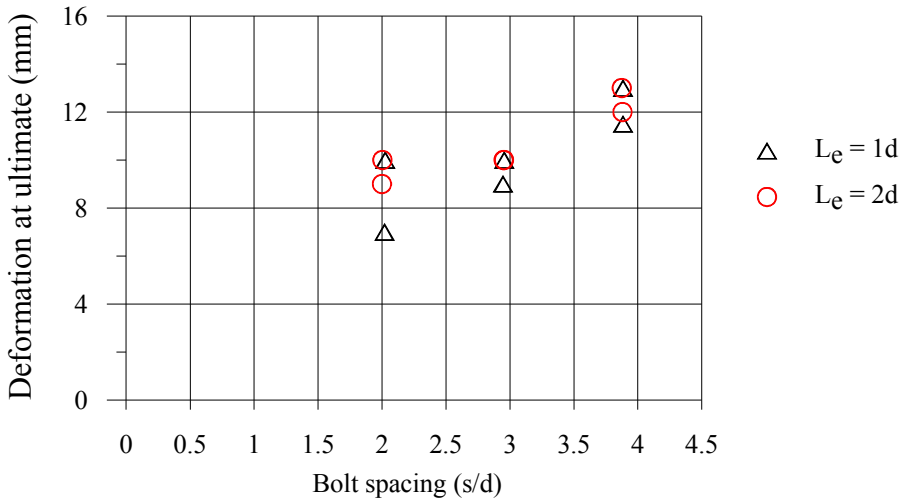

Figure 1.15: Effect of bolt spacing (Aalberg et al. 2002).

1.1.13. Effect of hole-making on the strength of double lap joints, Iwankiw and Schlafly (1982)

Iwankiw and Schlafly (1982) studied the effect of different types of holes on the ultimate strength of double lap joints failing their middle plate in the net section area. Six different types of hole-forming methods were looked at:

- Punching
- Punching with the burrs removed
- Sub-punching and reaming
- Drilling
- Flame-cutting
- Flame-cutting and reaming.

The authors stated that the lower ductility expected in the area worked by the punch in punched holes should have negligible effect on the performance of bolts in bearing, because the compressive strength is not affected by brittleness (Iwankiw et al. 1982).

Since end and edge distances are not dependent of the hole formation method, the authors did not consider these as parameters in their testing. A failure in tension on the net section area was expected to be the most affected by the hole formation method; the test specimens were therefore designed to fail in this manner.

The test specimens consisted of 18 double-lap joints with the interior ½" A36 steel plate designed to fail. One A325, 7/8" bolt was used. Three specimens were used for each hole-formation method. All specimens were tested under monotonic loading.

Of interest is the remark the authors made regarding the ultimate strengths of their specimens: the difference between the average ultimate strength of a connection fabricated with a particular hole-making procedure and the overall average of all connections is on the order of 5% or less. They concluded by saying hole-making procedures do not significantly affect the connection strength under static load, and that even flame-cut holes can be used as an alternative under exceptional circumstances (Iwankiw et al. 1982).

1.2. Literature Review of Low-Ductility Steel Braced Frames

Section 1.2 presents a review of the changes in NBCC 05 regarding the seismic design of conventional construction of concentrically braced steel frame structures, as well as a review of the research performed on these types of structures.

1.2.1. NBCC 05 and CSA S16.1

The 2005 National Building Code of Canada offers guidelines on the design of seismic force resisting systems (SFRS). The structural members not part of this system are to be designed to support the gravity loads.

The 2005 NBCC gives 5% damped spectral response accelerations, S_a, at periods of 0.2 s, 0.5 s, 1 s, and 2 s which are based on a probability of exceedance of 2% over 50 years. Local site conditions are accounted for by using site-dependent velocity- and acceleration-dependent coefficients F_v and F_a, respectively. Adapted from NBCC 05,

tables 1.7 and 1.8 give values for these coefficients. The design spectrum, S(T), is therefore calculated using the S values given by NBCC 05 and modified in the following manner:

$= F_a S_a(0.2)$ for $T \leq 0.2s$

$= F_v S_a(0.5)$ or $F_a S_a(0.2)$, whichever is smaller for $T= 0.5$ s

$= F_v S_a(1.0)$ for $T = 1.0$ s

$= F_v S_a(2.0)$ for $T = 2.0s$

$= F_v S_a(2.0)/2$ for $T \geq 4.0$ s

Table 1.7: F_a values used when determining S(T).

Site Class	Values of F_a				
	$S_a(0.2) \leq 0.25$	$S_a(0.2) = 0.50$	$S_a(0.2) = 0.75$	$S_a(0.2) = 1.00$	$S_a(0.2) = 1.25$
A	0.7	0.7	0.8	0.8	0.8
B	0.8	0.8	0.9	1.0	1.0
C	1.0	1.0	1.0	1.0	1.0
D	1.3	1.2	1.1	1.1	1.0
E	2.1	1.4	1.1	0.9	0.9

Table 1.8: F_v values used when determining S(T).

Site Class	Values of F_v				
	$S_a(1.0) \leq 0.1$	$S_a(1.0) = 0.2$	$S_a(1.0) = 0.3$	$S_a(1.0) = 0.4$	$S_a(1.0) \geq 0.5$
A	0.5	0.5	0.5	0.6	0.6
B	0.6	0.7	0.7	0.8	0.8
C	1.0	1.0	1.0	1.0	1.0
D	1.4	1.3	1.2	1.1	1.1
E	2.1	2.0	1.9	1.7	1.7

Two methods for seismic analysis are proposed in NBCC 2005: the first is a dynamic analysis and the second is an equivalent static force procedure. The latter can be used only in the following cases:

- where $I_E F_a S_a(0.2\ s)$ is less than 0.35;
- for regular structures that are less than 60 m in height and have a fundamental period less to 2 s in both orthogonal directions;
- and for structures with structural irregularities (except those with torsion sensitivity) that are less than 20 m in height and have a fundamental lateral period smaller than 0.5 s in both orthogonal directions.

The base shear from the equivalent static force procedure, V, is obtained through the following equation:

$$V = \frac{S(T) M_v I_e W}{R_o R_d} \tag{1.15}$$

where S(T) is the design spectral response acceleration, M_v is a factor accounting for higher modes, and W is the seismic weight. T is a fundamental period of vibration that is calculated by equation 1.16, which applies only to braced frames:

$$T = 0.025 h_n \tag{1.16}$$

where h_n is the total height of the structure. T may be determined by an eigenvalue analysis but this period may not exceed twice the fundamental period, T, as calculated with equation 1.16.

R_o and R_d are, respectively, overstrength and ductility related force modification factors. These factors are dependent upon the type of seismic force resisting system used. For braced frames, there are moderately ductile systems with R_d = 3.0 and limited ductility systems with R_d = 2.0. Both these types are subjected to special design and detailing provisions as given in Clause 27 of S16-01 (CSA 2001) to achieve the desired ductility levels as indicated by the R_d values. However, no such extensive ductility requirements exist for braced steel frames of the Conventional Construction (CC Type) category for an R_d factor of 1.5 is specified in NBCC 2005. For all three systems, an R_o = 1.3 is used as specified by Mitchell et al. (2003).

Past earthquake experience has shown that multi-storey buildings suffer more damage than low-rise structures. Since seismic force resisting systems with an $R_d \geq 2.0$ are expected to perform better under strong earthquakes, with greater ductility capacity, it was deemed necessary to specify their use for multi-storey building applications and thereby impose height limits for CC Type structures. Table 4.1.8.9 of the NBCC 2005, shown partly in Table 1.9, gives the ductility and overstrength factors related to all structural systems, as well as height restrictions. Seismic force resisting systems of the conventional category are limited to 15 metres in height under certain ground shaking intensities.

Table 1.10 shows a list of several major cities and their seismic characteristics. The values in bold indicate the application of the 15 m height limit described in Table 1.9. This height limit applies to almost all of these major cities, even in localities of moderate and low seismicity when the structure is located on soft soil.

In order to avoid brittle failures in connections of CC Type structures, Clause 27.10 in S16-01 (2001) requires structures in moderate to high seismic zones ($I_eF_aS_a(0.2\ s) > 0.45$) to either have connections be detailed to exhibit a ductile failure mode or be designed with seismic loads amplified by R_d, i.e. seismic forces obtained with $R_oR_d = 1.3$ rather than 1.5.

Much research has been done for Types MD and LD braced steel frames with $R_d \geq 2.0$. Significantly less research for structures of the conventional construction category has been done. Hynes and Gryniuk (2006) and Mullin and Cheng (2004) have looked at low-ductility structures and their results are reported in the following sections.

Table 1.9: Application of the 15 m height limit in conventional construction

Type of SFRS	R_d	R_o	Restrictions				
			Cases Where $I_E F_a S_a(0.2)$				Cases Where
			<0.2	≥0.2 to <0.35	≥0.35 to ≤0.75	>0.75	$I_E F_v S_a(1.0)$ >0.3
▪ Conventional construction of moment frames, braced frames or shearwalls	1.5	1.3	NL	NL	**15**	**15**	**15**

Table 1.10: Application of the 15 m height limit in cities across Canada

Site	$S_a(0.2)$ (g)	$S_a(1.0)$ (g)	$I_E F_a S_a(0.2)$ (g)					$I_E F_a S_a(1.0)$ (g)				
			A	B	C	D	E	A	B	C	D	E
Fredericton	0.39	0.2	0.27	0.31	**0.4**	**0.5**	**0.7**	0.1	0.1	0.2	0.26	**0.4**
Québec	0.59	0.14	0.43	**0.5**	**0.6**	**0.7**	**0.8**	0.1	0.1	0.14	0.19	0.29
Montréal	0.69	0.14	**0.5**	**0.6**	**0.7**	**0.8**	**0.8**	0.1	0.1	0.14	0.19	0.29
Ottawa	0.66	0.13	**0.5**	**0.6**	**0.7**	**0.8**	**0.8**	0.1	0.1	0.13	0.18	0.27
Toronto	0.26	0.06	0.18	0.21	0.26	0.34	**0.5**	0	0	0.06	0.08	0.12
Hamilton	0.33	0.06	0.23	0.26	0.33	**0.4**	**0.6**	0	0	0.06	0.08	0.12
Calgary	0.15	0.041	0.11	0.12	0.15	0.2	0.32	0	0	0.04	0.06	0.09
Kamloops	0.28	0.1	0.2	0.22	0.28	**0.4**	**0.6**	0.1	0.1	0.1	0.14	0.21
Vancouver	0.94	0.33	**0.8**	**0.9**	**0.9**	**1**	**0.9**	0.2	0.2	**0.3**	**0.4**	**0.6**
Victoria	1.2	0.38	**1**	**1.2**	**1.2**	**1.2**	**1.1**	0.2	0.3	**0.4**	**0.4**	**0.7**

1.2.2. Hines and Gryniuk: Preliminary Results: Collapse Performance of Low-Ductility Chevron Braced Steel Frames in Moderate Seismic Regions (2006)

Hines and Gryniuk (2006) of Massachusetts analysed 3-, 6-, 9-, 12-, and 15-storey buildings using chevron bracing systems designed with R values of 3 (equivalent of R_d = 1.5 in Canada). The authors included, for each building, a system with weak connections and a system with strong connections. The weak connection systems were thought to be non-ductile since the structures were designed with no specific seismic detailing requirements. The strong connection systems were thought to be semi-ductile, because their connection design reflected some attempt to provide post-buckling strength to the overall system. A total of 10 buildings were therefore analyzed with 14 different ground motions developed to reflect a typical Site Class D soil profile in Boston, Massachusetts.

The authors found that, in general, the strong connection system fared better than frames with weak connections. There was, however, an instance where the strong connection model experienced a collapse while the weak connection model did not, under the same ground motion. Higher mode effects were clearly visible in structures with more than 3 stories and demonstrated by collapses in the upper stories. The authors did not see any clear correlation between collapse probability and building height. The duration of a ground motion, the number and timing of large pulses, and the interaction between the ground motion and accumulated damage were found to significantly affect the collapse behaviour.

The authors pointed out that structural stiffness due to non-structural elements was not included in the analyses, but was included in the design of the structures by using an upper-bound limit on the design period.

1.2.3. Mullin and Cheng: Ductile Gusset Plates – Tests and Analyses (2004)

Nast, Grondin, and Cheng (1999) stated that gusset plates with edge stiffeners, combined with braces which remained elastic throughout the duration of the loading history, provide good energy absorption characteristics. Based on the research of Rabinovitch and Cheng (1993), Walbridge, Grondin and Cheng (1998), and Nast, Grondin, and Cheng (1999) who all concluded that gusset plates are considered good candidates to act inelastically in seismically loaded structures, Mullin and Cheng (2004) contributed to the introduction of the "weak gusset – strong brace" concept. This is the first of two of their articles with respect to this concept and presents tests performed on gusset plates with the goal of observing the ductility capacity of gusset plates undergoing monotonic loading in tension.

A total of ten gusset plates were tested; six were unreinforced and four were reinforced to prevent shear and tension block failure along the bolt lines. All specimens contained two lines of A325 ¾" bolts with two to eight bolt rows. All specimens were tested under monotonic tension. A typical specimen is shown in Figure 1.16.

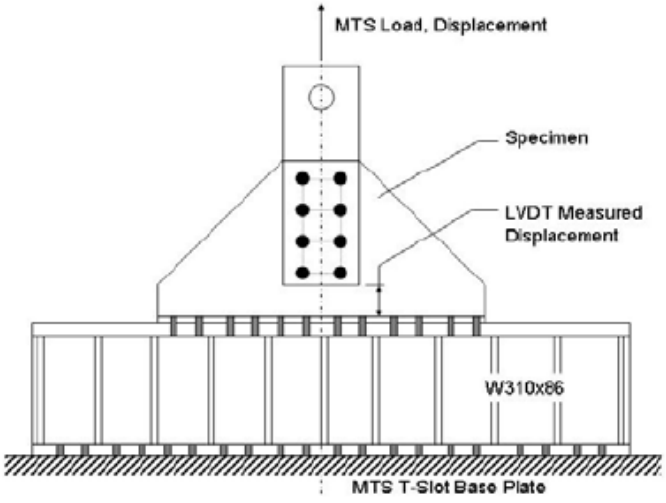

Figure 1.16: Typical specimen from Mullin and Cheng (2004)

In the unreinforced specimens, the typical failure started with a fracture in the gusset plate between the two bottom bolt holes shown in Figure 1.16. A sharp drop in load accompanied this fracture and corresponded to roughly the net area loaded in tension (clear bolt gauge multiplied by the plate thickness) times the material's measured ultimate stress. From this point, specimens with 4, 8, or 12 bolts developed shear fractures along the bolt lines parallel to the direction of loading to create a shear and tension block failure. Specimens with 14 and 16 bolts did not develop classic shear and tension block failure after the rupture of the net area loaded in tension.

In the reinforced specimens, the same fracture on the net tensile area occurred first. The presence of reinforcement, however, caused the fractures to propagate outwards at an angle of roughly 45 degrees. This rupture mode roughly corresponds to a fracture through the Whitmore section, which is described in section 4.4.4 of this thesis.

The authors reported the deformations at ultimate loads for the unreinforced and reinforced specimens were very similar, except for a slight increase in deformation at first fracture in the reinforced specimens. Between unreinforced and reinforced gusset plates, respectively, these deformations increased on average from 21 mm to 25 mm. The next part of the authors' study was to attempt to quantify the deformation demands on connections. This is reported in the following section, 1.2.4.

1.2.4. Mullin and Cheng: Response of Seismically Loaded Low Rise Steel CBF Structures with Inelastic Gusset Plate Connections (2004)

This is the second of two articles related to the "weak gusset – strong brace" concept by Mullin and Cheng (2004). They examined the possibility of using gusset plates as energy absorbing elements during earthquakes in structures. The authors examined the response of 1-, 2-, and 4-storey concentrically braced steel frames designed using the "strong brace-weak gusset" approach, meaning the inelasticity was confined to gusset plates during ground motions. The authors also reported that, at the time of writing, there was no research done in attempting to quantify the amount of deformation demand

in concentrically braced structures and that gusset plates have been found to maintain their tension and compression capacity. The authors attempted to quantify the deformation demand on brace connections.

All structures were designed according to the NBCC95 equivalent static lateral load procedure, using ductility factors of 1.5, 2.0, 3.0, and 4.0, but only the results for R = 1.5 are presented herein in view of the objectives of this study. The bracing system was made up of cross braced concentric frames over single stories. The gussets plates were modelled to yield at the maximum design bracing force arising from the equivalent lateral seismic loads. The braces were chosen to provide 1.5 times the modelled gusset plate ultimate resistance. This is to ensure ultimate limit states are reached in the gusset rather than the braces. Non-linear time history analyses were performed using ground motions records calibrated to provide peak accelerations and velocities consistent with NBCC design values for western Canada. Lumped masses were assigned at each floor of "dummy" leaning columns. These columns and the struts connecting them to the braced frame were assigned very large areas, essentially making them extremely stiff compared to the structure. P-delta effects were considered at all times.

Based on previous research, the authors adopted an inelastic deformation limit at first fracture of 15 mm for the gusset plates. They found that one-storey structures remained predominantly elastic. Two-storey structures underwent approximately 6mm of inelastic gusset deformation in a seismic zone 3 and approximately 10mm in a seismic zone 5.

In the four-storey buildings, the authors found that higher modes had a significant effect on structures designed with R = 1.5 in a seismic zone 5. Gusset plates underwent approximately 10mm of inelastic deformation in a seismic zone 3, and 23mm in a seismic zone 5. The 15mm deformation at first fracture was exceeded in zone 5 earthquakes.

The authors reported that the anticipation of predominantly elastic behaviour with the smaller ductility factors was not reflected in their analyses.

1.2.5. Walbridge, Grondin, and Cheng: Gusset Plate Connections Under Monotonic and Cyclic Loading (2005)

Walbridge, Grondin, and Cheng (2005) undertook a numerical study of gusset plates under monotonic and cyclic loadings using nonlinear finite element models. The authors performed this study to investigate the possibility of using structural systems with gusset plate – brace member subassemblies designed to have the gusset plate as the weak element instead of the brace, which was also introduced by Mullin and Cheng (2004, 2004).

The authors validated their finite element model by comparing their results with previous research that had been done on gusset plates. The modeling of their gusset plates is well explained in the article. The bolts were modeled as rigid links between the gusset plate and the splice plates connection the brace to the plate. Bolt slip is modelled through a series of elastic-perfectly plastic springs connecting the splice plates to the gusset plates. Inelastic deformations in the gusset plates took place on the form of buckling in compression and yielding in tension. Bearing deformations were not modelled. Their gusset plates subjected were subjected to monotonic tension and compression loading, as well as cyclic loading. Figure 1.17 shows the three different cyclic load sequences used.

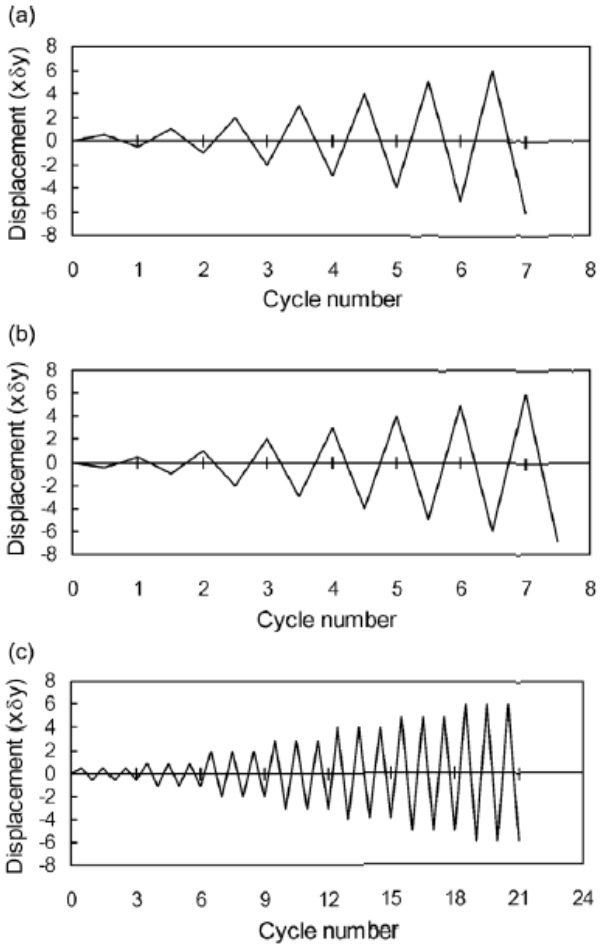

Figure 1.17: Load sequences used: (a) tension first, (b) compression first, (c) tension first with three cycles at each increment (Walbridge et al. 2005)

The numerical models closely matched the load resistance of previous experimental research on gusset plates in tension, as well as the buckling load and the subsequent decrease of post-buckling capacity in cyclic loading. Different gusset – brace designs were created:

- The brace member yields in tension before the gusset plate.
- The gusset plate yields in tension before the brace member.
- The brace member buckles before the gusset plate.
- The gusset plate buckles before the brace member.

Designs were done to provide some insight into the effect of having either the brace or the gusset plate both yield and buckle, or have a connection where the gusset would buckle and the brace yield, etc. The displacement range studied was approximately 15mm in compression or tension.

The authors came to the following conclusions (Walbridge et al. 2005):

- The load sequence had no significant effect on the cyclic behaviour of the gusset plates.
- Whether the governing tensile limit state was in the gusset plate or the brace member had no major change on behaviour in the displacement range studied.
- Buckling the gusset plates resulted only in a small reduction of the capacity and showed a very stable cyclic behaviour. This also showed better energy absorption characteristics
- Thicker gusset plates showed fuller hysteresis loops.
- In general, hysteresis plots for the weak gusset plate – strong brace showed less pinching and sustained higher post-buckling compressive loads than the conventionally designed connections. This means the use of weak gusset plates and strong beams could prove beneficial to low-ductility structures undergoing ground motions.

1.3. Summary

This chapter presented a literature review of two different subjects in two subsections: a review of bolt bearing connection failures and a review of low-ductility concentrically-braced steel frames. With regards to bolt bearing failures, it was found that:

- Longer end distances generally translate into higher deformations at the ultimate load (deformation at ultimate) (Cai et al. 2008; Kim 1996);

- Bolt pitch does also positively influence the deformation capacity but not as much as the bolt end distance (Aalberg et al. 2002);

- Drilled holes offer more deformation capacity than punched ones (Owens et al. 1981; Vasarhelyi et al. 1959; Wallin 1975)
- Bolt pre-tension does not affect the ultimate deformation of a connection undergoing bolt bearing failure (Frank et al. 1981);
- The ultimate stress to yield stress ratio has a negligible effect on the deformation capacity of a connection undergoing bolt bearing failure (Kim 1996; Kim et al. 1999);
- Slotted holes and standard round holes have insignificant differences in terms of ultimate deformations and load. Round holes, however, are stiffer that slotted holes in the early stages of loading (Frank et al. 1981);
- Transversely confined plates undergoing bolt bearing failures tend to show higher ultimate bearing stresses and consequently higher deformations (Cai et al. 2008);
- Increasing the end distance, L, and the bolt pitch, s, naturally increases a connection's bearing resistance (Cai et al. 2008; Kim 1996); and
- Shear and tension block failures should be avoided as they do not provide high deformation capacities (Cai et al. 2008).

With regards to the seismic behaviour of low-ductility steel braced-frames, it was found that:

- A study on frames with "strong" and "weak" connections showed that strong connections generally fared better under earthquake loading, but showed that weak connection did outperform systems with strong connections in some cases (Hines et al. 2006);

- Past research has shown that gusset plates are good candidates for use as energy dissipaters during severe ground motions (Mullin et al. 2004, 2004). These gusset plates were undergoing buckling and tensile yielding; and

- The “weak gusset – strong brace” system showed less pinching and sustained higher post-buckling compressive loads than the conventionally designed connections. This means the use of weak gusset plates and strong beams could prove beneficial to low-ductility structures undergoing ground motions. Again, the gusset plates were undergoing buckling and tensile yielding (Walbridge et al. 2005).

Chapter 2. EXPERIMENTAL PROGRAM: *PHASE I*

The experimental side of the project is split into two phases. Chapter 2 presents information and results on the first series of tests that was performed with the objective of investigating the ductility of several connection failure modes. Phase II is presented in Chapter 3 and deals with bolt bearing failures on gusset plates.

2.1. Introduction

Conventional construction and design of steel structures implies using a ductility factor, R_d, of 1.5. This implies the structure is designed for seismic loads larger than any other seismic force resisting system (SFRS) and is deemed to possess sufficient inherent ductility to undergo limited inelastic demand during an earthquake ground motion. CSA-S16 (CSA 2001) requires connections to be either detailed to exhibit a ductile failure mode or designed for amplified seismic loads. There is limited information available on how to detail for ductile connections.

One of the objectives of this report is to identify a ductile failure mode which could be used as an energy dissipater mechanism in a seismic load resistance system found in a structure designed using conventional construction. Six different connection failure modes were investigated with respect to their ductility. Chapter 1 gives a literature review on the failure mode expected to yield the most ductility: a bearing failure, which is often identified as an example of a ductile limit state (Muir 2007). Section 2.2 deals with the testing performed in the laboratory and presents the design of the specimens and the testing apparatus.

2.2. Test Program

Section 2.2 presents the test program used to evaluate the ductility of different connection failure mechanisms. The test specimens, the test setup, as well as the loading procedures are explained.

2.2.1. Test Specimens

Two back-to-back angles (L76x76x6.4) were used as the brace element. These angles were large enough to accommodate a bolt with the proper edge distances in one of its legs and were manageable in size enough for an average person to move them around by hand. A constant length of 916 mm (three feet) between centres of connections was used to, again, make the specimens easy to handle by hand and to maintain the same center to center brace length. A325 and A490 bolts with 19.05 mm (3/4 in.) in diameter (threads excluded) were used in 21 mm (13/16 in.) holes. E490XX weld electrodes were used for welding, and G40.21 350W steel (F_y = 350MPa, F_u = 450MPa) was specified for the angles and the plates. APPENDIX I shows the shop drawings for all Phase I specimens.

Three identical specimens for each target failure mechanism were tested, giving a total of 21 specimens. The specimens were numbered following the fabricator's shop drawings. D01X through D06X and D14X were used, and 01, 02, or 03 was suffixed to the latter to differentiate each of the three individual specimens for each target failure mechanism. Table 2.2 presents the numbering system used for all specimens.

All holes were punched except for specimen D14X which had drilled holes. Three more specimens identical to D06X but with drilled holes were to be tested for a shear and tension block failure, but a fabrication error rendered these specimens inadequate.

2.2.2. Apparatus

A tension-compression 2500 kN capacity Instron load frame was used to perform the testing. Data acquisition consisted of acquiring the load from the load cell mounted on the load frame actuator, while the displacements were acquired from two potentiometers attached to the gusset plates, their locations shown as black dots in Figure 2.1. As shown, all specimens had potentiometers with a gage length equal to the total length of the brace members (back-to-back angles). This means that the captured displacement was the total displacement for both connection ends, as well as elastic deformations in the angles.

Figure 2.1: Position of the potentiometers, as shown by the black dots.

Before installing the specimens in the load frame, the potentiometers were attached to the specimens with stems and nuts. The specimen was then placed in the load frame, its gusset plates centered in the grips. Once the specimen was centered the bottom hydraulic grips were actuated. The top grip was actuated afterwards, with care being taken not to load the specimen at the same time. The specimen was then ready to be tested.

No available potentiometer had the capacity to capture the expected deformations occurring in specimen D01X, yielding of the angles. Potentiometers were used to measure deformations almost to the point of ultimate load but had to be removed before the ultimate deformation occurred in order to avoid damaging them. The displacement measured from the LVDT located inside the load frame actuator was used to evaluate the deformation at ultimate. These deformations therefore include elastic deformations of the test setups as well as possible slip in the grips.

2.2.3. Procedure

The ultimate displacement was estimated for each failure mechanism and a displacement rate was calculated to make each test last approximately 15 minutes. To maintain static loading conditions and avoid increase in yield and tensile strengths due to high strain rate, the rate was kept below 100 με/sec. Another reason for using low strain rates was to validate design expressions that are based on a slow loading rate. Some loading rates were varied within a series of specimens to adjust the duration of the tests Table 2.1 presents the loading rate used for each specimen.

The gussets' and angles' thicknesses were measured using a Vernier calliper before each test. It is important to note that the steel had some amount of rust which may have yielded a lower level of precision in these measurements.

To ensure the proper failure mechanism was taking place, the deformations imposed on each specimen were sufficient to cause the entire failure mode to develop. All specimens were brought to the point where at least one failure crack appeared and the load had dropped significantly, indicating the ultimate load had been reached.

Table 2.1: Specimen loading rates used in Phase I

	Loading Rate (mm/min)		
Specimen #	- 01	- 02	- 03
D01X	5.0	3.0	4.7
D02X	0.3	0.4	0.4
D03X	3.5	3.5	3.5
D04X	3.0	3.0	3.0
D05X	0.7	0.8	0.8
D06X	3.0	3.0	3.0
D14X	3.0	3.0	3.0

2.2.4. Design of Specimens

Six specimens were designed to break in different manners under a tensile load. CANAM fabricated the specimens. The six different chosen failure mechanisms were:

1. Yielding of brace members
2. Weld rupture
3. Bolt bearing on gusset plate
4. Net area rupture of brace members
5. Bolt shear rupture
6. Shear and tension block failure of brace members

For comparison purposes, both CSA-S16-01 and AISC 360-05 were used when designing the specimens. The actual mechanical properties of the steel to be used in the fabrication of the specimens were not known at the time of design. In order to account for unavoidable variability in the material's characteristics, the load associated to the desired governing failure mode was calculated without any resistance factors, i.e., corresponding to the nominal resistance. R_y factors were not included, but an F_y value of 400 MPa (350 MPa steel was ordered) was used to obtain expected (conservative) nominal resistances. The resistance associated to the other failure modes to be checked were verified with the code prescribed resistance factors. This added to the certainty of achieving the target failure mechanism.

Table 2.2 shows the connection capacities for each failure mechanism calculated using references CSA (2001) and AISC (2005), along with their respective specimen numbers. P corresponds to factored (ϕP_n), nominal (P_n), and expected capacities (P_e), in kN, for both CSA and AISC standards. It is important to note that these values were calculated with F_y = 400 MPa, F_u = 450 MPa, and $R_y = R_t$ = 1.1. Nominal capacities calculated with F_y and F_u values coming from coupon tests are given in Table 2.10.

Table 2.2: CSA and AISC Phase I connection capacities

				CSA			AISC		
Failure Mode	ϕ_{CSA}	ϕ_{AISC}	Spec.	ϕP_n (kN)	P_n (kN)	P_e (kN)	ϕP_n (kN)	P_n (kN)	P_e (kN)
Brace Yielding	0.9	0.9	D01X	668	742	816	668	742	816
Weld Rupture	0.67	0.75	D02X	218	325	325	218	291	291
Bolt Bearing	0.67[1]	0.75	D03X	228	253	278	234	312	343
A_n Rupture	0.9	0.75	D04X	467	519	571	389	519	571
Bolt Rupture	0.8	0.75	D05X	227	284	312	177	236	260
Block Failure	0.9	0.75	D06X	446	495	545	371	495	545

[1] Actual governing failure of end bolt was a tearout. The ϕ factor in this case is 0.9.

2.2.4.1. Yielding of Brace Members

Table 2.3 shows the calculated nominal capacities of each failure mode investigated in the design of specimen D01X, as well as the design equations used. The specified yield strength of the steel was 350 MPa; a yield stress of 400 MPa was assumed to obtain an expected (conservative) value of the yield strength of the angles.

A 19.05 mm gusset plate is used to ensure yielding of the braces and not the gusset plate. As seen in Table 2.3, the calculated nominal resistance of the angles' net area could pose a problem. However, taking this non-factored resistance and multiplying it by $R_y = 1.1$ (variability of the angle material), the net area resistance is 14% greater than the yield load of the angles (847 kN). Nevertheless, this was deemed to be too close to ensure full yielding of the braces including strain hardening effects, and therefore an 8 x 50 x 200 mm reinforcement plate was welded to the horizontal leg of the angles to increase their net area to 1256 mm^2 from 856 mm^2.

Table 2.3: CSA and AISC nominal capacities for D01X

	CSA Equation #	$P_{n,CSA}$ (kN)	AISC Equation #	$P_{n,AISC}$ (kN)
Yielding of angles	13.2.(a).(i)	742	J4-1	742
Weld rupture	13.13.2.1.(a),)	746	J2-2, J2-3	748
Gusset plate yielding	13.2.(a).(i)	870	J4-1	870
Net area rupture	13.2.(a).(iii)	589	D2-2	579

2.2.4.2. Weld Rupture

Table 2.4 shows the calculated nominal capacities of specimen D02X and the design equation used for calculating these. E490XX electrodes are specified for welding 5 mm fillet welds. Two parallel welds were used: one on the heel and the toe of each angle. A 50 mm length was initially used but was changed to 70 mm to increase the net area to 560 mm^2 from 374 mm^2.

Table 2.4: CSA and AISC nominal capacities for D02X

	CSA Equation #	$P_{n,CSA}$ (kN)	AISC Equation #	$P_{n,AISC}$ (kN)
Weld rupture	13.13.2.1.(a), (b)	325	J2-2, J2-3	291
Yielding of angles	13.2.(a).(i)	584	J4-1	584
Gusset plate yielding	13.2.(a).(i)	731	J4-1	731
Net area rupture	13.2.(a).(iii)	406	D2-2	398

2.2.4.3. Bolt Bearing on Gusset Plate

Table 2.5 shows the calculated nominal capacities for specimen D03X and their respective design equations. This connection involved two bolts bearing onto a gusset plate confined by two angles.

Two A325 ¾" (19.05 mm) bolts are specified. A bolt spacing of 60 mm was used; CSA S16 specifies a minimum bolt pitch of 2.7 times the diameter, equalling 51 mm (CSA 2001). The end distance was 30 mm, whereas CSA specifies a minimum end distance of 1.5 times the bolt diameter, amounting to 28.5 mm. An 8 mm gusset plate is used and a tearout failure mode is expected.

Table 2.5: CSA and AISC nominal capacities for D03X

	CSA Equation #	$P_{n,CSA}$ (kN)	AISC Equation #	$P_{n,AISC}$ (kN)
Bolt bearing	13.10.(c), 13.11.(a)	253	J3-6b	312
Yielding of angles	13.2.(a).(i)	584	J4-1	584
Bolt rupture	13.12.1.1.(b)	452	J3-1	354
Gusset plate yielding	13.2.(a).(i)	365	J4-1	365
Net area rupture	13.2.(a).(iii)	327	D2-2	321
Block failure	13.11.(a)	371	J4-5	310

2.2.4.4. Net Area Fracture of Brace Members

Table 2.6 shows the calculated nominal capacities of specimen D04X and the design equations used. The net section area of the angle's outstanding leg was multiplied by a

factor to account for shear lag, thus giving an effective net section area to work with (Chesson et al., 1957). This factor is used in both the CSA and AISC standards.

Two A490 ¾" (19.05 mm) bolts are used. The factored bearing resistance of the bolts bearing on the angles was smaller than the net area capacity. Taking away the safety factors yields a bearing resistance 26% higher than the net area capacity and is deemed adequate. The factored shear and tension block failure capacity of the angles was also close to the capacity of the net area.

However, it is reasonable to exclude the safety factors in both these cases because both these limit states occur in the same connection element. The resistance factors are there to offer some security, but in our case, it is not unreasonable to ignore these when comparing failure modes in the same connection elements. The non-factored shear block failure capacity is 23% greater than the net area fracture capacity.

Table 2.6: CSA and AISC nominal capacities for D04X

	CSA Equation #	$P_{n,CSA}$ (kN)	AISC Equation #	$P_{n,AISC}$ (kN)
Net area rupture	13.2.(a).(iii)	519	D2-2	519
Yielding of angles	13.2.(a).(i)	584	J4-1	584
Bolt rupture	13.12.1.1.(b)	569	J3-1	445
Gusset plate yielding	13.2.(a).(i)	731	J4-1	731
Bolt bearing	13.10.(c), 13.11.(a)	441	J3-6b	492
Block failure	13.11.(a)	578	J4-5	480

2.2.4.5. Bolt Shear Rupture

Table 2.7 shows the calculated nominal capacities of specimen D05X and the respective design equations. One A325 ¾" bolt is used. The block failure of the angles and the failure of the angles in bearing could occur before the bolt rupture. An 8mm plate was welded to the horizontal leg of the angle around the bolt hole to increase the bearing resistance and the block shear capacity.

A single bolt was used in each connection. A connection with a single bolt is expected to undergo smaller amounts of deformations before failure. Longer joints experience the "unbuttoning" effect, which sees the connection go through larger deformations (Kulak et al. 1987).

Table 2.7: CSA and AISC nominal capacities for D05X

	CSA Equation #	$P_{n,CSA}$ (kN)	AISC Equation #	$P_{n,AISC}$ (kN)
Bolt shear rupture	13.12.1.1.(b)	284	J3-1	236
Yielding of angles	13.2.(a).(i)	584	J4-1	584
Gusset plate yielding	13.2.(a).(i)	731	J4-1	731
Net area rupture	13.2.(a).(iii)	328	D2-2	320
Block failure	13.11.(a)	264	J4-5	220
Bolt bearing	13.10.(c), 13.11.(a)	221	J3-6b	170

2.2.4.6. Shear and Tension Block Failure

Table 2.8 shows the calculated nominal capacities of specimen D06X along with the respective design equations. Three A325 ¾" (19.05 mm) bolts are used. A 240 x 50 x 6 mm plate was welded to the outstanding leg of each angle to increase their net area capacity.

Table 2.8: CSA and AISC nominal capacities for D06X

	CISC Equation #	$P_{n,CISC}$ (kN)	AISC Equation #	$P_{n,AISC}$ (kN)
Block failure	13.11.(a)	495	J4-5	495
Yielding of angles	13.2.(a).(i)	584	J4-1	584
Gusset plate yielding	13.2.(a).(i)	731	J4-1	731
Net area rupture	13.2.(a).(iii)	448	D2-2	439
Bolt bearing	13.10.(c), 13.11.(a)	604	J3-6b	630
Bolt rupture	13.12.1.1.(b)	677	J3-1	531

2.3. Post Test Measurements and Observations

After testing, each bolted specimen was disassembled to further investigate the connection deformations. The measurements of interests which could influence the ductility measure of a failure mechanism are the ovalization of bolt holes and elastic deformations of the two angles. The ductility measure is known as the ratio of the ultimate displacement to the yield displacement. However, the total displacement is the measure of interest in this case, since the SFRS would see connections undergoing their full capacity in displacement. The six failure mechanisms will therefore be compared with respect to their total deformation capacities. It is important to note, however, that the braces' elastic deformations will not be included in any of the results; this is explained in section 2.3.1.

It is important to know that the deformations include deformations at both connections ends. One never knows with certainty if the failure mechanism will happen at both ends at the same time. If both ends could undergo failure mechanisms at the same time, higher plastic deformations would be achieved. If all deformations happen at one end, this gives a lower ductility to the strong brace – weak connection mechanism.

The mechanical properties of the steel used in the gusset plates and angles were determined using ASTM-E8, in which a precise geometry and loading protocol is imposed. The results are shown in Table 2.9. The coupons were loaded in a force controlled press; the extensometer used to measure deformations therefore had to be removed before the ultimate load to avoid damaging it. Because of this, no ε_y and ε_{rupt} are available. New connection nominal capacities, P_a, are calculated based on the manual measurements made on the specimens and the latter values of F_y and F_u. Table 2.10 shows these new capacities along with the ultimate values measured in tests ($P_{u,exp}$). The capacities are nominal values obtained using the respective design equations from both the CSA and AISC standards.

Most connections failed at a load greater than the one predicted. The weld failure happened at a considerably greater load and this is due to the nature of the welding process. A 6 mm fillet weld was specified and it was evident that some weld lines were significantly greater in size. The capacities were calculated using no safety factors. More attention will be given to the bolt bearing failure mode because it is expected to give the most displacement capacity out of all the failure modes.

Table 2.9: Tensile coupon test results from Phase I

Coupon #	Thickness (mm)	Width (mm)	F_y (MPa)	F_u (MPa)	ε_y ( )	σ_{sh} ( )
1 - Gusset	8.00	38.09	394	485	0.0035	0.0100
2 - Gusset	8.02	38.05	411	503	0.0031	0.0071
3 - Gusset	7.99	38.08	410	500	0.0034	0.0069
4 - Gusset	8.00	38.06	391	486	0.0033	0.0081
5- Angle	6.49	37.96	347	491	0.0022	0.0194
6- Angle	6.41	37.84	366	503	0.0020	0.0207
7- Angle	6.41	37.96	364	503	0.0023	0.0214
		Gusset average:	**402**	**494**		
		Angle average:	**359**	**499**		

Table 2.10: Anticipated specimen capacities and experimental ultimate loads

	$P_{a,CSA}$ (kN)	$P_{a,AISC}$ (kN)	$P_{u,exp}$ (kN)
Yielding	666	666	676
Weld	390	291	629
Bearing	290	346	338
Net Area	393	393	532
Bolt	284	236	364
Block Failure	438	438	621

2.3.1. Member Yielding

This particular test consisted of yielding and rupturing the brace members. Engineers would typically not have any problems having this failure mode controlling the behaviour of the structure. However, no special design and detailing requirements are specified for ensuring this type of failure in CC Type SFRSs, and the objective of this

research project is to identify ductile connection limit states. With this being said, brace yielding was investigated for comparison purposes. Figure 2.2 shows the load vs. displacement graph of the three brace yielding specimens and include the elastic deformation of the braces. The deformations in this figure are those obtained from the LVDT located in the load frame actuator and hence include elastic deformations of the test setup as well as slip in the grips (there was no evidence pointing to slip taking place).

This test was relatively easy and had no complications. Both angles never ruptured at the same time; the first angle rupture happened at an average load of 885 kN. The two potentiometers attached to the gusset plates had deformation ranges smaller than the ultimate deformation anticipated for the angles and their strings were cut before the ultimate load. The potentiometers were therefore used to calculate the deformation at yield of the braces.

Photo 2.1: Picture representative of all D01X specimens.

The braces showed the classic shape and behaviour of structural steel yielding and rupturing under a tensile load. The yield point is clearly defined and the material shows typical strain hardening. The results from the three specimens were almost identical and fit nicely over one another in Figure 2.2. Table 2.11 shows the different pertinent characteristics of specimens D01X-01 through D01X-03. Included in this table as well as the other similar tables for the next five failure modes are the deformations at the

ultimate load, δ_u, and at the "rupture" point, δ_{rupt}, defined as 80% of the ultimate load after the latter is reached. The specimens showed excellent ductility. The average plastic deformation of these specimens is expected to be much greater than the other specimens.

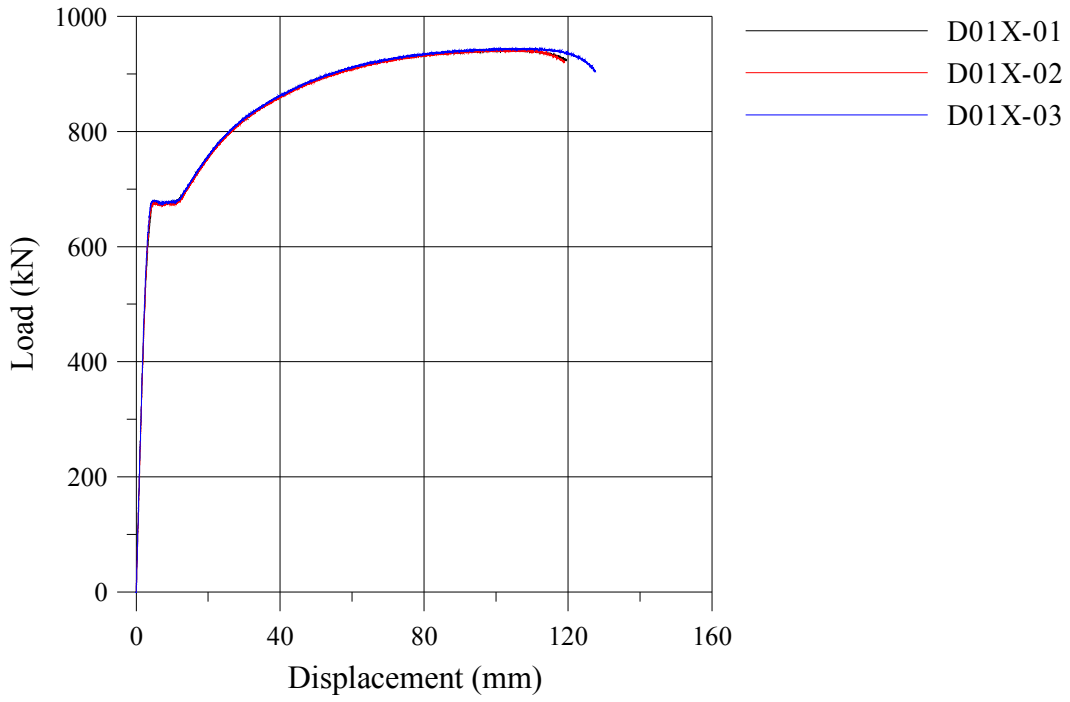

Figure 2.2: Brace yielding, D01X

Table 2.11: D01X experimental results

	Specimen		
	D01X-01	D01X-02	D01X-03
P_y (kN)	676	674	679
δ_y (mm)	5.70	5.78	5.47
$P_{u,exp}$ (kN)	941	942	944
δ_u (mm)	103.1	104.3	103.8
δ_{rupt} (mm)	115.5[1]	114.6[1]	122.3[1]

[1] δ_{rupt} corresponds to the deformation at rupture in this case, as explained below.

Deformations at rupture were not available in specimens D01X. Eighty percent of the ultimate load corresponds to approximately 754 kN for all three specimens. All three

specimens underwent their first rupture in an angle at an average load of 885 kN, the load immediately dropping well below 754 kN afterwards. The first brace fracture occurred at a strain of 0.126, 0.125, and 0.134 for specimens D01X-01, D01X-02, and D01X-03, respectively. Again, these strains were calculated based on a centre-to-centre length of brace.

As mentioned above, Figure 2.2 includes the elastic deformations of the braces. What is of interest in this research is the deformation capacity of the connections. To differentiate the two and explain what is done in future specimens, elastic deformations of the braces were eliminated from specimens D01X and both cases are shown in Figure 2.3, below. The elastic deformations ($\Delta_{elastic}$ = PL/AE) of the braces were taken away from the total measured average displacement from the potentiometers. The potentiometers offered a better quality of measurements over the elastic range of the braces than the load frame measurements and permitted us to measure the connection's and braces' deformations, while excluding any deformations in the gusset plates. The length between potentiometers was used as the brace length to be consistent with the measured elongations.

As can be seen in Figure 2.3, the plastic curve shows the displacement to be close to zero in the elastic range. After 600 kN, the braces seem to yield slowly until they reach 675 kN. This procedure will be used in the force-displacement curve of every specimen to show only the connection deformations.

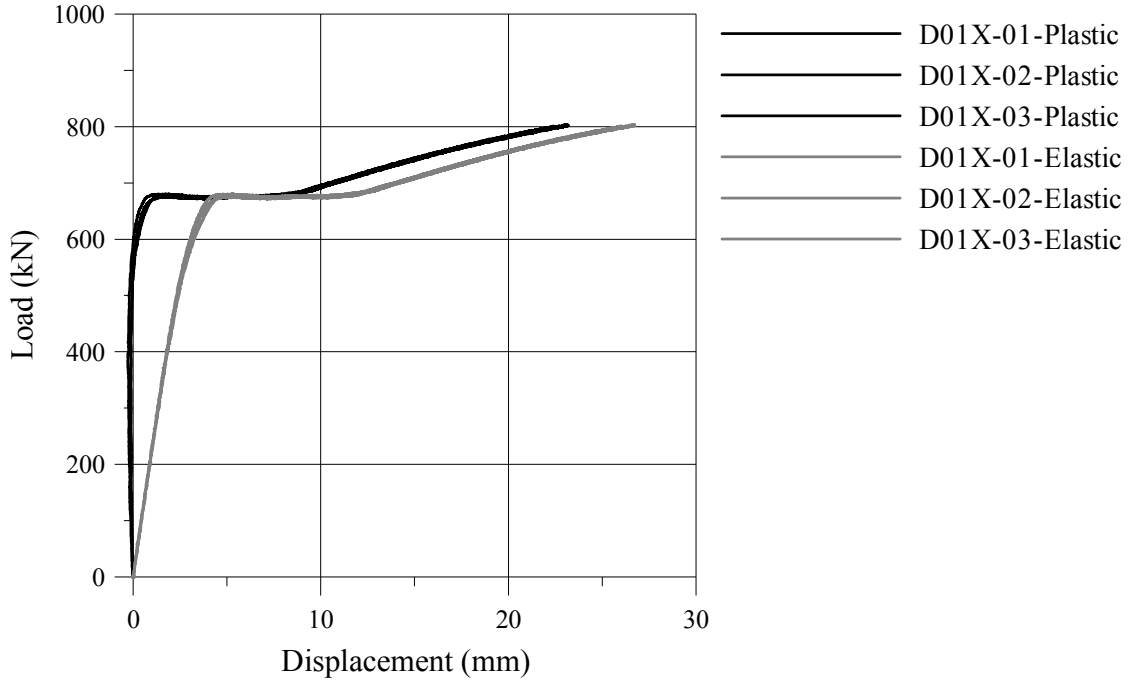

Figure 2.3: Comparison of plastic and elastic behaviour

2.3.2. Weld Rupture

Figure 2.4 shows the load vs. displacement response of the three specimens featuring a weld failure. Table 2.12 provides the key parameters measured in these tests. Photo 2.2, Photo 2.3, and Photo 2.4 show specimens D02X-01, 02, and 03.

In the tests, no visible deformation could be observed until a weld rupture happened without warning. There was an attempt made in trying to observe whether cracks were appearing in the weld itself or at the weld and base metal interface. Due to the rough nature of the welding process, no cracks were discernable at close range. For safety reasons, one could not approach the specimen near its rupture point in the hopes of observing a crack. It is believed the cracks formed in a rapid manner, leading to a brittle rupture.

The three plots are consistent with one another in the elastic range and part of the inelastic range. Specimen D02X-03 underwent more deformations, the explanation of which remains unknown. A probable explanation could be the yielding of the angles;

however, section 2.3.1 shows the yield load of the angles to be approximately 676 kN. However, with the inherent variability in steel the yielding of the angle cannot be ruled out. It is possible the angles yielded and the strain hardening brought on the weld failure. Simultaneous yielding and cracking may also have occurred at both ends of specimen D02X-03 and caused an increase in ultimate deformation. It is very difficult to point out the locations where extensive deformations occurred; white wash would have enabled us to identify the yielding zones.

Table 2.12 shows the pertinent information for the same three specimens. The three specimens underwent an average ultimate displacement of 7.3 mm, while the average deformation at rupture, δ_{rupt}, was 9.4 mm. It is important to note that the measured displacements are the sum of deformations at both connection ends.

Table 2.12: D02X experimental results

	Specimen		
	D02X-01	D02X-02	D02X-03
$P_{u,exp}$ (kN)	609	625	653
δ_u (mm)	5.2	6.3	10.4
δ_{rupt} (mm)	7.0	7.9	13.2

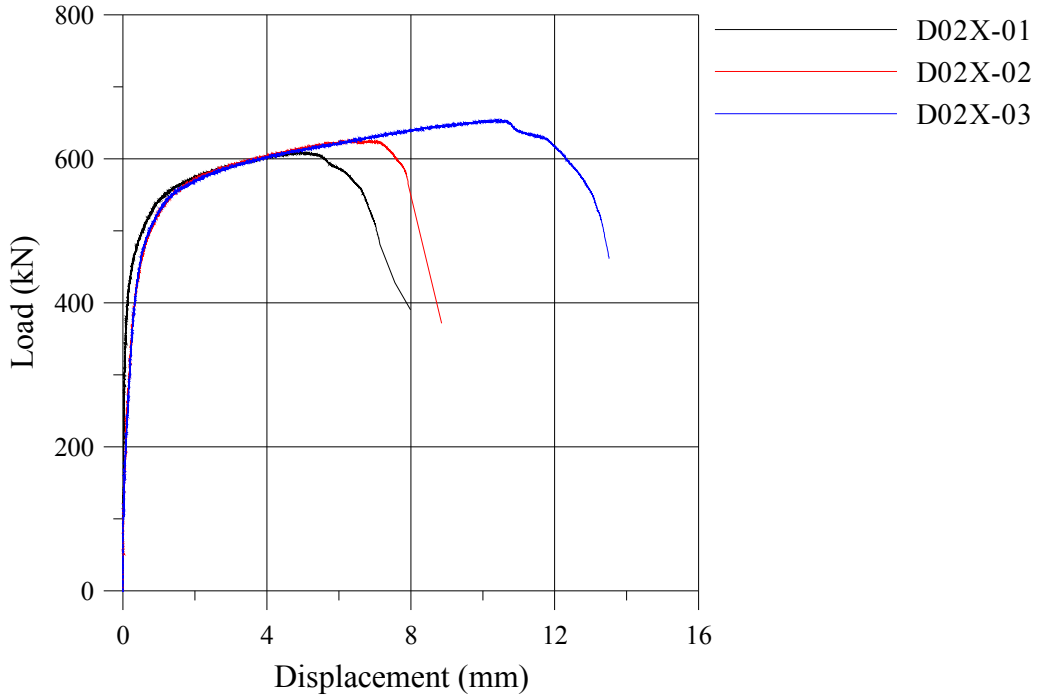

Figure 2.4: Weld failure, D02X.

Photo 2.2: Specimen D02X-01.

Photo 2.3: Specimen D02X-02.

Photo 2.4: Specimen D02X-03.

2.3.3. Bearing Failure of Gusset Plate

Table 2.13 shows the key parameters of the bearing failures shown in Figure 2.5. In Table 2.13, the F_u used is given in Table 2.9. All three tests gave very consistent results. Photos 2.5 through 2.8 show all bearing specimens.

The first part of Figure 2.5 shows the very steep elastic portion of the connection response. This corresponded to the response of the specimens before slip occurred, showing that a slip resistant connection is much more stiff than a bearing one. Once slip occurred loud noises could be heard, indicating different connection parts were moving relative to one another. Yielding initiated at approximately 250 kN for all specimens. Since the gusset plate was confined between the angles, it is difficult to point out precisely what happened at the ultimate load: whether shear cracks started to appear between the bolt holes and the end of the gusset plate or whether the pile-up of material was simply too great. It is noted, however, that a widening of the gusset plate occurred in all three specimens during the flattening of the load vs. displacement curve, such as experienced by Perry in his experiments (1981). This is shown in Photo 2.5. Pictures of specimens D03X-01, D03X-02, and D03X-03 are presented in Photo 2.6 through Photo 2.9. Specimens D03X-02 and D03X-03 did not have clean shear plane failures like D03X-01; a block of the gusset plate separated, as shown in photos Photo 2.7 and Photo

2.8. This was most likely due to the small cracks initiated by the hole punching process being expanded because of the widening of the plate.

Table 2.13: D03X experimental results

	Specimen		
	D03X-01	D03X-02	D03X-03
$P_{u,exp}$ (kN)	337	341	337
δ_u (mm)	24.7	23.5	19.9
δ_{rupt} (mm)	30.5[1]	32.0[1]	27.6[1]
$\sigma_{u,exp}$	$2.24F_u$	$2.26F_u$[2]	$2.24F_u$
$\sigma_{1/4"}$ (kN)	274	270	258
$P_{AISC\ Equ.\ J3\text{-}6a}$ (kN)	273	273	273

[1]:80% of the ultimate load could not be reached without taking a sharp drop in load after the ultimate load, indicating a rupture had happened. δ_{rupt} in this case corresponds to the deformation at this sharp drop in load.

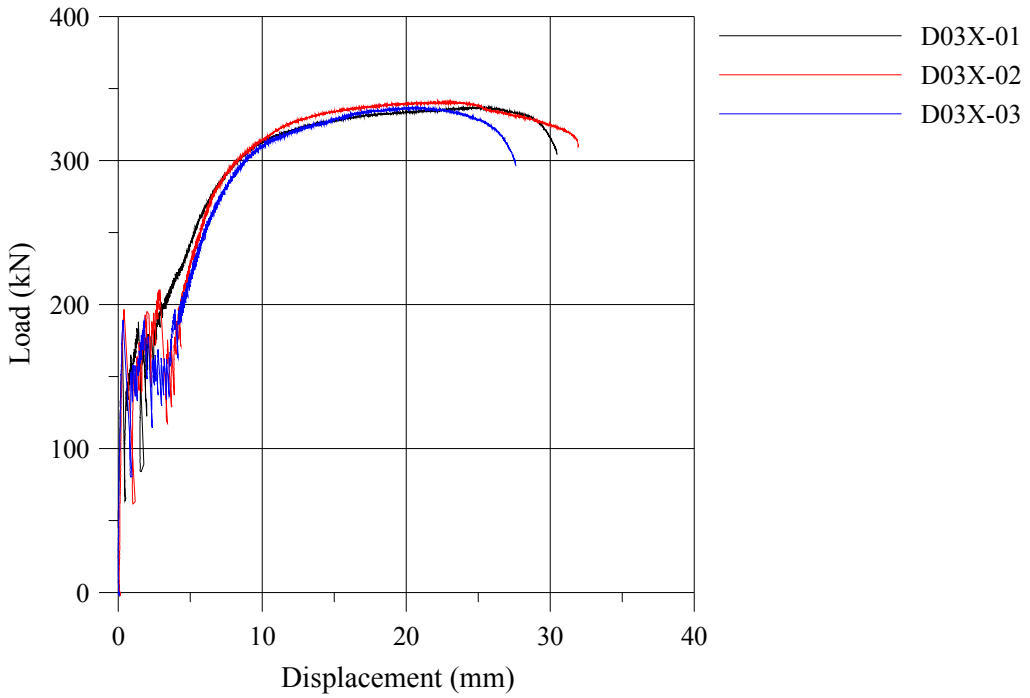

Figure 2.5: Bearing failure, D03X

Photo 2.5: Specimen D03X-01 mounted in the load frame, showing a widening of the gusset plate.

Photo 2.6: Specimen D03X-01, failed end.

Photo 2.7: Specimen D03X-02, failed end.

Photo 2.8: Specimen D03X-03, failed end.

Photo 2.9: Picture depicting the typical bearing deformations taking place in the intact end.

All three specimens underwent relatively consistent deformations at ultimate. The average ultimate displacement was 22.7 mm, and the ultimate deformation at rupture, δ_{rupt}, was 30.0 mm. The average $\sigma_{u,exp}$ was $2.25F_u$, significantly smaller than the $3F_u$ given in the S16 and AISC standards; the reason for this is the mode of failure calculated for the outside bolt (one closest to gusset plate edge). This bolt was calculated to have a bolt-tearout failure mode. If a longer end distance was used the load would have been able to achieve a higher level and therefore a higher bearing stress would have been witnessed.

Frank and Yura (1981) and the AISC (2005) both specify a maximum bearing stress of $2.4F_u$ when the displacement is limited to ¼" (6.35 mm). Table 2.13 shows the load at this displacement for specimens D03X (and includes any slip). The same table also includes the calculated connection nominal capacity when the displacement is limited to ¼", as given by AISC equation J3-6a.

We notice the loads obtained in the experiment at ¼" displacement are lower than calculated. It is important to note that slippage occurred during the test and can be seen within the first 5 mm in displacement on Figure 2.5. The bolt holes are 2 mm bigger than the bolt diameter to allow room for bolt installation. Though it is difficult to estimate closely the amount of slippage that occurred, the amount of slippage in each specimen is estimated to be approximately. The loads at a displacement of 11.35 mm (1/4" + 5 mm) in specimens D03X-01, D03X-02, and D03X-03 are, respectively, 319 kN (2.12Fu), 323 kN (2.15Fu), and 317 kN (2.11Fu), and much closer to the value of 329 kN obtained using the empirical formula.

In a bearing test performed by Frank and Yura (Frank et al. 1981) with a splice plate of similar width and geometry, an ultimate bearing ratio of 2.67Fu was obtained. In their experiments, the connections were supported during assembly in such a way that at least one bolt was brought into bearing. Since the bolt holes were not perfectly placed, some slip was recorded during the experiment. This slip was neglected in their calculations and their results shown; their deformations therefore include any slip deformations that

happened (although minimal). This ratio of $2.67F_u$ is significantly different from the results shown in Table 2.13 (values between 2.24 and $2.26F_u$). The difference can be attributed to the different Fu. Frank and Yura had an average F_u of 420 MPa, while the gusset plates in specimens D03X had an average of 494 MPa as the ultimate stress. Another explanation for the higher ductility in their specimens is the greater end distance used (76 mm versus 30 mm in D03X). As mentioned in section 1.1.5, longer end distance translates into the more ductility (Kim 1996). The governing failure mode for the outside bolt in D03X was a tearout; the exterior bolt's governing failure mode in Frank and Yura's specimen was a bolt bearing one. This is the main reason specimens D03X could not achieve a bearing stress of $3F_u$, as the one given in the CSA and AISC standards.

Photo 2.9 shows the typical bearing deformations that took place in the intact ends of specimens D03X. It is evident that these ends underwent important deformations; these were measured after the dismantling of the specimens and are reported in Table 2.14, under δ_{Int}. Taking away these deformations from δ_u, we obtain an average δ_{Br} of 18.3 mm, where δ_{Br} corresponds to the bearing deformation capacity of a single connection end.

Table 2.14: D03X deformations at both ends of the specimens

	Specimen		
	D03X-01	D03X-02	D03X-03
$\delta_{Int.}$ (mm)	5.1	3.3	4.8
δ_{Br} (mm)	19.6	20.2	15.1

2.3.4. Net Area Fracture of Brace Members

Specimens D04X had punched holes, while specimens D14X had drilled holes. Figure 2.6 and Figure 2.7 show the load vs. displacement behaviour of the specimens failing in their net sections and Table 2.15 shows the important parameters from these plots.

As with other bolted specimens, deformations were limited to elastic deformations at the beginning. Thereafter, a significant amount of slippage occurred when the load reached approximately 50 kN, as shown in the first portion of Figure 2.6. The first 3.5 to 4 mm of displacement can be attributed to slippage. At the end of the slippage phase, inelastic response was observed which can be attributed to localised bearing deformations as bolt bearing gradually took place in sequence. At a load of about 350 kN, softening of the response became more pronounced. This is most likely attributed to gradual yielding on the net area of the brace members. For all three specimens, the first crack appeared at the bolt hole and spread to the toe of the angle (on the leg bolted to the gusset plate). This location is shown in Photo 2.10-A. The peaks of each curve correspond to the appearance of the crack at this location. As can be seen in Photo 2.10-B, -C, and -D, specimens D04X did not break in a straight line across the angles' sections. A second crack then propagated to the heel and across the outstanding angle leg, again starting from the bolt hole. The crack found its way to the heel of the angle at an angle instead of being perpendicular to the direction of loading.

Table 2.15: D04X and D14X experimental results

	Specimen		
	D04X-01	D04X-02	D04X-03
$P_{u,exp}$ (kN)	536	537	523
δ_u (mm)	16.8	16.3	14.8
δ_{rupt} (mm)	20.8	21.0	18.6
	D14X-01	D14X-02	D14X-03
$P_{u,exp}$ (kN)	554	562	558
δ_u (mm)	32.8	33.9	31.8
δ_{rupt} (mm)	37.6	35.7	36.1

Specimens D04X failed in their net areas at an average ultimate load 532 kN and showed an average displacement at ultimate load of 16.0 mm. The deformation at rupture, δ_{rupt}, was on average 20.1 mm. The ultimate load was well approximated as Table 2.2 reports the calculated connection nominal capacity to be 519 kN. Photo 2.10-E shows the typical failure of specimens D14X, Figure 2.7 shows the load versus

displacement behaviour of all three specimens, and Table 2.15 shows the important parameters for Figure 2.7.

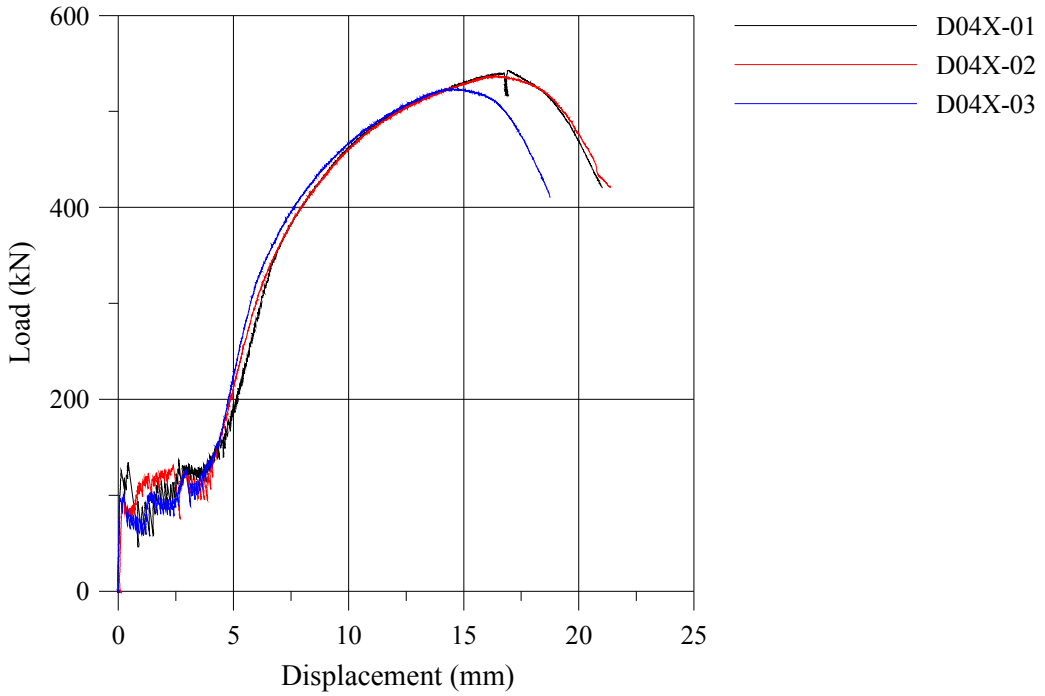

Figure 2.6: Net area rupture, D04X

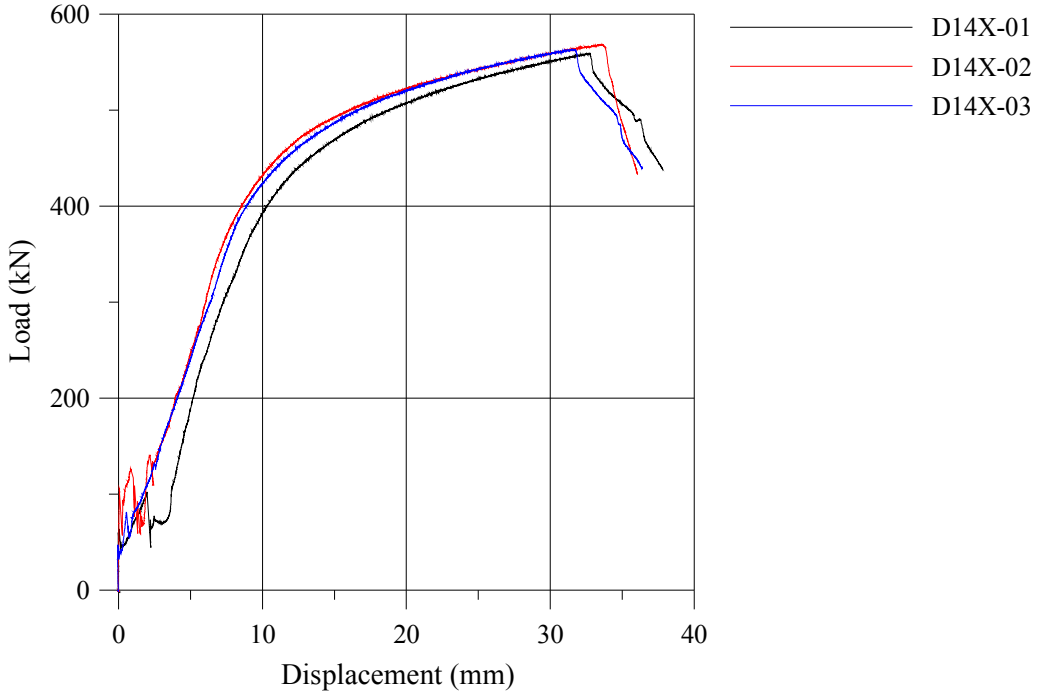

Figure 2.7: Net area rupture, D14X

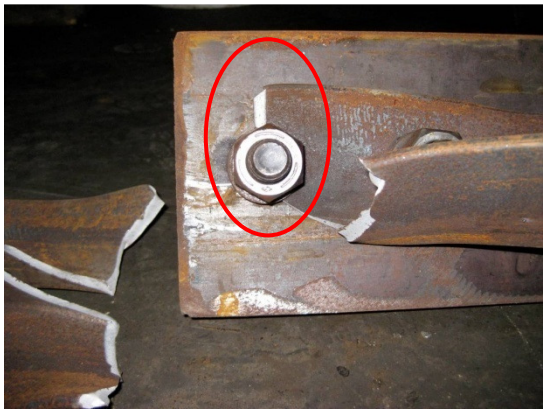

A): Picture showing the location of the first crack to appear in specimens D04X.

B): Specimen D04X-01.

C): Specimen D04X-02.

D): Specimen D04X-03.

E): Photo depicting a typical D14X specimen break.

F): Photo showing the significant bearing deformations in the angles.

Photo 2.10: Specimens D04X and D14X.

Specimens D14X did not break through their net areas. Other than their drilled holes, these specimens were identical to specimens D04X. In all cases, the peak of the curves

in Figure 2.7 corresponds to the appearance of the crack between the inside bolt and the toe of the angle, which was also experienced for specimens D04X. This crack appeared at an average load of 558 kN. In all D14X specimens, significant bearing deformations were visible in the angles after achieving a load of 500 kN or more. Specimen D14X-02 has bearing deformations so severe that the bolt hole in the angles could be seen at a load of 533 kN (see Photo 2.10-F). The crack then propagated from the bolt hole toward the end of the angles at a sharp angle, close to the line of bolts but not touching the bolt holes, as shown in Photo 2.10-E. This failure mode was close to indicating a shear and tension block failure. The specimen had an average ultimate load of 558 kN and average deformation at ultimate of 32.8 mm. The deformation at rupture, δ_{rupt}, was on average 36.5 mm. A plausible explanation for the significant differences in deformation values at ultimate load between D04X and D14X is that work hardened punched holes provided more resistance against bearing deformations in specimens D04X, consistent with the findings of Owens (Owens et al. 1981).

2.3.5. Bolt Shear Rupture

Figure 2.8 shows the load vs. displacement graphs of the D05X specimens and Table 2.16 gives its key parameters. Photo 2.11 and Photo 2.12 show, respectively, a ruptured and intact bolt from specimens D05X.

There was less slippage in these specimens than specimens D03X and D04X. This could be due to the fact that the bolts were brought closer to bearing because of the manner in which there were assembled at the fabrication shop. It could also be due to the small plate that was welded to the angle to increase the bearing capacity; this welded plate may not have been perfectly aligned with the angles' bolt holes, therefore restraining the possibility for bolt slippage. The first portion of the graphs show the load must be taken by friction forces since the load does not increase steadily.

The average ultimate load of the specimens was 364 kN, which does not compare well to the nominal calculated capacities of 284 kN (CSA) and 236 kN (AISC). The failure

was less ductile than in the previous specimens with a sharp drop in resistance following the ultimate capacity. The specimens averaged a total elongation of 15.7 mm at ultimate load and an average deformation at the rupture point, δ_{rupt}, of 16.2 mm. Both values include deformations at both ends of the braces. Kulak shows A325 bolts can undergo an ultimate shear deformation of approximately 5 mm (Kulak et al. 1987).

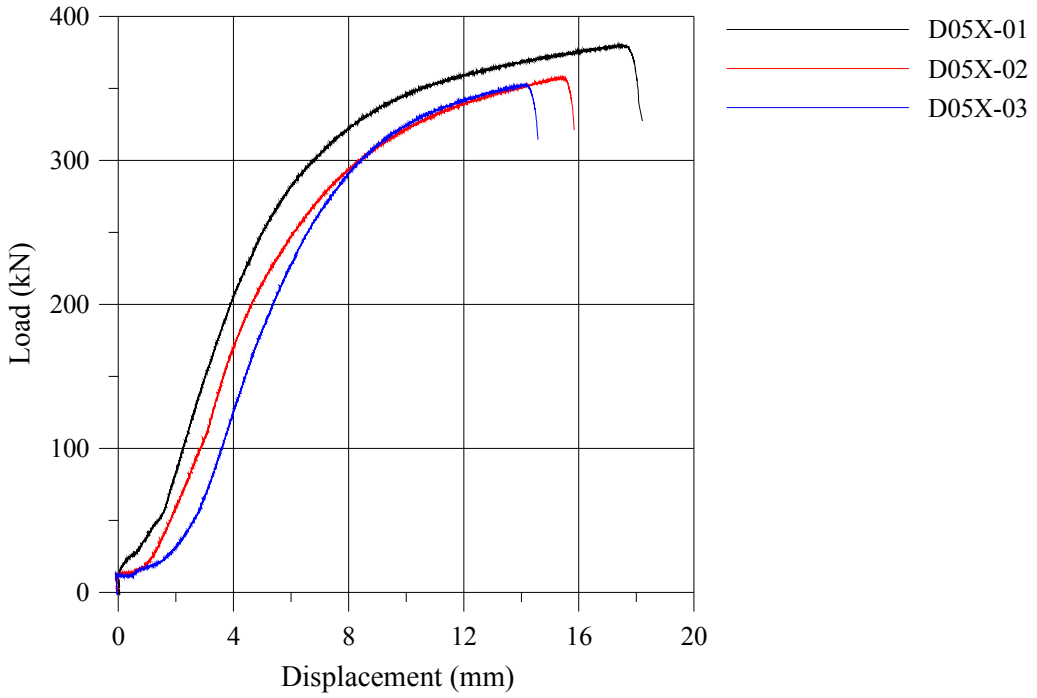

Figure 2.8: Bolt failure, D05X

Table 2.16: D05X experimental results

	Specimen		
	D05X-01	D05X-02	D05X-03
$P_{u,exp}$ (kN)	380	358	353
δ_u (mm)	17.4	15.4	14.2
δ_{rupt} (mm)	18.2	15.8	14.6

It is important to note that not all deformations in these tests came from shear bending of the bolts. There was significant bearing deformations at each bolt hole: D05X-01, 02, and 03 had approximately 4.7 mm, 4.1 mm, and 2.5 mm of total cumulative bearing

deformations, respectively, as measured after dismantling the specimens after testing. Photo 2.12 shows a bolt that did not break during the test and it is evident that more of the specimen deformation can be attributed to this bolt. Subtracting from the average specimen displacement (15.7 mm) the average bearing deformation (3.8 mm), the average amount of slippage (2 mm), and the unbroken bolt's deformation (3 mm to 4 mm, assuming it was on the verge of shear failure), we obtain results similar to Kulak's with a displacement of approximately 6 mm.

Photo 2.11: Typical bolt shear failure in specimens D05X.

Photo 2.12: Typical unbroken bolt from specimens D05X.

2.3.6. Block Shear and Tension Failure of Brace Members

Figure 2.9 shows the load vs. displacement of the D06X specimens and Table 2.17 shows their key parameters. Photo 2.13 and Photo 2.14 show typical failure angles.

Once again, we see the connection undergoing slippage at the start of the loading. Upon further investigation of the connected parts after the tests, there are no significant bearing deformations in the unbroken connections to be accounted for. All three specimens started to rupture in a manner similar to the specimens failing in their net areas by tension cracking between the bolt hole and the toe of the angle. This first crack had split wide open before the ultimate load was obtained, at approximately 600 kN. After rupturing in tension, a crack indicating a rupture in shear started to develop at the bolt hole closest to the end of the angle. This shear crack varied between the net shear

area and the gross shear area; the shear rupture never happened entirely along the net or the gross shear area. The ultimate load appeared to be reached just before the last intact section between bolts started to crack.

The average specimen deformation at ultimate load is 15.5 mm, with approximately 3.5 mm of slip before the connection behaved in an elastic manner. The average displacement at rupture, δ_{rupt}, was 19.7 mm. The average load at ultimate was 621 kN, while the CSA and AISC handbooks predicted a conservative 495 kN capacity.

Table 2.17: D06X experimental results

	Specimen		
	D06X-01	D06X-02	D06X-03
$P_{u,exp}$ (kN)	626	632	605
δ_u (mm)	15.5	15.8	15.3
δ_{rupt} (mm)	19.4	19.5	20.2

Photo 2.13: Typical failure in D06X specimens.

Photo 2.14: Typical failure in D06X specimens.

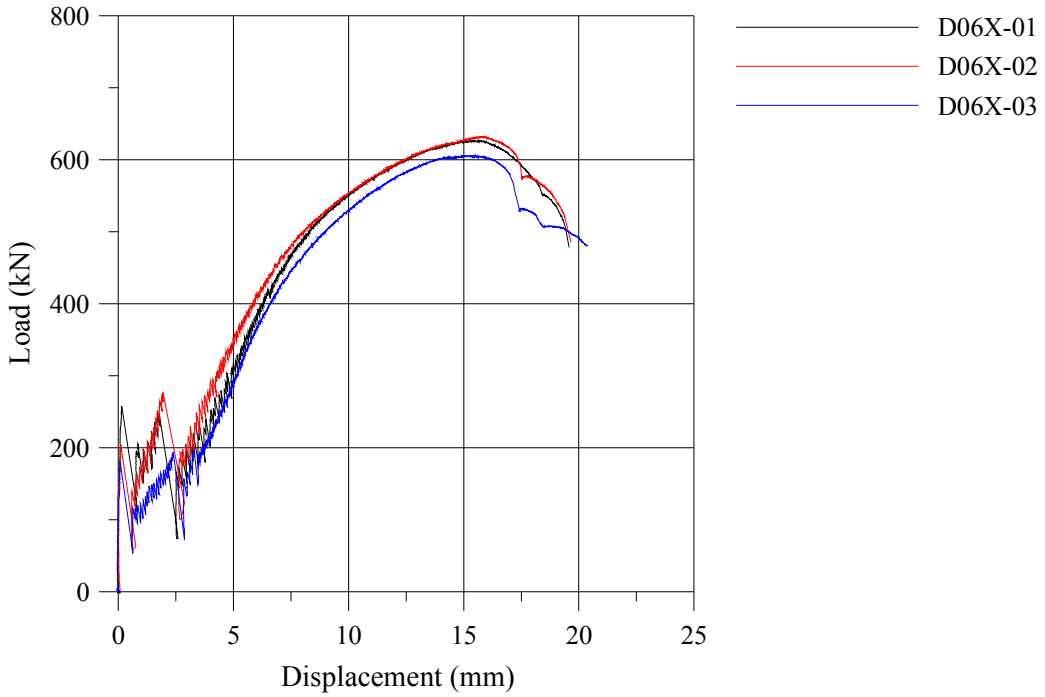

Figure 2.9: Shear and tension block failure, D06X.

2.4. Summary and Conclusions

Figure 2.10 shows the first specimen tested for each failure mechanism and Table 2.18 shows the average elongations at ultimate and at rupture for each of these. The brace yielding failure mechanism was not included because its maximum displacement was more than 3 times the deformation of a connection failing in bearing. It is evident that connections failing in bearing show more capacity for deformation than any other type of failing mechanism. Bearing failures averaged a deformation at ultimate load of 22.7 mm, as opposed to 16.0mm in net section area failures. Table 2.10 shows the connection capacities calculated using the F_y and F_u that were approximated in section 2.3.1. Most connections failed at a load greater than the ones predicted. The weld failure happened at a considerably greater load than expected, and this is due to the nature of the welding process. A 6 mm fillet weld was specified and it was evident that some weld lines were greater in size.

Table 2.18: Average deformations at ultimate and rupture for Phase I specimens

	Brace Yielding	Weld Failure	Bearing Failure	Net Area Failure (Punched)	Net Area Failure (Drilled)	Bolt Failure	Block Failure
δ_u (mm)	103.7	7.3	22.7	16.0	32.8	15.7	15.5
δ_{rupt} (mm)	117.5	9.4	30.0	20.1	36.5	16.2	19.7

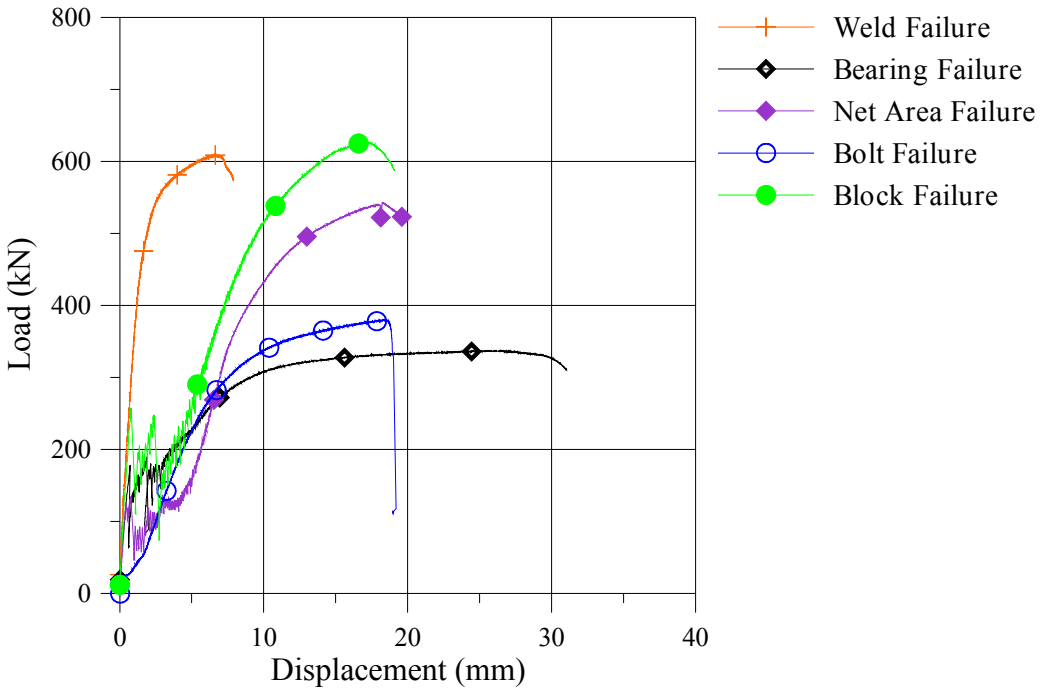

Figure 2.10: Specimen -01 of each failure mechanism, excluding member yielding.

The following is a list of negative and positive remarks that were found during the course of the Phase I Testing Program:

- The use of drilled holes was found to delay cracking of net section and to encourage bearing deformations.

- Slip reduced when adding reinforcement plates. This is not desirable, especially if a bearing failure mode is to be encouraged. The bearing capacity would have to be calculated based on two different materials, thus making it more difficult to predict.

- It is believed that confining the gusset plate was good, as it removed the possibility of introducing eccentricities and warping. A failure or rupture of the connection would most likely be brought on faster without a confined plate.

- The CSA bolt bearing equations were 25 % smaller than the experimental value, while the AISC bearing equations were 8 % smaller.

- Bolt shear and weld shear failures have less ductility. These should be excluded, possibly by using higher factors of safety during the connection design phase.

- Net section and shear and tension block failure modes both exhibit substantial deformation capacity and strain hardening responses. There is no need for higher safety factors when comparing these to bearing resistances.

- It is recommended using at least two bolts in each connection for Phase II. This will enable us to observe the effects of the bolt end distance and the bolt pitch.

- A rupture criterion should be established for Phase II. For example, the testing should at least go past 80 % of the ultimate load after the ultimate load has been reached. A specimen's deformation capacity would correspond to the deformation at this exact point, otherwise known as the rupture point.

- It would be wise to bolt the specimens in the structures lab of Ecole Polytechnique; this would enable us to control the bolt pretensioning.

The following is a list of positive and negative remarks, as well as recommendations, on the testing procedures used in Phase I of the testing program:

- No connection elements were white-washed. This made it difficult to identify zones which were undergoing yielding, especially for specimens D02X. It is recommended to use white-wash in Phase II of the testing program. Although the gusset plates will still be confined in the second phase, it may prove to be

beneficial to rule out any deformations due to yielding of a specific connection elements.

- The first phase had connections identical at both ends of the braces. It was difficult to quantify exactly how much deformation took place at the ruptured connection end, because of deformations also taking place at the unbroken connection. It would prove to be beneficial to bring to rupture only one connection. The opposite end would be the same for all specimens and would have a nominal resistance much higher than the other end, thus eliminating deformations taking place at the unbroken end.

- The potentiometers used in Phase I proved to be excellent. It is recommended to use potentiometers for Phase II. It would be worthwhile to change the gage length of the potentiometers to the length of the connection to capture only connection deformations at the end undergoing failure. Whether or not this is plausible, or practical, is talked about in the following chapter.

Chapter 3. EXPERIMENTAL PROGRAM: *PHASE II*

This chapter presents the second round of testing to be done. The objective of Phase II is to identify parameters that will optimize the deformation capacity of a connection failing in bearing. Section 3.1 will outline the parameters and specimens to be used.

3.1. Proposed Phase II Experimental Program

The focus of the Phase II test program is to identify a ductile connection failure mode and connection configuration, or connection details. It is recommended to proceed with and study the bearing failure mechanism, as it provided the most displacement capacity in Phase I. Some of the different connection parameters which could be investigated to improve ductility include the bolt end distance, bolt pitch, and standard or slotted holes; these are discussed below.

When designing the next specimens, a good tool in predicting which failure mode governs between net section failure and bearing failure is the bearing ratio, BR, as defined by equation 3.1 (Frank et al. 1981). Research reported by Jones (1957) states connections with bearing ratios of less than 2.25 would fail as net section failures under static loads. The BR of specimens D03X of the first round of testing was 3.26. If attention is given to this factor while designing the next round's specimens, bearing failures should be expected in the gusset plate.

$$BR = \frac{Bearing\ Stress}{Net\ Section\ Stress} = \frac{\frac{P}{A_{Br}}}{\frac{P}{A_n}} = \frac{A_n}{A_{Br}} \qquad 3.1$$

An important parameter in designing the specimens, and designing connections failing in bearing in the industry, is the ultimate bearing stress for which the connection is designed. CSA-S16-01 and AISC both use $3F_u$ when deformations are not a design consideration (AISC 2005; CSA 2001). Researchers that have reported few plates were capable of withstanding a bolt bearing stress of $3.0F_u$ limit were testing unconfined

plates (Frank et al. 1981; Lewis et al., 1996). Tests at the University of Alberta on confined plates failing purely in bearing showed that bearing stresses of $4.0F_u$ gave the most accurate connection capacities when used with the unified bearing equation (Cai et al. 2008). Although the authors do not explicitly state the cause of this increase in ultimate bearing stress capacity, it is believed to be due to the confinement of the plate in bearing.

CSA S16-01 states that the minimum bolt spacing (centerline to centerline) is 2.7 times the bolt diameter and that the minimum end distance (centerline to edge of connected part) is 1.5 times the bolt diameter. Lewis and Zwerneman (1996) reported that an end distance of 1.5d and a bolt spacing of 3d was not enough to develop a bearing force of $2.4dtF_u$ in their two-bolt, unconfined specimens; this statement also holds true for specimens D03X of Phase I, where bearing stresses of $2.4F_u$ were also not reached. This translates into less deformation capacity. As was found by Kim (1996), longer end distances (or bolt spacings) translate into more ductility. Figure 1.13 shows the effect of the end distance on the displacement capacity. Longer distances and spacings mean that bearing failures govern and it can be concluded that bearing failures give larger ultimate deformations.

Table 3.1 and Table 3.2 show the variation of the governing failure mode for different bolt diameters combined with different end distances and bolt spacings in an 8 mm thick steel plate (Fy = 350 MPa, Fu = 450 MPa). Table 3.1 and Table 3.2 use, respectively, $3.0F_u$ and $4.0F_u$ as the ultimate bearing stresses. In these tables, "Br" and "TO" indicate a bearing and a tear-out governing failure mode, respectively. Three design standards are used: CSA-S16-01, CSA-S16-09 (unified equation), and AISC 2005. Cai and Driver (2008) reported that, for confined plates, the use of the unified equation for bolt tear-out and an ultimate bearing stress of 4.0Fu gave the most accurate predictions of connection ultimate capacities when the governing failure modes are bolt tear-out and bearing failures. Cai and Driver's capacities were based on connections with inner bolts causing pure bearing failures and the outer bolts causing either a tear-out failure or a bearing

failure. Although more research is needed on this subject, the ultimate allowable bearing stress in practice is taken as $3.0F_u$ in either confined or unconfined plates. These tables show that the bolt diameter has no influence on the governing failure mode within each respective design standard. For example, looking at the CSA_{01} column across Table 3.1 in the three different bolt diameters shown, we see that the bearing failure mode governs at an end distance of 3.5d for exterior bolts, and at a bolt pitch of 3d for interior bolts. These spacings remain the same for different diameter bolts. This same consistency can be seen for CSA_{09} and $AISC_{05}$, but with different end distances and bolt pitches. In practice, end distances of 1.5 to 2.5 bolt diameters and bolt pitches of 3.5 and 4.0 bolt diameters are most widely used.

Table 3.1: Variation of governing failure mode when $3F_u$ is used as maximum bearing stress on 8 mm thick plate.

		d = 19.1 mm			d = 22.0 mm			d = 25.4 mm		
		CSA_{01}	CSA_{09}	$AISC_{05}$	CSA_{01}	CSA_{09}	$AISC_{05}$	CSA_{01}	CSA_{09}	$AISC_{05}$
Le (d)	1.5	TO	TO	TO	TO	TO	TO	TO	TO	TO
	2	TO	TO	TO	TO	TO	TO	TO	TO	TO
	2.5	TO	TO	TO	TO	TO	TO	TO	TO	TO
	3	TO	Br	Br	TO	Br	Br	TO	Br	Br
	3.5	Br	Br	Br	Br	Br	Br	Br	Br	Br
	4	Br	Br	Br	Br	Br	Br	Br	Br	Br
	4.5	Br	Br	Br	Br	Br	Br	Br	Br	Br
	5	Br	Br	Br	Br	Br	Br	Br	Br	Br
s (d)	3	TO	Br	Br	TO	TO	Br	TO	Br	Br
	3.5	Br	Br	Br	Br	TO	Br	Br	Br	Br
	4	Br	Br	Br	Br	Br	Br	Br	Br	Br
	4.5	Br	Br	Br	Br	Br	Br	Br	Br	Br
	5	Br	Br	Br	Br	Br	Br	Br	Br	Br
	5.5	Br	Br	Br	Br	Br	Br	Br	Br	Br
	6	Br	Br	Br	Br	Br	Br	Br	Br	Br

Table 3.2: Variation of governing failure mode when $4F_u$ is used as maximum bearing stress

		d = 19.1 mm			d = 22.0 mm			d = 25.4 mm		
		CSA_{01}	CSA_{09}	$AISC_{05}$	CSA_{01}	CSA_{09}	$AISC_{05}$	CSA_{01}	CSA_{09}	$AISC_{05}$
Le (d)	1.5	TO	TO	TO	TO	TO	TO	TO	TO	TO
	2	TO	TO	TO	TO	TO	TO	TO	TO	TO
	2.5	TO	TO	TO	TO	TO	TO	TO	TO	TO
	3	TO	TO	TO	TO	TO	TO	TO	TO	TO
	3.5	TO	TO	Br	TO	TO	Br	TO	TO	Br
	4	Br	Br	Br	Br	Br	Br	Br	Br	Br
	4.5	Br	Br	Br	Br	Br	Br	Br	Br	Br
	5	Br	Br	Br	Br	Br	Br	Br	Br	Br
s (d)	3	TO	TO	TO	TO	TO	TO	TO	TO	TO
	3.5	TO	TO	TO	TO	TO	TO	TO	TO	TO
	4	TO	Br	Br	TO	Br	Br	TO	Br	Br
	4.5	Br	Br	Br	Br	Br	Br	Br	Br	Br
	5	Br	Br	Br	Br	Br	Br	Br	Br	Br
	5.5	Br	Br	Br	Br	Br	Br	Br	Br	Br
	6	Br	Br	Br	Br	Br	Br	Br	Br	Br

To ensure the maximum amount of ductility is achieved, it is recommended to have an end distance and a bolt spacing with which bolt bearing will govern over the tear-out failure mode. As the specimens in Phase II will have confined plates, Table 3.2 shows that an end distance of 4d and a bolt spacing of 5d (round numbers are used for simplicity).

It is recommended to examine the combinations of end distance (L_e) and bolt spacings (s) shown in Table 3.3 in Phase II. The inside bolt always causes a bearing failure, while the failure caused by the end bolt is indicated. The last combination uses large spacings in order to ensure a pure bearing failure occurs. The first combination uses a small end distance to ensure a tear-out failure and to observe the distinctions between connections failing under the two different failure modes.

Table 3.3: Bolt spacings to be studied in Phase II

Le	s	End Bolt Failure Mode
2d	5d	Tear-out
4d	5d	Bearing
5d	6d	Bearing

In Frank and Yura's report (1981), it is shown that perpendicular long-slotted hole connections undergo more deformation than a standard hole connection under the same load. For the same bearing ratios, a connection with slotted holes has the same ultimate capacity as a connection with standard holes. It would prove interesting and beneficial to include in Phase II a specimen with slotted holes. Clause 27.1.6 of CSA-S16-01 states that long-slotted holes are not to be used in seismic force resisting systems. Short-slotted holes, however, are permitted as long as they are oriented perpendicular to the direction of the loading. Short-slotted holes are, following CSA-S16-01, 2 mm wider than the bolt diameter and at most 6 mm in length for bolts 22 mm or less in diameter, 8 mm for bolts 24 mm in diameter, and 10 mm for bolts 27 mm or more in diameter. Since a discussion with the steel fabricator CANAM showed that they had no objection to short-slotted because they use punches to make these, the Phase II test program will include one sub-group of specimens with a short-slotted hole.

As demonstrated by Owens and Iwankiw & T. Schlafly, punching does not significantly alter the bearing strength of a connection and deformations of punched holes at service loads are likely to be slightly less than drilled holes (Iwankiw et al. 1982; Owens et al. 1981). Owens showed that drilled holes sometimes underwent twice the deformation of a punched hole. This seems logical because punched holes feature material next to the bolt hole that has been work hardened. For this reason, it is proposed to use mainly drilled holes in the second round of testing in this research. One sub-group of specimens with punched holes will be tested to demonstrate the differences, if any, between the two types of holes.

It was reported by Frank and Yura that bolt pretensioning only changed the initial stiffness of bolted specimens in the outside splice plates of symmetric butt splices (confined) (Frank et al. 1981). For bearing failures, the ultimate load and displacement were the same, regardless of whether torqued or snug-tight bolts were used. Pre-tensioned bolts are more expensive because of installation but they may result in reduced deformation demand if friction can be maintained as an energy dissipation mechanism under cyclic loading. However, clause 27 of CSA-S16-01 does not state the need to have pretensioned bolts in braced frames of the conventional construction category. The RCSC, however, states that pretensioned bolts are to be used in joints where significant load reversals are expected. The AISC's stance on the subject of whether to use snug-tightened or pretensioned bolts in Phase II is to use snug-tight bolts, as this will give a baseline performance (Carter July 27, 2009). Snug-tightened bolts will therefore be used for all but one specimen.

3.2. Discussion of Proposed Connection Failure Mode

It is useful to compare the proposed specimens to real-life connections. In conventional construction, it is permitted to design connections for seismic loads calculated with R_dR_o equal to 1.95, as long as the governing connection failure mode is a ductile one, such as a bearing failure. The connection may also be designed for gravity loads combined with the same seismic load multiplied by R_d when the connection limit state is not a ductile one. To ensure the governing connection limit state is bearing failure, the resistance factors ϕ for tear-out and ϕ_{Br}, 0.9 and 0.67 respectively, should both be set equal to 0.9. The resistance factors of all other limit states remain as prescribed by CSA-S16-01.

It is useful to give a physical or practical representation of the specimens proposed in Phase II. From Table 3.10 of section 3.3.4.2, Specimen BRD4D5D of Phase II has, with the resistance factors proposed above, a bearing capacity of 495 kN (550 kN x 0.9). An HSS connected with two back-to-back angles on either side, such as the one shown in Figure 3.1, would have twice this capacity, 990 kN. Specimen BRD4D5D of Phase II would correspond to the two back-to-back angles used on one side of the HSS shown in

Figure 3.1. For a regular commercial building with X-bracings split over two storeys, or a Split-X SFRS, with a braced frame width of 9 m and a normal storey height of 3.75 m, the brace length is 5.86 m. Assuming an HSS is used as a brace, the corresponding section is an HSS203x203x8.0 with a C_r of 1153 kN, according to clause 13.3 of CSA S16 (2001). With the 127 mm leg of the angle connected to the gusset plate midway through its leg by two bolts, the bolt gage in the same plate becomes:

$$\frac{127}{2}+203+\frac{127}{2}=330mm$$

The corresponding shear and tension block capacity of this configuration is therefore 1269 kN using CSA-S16-01 and 1124 kN using the unified equation. Assuming the 76 mm leg of the angles are bolted to the HSS with enough bolts to ensure the failure is in the gusset plate (or $L_1<L_2$ because of the greater number of bolts), this connection configuration would be considered ductile.

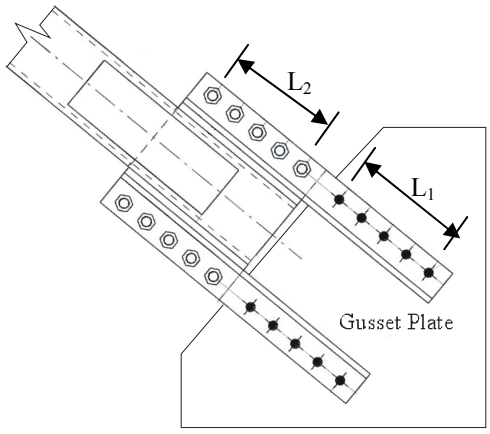

Figure 3.1: Typical HSS connection with two back-to-back angles on either side of the HSS brace.

It is also of importance that the connection limit state does not inherit too much overstrength. With R_ϕ equal to 1.11, R_y equal to 1.1, and R_{size} equal to 1.05 the associated overstrength is R_ϕ x R_y x R_{size} = 1.28, or 1.3 as prescribed by NBCC 05. Assuming the connection is designed perfectly for a bearing resistance just equal to the

factored brace axial load with R_dR_o equal to 1.95, its capacity may be as much as 30 per cent greater than the calculated capacity. The same applies to the bracing member. It would prove ineffective to have a so called "ductile" connection if it inherits too much overstrength and eventually concentrates the ductility demand on the bracing member, which could fail in tension rupture. The analytical aspect of this project will look at the probable force demand on braces (or connections) through linear time history analyses and is presented in the following chapter.

It is expected that specimen BRD4d5d will have the most deformation at ultimate; its end distance is 4d while its bolt spacing is 5d, both causing a bearing failure rather than a tear-out failure at each bolt. If a ductile connection is judged having to have all bolts cause a bearing failure (including the end bolts), then there are fewer parameters with which to play to adjust the connection resistance. These parameters are the plate thickness, the bolt diameter, and the plate's ultimate stress capacity. The smallest practical gusset plate is an 8 mm one and the smallest amount of bolts to be used in a brace connection is two. The corresponding bearing resistance, with ϕ equal to 0.9 and 19.1 mm bolts, is 371 kN for an ultimate bearing stress of $3F_u$ and 494 kN for an ultimate bearing stress of $4F_u$. This may pose problems for connections with smaller factored loads: connections in the top storeys of a braced bay, or connections for a light low-rise structure, for example. For these smaller connections, there exists the possibility of moving the bearing failure to two transfer plates slotted into an HSS. The gusset plate would have a larger thickness, thus not controlling the design. Two 4 mm thick transfer plates could be used with two 13 mm A490 bolts, giving a bearing resistance (ϕ_{Br} of 0.9) of 253 kN with an ultimate bearing stress of $3F_u$ (unconfined plates). The bolt shear capacity becomes 263 kN. The corresponding HSS for a cross-bracing over one storey for the same configuration described above is an HSS102x102x8.0, and the transfer plate width needed to avoid net area rupture is 122 mm (F_u = 450 MPa). This configuration seems to be one of the options for a ductile connection with a lower resistance.

Figure 3.2 and Figure 3.3 show the applicability of using bearing failures when it comes to designing connections with smaller factored resistances. These plots were obtained by calculating, for gusset plates 6 mm in thickness, the factored bearing resistance with ϕ_{Br} set to 0.9. Six mm gusset plates would be considered the absolute thinnest plate that could be used; 8 mm plates are used most of the time for small plates. Using gusset plates that are too thin means care must be exercised on the construction site, as well as the fabrication shop, to not bend or warp them.

Figure 3.2 and Figure 3.3 use, respectively, G40.21 350W steel and A36 steel to show the effect of using different materials. Using A36 steel would give slightly lower factored bearing capacities; A36 structural steel, however, is becoming less available as 350W is becoming more prominent. To obtain these capacities, ϕ_{Br} was set equal to 0.9 and $R_t = 1.1$ was used to account for the inherent variability in the steel's F_u. A490 bolts are used and are assumed to have two shear planes.

The main parameter which influences this range of factored capacities is the maximum bearing stress the gusset plate can sustain. CSA and AISC standard both provide $3F_u$ as the maximum bearing stress, as explained in sections 1.1.2. As was experienced by Cai and Driver (2008) and as will be seen in Phase II of this project, the allowable bearing stress is sometimes shown to be closer to $4F_u$. For this reason, both $3F_u$ and $4F_u$ are shown in the two latter figures. We see that if the connection is designed with $4F_u$, a 13 mm (1/2") bolt can not be used, as bolt shear rupture governs the design. Immediately, we see the effect of increasing the bearing stress to $4F_u$: the range of available lower bearing capacities is made smaller.

Theoretically, a factored bearing capacity can reach any higher level of force as long as, for any given bolt diameter, the plate thickness does not become too great such that the bearing capacity surpasses the bolt shear capacities. This statement assumes that bearing failure and bolt shear failure are the two governing failures modes in the connection.

When designing vertical bracing connections, one could develop design aids such as the one shown in Table 3.4, which shows connection factored capacities (using the same design parameters as in Figure 3.2) for a four-bolt double-shear connection. This connection would be similar to the one shown in Figure 3.1, but with two bolts on each side of the HSS tube rather than 5 as shown. Also shown in the table are the bolt shear capacities (V_r), just below the bolt diameter.

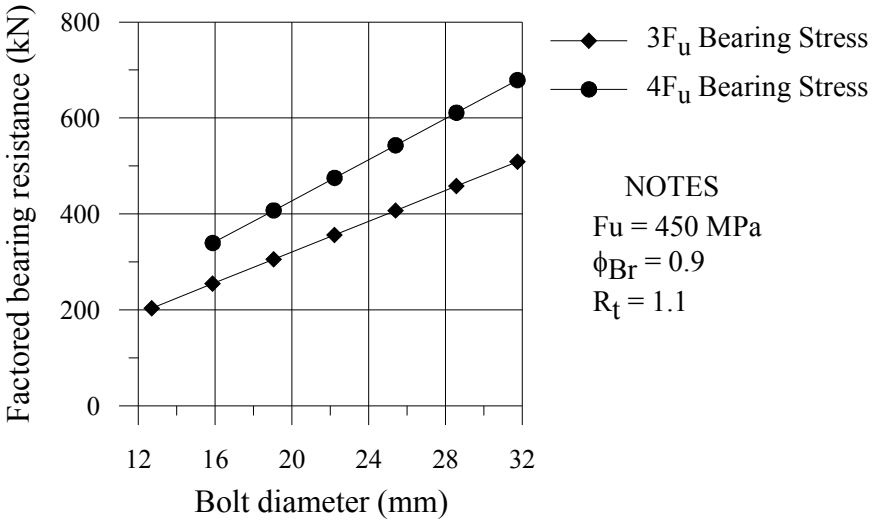

Figure 3.2: Range of B_r values in a two-bolt connection when G40.21 350W (F_u = 450 MPa) is used.

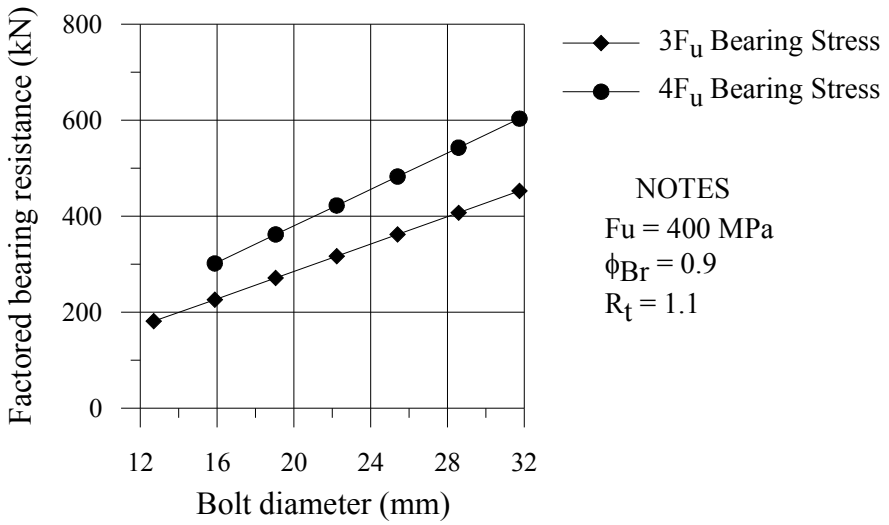

Figure 3.3: Range of B_r values in a two-bolt connection when A36 steel (F_u = 400 MPa) is used.

Table 3.4: Design aid when designing ductile bolted connections

	Bolt diameter and bolt shear capacity				
t	½	5/8	3/4	7/8	1
(mm)	V_r = 503 kN	V_r = 787 kN	V_r = 1133 kN	V_r = 1542 kN	V_r = 2014 kN
6	407	509	611	713	815
7	475	594	713	832	951
8		679	815	951	1086
9		764	917	1069	1222
10			1018	1188	1358
11			1120	1307	1494
12				1426	1629
13					1765
14					1901

An engineer can enter this table with a connection factored load of, for example, 1000 kN, and find that he or she has the choice to use a four-bolt connection with either ¾" bolts with a 10 mm plate, 7/8" bolts with a 9 mm plate, or 1" bolts with an 8 mm plate.

3.3. Phase II Test Program

Section 3.3 will present the test program used to evaluate the effect of certain parameters on the ductility of two-bolt connections failing under bearing stresses. The test specimens, the test setup, and the loading protocols will also be explained.

3.3.1. Test Specimens

As with Phase I, the Phase II test specimens will consist of two back-to-back angles connected by gusset plates bolted at one end and welded at the other. The bolted end is considered the "weak" end (the one undergoing failure) while the welded end is considered the "strong" end (remains elastic and undergoes negligible deformations during testing). Again, the angles were large enough to accommodate a bolt with the proper edge distances in one of its legs and were manageable in size enough for an average person to move them around by hand. All angles are approximately 1000 mm in length and 490 bolts (19.05 mm, or ¾", and 25.4 mm, or 1") were used to connect the angles to the gusset plate in all specimens. E490XX weld electrodes were used for welding the strong end, and G40.21 350W steel (F_y = 350 MPa, F_u = 450 MPa) was specified for the angles and plates.

Table 3.5 on page 96 shows the proposed Phase II test program specimens and Figure 3.4 to Figure 3.7 show the specimen shop drawings. There are 22 specimens including duplicates. Specimen identification numbers are given in Table 3.5. The first letter, B, refers to "Bearing". The second letter refers to either Round or Slotted holes. The third letter specifies whether the holes are Drilled or Punched. The following numbers and letters refer to the bolt end distance and bolt spacing in terms of bolt diameters, d. For example, 4D5D refers to a specimen with an end distance of four times the bolt diameters and a bolt spacing of five times the bolt diameter. If a "T" is appended at the end of the specimen number, a thicker gusset plate is used.

The bearing ratio of all specimens varies between 3.99 and 5.47, thus predicting a bearing failure rather than a net section failure in the gusset plates. The gusset plate

width is constant at 230 mm. The hole diameters in the gusset plates and angles are constant at a standard 2 mm (1/16") larger than the bolt diameter and are drilled in all but specimen: BRP4D5D. The bolt holes in the gusset plate vary between a standard hole and a slotted hole, and between punched and drilled. The welded gusset plate is the same for all but one specimen and is considerably stronger than the weaker bolt gusset plate.

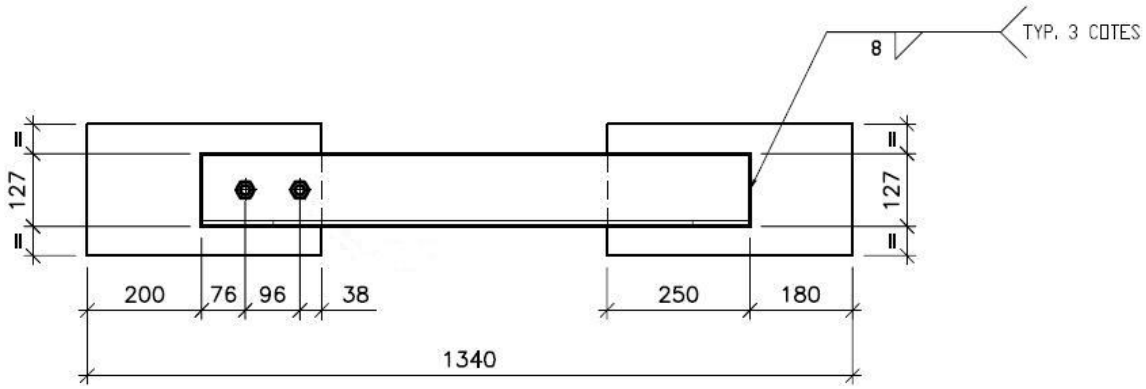

Figure 3.4: Specimen BRD2D5D

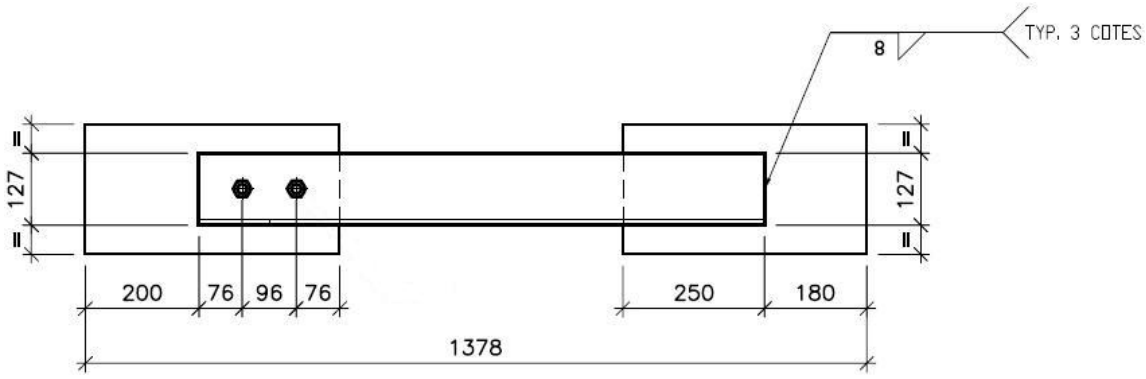

Figure 3.5: Configuration for specimens BRD4D5D, BRP4D5D, and BSD4D5D.

Table 3.5: Proposed Phase II specimens

Specimen #	Quantity	Angles	d (mm)	Hole Type	Hole Type	Bolt Grade	t_g (mm)	$L_{e,gusset}$ (mm)	s (mm)	$L_{e,angle}$ (mm)	L_{weld} (mm)
BRD2d5d	3	2L127x76x9.5	19.1	Standard[1]	Drilled	ASTM-A490	8	38	96	76	250
BRD4d5d	6	2L127x76x9.5	19.1	Standard	Drilled	ASTM-A490	8	76	96	76	250
BRD5d6d	3	2L127x76x9.5	19.1	Standard	Drilled	ASTM-A490	8	96	115	76	250
BRP4d5d	3	2L127x76x9.5	19.1	Standard	Punched	ASTM-A490	8	76	96	76	250
BSD4d5d	3	2L127x76x9.5	19.1	Short-Slotted[2]	Drilled	ASTM-A490	8	76	96	76	250
BRD15d3dT	4	2L152x102x16	25.4	Standard	Drilled	ASTM-A490	13	38	76	76	300

[1] Standard holes are 1/16" of an inch (1.6 mm) larger than the bolt diameter.

[2] Short-slotted holes are 21.1 mm x 25.1 mm, perpendicular to the direction of loading.

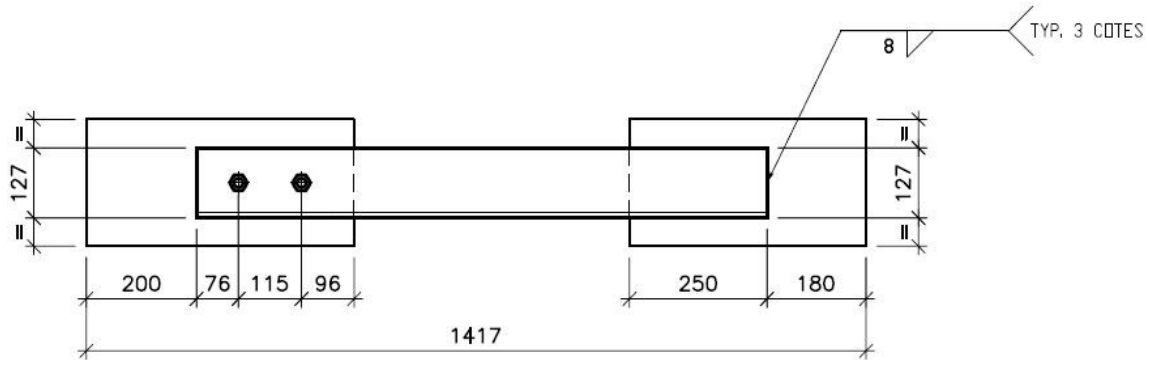

Figure 3.6: Specimen BRD5D6D

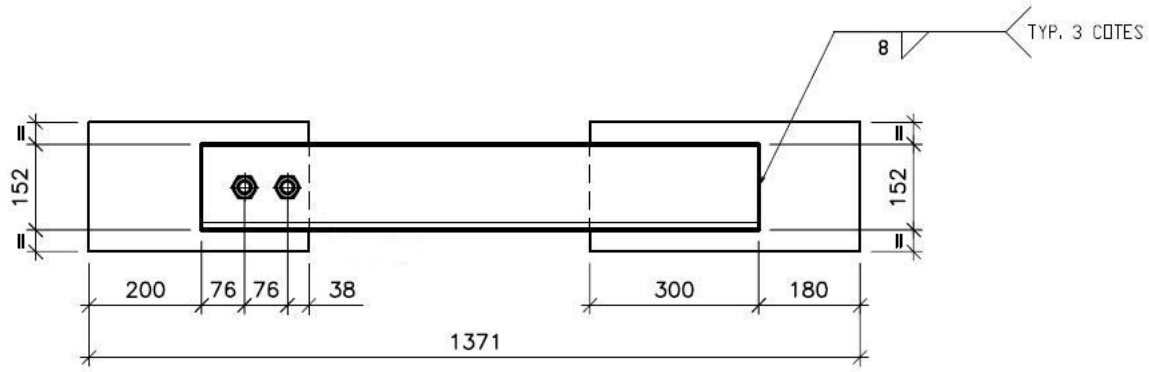

Figure 3.7: Specimen BRD15D3DT.

3.3.2. Apparatus

The same tension-compression 2500 kN capacity Instron load frame from Phase I was used to perform the testing in Phase II. Two LVDTs were used to capture deformations in the bolted gusset plate only. Each LVDT was mounted on a magnetic base and attached to the angle's outstanding leg, just above the interior bolt. The stems from both LVDTs then rested on two small aluminum angles which were clamped to the gusset plate. Photo 3.1-A shows a typical specimen mounted in the load frame, while Photo 3.1-B shows the placement of the LVDTs and the position of the aluminum angles on which the stems rest. The range of deformations captured is therefore equal to the distance from just above the press' grips (below which no deformations are taking place) to just above the interior bolt on the angles; all deformations measured therefore come from the connection, and elastic deformations of the angles are not captured, as

was the case in Phase I. Any slip taking place between the hydraulics grips on the gusset plates is also not captured by the LVDTs. The final deformation of the connection is taken as the average of the two LVDTs. As shown in Photo 3.1-B, the outstanding legs of the angles were coped to accommodate the width of the cavity in which the hydraulic grips are located.

A) Typical specimen in load frame

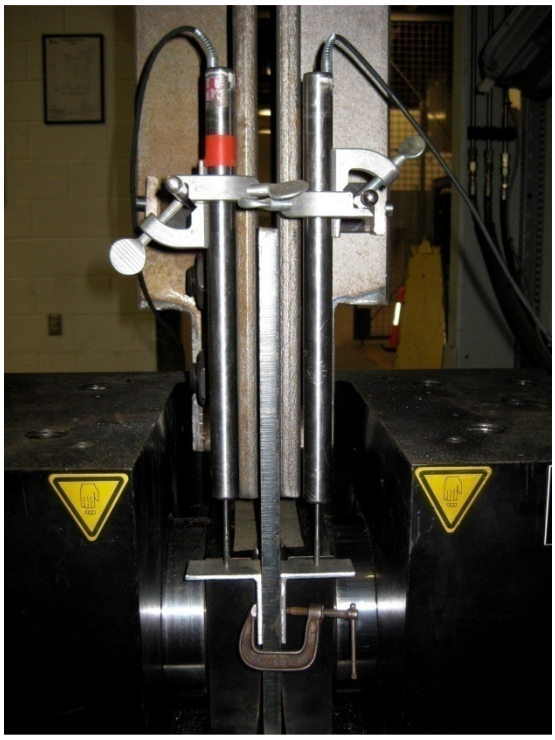

B) LVDTs and supports.

Photo 3.1: Specimen setup.

3.3.3. Procedure

All specimens arrived to the structures lab assembled and were unbolted and inspected before testing began. All specimens were then bolted to the snug-tight position except for specimen BRD4D5D-6, on which the turn-of-nut method was used to pretension the bolts.

ATC report P695 states the ultimate deformation capacity of a structural component can be conservatively measured at 80% of the ultimate load encountered in the test in the

post-peak region (ATC 2009). In order to ensure the tests would exceed this point, they were continued until the load had dropped to roughly 50% of the ultimate load. During cyclic loading, if the load had not reached this point during its last cycle another tension cycle was added afterwards.

3.3.3.1. Monotonic Loading Protocol

The displacement rate used in Phase I for specimen D03X, 3.5 mm/min as shown in Table 2.1, was kept for use for all specimens in Phase II. Static loading conditions were thus maintained for all specimens to better validate the bearing design equation as well as the tear-out equation for specimens BRD2D5D and BRD15D3DT.

3.3.3.2. Cyclic Loading Protocol

Contrary to Phase I, cyclic loading protocols were also used in Phase II to evaluate the degradation of the bolt bearing failure mode. In order to determine the number of cycles, two nonlinear OpenSees (McKenna et al., 2004) models from Chapter 4 were closely looked at: VaC15.6N04sSXE and VaC30.6N08sSXE. Both these models represent a 4- and an 8-storey building on site class C with X-bracing split over two storeys. Connections are modeled at the bottom of every brace to represent a bearing failure and these were looked at to determine the statistics regarding the number of excursions during an earthquake. Ten ground motions were looked at in both buildings and tension and compression cycles were looked at independently.

Figure 3.8 shows the number of cycles in both models. The frequency corresponds to the number of cycles a connection undergoes and includes any brace at any level. The figure shows the 4-storey building connections undergo a median of 4 cycles, while the 8-storey building connections underwent 3 cycles. Based on this graphic it was decided to use 4 cycles.

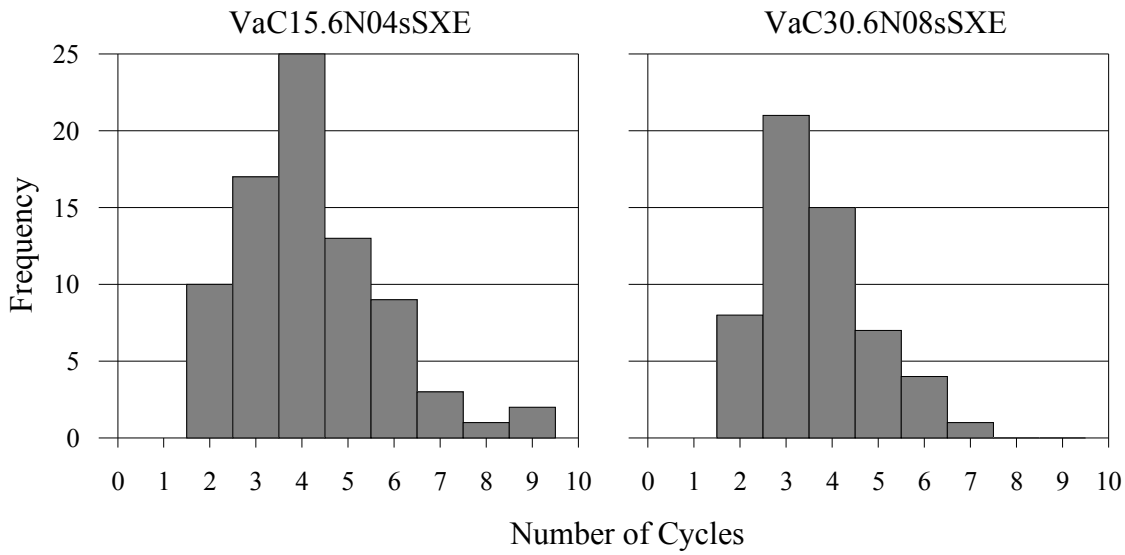

Figure 3.8: Number of cycles in 4- and 8-storey nonlinear OpenSees models.

The deformation at rupture was estimated to be approximately 30 mm for bearing failures, as shown in Table 2.18 of Phase I. The specimens in Phase II, who are undergoing bearing failure in only one end but have larger end distances and bolt spacings to promote a bearing failure, are expected to undergo roughly the same amount of deformation. A spacing between the bottom of the angles and the top of the grips from the Instron press of 40 mm was chosen. This enabled a compression deformation of up to 40 mm; a maximum deformation in compression of 36 mm (tension and compression) was chosen to further ensure the angles would not come into contact with the grips.

Albeit simple, it is important to visualize what is happening to a connection undergoing bearing failure during cyclic loading. Figure 3.9 visually depicts what is happening. After every load reversal, the bolt is simply traveling in a hole which has become slotted and parallel to the direction of the loading. Nothing of interest is happening here: we are simply seeing what kind of slip resistance is offered from the time the bolt leaves one end of the hole and makes its way to the opposite end and comes into bearing again. What is of interest is what is happening once the bolt is back into bearing and further elongates the hole. For this reason, it was decided to accelerate the rate of deformation

by a factor of 2.5 when the bolt is travelling inside the hole in order to reduce the testing time. There is also no need to follow up a completed cycle with another cycle that has a smaller amplitude, as the bolt would not come into bearing against the gusset plate. For this reason, four cycles of equal increasing amplitudes are used to observe the degradation of the gusset plate failing under bearing failure. To further observe the extent of degradation, two specimens were tested under cyclic loading with eight cycles of equal increasing amplitudes with the same total amplitude as the 4-cycle protocol.

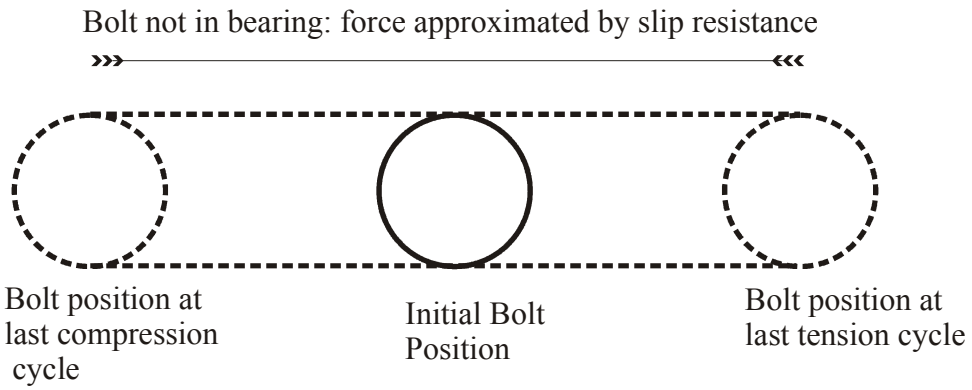

Figure 3.9: Drawing depicting the bolt movement during cyclic loading.

The four different cyclic loading protocols used in Phase II, along with their identification numbers, are shown in Figure 3.10. Protocol 4-36T36C is the standard protocol, and has 4 cycles totalling 36 mm in tension and 36 mm in compression. Table 3.6 shows the loading protocol used in all specimens. The rate of deformation used when the bolt is bearing against the gusset plate is the same as the rate used in monotonic tests: 3.5 mm/min. This rate is increased to 8.75 mm/min when the bolts are travelling between either ends of the deformed hole. The latter is dropped back down to 3.5 mm/min when the bolts are approximately 3 mm from coming back into bearing against the plate. As mentioned above, all protocols have cycles with amplitudes that increase by an equal amount.

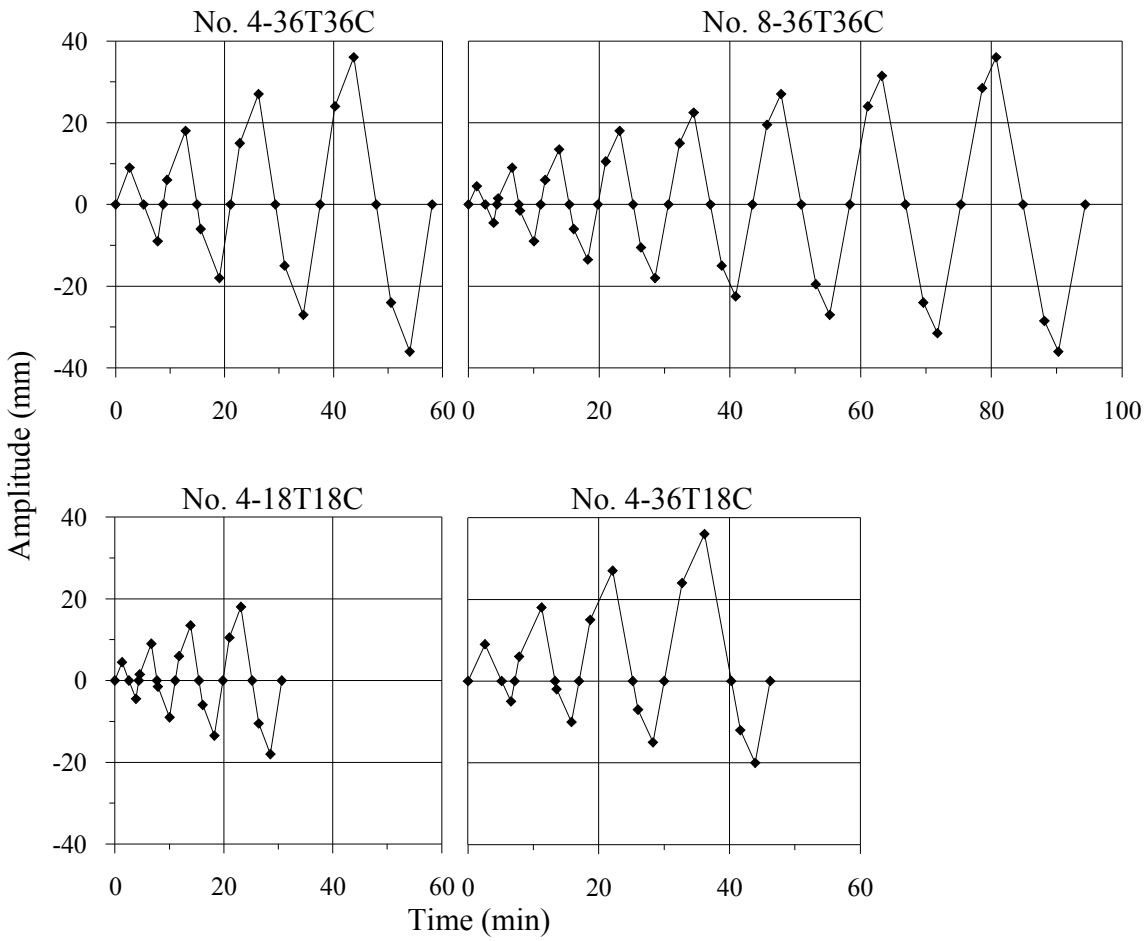

Figure 3.10: Cyclic loading protocols used and their identification numbers.

As shown in Table 3.6, the majority of the specimens are tested under the protocol 4-36T36C. Specimen BRD4D5D-4 and -5 were tested under 8-36T36C to look at the effect of having more cycles. Specimen BRP4D5D-3 was tested under 4-36T18C because of the presence of "free standing" drilled holes which would have come into play during the compression cycles; the total amplitude in compression deformations was reduced to 18 mm for this reason. The presence of these drilled holes is explained in section 3.4.4. Specimens BRD15D3DT-2 and -3 were tested under 4-18T18C, a protocol with half the total amplitudes, because of their smaller capacity for total deformation (smaller bolt spacings). Again, if 50% of the ultimate load after the latter

was not reached following 4 complete cycles, an additional tension cycle going up to 50 mm in deformation if needed was added.

Table 3.6: Loading protocol used for Phase I specimens

Specimen		Monotonic	Cyclic
BRD2D5D -	1	✓	
	2		4-36T36C
	3		4-36T36C
BRD4D5D -	1	✓	
	2		4-36T36C
	3		4-36T36C
	4		8-36T36C
	5		8-36T36C
	6		4-36T36C
BRD5D6D -	1	✓	
	2		4-36T36C
	3		4-36T36C
BRP4D5D -	1	✓	
	2	✓	
	3		4-36T18C
BSD4D5D -	1	✓	
	2		4-36T36C
	3		4-36T36C
BRD15D3DT -	1	✓	
	2	✓	
	3		4-18T18C
	4		4-18T18C

3.3.4. Design of Specimens

As shown in Table 3.5, there were a total of 22 specimens with six sub-group specimens to design. The connection nominal (P_n), factored (ϕP_n), expected (P_e), and anticipated capacities (P_a) for different connection failure modes are all reported in this section. It must be noted that during the design phase, the gusset plate coupon tests had not been performed and the design of the specimens was based on the expected capacities, which are calculated with R_y and R_t values. P_a values are given in this section for comparison purposes and for convenience as they became available at the time of writing. P_e values

were therefore used to judge as to whether or not a specimen would break in the desired manner.

For all specimen parts, G40.21 350W steel (F_y = 350 MPa, F_u = 450 MPa) was specified and its actual mechanical properties were used in the design phase. The CSA standard was used for design, and the AISC and the draft CSA-09 were used as well when determining the bearing and tear-out resistances.

Since specimens were undergoing cyclic loading in Phase II, the compression capacity, or the buckling capacity, of the gusset plate had to be checked. The standard equation from clause 13.11 of CSA was used with an effective length factor of 1; both the bottom and the top of the unsupported gusset plate length were restrained against rotation by the press' grips and by the angles.

Table 3.7 shows the connection capacities for each specimen calculated using references CSA-S16S1 (2001), CSA-S16-09 (2009), and AISC (2005). In all cases, the ultimate bearing resistance was taken as $4F_u$, rather than the $3F_u$ given in each standard. In addition to further ensuring that bearing failures were governing, this is consistent with the findings of Cai and Driver who found that the connection capacities in tear-out and bearing were better approximated with the unified equation (found in CSA-09) for bolt tear-out failures and $4F_u$ in the bearing resistance equation. This was explained in section 1.1.10.

Table 3.7 shows that CSA-01 gives more conservative connections capacities when bolt tear-out governs over bearing. Of course, when bearing failure governs the capacities are all the same as all standards use the same bearing resistance formula.

Table 3.7: Capacities of Phase II specimens

	CSA[1]				CSA-09[2]				AISC[3]			
	P_n	ϕP_n	P_e	P_a	P_n	ϕP_n	P_e	P_a	P_n	ϕP_n	P_e	P_a
Specimen	kN				kN				(kN)			
BRD2D5D	476	365	524	540	422	330	464	476	426	319	468	483
BRD4D5D	550	369	605	625	550	440	605	625	550	413	605	625
BRD5D6D	550	369	605	625	550	440	605	625	550	413	605	625
BRP4D5D	550	369	605	625	550	440	605	625	550	413	605	625
BSD4D5D	550	369	605	625	550	440	605	625	550	413	605	625
BRD15D3DT	731	556	804	817	604	453	664	643	548	411	603	613

[1] Clauses 13.10.(c) for bearing and 13.11.(a) for tear-out were used.

[2] Clauses 13.12.1.1.(a) for bearing and 13.11 for tear-out were used.

[3] Equation J3-6b, which looks at bearing and tear-out, was used.

3.3.4.1. Specimen BRD2D5D

Specimen BRD2D5D has a bolt end distance of 2 bolt diameters and a bolt spacing of 5 bolt diameters. The goal of this specimen was to observe the difference in behaviour and deformation capacity when the exterior bolt's governing failure mode is a tear-out, rather than a bolt bearing failure. Table 3.8 shows the bearing capacities calculated with CSA, CSA-09, and AISC, while Table 3.9 shows the other CSA connection capacities which were checked during the design phase.

The expected capacities, P_e, were used to judge whether or not the specimen was adequate and a bearing failure would govern. Conservatively, the maximum bearing capacity, in this case coming from CSA, was used to compare with the other failure modes. For specimen BRD2D5D, this bearing capacity was 540 kN in tension, which is well below the other important failure modes shown in Table 3.9. In compression, however, there is no end distance and both bolts are undergoing bearing failures. The expected capacity in this case is therefore equal to 605 kN, which is smaller than both the bolt shear capacities and the gusset buckling load.

Table 3.8: Bearing capacities of BRD2D5D specimen

	Tension				Compression			
	P_n	ϕP_n	P_e	P_a	P_n	ϕP_n	P_e	P_a
	(kN)				(kN)			
CSA	476	365	524	540	550	369	605	625
CSA-09	422	330	464	476	550	440	605	625
AISC	426	319	468	483	550	413	605	625

Table 3.9: Connection capacities of BRD2D5D specimen

		P_n	ϕP_n	P_e	P_a
	Equation #	(kN)			
Gusset - Ag	13.2.(a).(i)	644	580	708	705
Gusset - An	13.2.(a).(ii)	641	577	705	728
Gusset buckling	13.3.1	635	571	697	693
Bolt - Vr	13.12.1.1.(b)	712	569	712	712
Angles - Ag	13.2.(a).(i)	1295	1166	1295	-
Angles - An	13.2.(a).(iii)	906	815	906	-
Angles - Br	13.10.(c), 13.11.(a)	983	659	983	-
Angles - T + V	13.11.(a)	1060	795	1060	-

3.3.4.2. Specimens BRD4D5D + BRP4D5D + BRD5D6D

Specimens BRD4D5D, BRP4D5D, and BRD5D6D were grouped together since they all undergo bearing failures; their gusset plates all have the same capacities under the different failure modes that are looked at. The only difference comes in specimen BRD5D6D which has different spacings (with which bearing failures also govern). Table 3.10 shows the bearing capacities (no need to show tension and compression capacities such as Table 3.8, since a bearing failure is also expected under a tensile load) calculated using three different standards and Table 3.11 shows the connection capacities for other failure modes. The only difference between the three standards in Table 3.10 comes when ϕ factors are used: the three standards shown use 0.67, 0.8, and

0.75, respectively. Using 605 kN as the expected bearing capacity, we see that there are no other failure modes which govern over bearing.

Table 3.10: Bearing capacities of specimens failing under pure bolt bearing

	P_n	ϕP_n	P_e	P_a
	(kN)			
CSA	550	369	605	625
CSA-09	550	440	605	625
AISC	550	413	605	625

Table 3.11: Connection capacities of BRD4D5D, BRP4D5D, and BRD5D6D specimens

		P_n	ϕP_n	P_e	P_a
	Equation #	(kN)			
Gusset - Ag	13.2.(a).(i)	644	580	708	705
Gusset - An	13.2.(a).(ii)	641	577	705	728
Gusset buckling	13.3.1	635	571	697	693
Bolt - Vr	13.12.1.1.(b)	712	569	712	712
BRD4D5D + BRP4D5D angle capacities					
Angles - Ag	13.2.(a).(i)	1295	1166	1295	-
Angles - An	13.2.(a).(iii)	906	815	906	-
Angles - Br	13.10.(c), 13.11.(a)	983	659	983	-
Angles - T + V	13.11.(a)	1060	795	1060	-
BRD5D6D angle capacities					
Angles - Ag	13.2.(a).(i)	1295	1166	1295	-
Angles - An	13.2.(a).(iii)	847	847	847	-
Angles - Br	13.10.(c), 13.11.(a)	983	659	983	-
Angles - T + V	13.11.(a)	1147	861	1147	-

3.3.4.3. Specimen BSD4D5D

Specimens BSD4D5D had perpendicular slotted holes measuring 21.1 x 25.1 mm. After discussions with the CANAM group, who supplied and fabricated the specimens, it was believed these holes were to be made with a single punch. After dismantling the specimens and closely inspecting the holes, it was determined that these were actually

drilled; two 13/16" (20.6 mm) holes were drilled side-by-side to create a short-slotted hole.

Table 3.12 shows the different bearing capacities calculated with three different standards (with bearing failures under both compression and tension loads), while Table 3.13 shows the other important capacities under different failure mechanisms. As slotted holes offer the same bearing resistance as standard ones (Frank et al. 1981), the specimen's expected capacity is the same as specimen BRD4D5D. We see that no other failure mode is of concern against bearing failures.

Table 3.12: Bearing capacities of specimen BSD4D5D

	P_n	ϕP_n	P_e	P_a
	(kN)			
CSA	550	369	605	625
CSA-09	550	440	605	625
AISC	550	413	605	625

Table 3.13: Connection capacities of specimen BSD4D5D

		P_n	ϕP_n	P_e	P_a
	Equation #	(kN)			
Gusset - Ag	13.2.(a).(i)	644	580	708	705
Gusset - An	13.2.(a).(ii)	641	577	705	728
Gusset buckling	13.3.1	635	571	697	693
Bolt - Vr	13.12.1.1.(b)	712	569	712	712
Angles - Ag	13.2.(a).(i)	1295	1166	1295	-
Angles - An	13.2.(a).(iii)	906	815	906	-
Angles - Br	13.10.(c), 13.11.(a)	983	659	983	-
Angles - T + V	13.11.(a)	1060	795	1060	-

3.3.4.4. Specimen BRD15D3DT

Specimens BRD15D3DT were used to look at the effect of having a thicker gusset plate, and to observe whether or not bearing failures are attainable in them. Because of

limitations with the Instron press, a 13 mm (1/2") thick gusset plate was used with two bolts. Table 3.14 offers the bearing capacities in tension and compression, while Table 3.15 gives the capacities of other failure modes of interest.

Table 3.14: Bearing capacities of specimen BRD15D3DT

	Tension				Compression			
	P_n	ϕP_n	P_e	P_a	P_n	ϕP_n	P_e	P_a
	(kN)				(kN)			
CSA	731	556	804	817	1006	674	1106	1124
CSA-09	604	453	664	643	1006	804	1106	1124
AISC	548	411	603	613	1006	754	1106	1124

Table 3.15: Connection capacities of BRD15D3DT specimens

		P_n	ϕP_n	P_e	P_a
	Equation #	(kN)			
Gusset - Ag	13.2.(a).(i)	886	797	974	883
Gusset - An	13.2.(a).(ii)	854	769	940	955
Gusset buckling	13.3.1	880	792	967	878
Bolt - Vr	13.12.1.1.(b)	1259	1007	1259	1259
Angles - Ag	13.2.(a).(i)	2653	2388	2653	-
Angles - An	13.2.(a).(iii)	1466	1319	1466	-
Angles - Br	13.10.(c), 13.11.(a)	1922	1461	1922	-
Angles - T + V	13.11.(a)	1700	1275	1700	-

We see that bearing failure will govern comfortably in tension, but not so much in compression; buckling of the gusset plate may cause a problem. It was decided to go ahead with this design and use further restraints on the gusset plate to prevent buckling during testing.

3.4. Post Test Measurements and Observations

Such as in Phase I, each bolted specimen was dismantled to further investigate the connection deformations. Since the angles were designed not to yield during testing, the

only parameter which could influence the measure of ductility in the specimens were bearing deformations found in the angles, which were measured and recorded before disposing of the specimens. Elastic deformations taking place in the back-to-back angles were outside the range of deformations captured by the LVDTs. It was judged that no significant deformations took place within the connection in the angles (yielding, net area), other than for occasional bearing deformations. In order to better evaluate a gusset plate's capacity to deform in bearing failures, the tables of section 3.4 will report δ values which exclude bearing deformations in the angles.

The mechanical properties of the gusset plates used in the specimens were determined using ASTM-E8, such as in Phase I. No coupon tests were performed with steel coming from the angles, as no ruptures or plastic deformations were taking place in these. The coupons were loaded into the same Instron load frame used for testing specimens in Phase II, and were therefore loaded with a constant rate of deformation, contrary to the coupons tested in Phase I and whose results are reported in Table 2.9 of page 59. The extensometer was therefore allowed to remain on the coupons all the way through the test and through the rupture point; ε_{ult} and ε_{rupt} are therefore available. Table 3.16 offers a summary of these results. With the help of these results, anticipated capacities, P_a, are calculated for three codes and are shown in Table 3.17, along with average ultimate loads under monotonic and cyclic loading. Again, P_a capacities are calculated without ϕ factors and without R_y and R_t.

Table 3.16: Results of steel coupon tests

Coupon #	Thickness (mm)	Width (mm)	F_y (MPa)	F_u (MPa)	ε_y	ε_{sh}	ε_{ult}	ε_{rupt}
1	8.30	38.25	382	510.0	0.0021	0.0200	0.1457	0.2326
2	8.32	38.28	380	507.0	0.0020	0.0193	0.1368	0.2468
3	8.08	38.62	386	516.0	0.0019	0.0221	0.1613	0.2387
4	13.15	38.26	349	507.0	0.0018	0.0170	0.1821	0.2588
5	13.24	38.40	351	504.0	0.0018	0.0202	0.1930	0.2612
6	13.35	38.42	346	499.0	0.0018	0.0171	0.1770	0.2600
	8 mm plate average:		**383**	**511**				
	13 mm plate average:		**349**	**503**				

Table 3.17: Anticipated Phase II specimen capacities and experimental ultimate loads

	$P_{a,CSA}$ (kN)	$P_{a,CSA-09}$ (kN)	$P_{a,AISC}$ (kN)	Mono $P_{u,exp}$ (kN)	Cyclic $P_{u,exp}$ (kN)
BRD2D5D	540	476	483	485	486
BRD4D5D	625	625	625	683	632
BRD5D6D	625	625	625	769	729
BRP4D5D	625	625	625	679	645
BSD4D5D	625	625	625	661	640
BRD15D3DT	817	643	613	683	737

From Table 3.17, we see that very high load levels were achieved in both monotonic and cyclic tests in bearing failures (spacings 4D5D and higher). The 625 kN anticipated capacity was calculated with $4F_u$; all bearing failures achieved a higher load. The closest anticipated bearing capacity was that of the BRD4D5D specimens undergoing cyclic tests. In every bearing failure, monotonic tests lead to higher ultimate loads; material degradation therefore exists in bearing failures. Specimen BRD2D5D had very similar ultimate loads for both monotonic and cyclic tests. Specimen BRD15D3DT experienced a higher ultimate load under cyclic loading. CSA-09 and AISC gave better capacity estimates in specimen BRD2D5D, while CSA-01 gave better estimates of specimen BRD15D3DT's capacity.

3.4.1. Specimen BRD2D5D

Figure 3.11 shows the load versus displacement behavior of specimen BRD2D5D and Table 3.18 gives the relevant information from these plots. Pictures of the specimens are seen in Photo 3.2 through Photo 3.4.

The monotonic test began with sharp noises such as those heard in Phase I, indicating some slippage was taking place. However, the slippage is not noticeable in Figure 3.11 as it was in the load versus displacement behavior of the specimens from Phase I, most likely because all specimens from Phase II had bolts which were snug-tightened at the laboratory. Approximately 1 mm can be attributed to slippage. The specimen remained elastic up to a deformation of approximately 6 mm, from where the load flattened

gradually. At 11 mm of deformation, or 440 kN, a small bulge could be seen on top of the gusset plate, above the interior bolt. This indicates the bearing resistance of the gusset plate at the exterior bolt was most likely exceeded, and the two shear planes extending from the side of the hole to the edge of the plate were yielding, or close to rupturing. The bolt was therefore forcing a "plug" of material outwards as seen in Photo 3.2-C, which was seen as a bulge on the edge of the plate during testing. A small crack started to form in the gusset plate above the interior (top) bolt at approximately 20 mm in deformation and became fully open at about 24.5 mm. This corresponds to the sharp drop in load in the plot. From this point on, the entire resistance is provided by the exterior (bottom) bolt bearing against the material between the two bolts, as seen in Photo 3.2-D. The shear planes on either side of the exterior bolts can also be seen in this picture. Like that of specimens D03X in Phase I, there was clear widening of the gusset plate at failure.

In the cyclic testing of specimens BRD2D5D-2 and -3, specimen -3 was tested first. Similar to specimen -1 loaded in tension, a bulge above the top bolt was discernable at a deformation of 10 mm in tension (2^{nd} tension cycle). Before the end of this 2^{nd} tension cycle, a crack could not be noticed atop the interior bolt in the gusset plate. In compression, once the bolt comes back into bearing against the gusset plate, the load returns to where it last left better than what can be seen in tension. This is most likely due to the fact that the plate is undergoing a pure bearing failure in compression, whereas the interior bolt is undergoing a tear-out failure in tension. In the third tension cycle, a crack started to form above the top bolt before the bolts were allowed to come back into bearing. This prevented the load from returning to where it was at the end of the 2^{nd} cycle. In the third compression cycle, significant gusset buckling could be seen and it was decided to stop the test for fear of having invalid results. The buckling of the gusset plate can be seen in Photo 3.3-A. The gusset plate's buckling capacity was calculated using an unsupported length of 40 mm and an effective length factor of 1.0 to represent both ends being restrained against rotation, but with one end allowed to move laterally. It is believed the gusset plate buckled because the grips only restrained 160

mm of the gusset plate in width; 35 mm strips of plate were therefore on either side of the grips and were not restrained. For future tests, four steel plates were wedged between the gusset plate and the cavity of the press for added support. Some buckling was still seen in the future tests, but this was restrained to the far edges of the gusset plates and is not believed to have affected the results to a significant degree.

With its gusset plate restrained from buckling, specimen BRD2D5D-2 underwent the complete cyclic protocol 4-36T36C. Nothing pertinent took place during the first complete cycle. During the 2nd tension cycle, a small bulge could be seen above the top bolt at 9 mm, with a crack starting to form at 13 mm. At the start of the third tension cycle, the crack continued to spread and was completely open (as indicated by a loud noise) at a deformation of about 17 mm. During the third compression cycle, the angles were separating from the gusset plate; this is most likely due to a pile-up of the material next to the bolt hole, typical of a bearing failure. The material pile-up was spreading outwards and pushing the angles out. In the 4th tension cycle, the load never reached the load level of the 3rd cycle. At a deformation of 17 mm, loud noises were heard, indicating the material above the top bolt had split, and a sharp drop in load immediately followed. In the 4th compression cycle, a small amount of warping took place on the edge of the gusset plate as shown in Photo 3.3-B. Photo 3.4 offers a look at the shear planes undergoing rupture on both sides of the outer bolt.

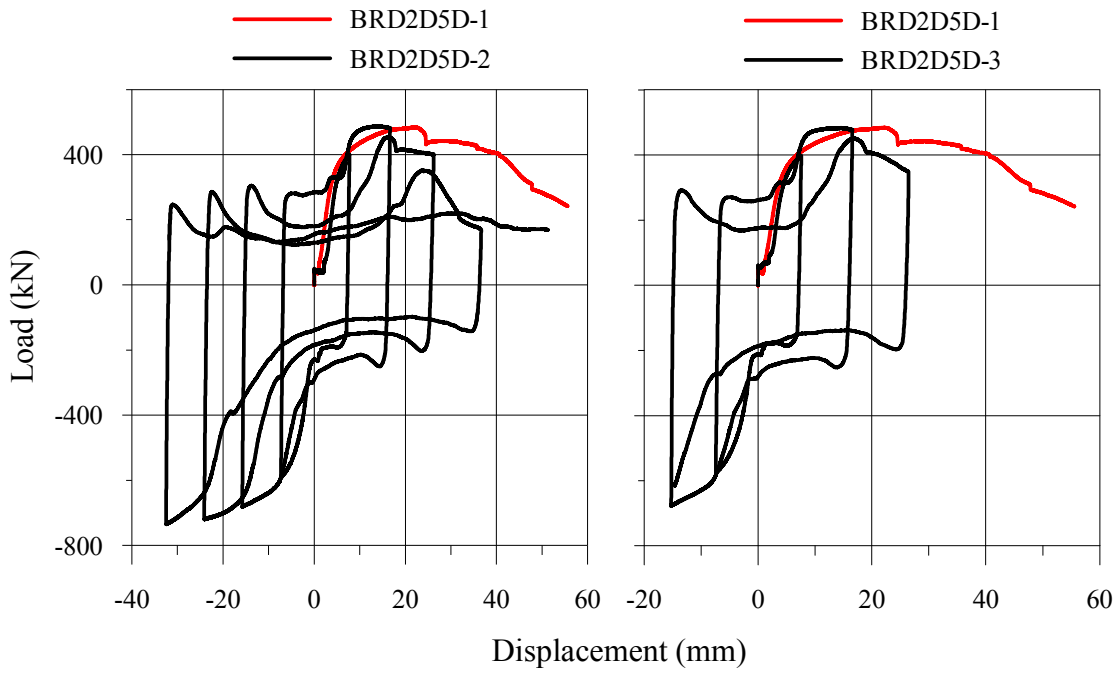

Figure 3.11: Monotonic and cyclic testing of specimen BRD2D5D.

Table 3.18: BRD2D5D experimental results

Specimen #	$P_{u,exp}$ (kN)	δ_u (mm)	δ_{rupt} (mm)	Loading
BRD2D5D-1	485	22.2	41.7	Mono
BRD2D5D-2	488	13.8	22.0[1]	4-36T36C
BRD2D5D-3	484	14.6	25.0	4-36T36C

[1] 80% of the load was never actually achieved. As the load was dropping during the second tension cycle, the load reverses before this 80% was reached. Upon the third tension cycle, the load never reached 80% of the maximum load. The deformation at 80% was thus taken as the deformation at the end of the third tension cycle.

A) Failed gusset plate.

B) Close-up of both failed holes.

C) Close-up of exterior bolt hole.

D) Close-up of interior bolt hole.

Photo 3.2: Specimen BRD2D5D-1, tested under monotonic loading.

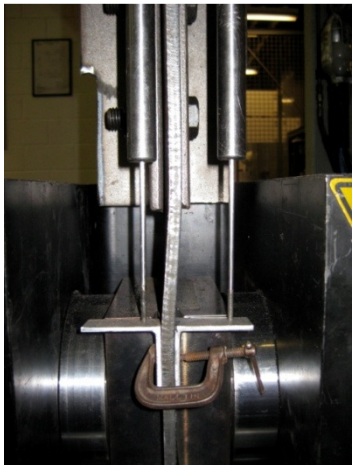

A) Plate buckling in specimen BRD2D5D-3.

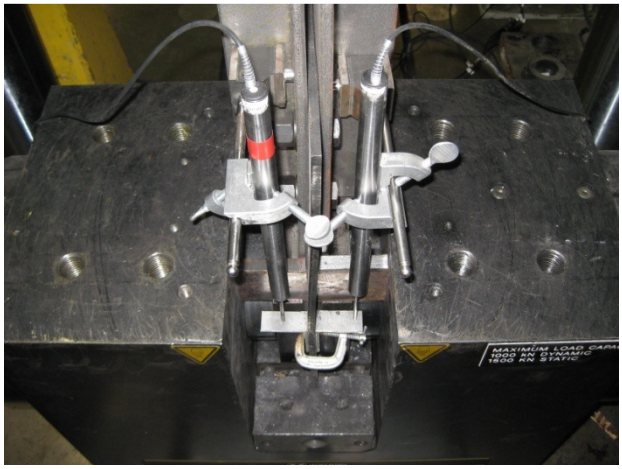

B) Warping of gusset plate edge in BRD2D5D-2

Photo 3.3: Buckling of the gusset plate in specimen BRD2D5D-3.

A) Specimen -2

B) Specimen -3

Photo 3.4: Specimen BRD2D5D tested under cyclic loading.

The average ultimate load seen in the specimens was 486 kN, which was estimated best by CSA-09 and AISC with calculated capacities of 476 kN and 483 kN, respectively. CSA-01 estimated the capacity at 540 kN, suggesting that the shear capacity term of equation 13.11.(a).(ii) did not provide a good estimate of the tear-out capacity of the exterior bolt. Under cyclic loading, the deformation at ultimate was on average 36% smaller than δ_u under monotonic loading while deformation at rupture was on average 44% smaller.

3.4.2. Specimen BRD4D5D

Figure 3.12 shows the 5 different plots of specimens BRD4D5D, with the monotonic results plotted with the cyclic tests. The monotonic results (specimen BRD4D5D-1) are shown on every plot as the lighter coloured line. Table 3.19 provides the key parameters of these plots. Photo 3.5 and Photo 3.6 show selected pictures of the monotonic and cyclic loading tests, respectively.

The monotonic test, specimen BRD4D5D-1, started with very little noise compared to what was heard in Phase I specimens. This is due to the fact that bolts were manually snug-tightened in the laboratory. As with specimen BRD2D5D, the specimen behaved elastically up to a deformation of roughly 6 mm, after which the load gradually flattened. The first noticeable change in the specimen was a bulge that could be seen

atop the gusset plate, above the interior (top) bolt, at a deformation of roughly 20 mm. This is the same bulge that was seen in specimen BRD2D5D and which will be seen in the subsequent tests. Cracks started to appear in the location of the bulge as the ultimate load was reached, and this crack further opened at the first sharp drop in load at a deformation of 32 mm. The same crack split wide open at a deformation of 40 mm, where a drop in load is clearly discernable.

Specimens BRD4D5D-2 and -3 were subjected cyclic loading protocol 4-36T36C. In both specimens, no changes to the gusset plate were noticeable during the first two complete cycles. During the third tension cycle, the familiar bulge atop the gusset plate above the top bolt could be seen at a deformation of roughly 20 mm, such as the specimen BRD4D5D-1. Before the load reversed, some necking had taken place and a small crack had begun to develop across the gusset plate in the same area. Some separation of the angles could be seen during the third compression cycle, caused by the piling-up of material in the immediate vicinity of the bolt hole. A small amount of warping took place on the edges of the gusset plate and is not believed to have affected the results, as there is good agreement between the third and second compression cycles. During the fourth tension cycle, the crack which had developed during the third tension cycle continued to widen and caused the load to drop gradually. The load dropped sharply at a deformation of 26 mm and 24 mm, respectively, for specimens BRD4D5D-2 and -3 after the crack had split open. This crack is shown in Photo 3.6-B.

Specimens BRD4D5D-4 and -5 were tested under cyclic loading protocol 8-36T36C, with the goal of observing whether an increase in cycles would increase the degradation of the gusset plate. Both specimens behaved very similarly, as can be seen in Figure 3.12. Nothing of interest happened during the first four cycles, except for some separation of the angles in the fourth tension cycle of specimen -5, indicating piling-up of the material close to the bolt hole was taking place. Both specimens had necking above the interior bolt appear before the end of the fifth tension cycle at a deformation of roughly 19 mm. Necking continued to take place during the subsequent cycles, with

cracks appearing before the end of the sixth cycle, at a deformation of 25 mm. In both specimens, this crack continued to widen during the seventh tension cycle, causing the load to drop, and appeared to split open and cause a quick drop in load just moments before the load reversed for the seventh compression cycle.

Specimen BRD4D5D-6 had pretensioned bolts and underwent the cyclic loading protocol 4-36T36C. Since bolts were pretensioned and thus had a high initial axial strain, safety precautions were taken to avoid injuries from a bolt rupturing in tension since the pile-up of material may cause separation of the angles and further axial straining of the bolts. A slip resistance of approximately 240 kN was seen at the start of the test, and nothing else was noticeable during the first complete cycle. Some separation of the angles from the gusset plate was noticed during the second tension cycle. A small amount of necking had taken place above the top bolt during the third tension cycle just before the reversal of the load. A crack began to form at this same location as the load dropped during the fourth tension cycle. The same crack widened and split open as the load dropped sharply during the fourth tension cycle. A drop in strength in compression during the fourth compression cycle can by noticed and is believed to be due to accumulated damage to the bolt hole and the material between the two bolts.

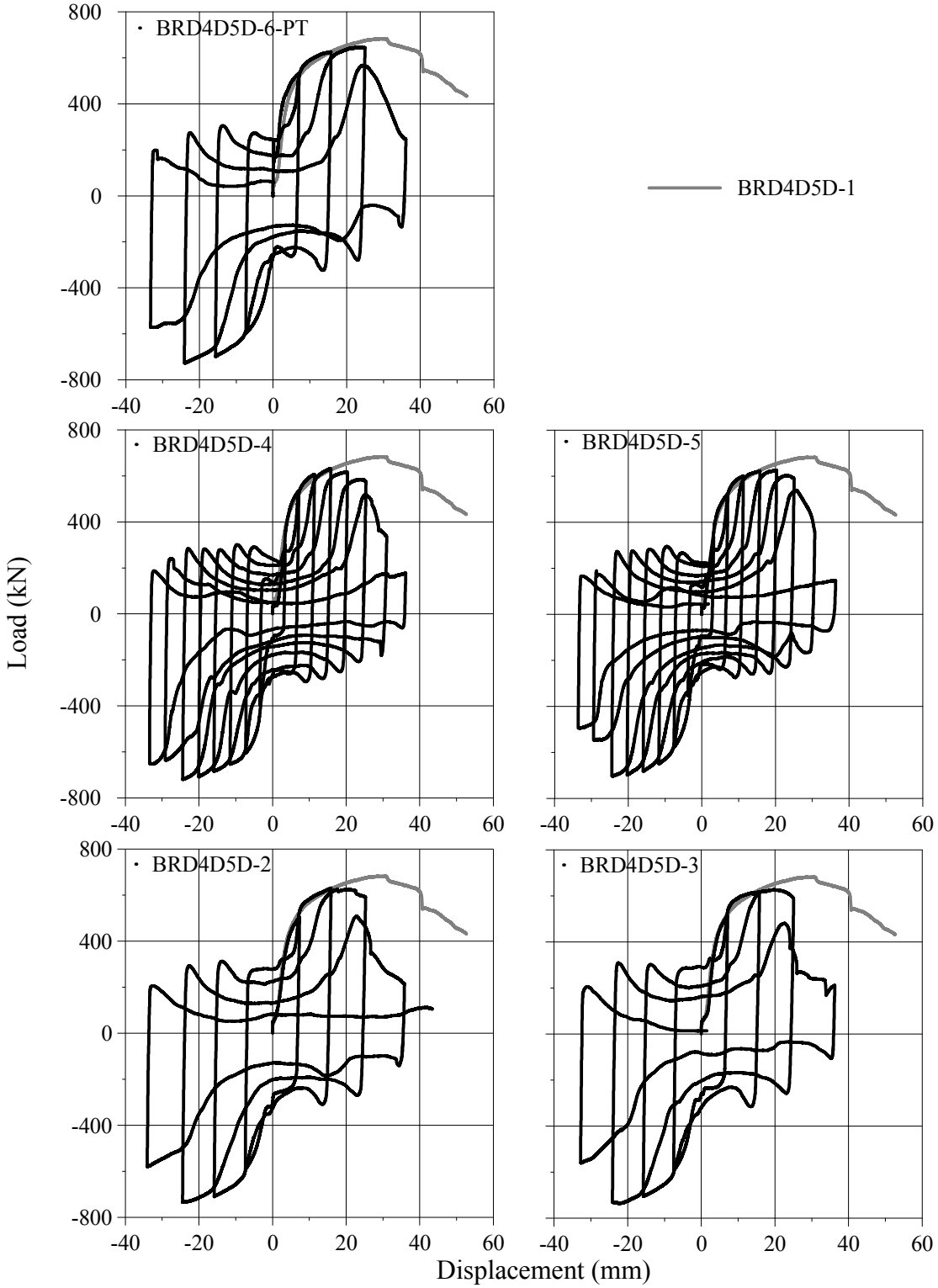

Figure 3.12: Monotonic and cyclic testing of specimen BRD4D5D.

Table 3.19: BRD4D5D experimental results

Specimen #	$P_{u,exp}$ (kN)	δ_u (mm)	δ_{rupt} (mm)	Loading
BRD4D5D-1	683	30.3	41.0	Mono
BRD4D5D-2	630	15.9	25.0[1]	4-36T36C
BRD4D5D-3	628	19.8	25.0[1]	4-36T36C
BRD4D5D-4	631	15.8	26.0	8-36T36C
BRD4D5D-5	626	20.3	27.5	8-36T36C
BRD4D5D-6	646	24.0	28.0	4-36T36C

[1] 80% of the maximum tension load was never actually achieved. As the load was dropping the third tension cycle, the load reversed before this 80% was reached. Upon the fourth tension cycle, the load never reached 80%; the deformation at 80% was thus taken as the deformation at the end of the third tension cycle, 25 mm.

A) Failed gusset plate under monotonic loading.

B) Failure of gusset plate on end distance.

C) Failure of material between bolts.

Photo 3.5: Specimen BRD4D5D-1, tested under monotonic loading.

A) Typical gusset plate bearing failure in specimen BRD4D5D-2.

B) Crack having split open after necking in specimen BRD4D5D-3.

C) Failure of specimen BRD4D5D-5, which underwent 8 cycles.

D) Close-up of material between bolts which became loose.

E) Failure of end material.

F) Failure of specimen BRD4D5D-6.

Photo 3.6: Specimen BRD4D5D under cyclic loading.

As with specimen BRD2D5D, specimen BRD4D5D saw a drop in bearing strength when subjected to cyclic loading. The monotonic test gave a bearing strength of 683 kN, while the four specimens with snug-tightened bolts tested under cyclic loading had an average strength of 629 kN. The pretensioned specimen saw a slight increase in strength with 646 kN. All these strengths are higher than the bearing capacity of 625 kN, calculated with an ultimate bearing stress of $4F_u$ and shown in Table 3.10. Table 3.19 shows the first specimen, tested under monotonic loading, underwent a deformation at ultimate and rupture of, respectively, 30.3 mm and 41.0 mm. Specimens tested with four cycles had average deformations at ultimate and rupture of 17.9 mm and 25 mm, while these deformations were 18.1 mm and 26.8 mm when tested with eight cycles. The deformation at ultimate was therefore similar for different cyclic loading protocols, while the deformation at rupture was higher for specimens undergoing eight cycles. This is due to the fact that, as explained in note 1 of Table 3.19, specimens BRD4D5D-2 and -3 never reached the point defined as rupture: 80% of the ultimate load, past the ultimate load. Their deformations at rupture had to be taken as the deformation at the end of the third tension cycle.

Specimen BRD4D5D-6, which had pretensioned bolts, underwent a deformation at ultimate of 24.0 mm and deformation at rupture of 28 mm, which were both higher than the deformations seen in snug-tightened specimens. It is believed this is due to the fact that the load was shared between bolt bearing and friction forces between the gusset plate and the angles; the load could therefore reach a higher level and be maintained longer.

3.4.3. Specimen BRD5D6D

Figure 3.13 shows the load versus displacement behaviour of the BRD5D6D specimens tested under monotonic and cyclic loading, while Table 3.20 shows the important parameters of these plots. Photo 3.7 shows selected pictures of the gusset plates tested under monotonic and cyclic loadings.

Tested under monotonic loading, specimen BRD5D6D-1 behaved similarly to specimen BRD4D5D. The test began quietly, as the bolts were snug-tightened and did not provide a large initial slip resistance. The bulge above the interior (top) bolt seen in other specimens did not become visible until approximately 37 mm in deformation. This indicates the gusset plate underwent significant bearing deformations before the tear-out shear capacity was reached. The ultimate load came as a small crack above the top bolt was widening, after which the load gradually dropped. This crack came after some necking was noticed above the top bolt. The sharp drop in load seen in Figure 3.13 is caused by the opening of this crack, after which the resistance is provided by the exterior (bottom) bolt bearing against the material between the two bolts. A picture of this crack is shown in Photo 3.7-A and B and a picture showing the necking is shown in Photo 3.7-C.

Both specimens tested under cyclic loading behaved very similarly. A picture of a typical failed BRD5D6D gusset plate subjected to cyclic loading is shown in Photo 3.7-D. Nothing of interest happened during the first complete cycle. During the second cycle, the angles seemed to be separating from the gusset plate, an indication that the steel in the vicinity of the bolt hole was piling-up and pushing against the angles. During the reversal of the load after this point, loud noises could be heard and were most likely caused by the angles rubbing against this pile-up of material. During the third cycle, no bulging or necking above the top bolt could be seen, except for a very small amount of necking in specimen -2 just before the reversal of the load. A small amount of warping on the edge of the gusset plate appeared at a deformation of approximately 23 mm in compression. It is not believed that this affected the results or the strength, as the envelope of the compression cycles creates a smooth curve because of the good concordance between cycles. Only a small amount of warping took place and never seemed to get any worse because the entire load would be taken from the bolt bearing on the gusset. For both specimens, necking started to become quite noticeable above the top bolt in the fourth tension cycle. A fifth tension cycle was added after the complete loading protocol to cause the tension load to drop to roughly 50% of the ultimate load.

In both specimens, necking of the gusset plate continued to take place, only to cause a rupture of the material above the exterior bolt at approximately 40 mm, which corresponds to the last sharp drop in load. This last rupture was indicated by a loud cracking noise after which the test was stopped, and is shown in Photo 3.7-E. Photo 3.7-F shows a typical bolt after cyclic testing; this bolt did undergo some deformations (negligible compared to the bearing deformations) because of the higher strength encountered in specimens BRD5D6D.

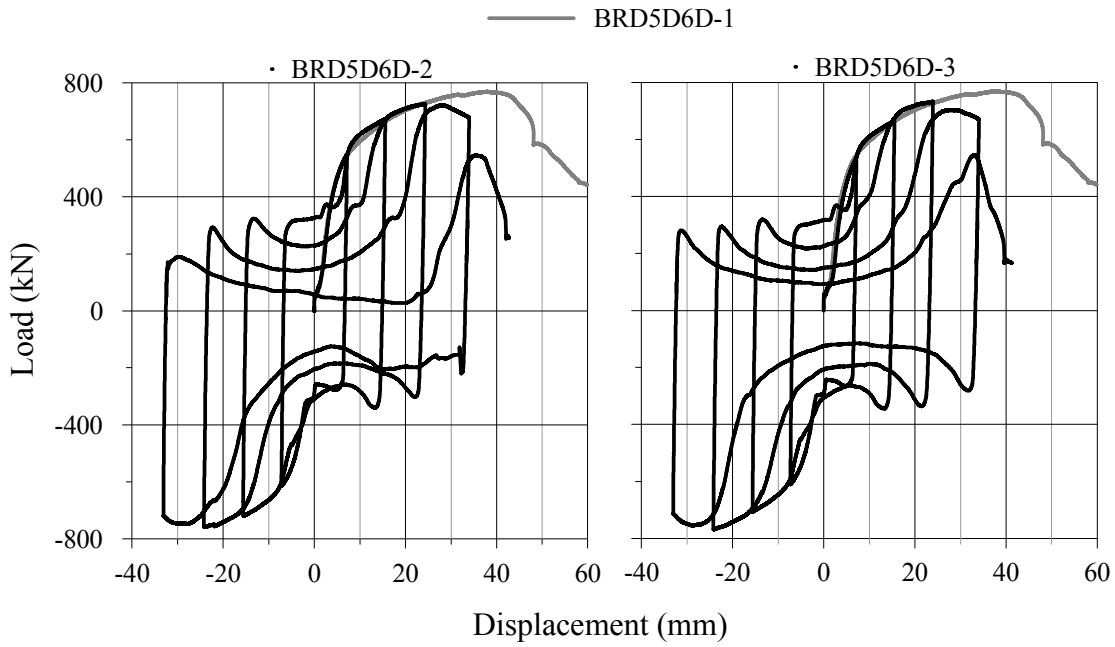

Figure 3.13: Monotonic and cyclic testing of specimen BRD5D6D.

Table 3.20: BRD5D6D experimental results

Specimen #	$P_{u,exp}$ (kN)	δ_u (mm)	δ_{rupt} (mm)	Loading
BRD5D6D-1	769	38.3	47.0	Mono
BRD5D6D -2	726	24.2	34.0[1]	4-36T36C
BRD5D6D -3	733	24.0	34.0[1]	4-36T36C

[1]: 80% of the maximum tension load was never actually achieved. As the load was dropping during the third tension cycle, the load reversed before this 80% was reached. In the fourth tension cycle, the load never reached 80% of the maximum load. The deformation at 80% was thus taken as the deformation at the end of the third tension cycle.

The three specimens had an average ultimate strength of 743 kN, which is considerably higher than the bearing capacity calculated at 625 kN with a maximum bearing capacity of $4F_u$, and also higher than the strength seen in specimens BRD4D5D. A probable explanation for this is the fact that bearing deformations can only take place as long as the bolt end distance is large enough that tear-out capacities do not govern. Once bearing deformations have gotten significant enough we see a failure mode that is not that of a classic bearing failure: a tear-out or necking of the material between the bolt hole and gusset plate edge due to the widening of the plate. Specimens BRD5D6D suggest that the bearing resistance could be proportional to the end distance, even when bolt spacings are large enough that a bearing failure is assured.

Specimen BRD5D6D underwent large deformation under monotonic loading; 38.3 mm and 47.0 mm at ultimate and rupture. As with specimen BRD4D5D, a significant drop is seen with cyclic loading as the ultimate deformation drops 37% to an average of 24.1 mm, and the deformation at rupture drops 28% to 34 mm.

A) Specimen BRD5D6D-1 under monotonic loading.

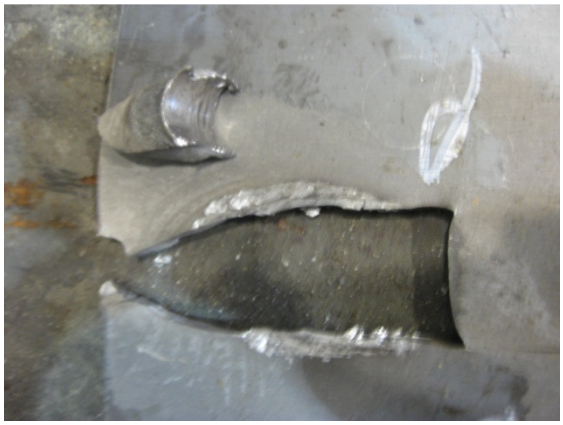

B) Rupture of material above top bolt.

C) Example of necking phenomenon.

D) Typical failed gusset plate after cyclic loading.

E) Photo showing formation of crack above top bolt after necking.

F) Photo showing typical bolt after testing.

Photo 3.7: Specimen BRD5D6D tested under monotonic and cyclic loading.

3.4.4. Specimen BRP4D5D

Figure 3.14 shows the load versus displacement behaviour of the specimens tested under monotonic and cyclic loading, while Table 3.21 shows the important parameters from this plot.

Specimen BRP4D5D is geometrically identical to specimen BRD4D5D, with the only difference being the types of holes used; punched versus drilled holes, respectively. After dismantling, the BRP4D5D specimens delivered to the laboratory were thought to have drilled holes instead of punched ones. The three specimens were taken back to the CANAM fabrication shop, where it was determined with the help of experienced shop workers that the holes were indeed drilled. Two additional holes were punched in the opposite ends of the gusset plates. Pictures of the two types of holes are shown in Photo 3.8-A and -B. During testing, one drilled hole was restrained by the hydraulic grips while the second drilled hole was above the grips; this second hole was therefore free to expand and lose its round shape during testing. For this reason, the diameter of the free drilled hole after testing was measured parallel to the loading and is reported in Table 3.21 as $\delta_{\text{Drilled Hole}}$. δ_u and δ_{rupt} as reported in Table 3.21 are the deformations from Figure 3.14 with $\delta_{\text{Drilled Hole}}$ subtracted. This is not done in this third specimen because of cyclic loading, but one could assume the deformation of the hole was also close to 1.0 mm.

Both specimens tested under monotonic loading behaved similarly and a typical failure gusset plate is shown in Photo 3.8-C. Both specimens remained relatively elastic up to roughly 6 mm of deformation, after which the load gradually flattened. Nothing was noticeable during testing until a small bulge could be seen above the interior bolt at 20 mm of deformation. Necking of this material then took place at 26 mm, with a small crack appearing across the width of the gusset plate at 31 and 32 mm for both specimens. This crack, shown in Photo 3.8-C, was widening as the load dropped, and split open when the load dropped sharply. Again, a separation of the angles was seen in these specimens as a pile-up of material was taking place in the vicinity of the bolt

holes. Photo 3.8-F shows the typical shape of the free-standing hole in each specimen after monotonic testing.

The cyclic loading protocol used for specimen BRP4D5D-3 had a maximum compression deformation of 18 mm, half that of the normal 4 cycle protocol. This was to avoid complications with the free standing drilled hole immediately below the bottom of the angles. Photo 3.9-A shows the failed gusset plate. Nothing of interest took place during the first complete cycle. During the second tension cycle, separation of the angles could be observed because of a pile-up of material, and a very small amount of necking could be seen before the load reversed. During the third tension cycle, necking continued to take place but no crack could be seen before the load reversed. Necking was quite visible at the start of the fourth tension cycle (5 mm) and a small crack had formed by 25 mm. The drop in load was caused by the widening of this crack, which split open at a deformation of approximately 32 mm and can be seen in Photo 3.9-B. As opposed to having only one crack like that of the specimen shown in Photo 3.8-E, two cracks developed roughly on each side of the bolt. A fifth tension cycle was added to the end of the loading protocol since the load had not dropped to 50% of the ultimate load prior to reversing direction. The gusset plate was damaged enough such that the load did not reach 50% of the ultimate load during this added cycle.

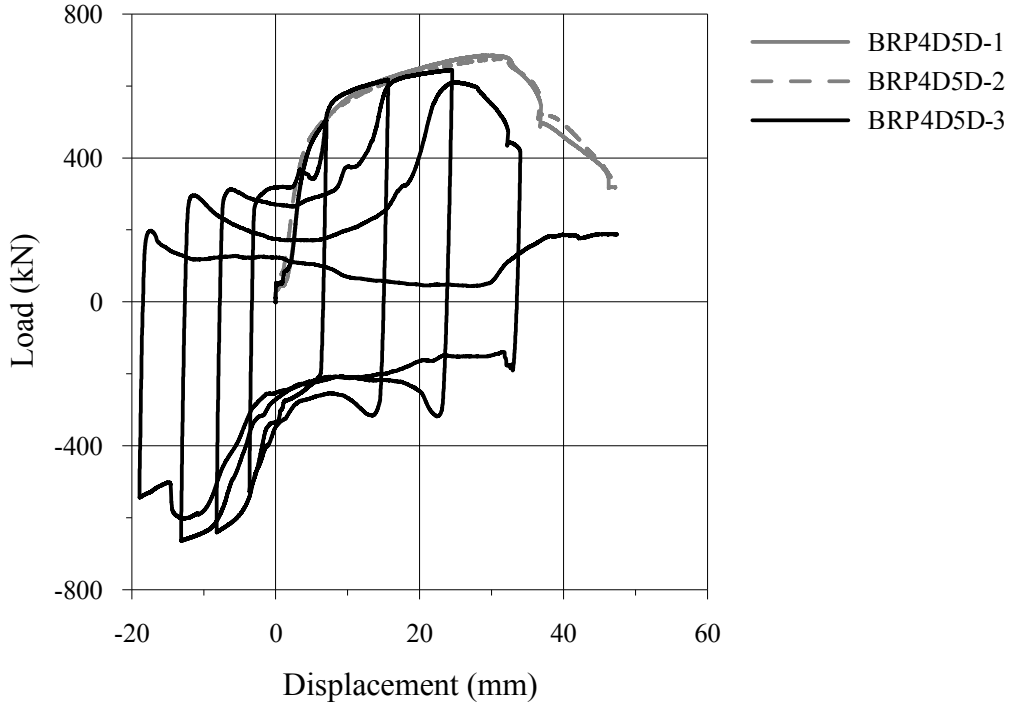

Figure 3.14: Monotonic and cyclic testing of specimen BRP4D5D.

Table 3.21: BRP4D5D experimental results

Specimen #	$P_{u,exp}$ (kN)	$\delta_{Drilled\ Hole}$ (mm)	δ_u (mm)	δ_{rupt} (mm)	Loading
BRP4D5D-1	684	1.0	28.0	36.0	Mono
BRP4D5D -2	675	1.1	30.2	35.9	Mono
BRP4D5D -3	645	N/A	24.5	31.0	4-36T18C

Specimens BRP4D5D and BRD4D5D had almost the same strength when tested under monotonic loading. Under monotonic loading, the average deformation at ultimate and at rupture was, respectively, 29.1 mm and 36 mm. Under cyclic loading, these deformations dropped to 24.5 mm and 31 mm. The lone cyclic test on punched holes had a higher strength than the average strength of drilled hole specimens.

A) Specimen with drilled hole as delivered to the lab.

B) Hole punched in the opposite end of the plate following discussions with CANAM.

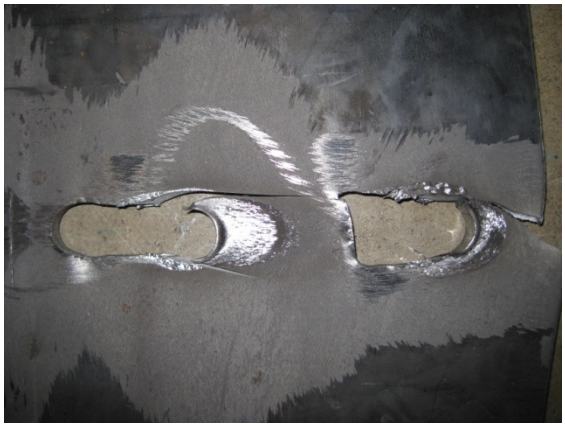

C) Typical failure in gusset plate.

D) Exterior (bottom) bolt showing formation of transverse crack.

E) Interior bolt, showing typical crack that forms after necking.

F) Typical free-standing drilled hole deformations.

Photo 3.8: Drilled and punched holes and specimen BRP4D5D tested under monotonic loading.

A) Failed gusset plate under cyclic load. B) Close-up of edge material.

Photo 3.9: Cyclic testing of BRP4D5D-3.

3.4.5. Specimen BSD4D5D

Figure 3.15 shows the load versus displacement behaviour of the BSD4D5D specimens tested under monotonic and cyclic loading, while Table 3.22 gives the important parameters from these plots. Photo 3.10 gives selected pictures of the failed gusset plates.

The specimen BSD4D5D behaved similarly to any other specimen undergoing bearing failure under a monotonic loading. Up to approximately 6 mm, the behaviour remained elastic, followed by a flattening of the curve. Up to 10 mm in deformation, nothing could be seen in the specimen. Before the ultimate load was reached, necking of the material between the interior bolt and the edge of the gusset plate could be seen. A crack started to appear in the same location as the ultimate load was reached. This crack continued to widen as the load dropped, and split open as the load dropped sharply.

Both specimens subjected to cyclic loading behaved similarly. Nothing of interest took place during the first complete cycle. No bulging of the gusset plate and no necking was seen during the second tension cycle. Some warping of the gusset plate was seen during the second compression cycle, but this does not seem to have affected the results, as there is good agreement between the first and second compression cycles. Both specimens had visible necking of the material above the interior bolt at a deformation of

approximately 25 mm during the third tension cycle. No crack has appeared at this point. For both specimens, the crack appeared and began to noticeably widen at a deformation of 26 mm during the fourth tension cycle. The crack gradually continued to widen and, like other specimens, caused a sharp drop in load as it split open.

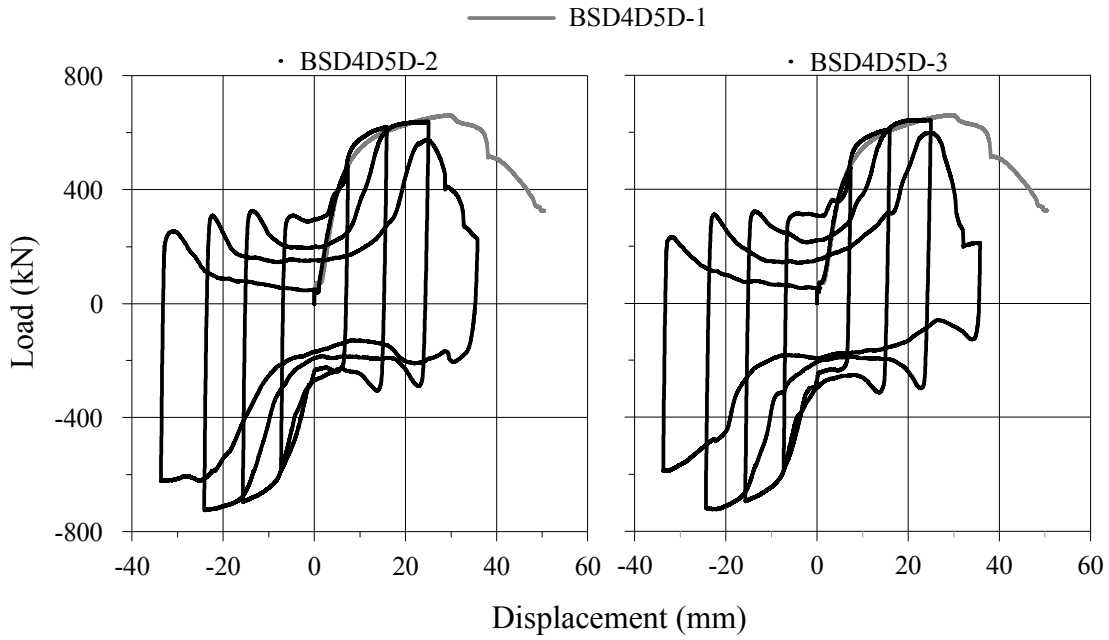

Figure 3.15: Monotonic and cyclic testing of specimen BSD4D5D.

Table 3.22: BSD4D5D experimental results

Specimen #	$P_{u,exp}$ (kN)	δ_u (mm)	δ_{rupt} (mm)	Loading
BSD4D5D-1	661	29.5	38.0	Mono
BSD4D5D -2	637	25.1	27.0	4-36T36C
BSD4D5D -3	643	21.2	28.0	4-36T36C

A) Failure of gusset plate under monotonic loading.

B) Shear planes between two bolts, monotonic loading.

C) Typical failed gusset plate under cyclic loading.

D) Close-up of end material.

Photo 3.10: Specimen BSD4D5D subjected to monotonic and cyclic loading.

The bearing strength under monotonic loading was 661 kN, while the strength under cyclic loading was 640 kN. As with other specimens, the slotted holes underwent more deformations at ultimate under monotonic loading with a deformation of 29.5 mm compared to the average of 23.2 mm seen under cyclic loading. The same can be said about the deformation at rupture, where 38.0 mm and 27.5 mm were seen under monotonic and cyclic loading, respectively.

3.4.6. Specimen BRD15D3DT

Figure 3.16 shows the four BRD15D3DT specimens tested under monotonic and cyclic loading, while Table 3.23 shows the important parameters from these plots. Photo 3.11 on page 137 shows selected pictures of this specimen.

Both specimens subjected to monotonic loading are performing similarly. The ultimate load appeared to be reached when a crack was forming above the interior bolt in the gusset plate at the same time that necking could be observed in the same area. The first sharp drop in load corresponded to the opening of this crack above the top bolt, after which the resistance is offered by the exterior (bottom) bolt. The load plateaued until the material between the two bolts reached its shear capacity.

Table 3.23 shows that specimen -3 was able to achieve a higher load. The reason for this is unclear, but a small defect in the gusset plate above the interior bolt may be the explanation. This defect is partially captured in Photo 3.11-C and D and looks as if something was spot welded to the plate and later removed. Nothing of interested took place during the first two cycles of testing for specimen -3. The material on top of the interior bolt seemed to be necking as the load flattened in the third tension cycle. During the 4^{th} tension cycle, a crack above the top bolt is slightly splitting open as the load starts to drop. Before the load reversed, the crack split wide open and the bolt shaft could actually be seen. In compression, nothing of interest could be seen on the specimens. After the fourth compression cycle, there was still no buckling or warping of the gusset plate; however, the load in the fourth cycle did not reach the load level attained during the third cycle. This may be explained by the smaller bolt pitch used in the specimen, which would give the material between the two bolts a smaller tear-out capacity.

Specimen BRD15D3DT-4 has the same behaviour as that of specimen -3, except that a small crack over the width of the gusset plate above the interior bolt appeared during the 2^{nd} tension cycle. During the third tension cycle, the crack continued to widen as the

interior bolt came back into bearing and caused the load to flatten. This crack split open during the last tension cycle, causing a drop in the load at approximately 13 mm. Like specimen -3, there was no buckling or warping of the gusset plate. A fifth tension cycle was added at the end of the cyclic protocol in specimen BRD15D3DT-4 in order to get the load to drop to roughly 50% of the ultimate load. However, large noises could be heard before the bolts came back into bearing, indicating a final rupture of the material between the two bolts; this can be seen as two sharp load drops at approximately 300 kN.

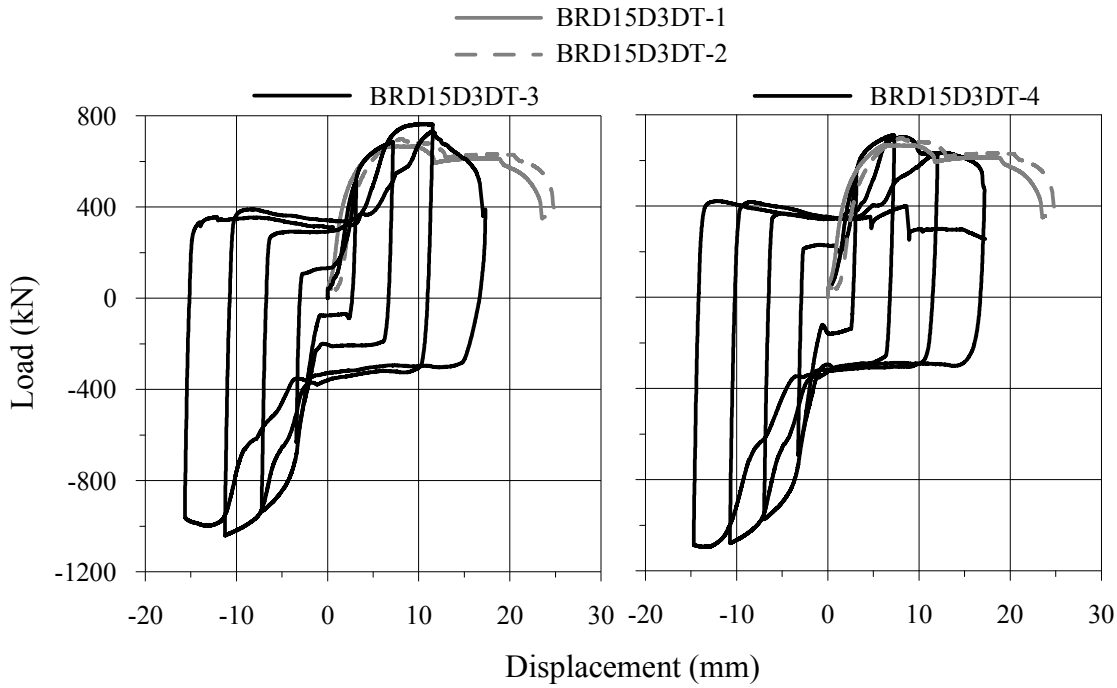

Figure 3.16: Monotonic and cyclic testing of specimen BRD15D3DT.

Table 3.23: BRD15D3DT experimental results

Specimen #	$P_{u,exp}$ (kN)	δ_u (mm)	δ_{rupt} (mm)	Loading
BRD3D15DT-1	667	6.2	21.6	Mono
BRD3D15DT-2	699	8.1	23.3	Mono
BRD3D15DT-3	764	10.1	14.8	4-18T18C
BRD3D15DT-4	711	7.3	16.9	4-18T18C

The CSA, CSA-09, and AISC anticipated capacities were, respectively, 817 kN, 643 kN, and 613 kN. In all tests, CSA over-estimated the capacity of BRD15D3DT as it did for specimen BRD2D5D. CSA-09 and AISC were on the safe side while under-estimating the capacity and CSA-09 provided the best estimates. These estimates were not as good as the ones for specimen BRD2D5D.

After dismantling the specimens, transverse cracks, as seen in Photo 3.11-E and –F, developed in the specimens which underwent cyclic loading. These types of cracks had only been seen in punched-hole specimens up to this point and the reason for their appearance in a drilled-hole specimen remains unknown.

It is worth noting the deformation at rupture, δ_{rupt}, was not reached in compression for both specimens tested under cyclic loading. The specimens still obtained approximately 16 mm of deformation even with a small bolt pitch of 3 bolt diameters. This leads one to believe thicker gusset plates can undergo large deformations such as the ones witnessed in the bearing failures of Phase II on thinner gusset plates.

A) Typical failure under monotonic load.

B) Close-up of shear planes in monotonic test.

C) Apparent defect in gusset plate of specimen 3

D) Specimen BRD15D3DT-3

E) Specimen BRD15D3DT-3

F) Specimen BRD15D3DT-4

Photo 3.11: Specimen BRD15D3DT.

3.4.7. Drilled versus Punched Holes

Table 3.24 shows a summary of the results for specimens with drilled and punched holes having a bolt end distance of 4d and bolt spacing of 5d. Specimens subjected to cyclic loading protocol 4-36T36C only are shown. Figure 3.17 shows the monotonic test results for both drilled and punched holes.

Under monotonic loading, both types of bolt holes performed very similarly in terms of strength and deformation capacity at ultimate, as shown in Figure 3.17 and Table 3.24. This supports the findings of Iwankiw and Schlafly (1982). The only difference comes in the deformation capacity at rupture, where the drilled hole specimens achieve a higher deformation under monotonic loading. This leads one to believe punched holes may deteriorate faster than drilled holes. This is believe to be due to the hole punching process; the work-hardened material surrounding the bolt hole and small micro-fissures which are introduced in the vicinity of the bolt hole are likely causing a higher rate of degradation once the ultimate load has been reached. Specimen BRP4D5D-2 developed a transverse crack next to a bolt hole as shown in Photo 3.8-D and similar to two of the D03X specimens in Phase I which also had punched holes. This type of crack did not appear in any of the drilled hole specimens, other than specimen BRD15D3DT-3 shown in Photo 3.11-E. The latter specimen had a thicker gusset plate and underwent cyclic loading.

Under cyclic loading, punched holes surprisingly underwent more deformations at ultimate and at rupture than drilled holes. This contradicts the monotonic test results as well as previous academic research (Owens et al. 1981). The reason for higher deformation at ultimate remains unclear, while there is a clear explanation for the difference in deformation at rupture: the drilled hole specimens never went through the point of rupture, defined as the point where the load was equal to 80% of the ultimate load, once the latter had been passed. The deformation at rupture had to be taken as the deformation at the end of the third cycle, instants before the load changed direction. Punched hole specimens were able to go through this point because they reached a

higher load level in their fourth tension cycle and therefore were calculated to have larger deformation at rupture.

Table 3.24: Results of drilled and punched hole specimens

	$P_{u,exp}$ (kN)	δ_u (mm)	δ_{rupt} (mm)
MONOTONIC			
BR**D**4D5D-1	683	30.3	41.0
BR**P**4D5D-1	684	28.0	36.0
BR**P**4D5D-2	675	30.2	35.9
CYCLIC			
BR**D**4D5D-2	630	15.9	25.0
BR**D**4D5D-3	628	19.8	25.0
BR**P**4D5D-3	645	24.5	31.0

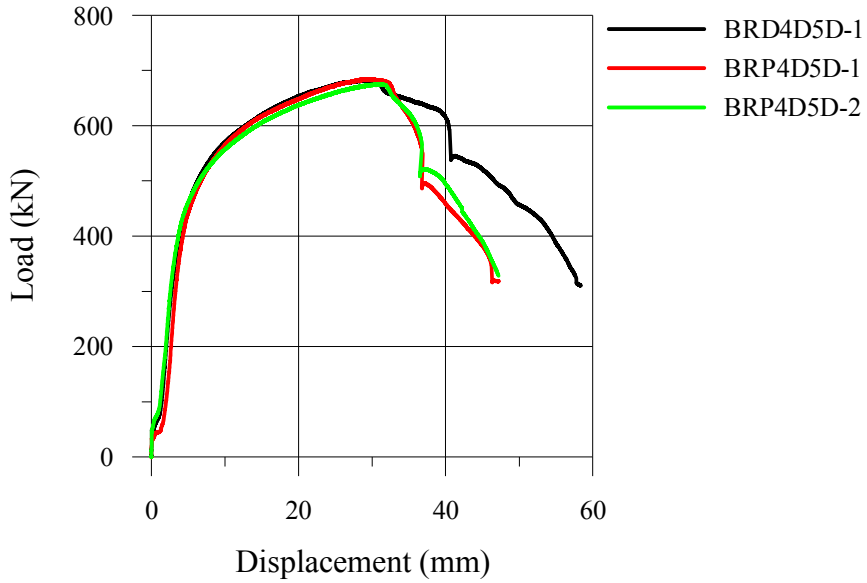

Figure 3.17: Monotonic test results on drilled and punched holes.

3.4.8. Slotted versus Standard Holes

Table 3.25 shows a summary of the results for specimens with drilled and punched holes having a bolt end distance of 4d and bolt spacing of 5d. Specimens subjected to cyclic

loading protocol 4-36T36C only are shown. Figure 3.18 shows the monotonic test results of specimens BRD4D5D-1 and BSD4D5D-1.

As stated in 1.1.7, slotted holes have only slight differences in ultimate loads but show more displacement per load in the early stages on loading than round holes. This is illustrated in Figure 3.18 as a different initial slope in the load versus displacement response. The cause of this is explained or illustrated, by Frank and Yura (1981), as an increase in "bending" deformations because slotted holes introduce "deep beams" between bolts, and this introduce more flexibility. Table 3.25 shows the data obtained during Phase II supports the statements made by Frank and Yura, as only a slight difference in ultimate loads was seen and similar ultimate displacements were observed.

Table 3.25: Results of standard and slotted hole specimens

	$P_{u,exp}$ (kN)	δ_u (mm)	δ_{rupt} (mm)
MONOTONIC			
B**R**D4D5D-1	683	30.3	41.0
B**S**P4D5D-1	661	29.5	38.0
CYCLIC			
B**R**D4D5D-2	630	15.9	25
B**R**D4D5D-3	628	19.8	25
B**S**D4D5D-2	637	25.1	28.0
B**S**D4D5D-3	643	21.2	28.0

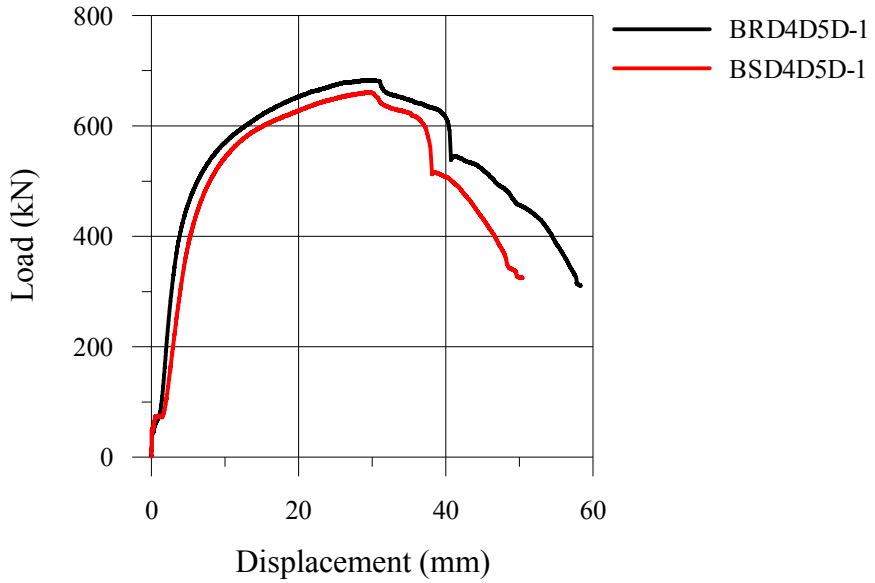

Figure 3.18: Monotonic test results on standard and slotted bolt holes.

3.4.9. Effect of Bolt Spacings

As explained by Kim (1996), smaller ultimate deformations were expected in specimens where the end distances were smaller. Table 3.26 shows results for the three specimen sub-groups used to observe the effect of different bolt spacings, and Figure 3.19 shows the monotonic test results on specimens of different bolt spacings.

There exists an obvious difference in deformation at ultimate under monotonic loading when the end distance is reduced to 2 bolt diameters, with specimen BRD2D5D-1 undergoing 22.2 mm versus 30.3 mm and 38.3 mm in specimens BRD4D5D-1 and BRD5D6D-1, respectively. This supports the findings of Kim (1996), who stated that longer end distances translate into larger ultimate deformations. BRD2D5D actually had a similar deformation at rupture to that of specimen BRD4D5D, which is most likely due to the similar bolt spacing of 5d; once the tear-out failure had occurred in BRD2D5D the load was sustained by the material between the two bolts until its tear-out capacity was reached.

Specimen BRD5D6D underwent the most deformation at both ultimate and rupture by a significant amount, as shown in Table 3.26. However, the bearing capacity of this specimen was poorly estimated by equation 1-5, as it had a bearing capacity of $4.9F_u$. Using spacings of 5d and 6d may prove too drastic a change when trying to accurately evaluate a connection's capacity.

Table 3.26: Results of different bolt spacing configurations

	$P_{u,exp}$ (kN)	δ_u (mm)	δ_{rupt} (mm)
MONOTONIC			
BRD**2D5D**-1	485	22.2	41.7
BRD**4D5D**-1	683	30.3	41.0
BRD**5D6D**-1	769	38.3	47.0
CYCLIC			
BRD**2D5D**-2	488	13.8	22.0
BRD**2D5D**-3	484	14.6	25.0
BRD**4D5D**-2	630	15.9	25.0
BRD**4D5D**-3	628	19.8	25.0
BRD**5D6D**-2	726	24.2	34.0
BRD**5D6D**-3	733	24.0	34.0

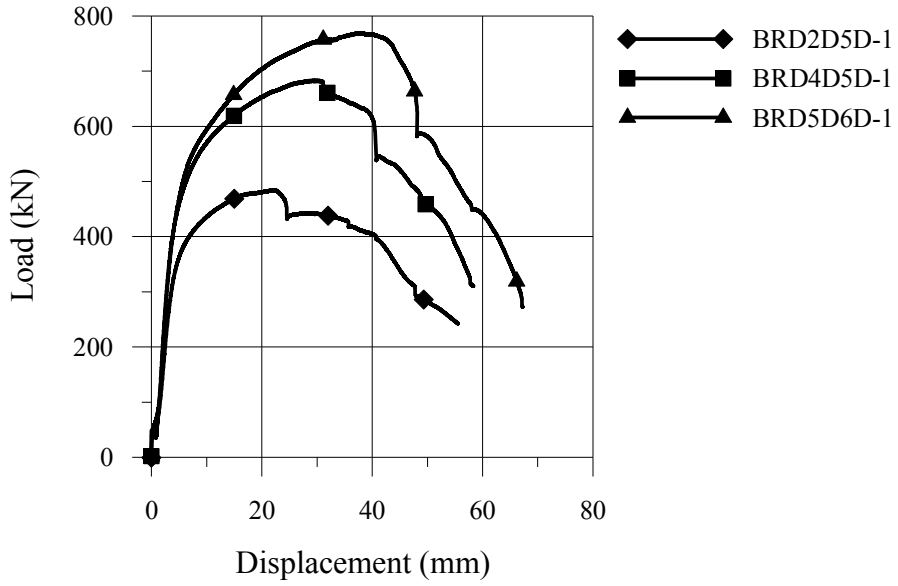

Figure 3.19: Monotonic test results on specimens of different bolt spacings.

3.4.10. Observations on the Ultimate Bearing Stresses Encountered

As mentioned in section 3.3.4, the specimens designed to fail under bolt bearing were designed with an ultimate bearing capacity equal to $4F_u$. Higher ultimate bearing stresses were observed for all but one specimen. Table 3.27 shows the bearing stresses at ¼" (6.35 mm) and at ultimate load for specimens designed to fail under bolt bearing only. Slip amounts were estimated as 0.5 mm in all specimens, and $\sigma_{1/4"}$ is thus taken as the load corresponding to a displacement of 6.85 mm divided by the bearing area (2 bolts x bolt diameter x plate thickness) and normalized with respect to the material's ultimate stress (F_u). Bearing stresses in Table 3.27 are given for both monotonic and cyclic tests and the monotonic tests are shown in Figure 3.20. Cyclic test results shown are only for loading protocol 4-36T36C.

Table 3.27: Bearing stresses attained in specimens failing under bolt bearing

	$\sigma_{1/4"}$	$\sigma_{u,exp}$
MONOTONIC		
BRD4D5D-1	$3.3F_u$	$4.4F_u$
BRP4D5D-1	$3.2F_u$	$4.4F_u$
BRP4D5D-2	$3.3F_u$	$4.3F_u$
BSD4D5D-1	$3.0F_u$	$4.2F_u$
BRD5D6D-1	$3.4F_u$	$4.9F_u$
CYCLIC		
BRD4D5D-2	$3.2F_u$	$4.1F_u$
BRD4D5D-3	$3.3F_u$	$4.0F_u$
BRP4D5D-3	$3.2F_u$	$4.2F_u$
BSD4D5D-2	$3.0F_u$	$4.1F_u$
BSD4D5D-3	$3.0F_u$	$4.1F_u$
BRD5D6D-2	$3.5F_u$	$4.7F_u$
BRD5D6D-3	$3.4F_u$	$4.7F_u$

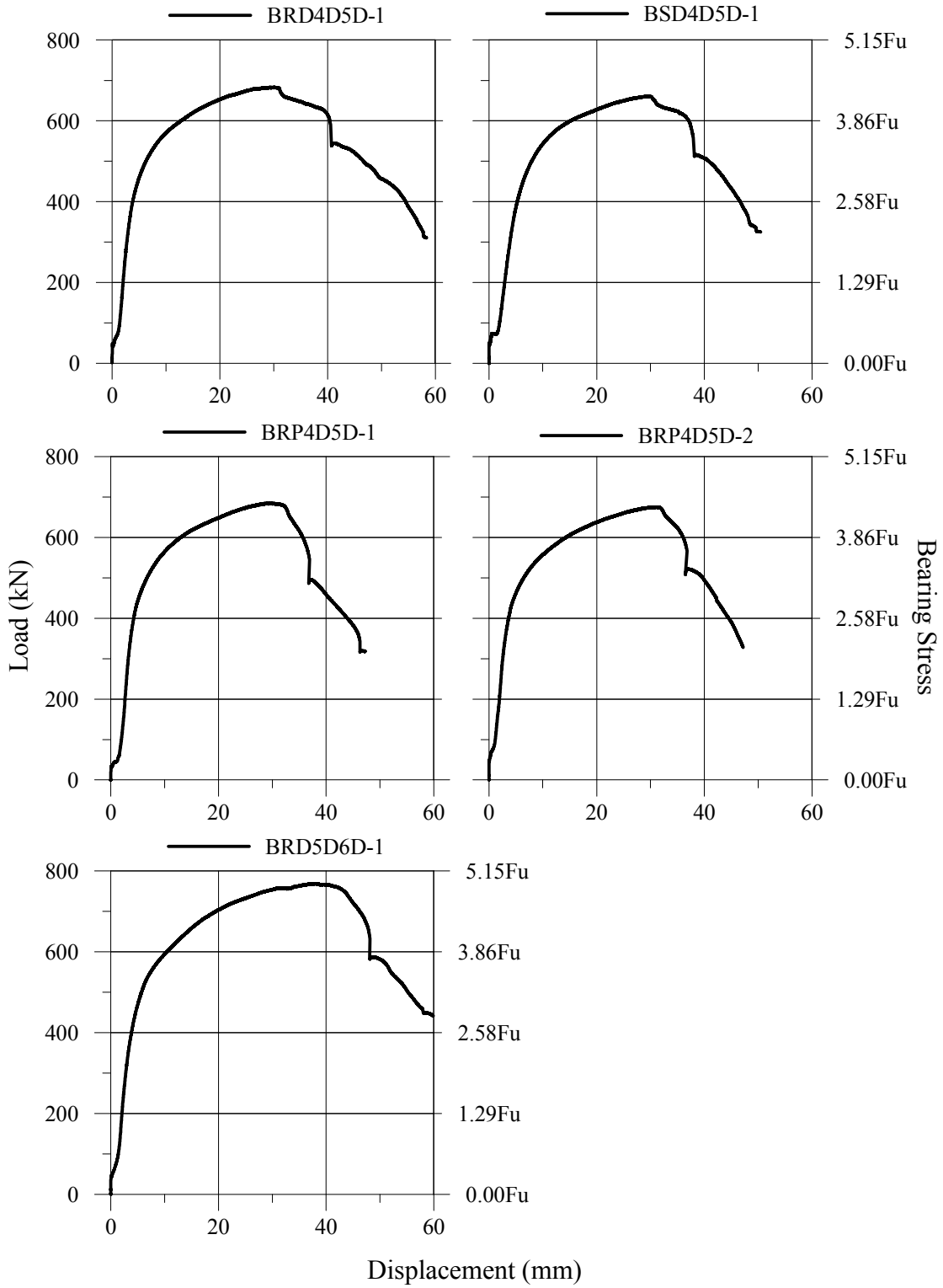

Figure 3.20: Monotonic test results of specimens designed to fail under bolt bearing.

All specimens exceeded by a significant amount the $3.0F_u$ bearing stress limit suggested in both Canadian and American standards. We also see that specimen BRD5D6D, with its larger bolt spacings, was able to sustain larger ultimate bearing stresses than any other specimens. The reason for these higher bearing stresses is believed to be the confinement of the gusset plates between the two angles, as most of the literature has bolt bearing tests performed on unconfined plate. Cai and Driver came to similar conclusions in their work, which also involved confined plates (Cai et al. 2008).

As mentioned in section 2.3.3, Frank and Yura (1981) specify a maximum bearing stress of 2.4Fu when the deformation is limited to 6.35 mm (1/4"). Table 3.27 shows even this limit was considerably exceeded by the specimens of Phase II. Specimens with 4D5D had similar bearing stresses at this deformation under both monotonic and cyclic loading. Specimen BRD5D6D had a higher bearing stress at this same deformation.

Under cyclic loading, ultimate bearing stresses were closer to the $4F_u$ assumed during design. Using this limit to design ductile connection in seismic force resisting systems may prove to be the better option, as seismic loads are obviously cyclic load.

As with section 3.4.8, we can conclude that slotted holes undergo more displacement per load, as Table 3.27 shows specimens BSD4D5D had smaller bearing stresses at a deformation of 6.35 mm when compared with regular bolt holes.

3.5. Summary and Conclusions

The following is a summary of the findings from Phase II:

- The use of punched or drilled holes does not seem to significantly affect the strength of ductility of bearing failures. Punched holes, however, seem to be prone to developing fractures transverse to the direction of the loading. This is most likely due to micro-cracks introduced in the surroundings on the bolt hole during the punching process and to the brittleness of the work hardened material after punching.

- No benefits to using slotted holes were observed during Phase II. All they did was provide more flexibility to a connection during its initial loading stage. Table 3.25 does show slotted holes had higher deformations at rupture and this was due to the fact that the specimens with drilled holes had a deformation at rupture equal to the deformation at the end of the third tension cycle. Under monotonic loading, drilled holes actually had a greater deformation at rupture than slotted holes.

- The use of larger bolt spacings yielded higher deformations at both ultimate and rupture. However, with higher bolt spacings came ultimate bearing stresses much higher than the limit of $3F_u$ proposed by codes and shown in equation 1.7. The findings of Cai and Driver, who stated CSA S16 was too conservative in using a bearing stress limit of $3F_u$ and that $4F_u$ was more appropriate, were supported in this study. Under cyclic loading, all specimens with spacings 4D5D had an ultimate bearing stress close to $4F_u$.

- Specimens with thicker gusset plates, BRD15D3DT, achieved a deformation in compression of 16.0 mm and had not yet reached the deformation at rupture. This deformation was reached even though a bolt pitch of only 3 bolt diameters was used in these specimens, as opposed to the minimum of 5 bolt diameters that was used in all other specimens. This is promising in the sense that bearing failures can be expected to behave the same in thicker gusset plates.

The following is list of conclusions drawn after the completion of the second phase of the test program:

- It is recommended to use an end distance of 4d and a bolt pitch of 5d.

- It is recommended to use drilled holes instead of punched holes, and standard round holes instead of slotted ones.

- More research is recommended to study the effect of introducing large bolt spacings on the bearing strength. Phase II indicated that ultimate bearing stresses climbed with higher bolt spacings. It would prove interesting to determine at what percentage of the tear-out capacity the ultimate load is taking place when large distances are used, as the bolt bearing capacity is upper bound by this capacity.

- More research is also recommended to study the effect of confining the plate undergoing bolt bearing failure. Based on literature and the results of Phase II, confinement has the effect of increasing the ultimate bearing stress because the material in the vicinity of the bolt hole is not able to expand outwards in the third dimension. However, even with confinement, a pile-up of material next to the bolt hole was seen pushing the angles outwards in most of the specimens in Phase II.

Chapter 4. ANALYTICAL PHASE

4.1. Introduction

The purpose of the experimental phase of this project, presented in chapters 2 and 3, was to evaluate the ductility capacity of connections. As CSA S16 permits the use of the seismic load reduction factor R_d when designing ductile bracing member connections, the ductility demand on these connections needs to be evaluated in order to determined whether these "ductile" connections are sufficiently ductile. This chapter gives the results of detailed finite element analyses using the OpenSees software (McKenna et al. 2004) performed on 24 regular commercial buildings situated in two locations in Canada prone to earthquakes: Montreal and Vancouver. The first section presents buildings chosen to be studied and the justification of their use. The following section presents the design procedures taken to design the 24 buildings. Afterwards, the OpenSees analytical models used for analysis are presented, followed by the analytical phase results.

The analyses were separated into three series: linear (non-ductile connections), non-linear (ductile connections), and non-linear incremental analyses (with ductile connections). The objectives of these analyses were to 1) study the force demand on non-ductile connections, 2) study the ductility (deformation) demand on ductile connections, 3) establish a level of confidence against collapse for two of the twenty-four buildings, and 4) on the basis of the results generated, revisit the NBCC 15 m height limit.

Due to the large amount of analyses performed in the analytical part of this project, the tasks were separated in equal parts with a fellow graduate student, Kim Guilini-Charette. Both the author and Ms. Guilini-Charette contributed equal parts to this phase. However, a detailed report on the selection and scaling of the ground motions used can be found in Guilini-Charette (2009).

4.2. Buildings Studied

Vancouver and Montreal were chosen as the locations to be studied in this project. This will enable us to observe the effects of having buildings located in either eastern or western Canada, which both see different types of earthquakes (low-frequency versus high-frequency waves, respectively). Figures 4.1 and 4.2 show the buildings studied in Montreal and Vancouver, respectively. For each city, five structures were chosen as the standard buildings. These standard buildings had normal storey heights, split-X bracing, braced bays located on the perimeter of the building, and were located on site class C. From these standard buildings, several parameters were chosen to study in order to examine their effects on the seismic behaviour of the structure. These parameters included:

- Site class: The effect of having structures located on site classes C or E.
- Building height: The effect of the building height (number of storeys).
- Storey height (or pattern) within a given building height: The effect of having different storey height patterns within a given building height.
- Bracing configuration (chevron vs Split-X): The effect of using chevron versus split-X bracing.
- Position of the bracing bent in the building (external and internal): The effect of having the bracing bent placed on the perimeter of the building or inside the building (higher accidental torsional loads, higher gravity loads).

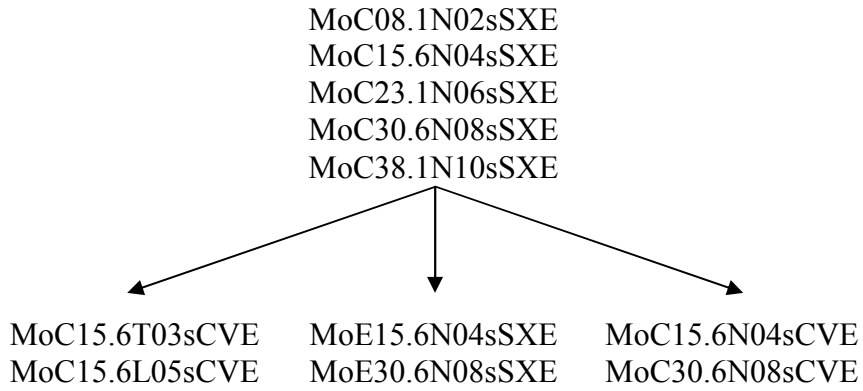

Figure 4.1: Buildings studied in Montreal.

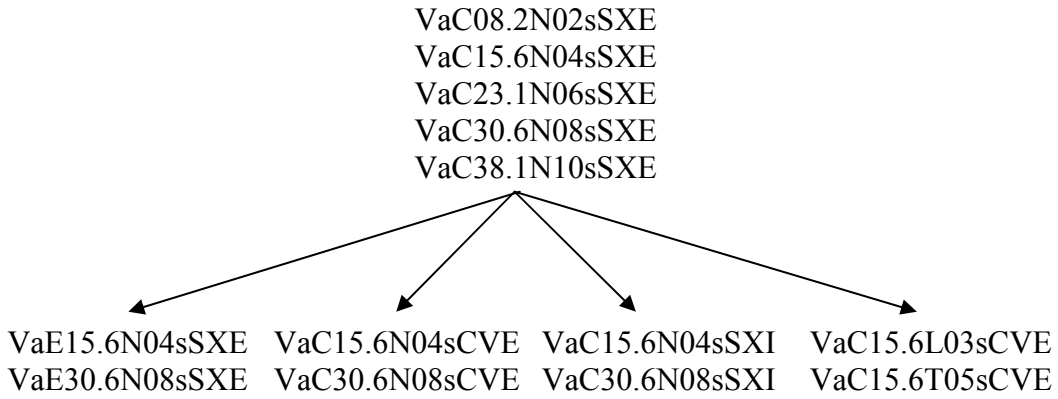

Figure 4.2: Buildings studied in Vancouver.

The following convention was used to identify all models. The first two letters correspond to the location of the building: Montreal or Vancouver. The third letter corresponds to the site class: C or E. The following four digits correspond to the total building height: 8.2, 15.6, 23.1, 30.6, or 38.1 m. The following letter corresponds to the storey height pattern: Normal, Low, or Tall. The next two numbers correspond to the number of storeys and the next letter to the word "storeys": 02s, 03s, 04s, 05s, 06s, 08s, or 10s. The following two letters refer to the bracing system used: Split-X (SX) or Chevrons (CV) bracings. The final letter refers to the position of the bracing bays: either on the Exterior or Interior of the building.

The buildings presented in figures 4.1 and 4.2 were used to perform the first two series of analyses (linear and nonlinear). Two buildings only were chosen to perform nonlinear incremental analyses (VaC15.6N04sSXE and VaC15.6L05sCVE) and are discussed further in section 4.5.3.

4.2.1. Building Geometry and Gravity Loads

All buildings have the plan geometry shown in Figure 4.3, with 5 bays of 9 m width for a total length of 45 m on all four sides. A typical overhang of 250 mm was used on the perimeter of the building for applying all gravity loads. The two positions and configurations of the bracing bents used are also shown in Figure 4.3.

Table 4.1 shows the different storey height patterns used. Only the standard four-storey building with normal storey heights had varied storey heights to study its effects; of course, the total building height is kept constant at the same height as the conventional four-storey building. Table 4.2 shows the different number of storeys available when using the three different storey height patterns with the same total height. Table 4.3 gives a detailed look at all storey heights for all combinations used in the 24 buildings.

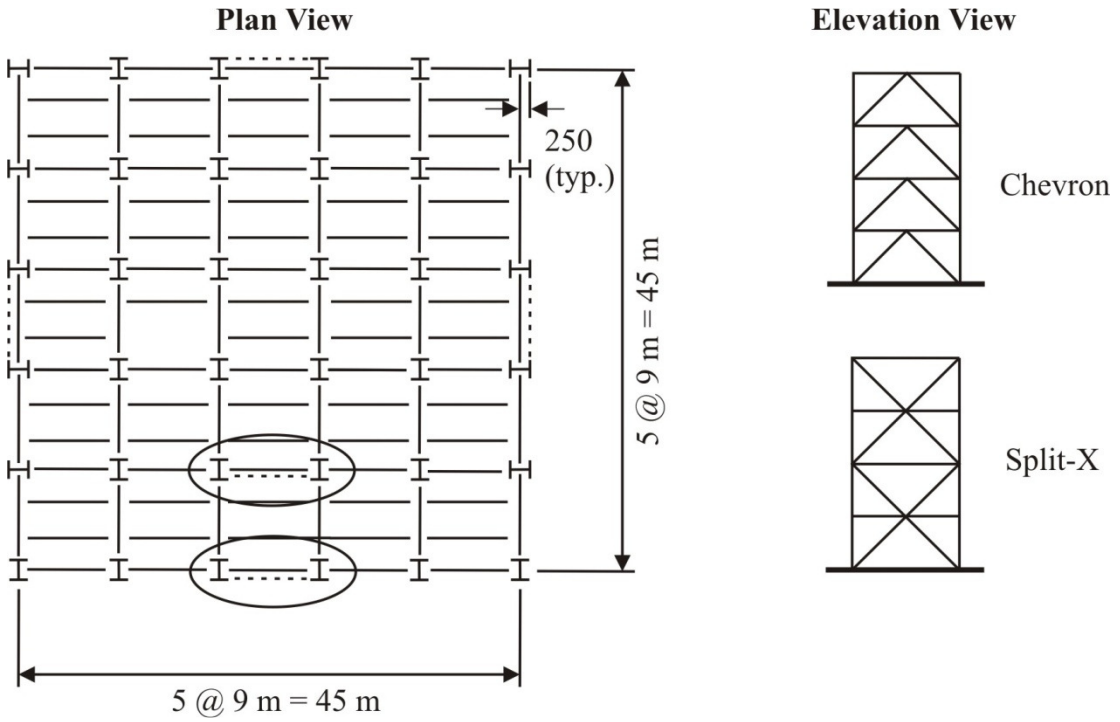

Figure 4.3: Plan layout of the structures showing the location of both exterior and interior bracing location.

Table 4.1: Storey height patterns.

Storey height pattern	Storey height	
	1st	>= 2nd
N	4.35	3.75
T	5.60	5.00
L	3.60	3.00

Table 4.2: Different height patterns used with standard building heights.

h_n (m)	Number of storeys with respect to storey height pattern		
	Normal, N	Tall, T	Low, L
8.1	2	N/A	N/A
15.6	4	3	5
23.1	6	N/A	N/A
30.6	8	N/A	N/A
38.1	10	N/A	N/A

Table 4.3: Storey heights of buildings studied.

	Number of storeys and storey height pattern						
	2	3	4	5	6	8	10
Storey	N02s	T03s	N04s	L05s	N06s	N08s	N10s
1	4.35	5.60	4.35	3.60	4.35	4.35	4.35
2	8.10	10.60	8.10	6.60	8.10	8.10	8.10
3		15.60	11.85	9.60	11.85	11.85	11.85
4			15.60	12.60	15.60	15.60	15.60
5				15.60	19.35	19.35	19.35
6					23.10	23.10	23.10
7						26.85	26.85
8						30.60	30.60
9							34.35
10							38.10

Table 4.4 shows the gravity loads used in the design of all 24 commercial buildings and are representative loads currently used in practice. The snow loads were calculated as per NBCC 05 (NBCC 2005).

Table 4.4: Gravity loads used in design.

			Load (kPa)
Roof	Dead load		3.0
	Live load (snow)	- Montreal	2.48
		- Vancouver	1.64
Floor	Dead load		3.5
	Partitions dead load		1.0
	Live load		3.8
Exterior walls	Dead load		1.2

4.3. Building Design

Automated design of the buildings was performed with the commercially available Graitec Advanced Design America (ADA) program according to NBCC 05 and CSA S16 (CSA 2001; NBCC 2005). ADA uses an iterative design process until convergence

is achieved and no sections need to be changed. ADA has built in procedures to account for seismic loads using the response spectrum analysis method.

4.3.1. Seismic Design

According to NBCC, the member forces from the analysis are adjusted such that the base shear from the spectrum analysis is equal to V_d from equation 4.1, where V_e is the elastic base shear from the response spectrum analysis, I_e is the importance factor (taken as 1.0 for the buildings studied herein), and R_o and R_d are, respectively, overstrength and ductility force reduction factors. R_o and R_d, as shown in Table 1.9, are equal to 1.3 and 1.5, respectively, for structures of the conventional construction category.

$$V_d = \frac{V_e I_e}{R_o R_d} \tag{4.1}$$

The value of V_d need not exceed 80% of V, which NBCC 05 provides as an equivalent static base shear calculated using equation 1.15. NBCC 05 states the base shear V need not exceed 2/3 the value of V calculated with T_a = 0.2 s and must be greater than the value obtained with T_a = 2.0 s. The NBCC 05 response spectral ordinates are shown in Table 4.5 for Montreal and Vancouver.

Table 4.5: Maximum considered earthquake response spectrum ordinates.

	S_a (g)	
T (sec)	Montreal	Vancouver
0.0	0.690	0.940
0.2	0.690	0.940
0.5	0.340	0.640
1.0	0.140	0.330
2.0	0.048	0.170
4.0	0.024	0.085

The seismic loads were distributed between the bracing bents, including 10% accidental in-plane torsional effects, and were amplified to account for inelastic P-Δ effects by the factor U_2 of CSA, shown in equation 4.2.

$$U_2 = 1 + \frac{\sum C_f R_d \Delta_f}{\sum V_f h} \qquad 4.2$$

The buildings' seismic design characteristics are shown in Table 4.6. Of particular interest is the ratio V_e/V_{de}, which reflects the impact of the design rules imposed by the NBCC, such as period limits and upper and lower bounds on the base shear forces. The base shear V_{de} is obtained by multiplying the design base shear, V_{Chosen}, by R_oR_d. This enables the direct comparison of the elastic design base shear to the expected elastic demand from the response spectrum analysis, V_e. As shown, the ratios are significantly lower than 1 in Montreal, indicating that these structures possess additional overstrength compared to those in Vancouver. This can come from the limitations on the structural periods used to select the base shear. A structure located in Vancouver will be much stiffer than the same structure located in Montreal because of the greater maximum considered earthquake in Vancouver as specified by the NBCC. However, the two can be designed for the base shear based on the same empirical period, calculated as 0.05h, which is used as an upper limit. The Montreal buildings have dynamic base shears below the 80% of the equivalent static base shear, while the Vancouver buildings have dynamic base shears between 80% and 100% of the equivalent static base shear. However, even if the dynamic period, T_1, is greater than the fundamental period, T, the design base shear may still be based on the base shear calculated with the spectral analysis due to the design base shear being allowed to be as low as 80% of the base shear calculated using the equivalent static force procedure.

Table 4.6: Seismic design characteristics of buildings.

Model	V (kN)	V_e (kN)	V_d (kN)	V_{Chosen} (kN)	T (s)	$T_{1\text{-}ADA}$ (s)	$T_{1\text{-}L}$ (s)	$T_{1\text{-}NL}$ (s)	V_e/V_{de}
MoC08.1N02sSXE	3943	5346	2742	3154	0.41	0.52	0.54	0.55	0.87
MoC15.6N04sSXE	4120	5192	2663	3296	0.78	0.97	1	1.04	0.81
MoC23.1N06sSXE	3546	4582	2350	2837	1.16	1.65	1.7	1.78	0.83
MoC30.6N08sSXE	3817	4131	2119	3053	1.53	2.38	2.4	2.55	0.69
MoC38.1N10sSXE	3612	4237	2173	2890	1.91	3.20	3.24	3.52	0.75
MoE15.6N04sSXE	9313	15093	7740	7740	0.78	0.72	0.73	0.75	1.00
MoE30.6N08sSXE	7863	10799	5538	6290	1.53	1.98	2.00	2.1	0.88
MoC15.6T03sCVE	3136	3561	1826	2509	0.78	1.01	1.03	1.06	0.73
MoC15.6L05sCVE	5097	4797	2460	4078	0.78	1.23	1.22	1.25	0.60
MoC15.6N04sCVE	4120	4310	2210	3296	0.78	1.1	1.12	1.14	0.67
MoC30.6N08sCVE	3817	3365	1725	3053	1.53	2.47	2.52	2.73	0.57
VaC08.1N02sSXE	5341	11142	5714	5714	0.41	0.43	0.43	0.43	1.00
VaC15.6N04sSXE	8912	14513	7442	7442	0.78	0.73	0.73	0.74	1.00
VaC23.1N06sSXE	8292	13703	7027	7027	1.16	1.21	1.23	1.25	1.00
VaC30.6N08sSXE	8948	14229	7297	7297	1.53	1.71	1.72	1.77	1.00
VaC38.1N10sSXE	8485	14316	7342	7342	1.91	2.31	2.33	2.41	1.00
VaE15.6N04sSXE	10602	23214	11905	11905	0.78	0.61	0.57	0.57	1.00
VaE30.6N08sSXE	19788	29988	15379	15830	1.53	1.22	1.17	1.18	0.97
VaC15.6T03sCVE	6354	10985	5634	5634	0.78	0.77	0.79	0.81	1.00
VaC15.6L05sCVE	10323	13702	7027	8258	0.78	0.93	0.91	0.95	0.85
VaC15.6N04sCVE	8323	12328	6322	6658	0.78	0.87	0.88	0.91	0.95
VaC30.6N08sCVE	8948	12450	6384	7158	1.53	1.82	1.84	1.92	0.89
VaC15.6N04sSXI	9249	15269	7830	7830	0.78	0.70	0.75	0.76	1.00
VaC30.6N08sSXI	9124	16033	8222	8222	1.53	1.27	1.37	1.39	1.00

4.3.2. Member Design

As mentioned, automated member design using the Advanced Design America program was performed. The structural steel was designed to CSA 2001. The base of a braced column was assumed to be fixed, while the base of gravity columns were taken as pinned. The columns were continuous over two floors and the splice connections were taken as pinned. The connections of beams framing into columns were taken as pinned.

The slabs were modeled using the "joist floor" elements included in the program and distributed the gravity loads in the east-west direction as shown in Figure 4.3,. Rigid diaphragms were not used: a concrete slab was modeled to properly distribute the seismic loads to the beams part of the brace bents. The slab thickness was adjusted so as not to affect the structural period by more than 10%.

Table 4.7 shows the steel grades used for all structural members: beams and columns were W-shapes, while the braces were square HSS tubes. Sections of classes 1 through 4 were allowed in ADA, as there are no member class requirements in Clause 27 of CSA with respect to conventional construction. Table 4.8 shows the load combinations used for design as well as their types and the seismic weight load combination.

Table 4.7: Steel grades used in design.

Member	Steel	Fy (MPa)	Fu (MPa)
Beams	G40.21-350W	350	450
Columns	G40.21-350W	350	450
Braces	ASTM A500-C50	345	427

Table 4.8: Load combinations used for design.

Load Combinations	Type
1.4D	Ultimate
1.0D + 0.5L + 0.25S	Ultimate
1.25D + 1.5L + 0.5S	Ultimate
1.25D + 1.5S + 0.5L	Ultimate
1.0D + 1.0E + 0.5L + 0.25S	Ultimate
0.9D + 1.0E + 0.5L + 0.25S	Ultimate
1.0L + 1.0S	Deflection
1.0D + 0.25S	Seismic weight

All braces and columns were designed with an effective length coefficient of 0.9 and 1.0, respectively, with the KL/r_{max} set equal to 200. Columns were taken as continuous over two floors; however, braces were forced in pairs only at each level and were therefore not always of the same size over two floors in a split-x bracing system. Live

loads were reduced according to NBCC and following equation 4.3, in which B is the tributary area in m^2.

$$0.3 + \sqrt{9.8/B} \qquad 4.3$$

4.4. Modeling

All analytical models were created with OpenSees – Open System for Earthquake Engineering Simulation, a software framework which uses the finite element method for the analysis of structural and geotechnical systems subjected to ground motions (McKenna et al. 2004). This section presents the analyses performed, the structural modeling, the sizing and modeling of the gusset plates, the hysteretic material used to model the ductile links at the ends of the braces, the ground motion selection and scaling methods, and the validation of the nonlinear model.

A validation of the OpenSees model developed for the analytical phase is presented in APPENDIX I.

4.4.1. Analyses Performed

Several aspects were studied in the analytical phase: the force and ductility demand on brace connections, as well as establishing a level of confidence against collapse when using ductile connections in structures of the conventional construction category. The three series of analyses performed are presented in Table 4.9: linear, nonlinear, and nonlinear incremental. The use of second-order effects, or P-Delta effects, is also specified in the same table: large deformation analysis was performed for all series except the linear. Past studies showed that P-delta effects on the linear seismic response of structures are generally small and can be neglected (Bernal 1987; Humar et al. 2006). The procedure used for performing incremental analysis is described in section 4.5.3.

Table 4.9: Different properties of the three analysis series.

	Analysis series		
	Linear	Nonlinear	Nonlinear Incremental
Material Linearity	Linear	Nonlinear	Nonlinear
Use of ductile links?	No	Yes	Yes
Connections with limited ductility?	No	No	Yes
Braced column buckling?	No	Yes	Yes
Brace buckling?	No	Yes	Yes
Second-order effects	Linear	Corotational	Corotational

4.4.2. Structural Modeling and Gravity Loads

Figure 4.4 shows an example of the OpenSees models used for this study. All models included one half of the entire building, or only one of the two braced frames as well as half of all the gravity columns. For simplicity, all identical gravity columns were lumped together, as shown in Figure 4.4, and resulted in five different gravity columns: the corner columns oriented in their weak axis (Y-Y), the perimeter columns oriented in the weak axis, the interior columns oriented in their weak axis, the perimeter columns oriented in their strong axis (X-X), and the north-south braced columns oriented in their strong axis. A rigid diaphragm was used, as all gravity columns were restrained at every storey to the displacements of the right braced column.

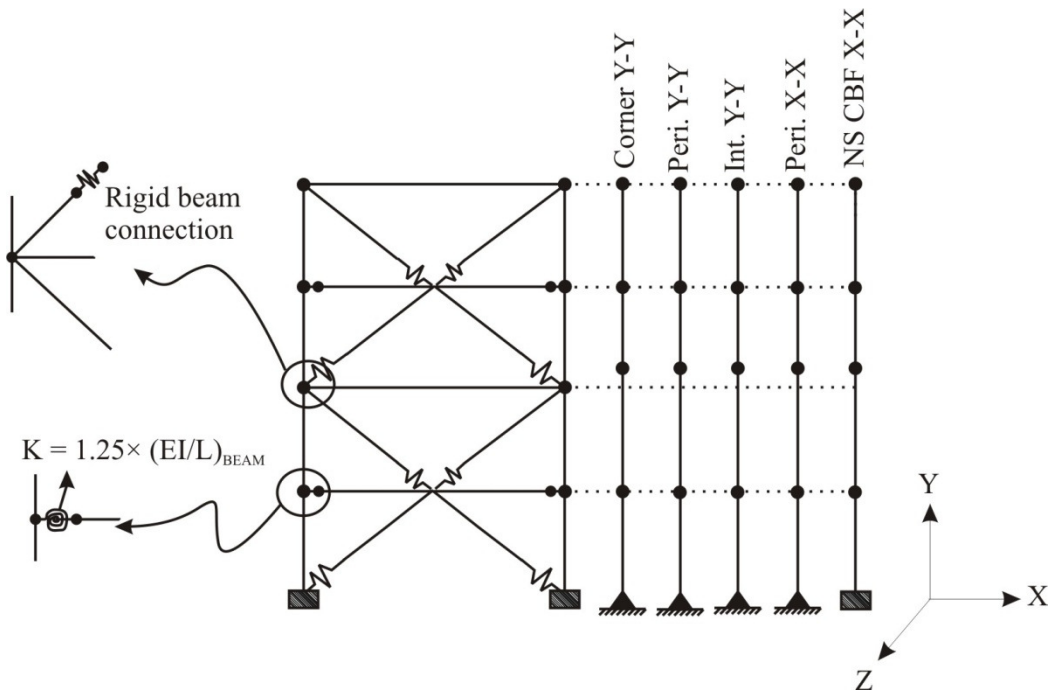

Figure 4.4: A four-storey example of an OpenSees model.

The braced frame modeled is essentially analyzed in two dimensions, but three dimensions were needed to model the out-of-plane (Z-direction) imperfections of the braces and braced columns in order to model buckling of these members. The braces and columns were assigned initial imperfections of L / 1000 at their midpoints, as such is allowed by CSA S16.

The mechanical properties of the steel were the same as those used in the design phase using ADA. R_y and R_t both equal to 1.1 were used when defining the material properties in OpenSees.

No column splices were modeled in the braced columns. A splice at every second storey and 1 m above the floor level was modeled in the gravity columns and assigned a stiffness. As proposed by Izvernari (2007), the flexural capacity of the splice was taken as 10% of the smallest attached column's plastic moment and the stiffness was dependent upon the orientation of the column and is defined by equations 4.4 and 4.5.

$$C_{Strong\ axis} = \frac{EAd^2}{L} \quad 4.4$$

$$C_{Weak\ axis} = \frac{9}{16}\frac{EAb_f^2}{L} \quad 4.5$$

In equation 4.4, A is the area of the splice plates connecting the column flanges and is equal to $b_f \times t_{splice}$, where b_f is the width of the column flange and t_{splice} is the thickness of the splice plate. In all cases, the thickness of the splice plate was taken as 13 mm (1/2"). L represents the length of the splice plate connection. In equation 4.5, A is taken as $\frac{b_f}{2} \times t_{splice}$. Details on these formulas are given in Appendix VI of Izvernari (2007).

The seismic weight, or mass, used for all analyses was calculated with the following load combination, as specified by clause 4.1.8.2 of NBCC 2005: 1.0D + 0.25S. Fifty (50) per cent of the partition load (1 kPa) was used as part of the dead load. The gravity load was applied as a point load at every storey of every column and calculated as follows: 1.0D + 0.5L + 0.25S.

4.4.3. Modeling of HSS and W-Shape Sections

Recommendations from Izvernari (2007) were followed regarding the modeling of HSS braces and W-shape beams and columns. Izvernari conducted studies with the goal of determining the optimum parameters when modeling these members; the number of elements, the number of fibres used in modeling the cross-section, and the number of integration points used are all examples of the parameters which were optimized in the latter studies.

Braces were modeled with nonlinear beam-column elements with the plasticity spread along the length of the member rather than at its ends. Each brace was represented with 8 elements having a cross-section modeled with 16 fibres as shown in Figure 4.5-B and

four integration points. Each fibre of the cross-section was assigned the uniaxial Steel02 Giuffré-Menegotta-Pinto material represented by a force-deformation relationship which included isotropic strain-hardening in both tension and compression. An example of the Steel02 material with isotropic strain-hardening in tension is shown in Figure 4.5-A. The Steel02 enables the use of residual stresses; however, no residual stresses were included in the HSS braces. The brace cross-section was first constructed using the "section" command of OpenSees (McKenna et al. 2004) with fibres and aggregated to an elastic material to include the torsional stiffness using the object "Section Aggregator".

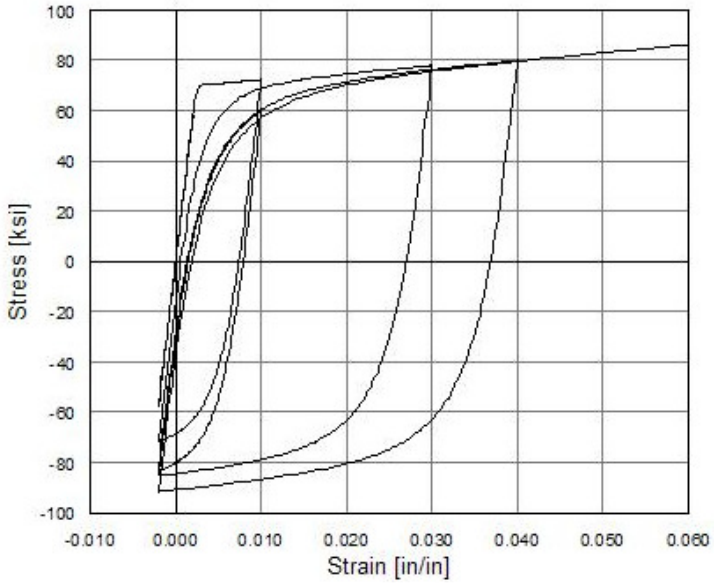

A) B)

Figure 4.5: A) Example of Steel02 material with isotropic strain-hardening in tension (McKenna et al. 2004), B) fibre discretization of a HSS cross-section.

The beams and columns were modeled using a "Beam with Hinges" element; this element was described and validated in Chapter 4 of Izvernari (2007). The depth of the hinges was set equal to the depth of the members. As shown in Figure 4.4, beams were assumed to be fixed at brace connection locations. Other beam-to-column connections were assigned a flexural stiffness equal to 1.25 times the beam's flexural stiffness and a maximum moment capacity equal to 1% of the the beam's plastic moment. This 1.25

value was based on the results of Liu and Astaneh (2000), who studied the cyclic behaviour of typical beam shear connections including the effects of concrete slabs. The torsional response of the beams and columns was prevented by using, again, the section aggregator and aggregating a linear material with very high stiffness. In the columns, ten fibres were used to model the web, while twenty fibres (two rows of ten) were used to model the flanges. For the beams, eight fibres were used to model the web and 40 (four rows of then) were used to model the flange. Columns were modeled using 8 elements over each storey and beams were modeled using two elements at each floor.

4.4.4. Sizing and Modeling of Gusset Plates

Figure 4.6 shows the typical layout of the brace connections used in this study. Based on the findings of the second experimental phase, a bolt spacing of 5d and an end distance of 4d was chosen to provide ductile behaviour of the connection failing under bolt bearing. A490, 19.05 mm (3/4") diameter bolts were used to establish an estimate of the length of the connection. Rather than detailing the typical $2t_g$ clearance between the gusset plate and the attaching beam and column, a minimum clearance of 20 mm was used between the edge of the angle and the beam flange as well as with the column flange as shown in Figure 4.6. The angles used for the connection were assumed not to enter the area between the column flanges.

The design of the gusset plates was performed using the findings of Whitmore (1952). Whitmore defined the effective width, b_w, of a gusset plate "as the length of the line passing through the bottom row of fasteners and intercepted by two 30º lines originated at the outside fasteners of the first row". Using the number of bolts, a Whitmore width was calculated and, as shown in Figure 4.7, the average length of three imaginary strips was used as the unsupported length of the gusset plate. Lin et al. concluded that an effective length factor, K, of 2.0 could be used (Lin et al., July 19-21, 2005), while Thornton (1984) recommended a K of 0.65. As was done in Izvernari's study (2007), an effective length factor of 1.2 was used. The factored force for which the gusset plate was designed depended upon the type of analysis series and was taken as follows:

- Non-ductile: The brace's C_f force coming from the ADA design composed of the axial load coming from gravity loads plus the seismic load multiplied by R_d. This gusset plate represents a non-ductile connection.
- Ductile: The brace's C_f force coming from the ADA design, composed of the axial load coming from gravity loads plus the seismic load which includes R_d.

The thickness of the gusset plate was then determined from its tensile and compression resistance, shown by equations 4.6 and 4.7. Plate material was assumed to be G40.21-350W with a F_y of 350 MPa.

$$T_r = \phi F_y b_w t_g \tag{4.6}$$

$$C_r = \phi A_w F_y (1 + \lambda^{2n})^{-1/n} \tag{4.7}$$

where

$$\lambda = \frac{KL}{t_g}\sqrt{\frac{12F_y}{\pi^2 E}} \tag{4.8}$$

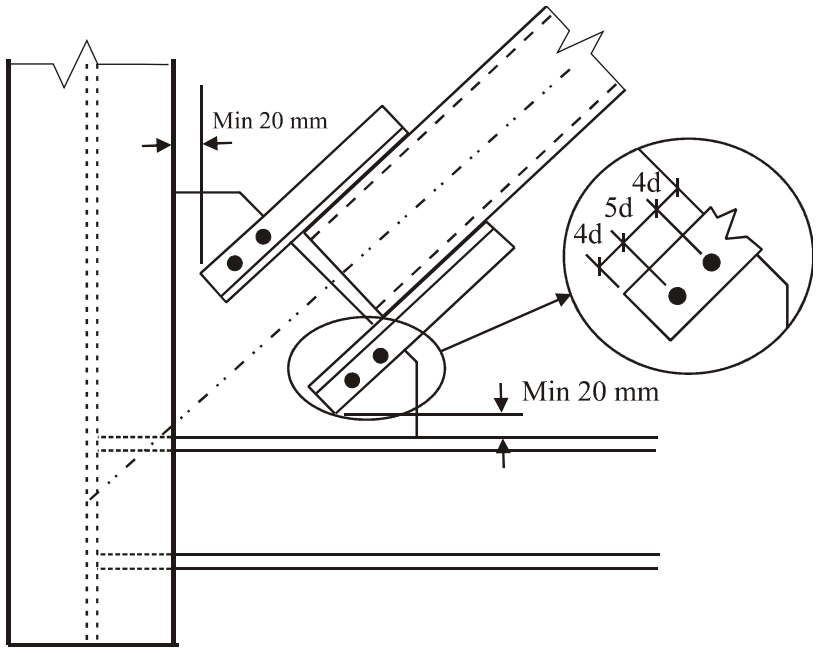

Figure 4.6: Connection layout and clearances.

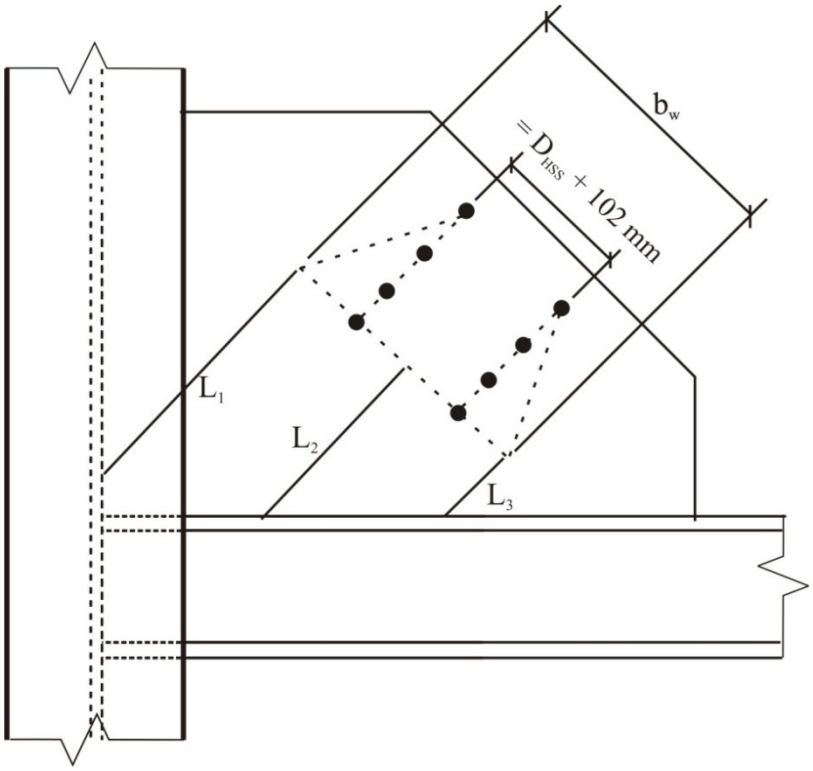

Figure 4.7: Connection details.

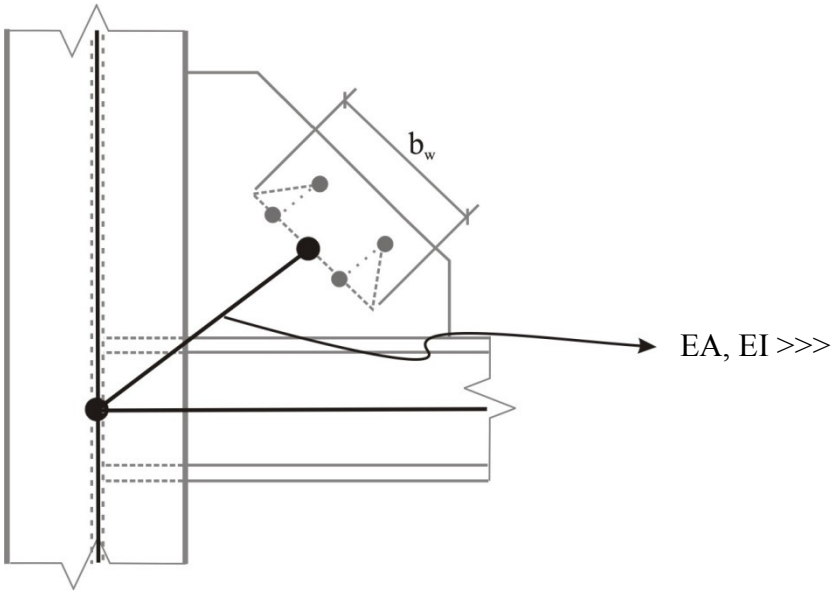

Figure 4.8: Rigid element used to model length of gusset plate.

In modeling the gusset plate, the length of the rigid element was taken as the distance between the intersection of the beam and column and the midpoint of the Whitmore width, as shown in Figure 4.8. This length was modeled with an elastic beam-column element with infinite stiffness and strength as illustrated in the same figure. The rigid elastic beam-column element was connected to the brace using a zero-length element. The degrees of freedom of this element's two nodes were restrained in such a way as to prevent in-plane rotation of the brace extremities as these were assumed to be fixed in the plane of the frame. The zero-length element was assigned out-of-plane and torsional stiffness according to equations 4.9 and 4.10. Equation 4.11 gives the flexural capacity of the gusset plate. These equations were adapted from Izvernari (2007) to include the 20 mm clearance shown in Figure 4.6, rather than the $2t_g$ clearance used for higher ductility bracing systems to help develop a plastic hinge in the gusset plate.

$$C_b = 1.5\frac{EI}{2\times\left(20/\sin\theta_{brace}\right)} \tag{4.9}$$

$$C_t = 1.5\frac{GJ}{2\times\left(20/\sin\theta_{brace}\right)} \tag{4.10}$$

$$M_p = \frac{1}{4}b_w t_g F_y \tag{4.11}$$

The two nodes of the zero-length element connecting the rigid elastic element, representing the gusset plate length, to the first brace element were restrained in such a way as to enable them to be free to move in the longitudinal direction of the brace. Two different hysteretic materials were used to represent the axial force-deformation behaviour and are presented in sections 4.4.5 and 4.4.6.

4.4.5. Hysteretic material calibrating for ductility demand analyses

The "Hysteretic" material in OpenSees was used to represent the axial cyclic behaviour of the gusset plate failing under bolt bearing in the second series of analyses, used to

determine the ductility demand on connections. This material is used to construct a uniaxial bilinear hysteretic material object with pinching of force and deformation, damage due to ductility and energy, and degrading unloading stiffness based on ductility (McKenna et al. 2004). Only the material's pinching parameters were used, as no damage or degrading unloading stiffness was needed for this series of analyses. This material is specified with the identification of three points in compression and tension, as shown in Figure 4.9.

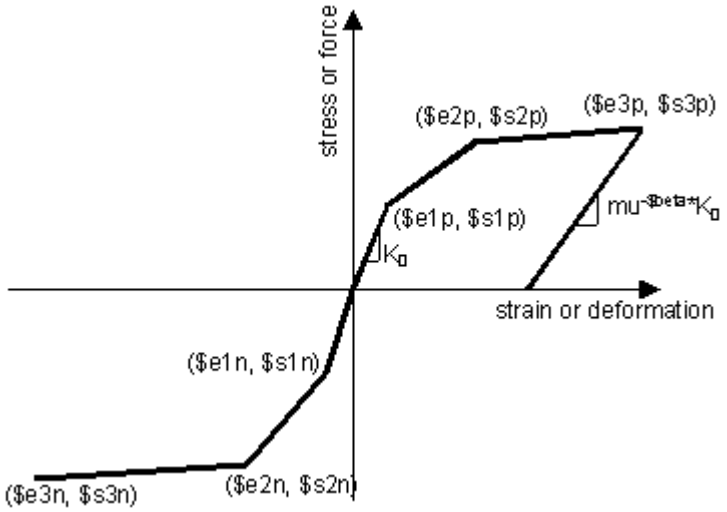

Figure 4.9: OpenSees' hysteretic material (McKenna et al. 2004).

When the OpenSees models were being developed for the second series of analyses, only Phase I of the experimental section had been performed. The hysteretic material was thus calibrated to specimens D03X-01 as shown in Figure 4.10, where the coordinates are of each are also given. Engineering judgement was used in calibrating the material to the experimental results from Phase I.

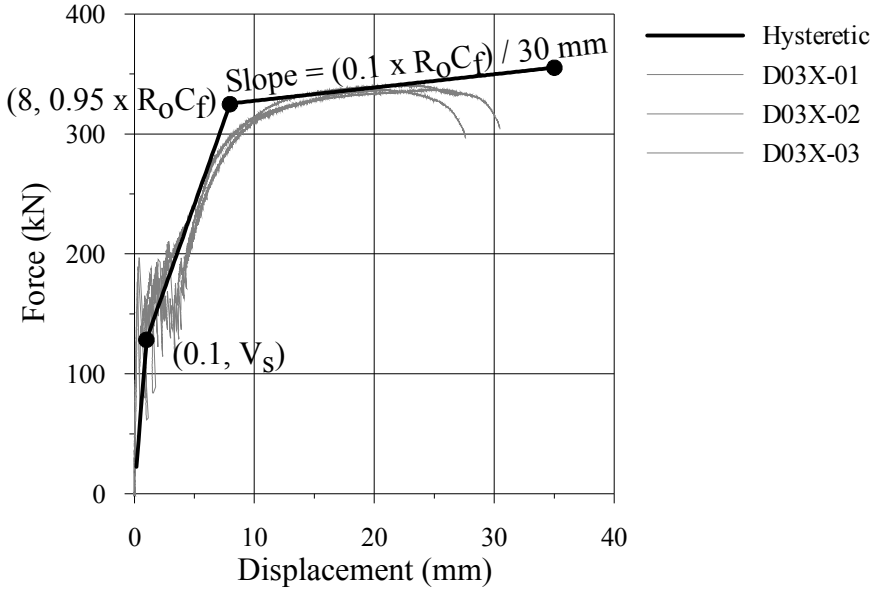

Figure 4.10: Calibrating of the Hysteretic material to the D03X specimen results.

The first point was used to specify the slip resistance, V_s. The second point was dependent on the slope of the third line: this slope was chosen as 10% of the brace's factored compressive force (the compression force always governs over the tensile one, and as the failure mode is one of bolt bearing the capacity of the plate is the same in both compression and tension) multiplied by R_o over a deformation of 30 mm. The overstrength factor, R_o, was used to increase the C_f in order to account for the minimum overstrength likely to be present in the connection (Mitchell et al. 2003): nominal to factored resistance ($1/\phi = 1.11$), actual to nominal material properties (1.1), supplied to required strength (1.05). These three factors multiplied together give a value of 1.28 and was rounded off to 1.3, which is equal to R_o in conventional construction. In order to have a load of R_oC_f at a deformation of 20 mm, an estimate of the deformation at ultimate based on the results of the first experimental phase, the third point's load value was taken as 98% of R_oC_f. The three points are summarize in Table 4.10 and are the same for compression and tension. The second point's displacement, 8 mm, was used to represent the soft behaviour of the bolts bearing against the gusset plate in the earlier stages of loading as seen in the first experimental phase. The third point's large

deformation value was used to enable large deformations and to observe the ductility demand.

Table 4.10: Coordinates of the force-deformation curve for ductile connections in nonlinear analyses.

Point #	Deformation (mm)	Load (kN)
1	0.1	V_s
2	8	98% of R_oC_f
3	5000	Calculated with third slope

Based on the number of 19.05 mm bolts in the connection, its slip resistance was calculated based on the equations provided by CSA S16 and as shown in equations 4.12 and 4.13.

$$T_o = 0.7 \times [0.75 A_b F_u] \quad 4.12$$

$$V_s = nmC_1 k_s T_o \quad 4.13$$

where T_o represents the initial tensile load in the fasteners, n is the number of bolts, m is the number of shear planes (2), C_1 is a coefficient relating the specified initial tension and mean slip to a 5% probability of slip (taken as 1.0 to bring the probability of slippage to 50%), and K_s is the mean slip coefficient (taken as 0.33 as per CSA S16 for clean mill scale). However, to represent snug-tightened bolts, 50% of T_0 as calculated with equation 4.12 was used in calculating V_s. A small deformation of 0.1 mm was used as the deformation at which the slip resistance is exceeded.

As for its cyclic behaviour, the hysteretic material was calibrated to provide the behaviour shown in Figure 4.11. The behaviour of a bolt bearing against a plate and undergoing cyclic loading was judged to have this behaviour; with the monotonic behaviour shown in Figure 4.10, the load dropped to a value of zero with the reversal of the load. The load would not increase again until the bolt bears against the opposite end

of the hole, which is now in the form of a slotted hole. As the goal of this series of analyses was to observe the ductility demand on connections failing under bolt bearing and not to observe the effect of the degradation of the connection, no degradation or damage to the force-deformation behaviour was specified. The hysteretic parameters are defined as follows to obtain this behaviour (McKenna et al. 2004):

PinchingX: Pinching factor for deformation during reloading. Set to 0.99 to have the load rise again only when the bolt bears against the hole.

PinchingY: Pinching factor for force during reloading. Set to 0.01 to have the load return to the level it was when it last lost contact against the bolt hole.

Damage1: Damage due to ductility. Set to zero.

Damage2: Damage due to energy. Set to zero.

Beta: Power used to determine the degraded unloading stiffness based on ductility. Set to zero.

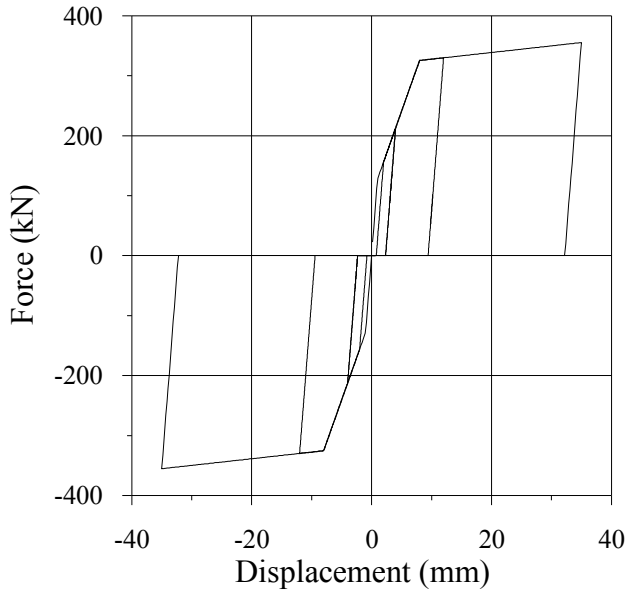

Figure 4.11: Hysteretic material under cyclic loading.

4.4.6. Pinching4 Material Calibrating for Incremental Analyses

In the incremental analyses, it was wished to model a connection breaking off, or reaching its rupture point, after a specified deformation. A different material was used to achieve this because the Hysteretic material used in the second series did not provide a fourth point to enable modeling a connection losing strength after a certain deformation. The Pinching4 material from OpenSees provided this fourth point, as shown in Figure 4.12. The Pinching4 material is essentially the same material as Hysteretic.

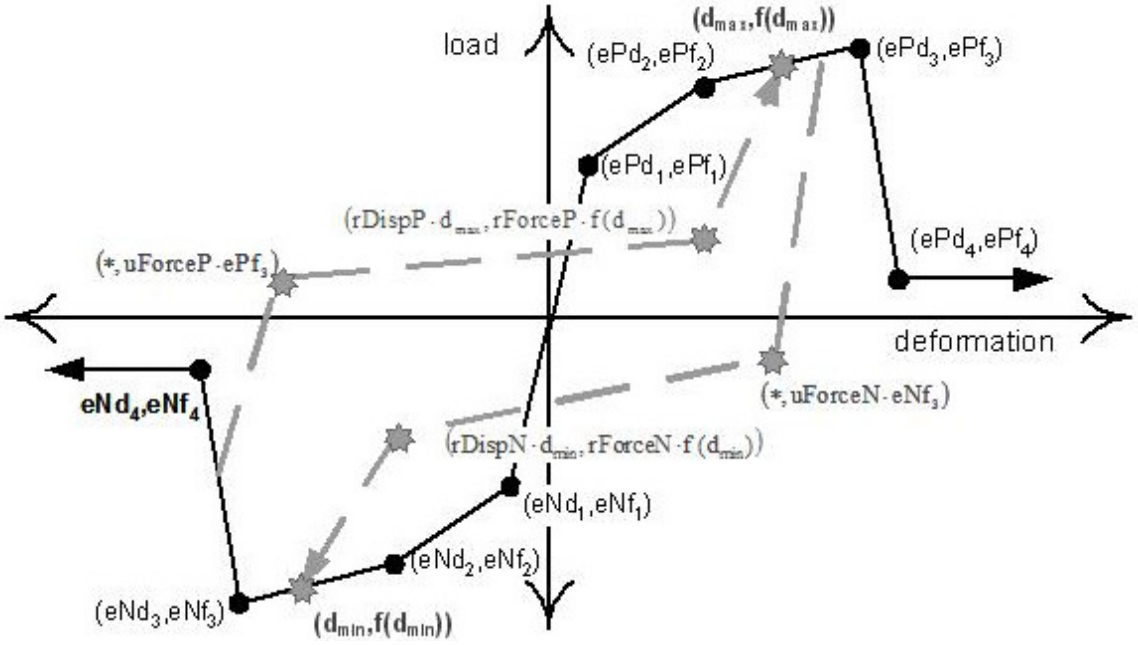

Figure 4.12: Pinching4 material of the OpenSees program (McKenna et al. 2004).

At the time of the incremental analyses preparation, the results from the second experimental phase were available. As these results included connections undergoing bolt bearing failures under cyclic loading, they provided a point of reference for calibrating the Pinching4 material. First, the deformation breaking point of the connection had to be estimated from the results of Chapter 3, as well as those from Chapter 2. Experimental phase II had test specimens undergoing failure in one end only and it was desired to account for the deformations taking place at the opposite end of the

brace as well. The deformations at rupture measured from Phase II specimens undergoing pure bearing failure, which are repeated in Table 4.11 for convenience, were used to establish the capacity in deformation of one connection (one end of the brace). Based on the Chapter 3 recommendations of using of a bolt pitch of 5d and an end distance of 4d, a deformation at rupture of 25 mm was chosen as a conservative connection break off point. Since this deformation is in one connection (one brace end) only, the results from specimen D03X in Phase I were used to estimate the amount of deformation taking place at the opposite end of the brace. From Table 4.12, the average δ_{Int} / δ_{Br} ratio for specimen D03X is 0.25, showing that the opposite end underwent, on average, 25% of the deformations of the end undergoing bolt bearing failure. The connection break off deformation was therefore chosen as 25 mm × 1.25 = 31 mm. The general behaviour of the calibrated Pinching4 material is shown in Figure 4.13, along with the cyclic testing of several Phase II experimental tests. Figure 4.14 shows the behaviour and the coordinates of the four Pinching4 points of the connection under monotonic loading. The negative slope after the third point was based on the degrading slope of specimen BRD4D5D-3, which underwent cyclic loading, and calculated as -32 kN/mm. The residual force after the breaking point was taken as 10% of R_oC_f, which is the connection ultimate load.

Table 4.11: Deformations at rupture and ultimate of selected specimens from Phase II.

Specimen	δ_u (mm)	δ_{rupt} (mm)
BRD**4D5D**-2	15.9	25.0
BRD**4D5D**-3	19.8	25.0
BRD**4D5D**-4	15.8	26.0
BRD**4D5D**-5	20.3	27.5
BRD**5D6D**-2	24.2	34.0
BRD**5D6D**-3	24.0	34.0

Table 4.12: Bearing deformations at failed end (δ_{Br}) and intact end ($\delta_{Int.}$) of Phase I specimens.

	Specimen		
	D03X-01	D03X-02	D03X-03
$\delta_{Int.}$ (mm)	5.1	3.3	4.8
δ_{Br} (mm)	19.6	20.2	15.1

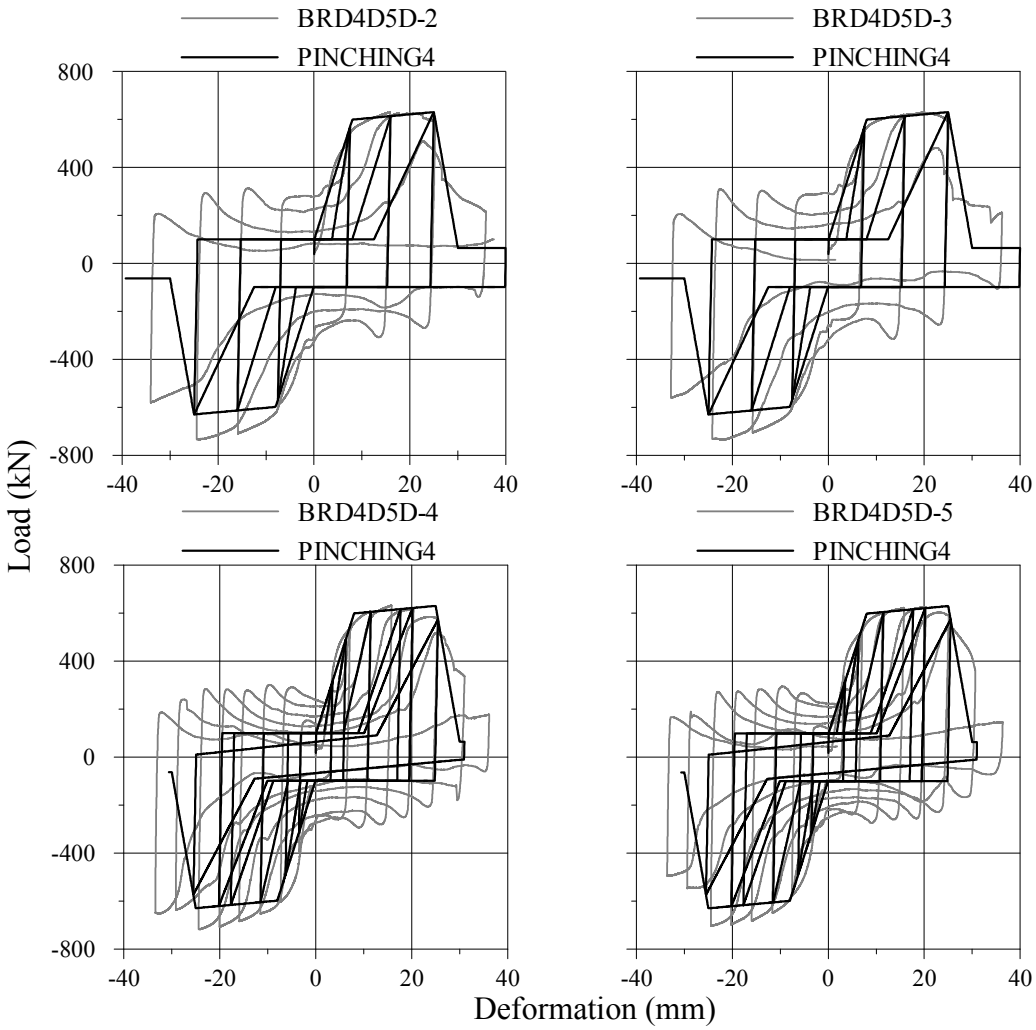

Figure 4.13: Calibrating of Pinching4 to cyclic results of chapter 3.

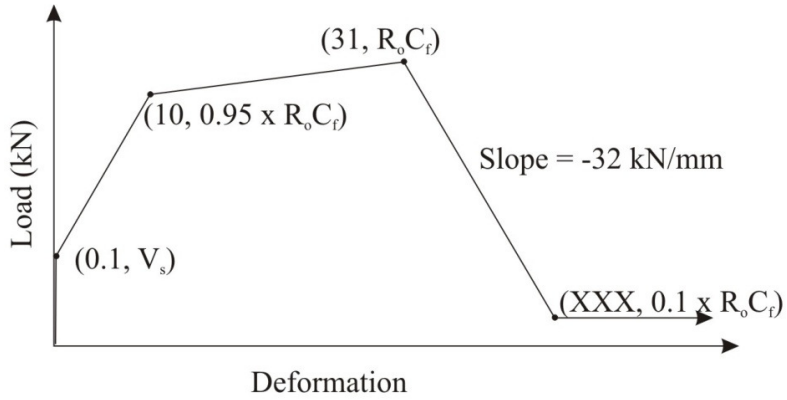

Figure 4.14: Pinching4 material used for incremental analyses brace connections.

Worth noting is the non-zero load when the bolts are not bearing against the gusset plate. This load was set equal to the calculated connection slip resistance, V_s, as explained in section 4.4.5. The list of parameters defined when creating the Pinching4 material is as follows (McKenna et al. 2004):

- rDispP, rDispN: Both set to 0.5. Defined as ratio of the deformation at which reloading occurs to the maximum historic deformation demand. The load therefore climbs once the deformation is equal to half that of the maximum historic deformation.

- rForceP, rForceN: Both set to the ratio of V_s over R_oC_f. Defined as the ratio of the force at which reloading begins to force corresponding to the maximum historic deformation demand. Enables the load to be equal to the slip resistance when the bolts are travelling inside the bolt holes.

- uForceP, uForceN: Both set to the ratio of V_s over R_oC_f. Defined as the ratio of strength developed upon unloading from negative load to the maximum strength developed under monotonic loading. Enables the load to unload to the slip resistance when the bolts lose contact with the gusset plate.

- gammaK: Set to 0.0. Defined as values controlling cyclic degradation model for unloading stiffness degradation.

- gammaD: Set to 0.0. Defined as values controlling cyclic degradation model for reloading stiffness degradation.

- gammaF: Set to 0.0. Defined as values controlling cyclic degradation model for strength degradation.

- gammaE: Set to 0.0. Defined as values used to define maximum energy dissipation under cyclic loading.

- damageType: Set to "cycle", but does not come into effect because of the definition of the gamma parameters.

4.4.7. Damping and Solution Algorithms Used

The "region" command from OpenSees was used to assign a damping equal to 3% of the critical damping in the first two modes of vibration to all structural members except the ductile links. Since the damping was specified as dependent upon the initial structural stiffness matrix, the ductile links (hysteretic and pinching4 material) had to be assigned a damping of 0.1% in order to keep from distributing the axial load between viscous damping and internal forces once the link underwent plastic deformations. This was not done at first try and thus axial forces from the first brace element and the ductile link were not equal after yielding of the link.

A time history analysis was performed in two steps: the gravity loads were first applied to the structure as a single load pattern and a second load pattern holding the ground acceleration record specified at a base node was used to apply the ground motion record.

As was done by Izvernari (2007), the equations were numbered using an RCM numberer, which optimizes the node numbering in order to reduce the storage bandwidth. The constraints were applied by using the transformation method, which

transforms the stiffness matrix by condensing out the constrained degrees of freedom as recommended for transient analyses. The system of equations was formed using a SparseGeneral scheme and was factored and solved during the analysis using the SuperLU solver. Because of convergence problems during nonlinear analyses, the Newton type solution algorithm was substituted for the Newton with Line Search algorithm procedure. This uses the Newton-Raphson method with line search to advance to the next time step. A norm displacement increment test was used to test positive force convergence if the 2-norm of the displacement increment in the system of equations is less than the specified tolerance.

For the first analysis step, a Load Control integrator was used to apply the gravity loads. For the dynamic analysis, a Newmark-Beta type integrator is defined with γ equal to 0.5 and β equal to 0.25 (average acceleration method). A transient analysis is then performed with an analysis time step of 0.001 s. The number of time steps varied upon the duration of the ground motion being used.

4.4.8. Ground Motion Selection and Scaling

The ground motions used in this project were based on the findings of Guilini-Charette (Guilini-Charette 2009), who underwent an in-depth study on the effect of the selection and scaling of ground motion records on structures. The reader is referred to chapter 4 of Guilini-Charette's M.Sc. thesis for detailed records. A brief overview of the ground motions used in the three series of analyses is provided in this section. The first subsection provides an overview of the earthquakes (synthetic and historical) used for the linear and nonlinear series of analyses and the second provides those used for the incremental analyses.

All graphics in the subsequent sections showing the ground motion response spectra include all respective ground motions and their response spectra as well as the NBCC uniform hazard spectrum for the site.

4.4.8.1. Linear and Nonlinear Series of Analyses

The linear and nonlinear analyses used the same suite of ground motions. For both Montreal and Vancouver, each structure was subjected to 10 synthetic ground motions generated by the method outlined by Atkinson (2009). A first selection of synthetic ground motions was done by choosing representative magnitude-distance scenarios for the sites studied. From this group of preselected earthquakes, the 10 accelerograms closest to the NBCC 2005 uniform hazard spectrum between the periods of 0.2 and 2.0 s were chosen and applied to the structures in the transient analyses without any calibration.

The availability of historical ground motions in the western part of Canada permitted the use of an additional 10 ground motions applied to structures located in Vancouver on soils of both class C and E. The selection of these historical ground motions depended on how well they were characteristic of western ground motions. Several guidelines were used to determine this: the site on which the seismograph was located needed to have an appropriate shear wave velocity (360 to 760 m/s for a site class C and less than 200 m/s for a site class E); the magnitude-distance scenarios needed to be representative of the city of Vancouver; and, the site's peak ground acceleration was to be similar to the one given by NBCC 05 for the given site. These historical ground motions were then calibrated such that the area under their spectra were equal to the area under the design spectrum between periods of 0.2 and 2.0 s for a site class C and 0.5 and 2.0 s for a site class E. For site class E, an additional criterion was used in order to limit the peak spectral acceleration, which was sometimes found to be unreasonably high. Calibration for these ground motions was performed such that their spectra never surpass twice the design spectral acceleration for any period past 0.1 s.

Tables of the ground motions used, as well as plots of their responses spectra, are presented in APPENDIX III. Table III.1 shows the synthetic ground motions used for Montreal and Tables III.2 and III.3 show the synthetic and historical ground motions used for Vancouver for site classes C and E, respectively.

4.4.8.2. Nonlinear Incremental Analyses

Nonlinear incremental analyses were performed on two structures located in Vancouver on site class C. As is done in FEMA Report P695 (ATC 2009), only historical ground motions are used for this series of analyses. Ten ground motions were added to the existing ten historical ground motions used in the linear and nonlinear analyses to provide better statistics and were calibrated using the same method outlined in section 4.4.8.1 for historical records.

In order to study the effect of using simulated ground motions versus historical ones when performing incremental analyses, the 10 simulated earthquakes presented in section 4.4.8.1 will also be used to perform incremental analysis on one of the two buildings chosen to study. This will indicate whether simulated earthquakes are representative of the historical ones in practical terms and whether these simulated ground motions allow users to come to the conclusions. The complete list of historical ground motions used for incremental analysis is given in APPENDIX III. Table III.4 shows the response spectra of the twenty historical ground motions used, while the ten simulated ground motions are shown in Table III.2.

4.5. Results

This section provides the results in three different sub-sections, according to the analysis series: linear, nonlinear, and nonlinear incremental. For the first two series, every building was subjected to ten synthetic earthquakes in Montreal. In Vancouver, structures on site class C were subjected to ten synthetic and historical earthquakes, while structures on site class E were subjected to ten synthetic and twelve historical ground motions. In total, 748 time history analyses (linear + nonlinear) were performed, in addition to the incremental analyses. These results are given in the form of figures showing the 50^{th}, 84^{th}, and 100^{th} percentile and tables showing the median of the peak response value at every storey; connection force demands for the linear series and connection axial deformations for the nonlinear series. The incremental nonlinear

dynamic analyses are presented in the format suggested by FEMA P695 (ATC 2009). Brief statistics on the column C_f/C_u ratio are also presented in a fourth sub-section to demonstrate the benefits of using ductile connections on column performance.

The results are presented for the standard buildings, followed by comparisons between the standards buildings and chevrons, site class E, different storey heights, and the location of the brace bents. For each category, the V_e/V_{de} ratios of Table 4.6 are given for the respective buildings and repeated in the linear and nonlinear analysis series for convenience.

It should be noted that a critical damping of 3% was used in all time history analysis, as opposed to the 5% used in the NBCC's design response spectrum. A smaller damping ratio has the effect of increasing the internal forces seen in the members and this is part of the reason connection force demands are greater than the elastic design brace axial loads.

4.5.1. Linear Analyses – Connection Force Demand

The linear results are presented as a P/P_{de} ratio for every storey. P corresponds to the maximum axial load found in the rigid link from the brace connections in the analytical models. P_{de} corresponds to the brace axial load obtained from the response spectrum analysis multiplied by R_oR_d; gravity loads were not included in the linear dynamic analyses and are therefore not reflected in the P/P_{de} ratios. A ratio P/P_{de} equal to 1.0 means the force demand from the time history analyses is identical to the expected resistance of a non-ductile connection, i.e. R_o (1.3) times the design seismic force which was amplified by the R_d (1.5) factor to design the connection.

Standard Buildings. Figures 4.15 and 4.16 show the statistics of the P/P_{de} ratio for both Montreal and Vancouver (synthetic and historical), respectively. The median statistics are shown in tables 4.13 and 4.14 for Montreal and Vancouver, respectively. For Montreal, the V_e/V_{de} ratios are, in increasing order of number of storeys, 0.87, 0.81, 0.83, 0.69, and 0.75. For Vancouver, the V_e/V_{de} ratios are all equal to 1.0.

In Montreal, the median P/P_{de} values were generally below 1.0. However, in the 6- and 8-storey structures, two of the storeys had median connection force demands greater than 1.0, indicating the 15 m height limit is applicable to buildings with non-ductile connections in Montreal. These same statistics vary between 1.06 and 1.47 for synthetic ground motions and 0.96 and 1.50 for historical ground motions in Vancouver. The generally lower demands in Montreal are due to the inherent overstrength of the buildings in Montreal, as indicated by the V_e/V_{de} ratios from Table 4.6 being less than 1.0, versus being equal to 1.0 for most of the buildings in Vancouver. In general, the force demand in Vancouver tends to decrease with the building height. However, structures in Vancouver are clearly subjected to greater connection force demands, suggesting conventional construction with non-ductile connections is not suitable for Vancouver, or that the connection design forces should be increased. On average over the building heights and for simulated ground motions, the ratio Vancouver to Montreal for P/P_{de} ratios varied between 1.3, 1.4, 1.4, 1.5, and 1.4 for buildings with 2, 4, 6, 8, and 10 storeys, respectively. Connections in Vancouver are therefore subjected to between 30 and 50 per cent more connection demands than Montreal. To avoid any heights limits, connections would have to be designed for seismic forces corresponding to R_oR_d of 0.8 and 0.65 for Montreal and Vancouver, respectively.

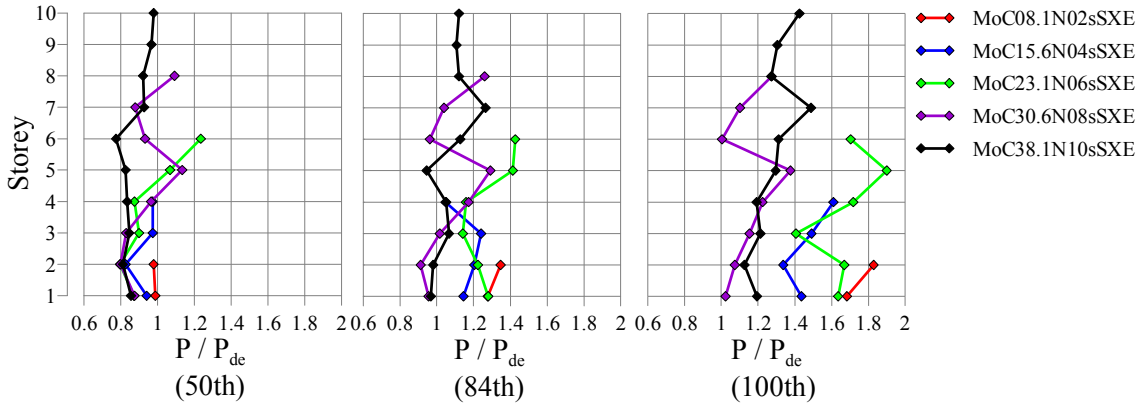

Figure 4.15: P/P_{de} statistics for Montreal standard buildings.

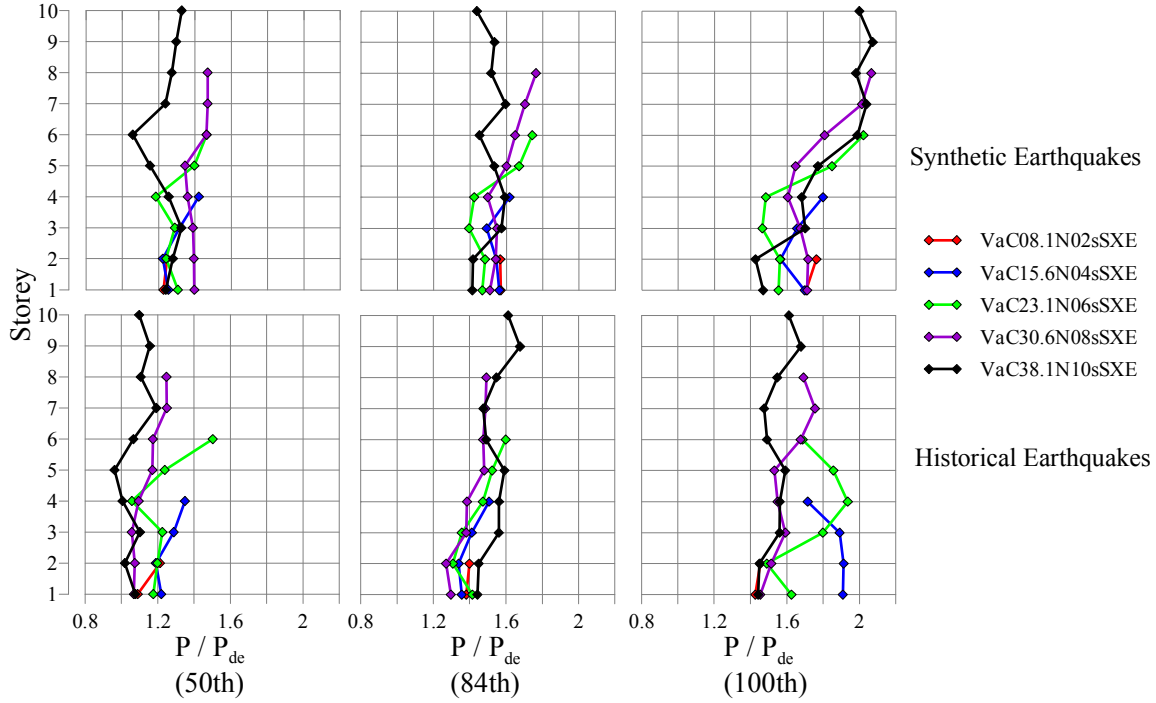

Figure 4.16: P/P_{de} statistics for Vancouver standard buildings.

Table 4.13: Median P/P_{de} ratio in Montreal standard buildings.

Storey	MoC08.1N02sSXE	MoC15.6N04sSXE	MoC23.1N06sSXE	MoC30.6N08sSXE	MoC38.1N10sSXE
10					0.98
9					0.97
8				1.09	0.92
7				0.88	0.93
6			1.23	0.93	0.77
5			1.07	1.13	0.83
4		0.97	0.87	0.97	0.83
3		0.97	0.90	0.83	0.85
2	0.98	0.83	0.80	0.80	0.81
1	0.99	0.94	0.87	0.87	0.86

Table 4.14: Median P/P_{de} ratios for Vancouver standard buildings.

	Synthetic					Historical				
Storey	VaC08.1N02sSXE	VaC15.6N04sSXE	VaC23.1N06sSXE	VaC30.6N08sSXE	VaC38.1N10sSXE	VaC08.1N02sSXE	VaC15.6N04sSXE	VaC23.1N06sSXE	VaC30.6N08sSXE	VaC38.1N10sSXE
10					1.33					1.10
9					1.30					1.16
8				1.47	1.27				1.25	1.11
7				1.47	1.24				1.25	1.19
6			1.46	1.46	1.06			1.50	1.17	1.07
5			1.40	1.35	1.15			1.24	1.17	0.96
4		1.42	1.18	1.36	1.26		1.35	1.06	1.10	1.01
3		1.31	1.29	1.39	1.32		1.29	1.23	1.06	1.10
2	1.25	1.22	1.24	1.39	1.28	1.21	1.19	1.20	1.07	1.02
1	1.23	1.25	1.31	1.40	1.24	1.09	1.22	1.18	1.07	1.08

Chevron bracings. Figures 4.17 and 4.18 show, respectively, a comparison of the complete statistics between buildings with chevrons and split-x bracing in Montreal and Vancouver. Table 4.15 shows the median statistics only of the same buildings. In Montreal, the V_e/V_{de} ratios are 0.81 and 0.69 for the split-x and 0.67 and 0.57 for chevrons for the 4- and 8-storey buildings, respectively. In Vancouver, the same ratios are equal to 1.0 for split-x, and 0.95 and 0.89 for 4- and 8-storey chevrons. Table 4.6 shows that split-x and chevron bracings are designed for the same base shear but that chevrons are more flexible, based on the structural periods.

It is evident that chevron connections have lower force demands than split-x ones, especially at the 84^{th} and 100^{th} statistics. This is due to the lower V_e/V_{de} ratios for the chevron buildings. The median ratios for chevrons in Montreal vary between 0.80 and 0.88 (0.83 and 0.97 for split-x) for 4 storeys and 0.68 and 0.98 (0.80 and 1.13 for split-

x) for 8 storeys. Based on these numbers, the 15 m height limit need not be applied for non-ductile connections in chevron bracings, contrary to split-x bracing. For synthetic ground motions in Vancouver, the P/P_{de} ratios for chevrons vary between 1.11 and 1.40 (1.22 and 1.42 for split-x) for 4 storeys and 1.17 and 1.45 (1.35 and 1.47 for split-x) for 8 storeys. For historical ground motions, the same ratios vary between 1.17 and 1.35 (1.19 and 1.35 for spit-x) for 4 storeys and 0.93 and 1.29 (1.06 and 1.25 for split-x) for 8 storeys. The lower ratios in Montreal can, again, be attributed to the lower V_e/V_{de} ratios. Even with the smaller force demand in the chevrons, chevron-braced structures in Vancouver still exhibit median P/P_{de} ratios greater than 1.0 in both the 4- and 8-storey buildings, suggesting conventional construction with chevrons is not suitable, like the split-x bracing, in Vancouver unless the connections design forces are increased in addition to the existing R_d increase. An additional increase of 50% in the connection design force (which used R_oR_d of 1.3) would provide safe non-ductile connections in Vancouver. This corresponds to a R_oR_d of 0.65.

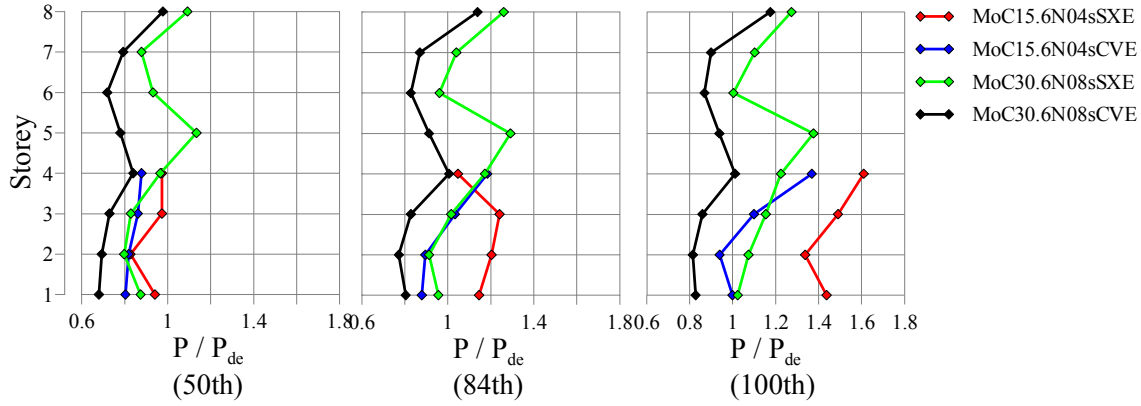

Figure 4.17: P/P_{de} statistics for chevron and split-x bracings in Montreal.

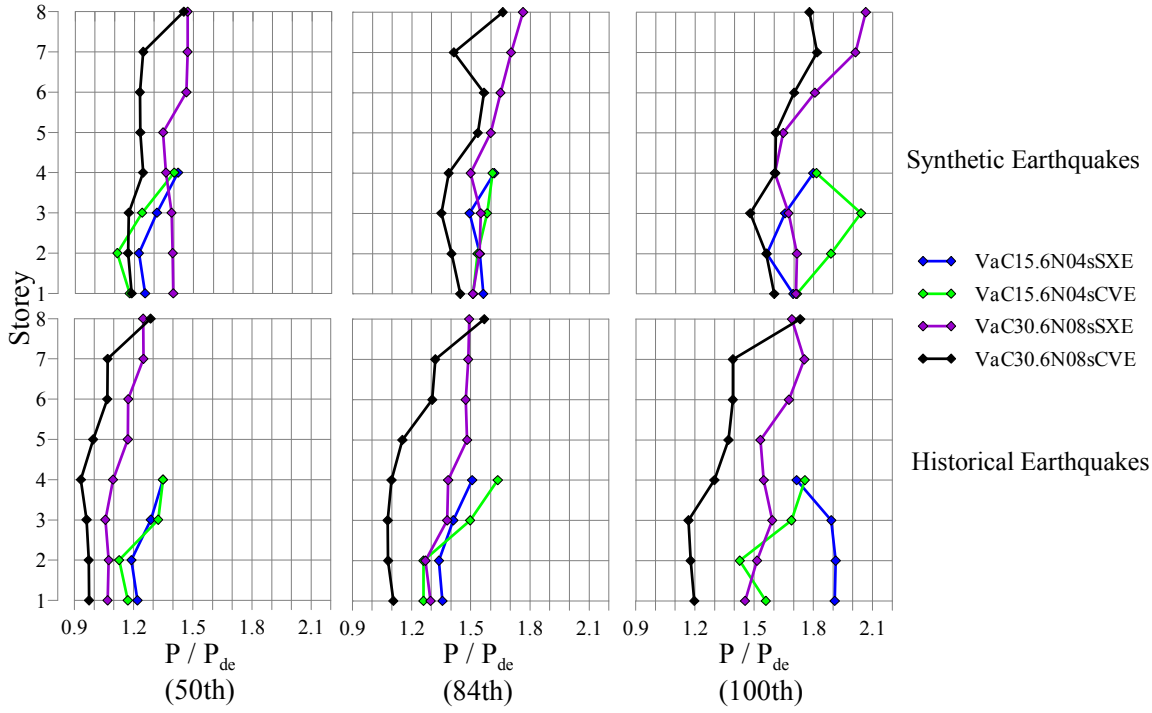

Figure 4.18: P/P_{de} statistics for chevron and split-x bracings in Vancouver.

Table 4.15: Median P/P_{de} ratios for chevrons and split-x in Montreal and Vancouver.

					Synthetic EQs				Historical EQs			
Storey	MoC15.6N04sSXE	MoC15.6N04sCVE	MoC30.6N08sSXE	MoC30.6N08sCVE	VaC15.6N04sSXE	VaC15.6N04sCVE	VaC30.6N08sSXE	VaC30.6N08sCVE	VaC15.6N04sSXE	VaC15.6N04sCVE	VaC30.6N08sSXE	VaC30.6N08sCVE
8			1.09	0.98			1.47	1.45			1.25	1.29
7			0.88	0.79			1.47	1.24			1.25	1.07
6			0.93	0.72			1.46	1.23			1.17	1.07
5			1.13	0.78			1.35	1.23			1.17	1.00
4	0.97	0.88	0.97	0.84	1.42	1.40	1.36	1.24	1.35	1.35	1.10	0.93
3	0.97	0.86	0.83	0.73	1.31	1.24	1.39	1.17	1.29	1.32	1.06	0.96
2	0.83	0.82	0.80	0.69	1.22	1.11	1.39	1.17	1.19	1.13	1.07	0.97
1	0.94	0.80	0.87	0.68	1.25	1.18	1.40	1.19	1.22	1.17	1.07	0.97

Site Classes C and E. Figures 4.19 and 4.20 show the complete statistics on the effects of having site classes C and E in Montreal and Vancouver, respectively. Table 4.16 shows the median statistics for both cities. In Montreal, the V_e/V_{de} ratios are 0.81 and 0.69 for site classes C and 1.0 and 0.88 for site classes E for 4- and 8-storey buildings, respectively. The same ratios are, in Vancouver, equal to 1.0 for site classes C and to 1.0 and 0.97 for site classes E for 4- and 8-storey buildings, respectively.

Designing for a site class E has the effect of increasing the design seismic loads, which in turn increases the lateral stiffness and decreases the structural period. This has the effect of increasing the V_e/V_{de} ratio for buildings located on a soil of site class E, as shown in Table 4.6 and mentioned above. The differences between the two site classes are as noticeable in Montreal as they are in Vancouver. The median ratios for site class E in Montreal vary between 1.06 and 1.29 (0.83 and 0.97 for C) for 4 storeys and 0.97 and 1.20 (0.80 and 1.13 for C) for 8 storeys. For simulated ground motions in Vancouver, the median ratios vary between 1.32 and 1.48 (1.22 and 1.42 for C) for 4 storeys and 1.63 and 1.88 (1.35 and 1.47 for C) for 8 storey, while for historical ground motions these ratios vary between 1.17 and 1.35 (1.19 and 1.35 for C) for 4 storeys and 1.27 and 1.51 (1.06 and 1.25 for C) for 8 storeys. From these figures, we see that the synthetic earthquakes yielded significantly larger ratios for site class E and that the differences between the two site classes are greater in Vancouver. Based on these results, conventional construction is not suitable for site classes E in either Montreal or Vancouver with non-ductile connections. Alternatively, the structures could be used provided that the connections are designed for seismic forces corresponding to a R_oR_d of 0.76 in Montreal and 0.65 in Vancouver. These numbers would allow structures of any height up to 30.1 m and structures up to 15 m in height to be built in Montreal and Vancouver, respectively.

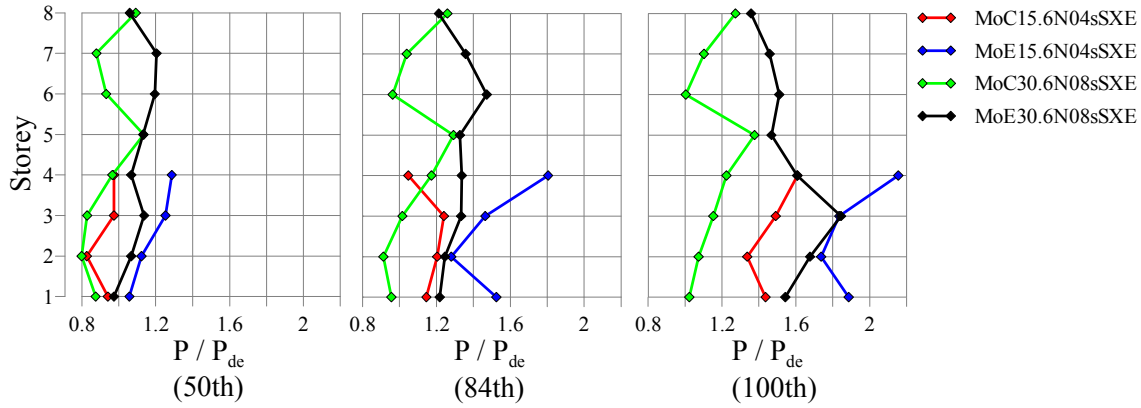

Figure 4.19: P/P_{de} statistics for site classes C and E in Montreal.

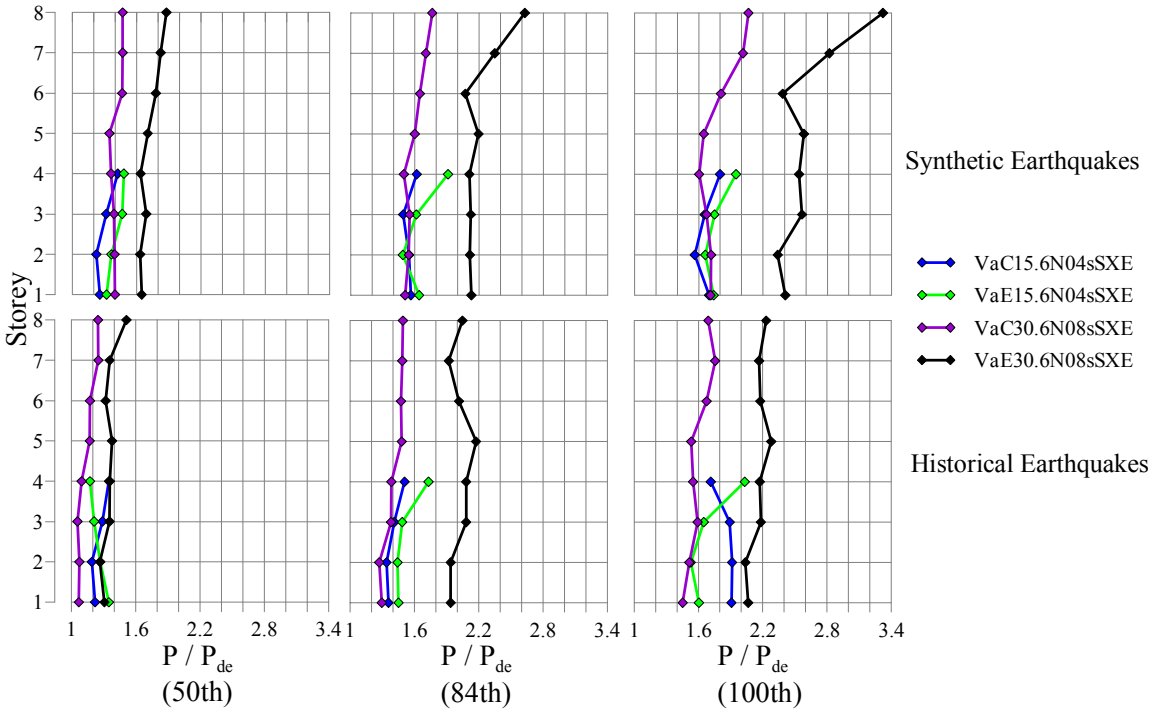

Figure 4.20: P/P_{de} statistics for site classes C and E in Vancouver.

Table 4.16: Median P/P_{de} ratios of site classes C and E in Montreal and Vancouver.

					Synthetic EQs				Historical EQs			
Storey	MoC15.6N04sSXE	MoE15.6N04sSXE	MoC30.6N08sSXE	MoE30.6N08sSXE	VaC15.6N04sSXE	VaE15.6N04sSXE	VaC30.6N08sSXE	VaE30.6N08sSXE	VaC15.6N04sSXE	VaE15.6N04sSXE	VaC30.6N08sSXE	VaE30.6N08sSXE
8			1.09	1.06			1.47	1.88			1.25	1.51
7			0.88	1.20			1.47	1.82			1.25	1.36
6			0.93	1.20			1.46	1.78			1.17	1.32
5			1.13	1.13			1.35	1.70			1.17	1.38
4	0.97	1.29	0.97	1.07	1.42	1.48	1.36	1.64	1.35	1.17	1.10	1.36
3	0.97	1.25	0.83	1.14	1.31	1.46	1.39	1.69	1.29	1.21	1.06	1.36
2	0.83	1.12	0.80	1.07	1.22	1.36	1.39	1.63	1.19	1.27	1.07	1.27
1	0.94	1.06	0.87	0.97	1.25	1.32	1.40	1.65	1.22	1.35	1.07	1.31

Storey heights. Figures 4.21 and 4.22 show the complete statistics on the effects of having different storey heights for the same total building height in Montreal and Vancouver, respectively. Table 4.17 shows the median statistics for both cities. The V_e/V_{de} ratios are equal to 0.73, 0.67, and 0.60 in Montreal and 1.0, 0.95, and 0.85 in Vancouver for 3-, 4-, and 5-storey buildings, respectively.

In both locations, the 5-storey building has the lowest V_e/V_{de} ratio and should be expected to have the lowest P/P_{de} ratios. The following two figures show this is the case for the 50^{th}, 84^{th}, and 100^{th} percentile in both locations. This is due to the fact that the 5-storey buildings have the lowest V_e/V_{de} ratios of the three buildings. No obvious trend exists between the three different storey height patterns other than this one. In Montreal, the median ratios vary between 0.77 and 0.85, 0.80 and 0.88, and 0.64 and 0.84 for the 3-, 4-, and 5-storey buildings, respectively. For simulated earthquakes in Vancouver, the same ratios vary between 1.16 and 1.36, 1.11 and 1.40, and 1.05 and 1.38. For historical earthquakes in Vancouver, these ratios vary between 1.18 and 1.32, 1.13 and 1.35, and .97 and 1.22. From figures 4.21 and 4.22, it can be seen that chevrons tend to have the

highest connection demands in the uppermost storey; this is not the case with split-x bracings. This may lead to higher connection ductility demand in the upper storeys, and is discussed in section 4.5.2.

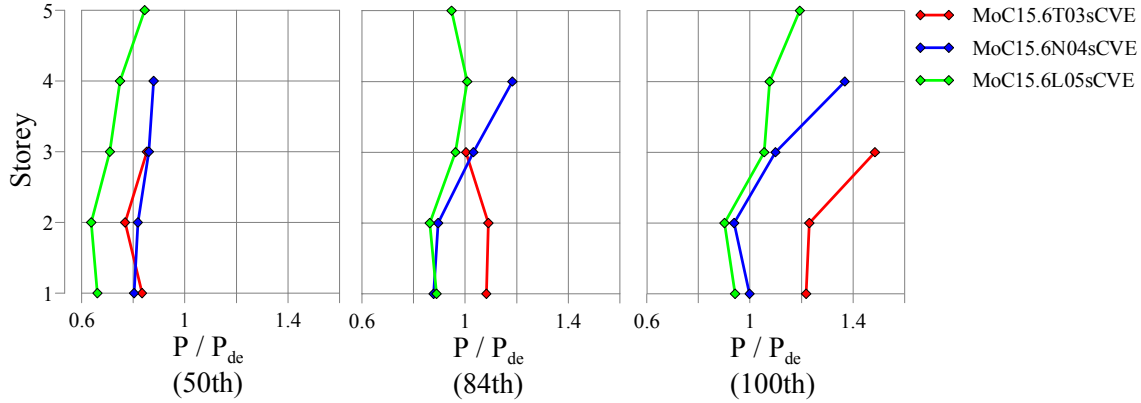

Figure 4.21: P/P_{de} statistics for different storey heights in Montreal.

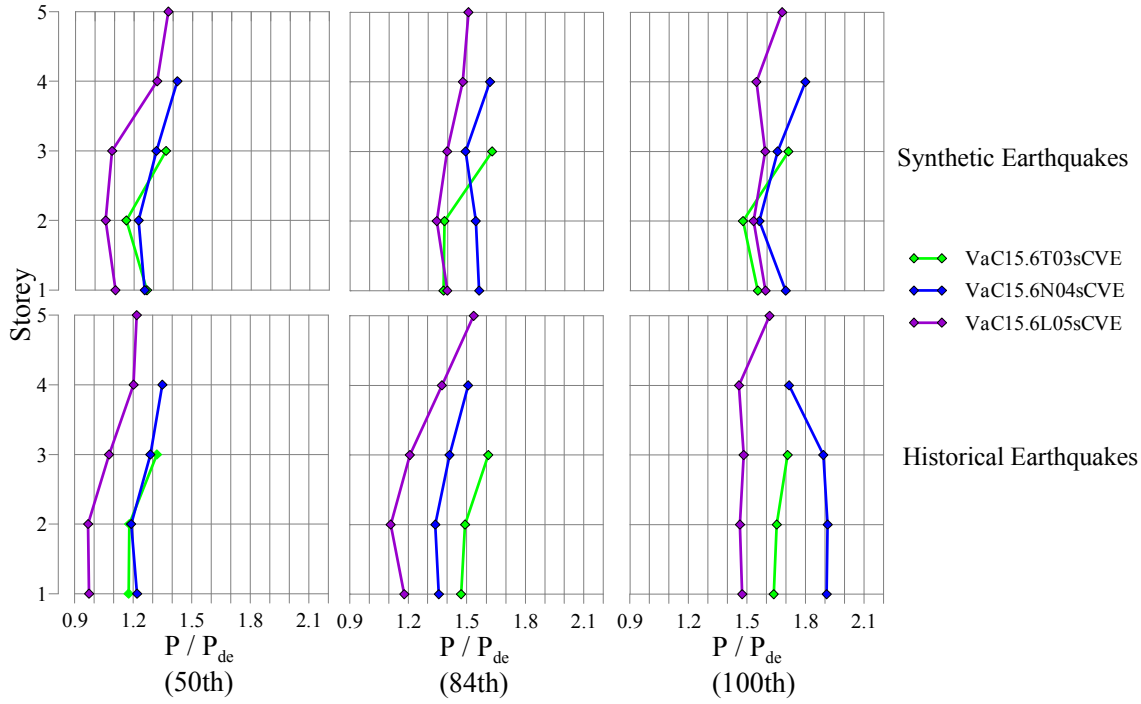

Figure 4.22: P/P_{de} statistics for different storey heights in Vancouver.

Table 4.17: Median P/P_{de} ratios of different storey height effects in Montreal and Vancouver.

				Synthetic EQs			Historical EQs		
Storey	MoC15.6N04sCVE	MoC15.6T03sCVE	MoC15.6L05sCVE	VaC15.6N04sCVE	VaC15.6T03sCVE	VaC15.6L05sCVE	VaC15.6N04sCVE	VaC15.6T03sCVE	VaC15.6L05sCVE
5			0.84			1.38			1.22
4	0.88		0.75	1.40		1.32	1.35		1.20
3	0.86	0.85	0.71	1.24	1.36	1.09	1.32	1.32	1.08
2	0.82	0.77	0.64	1.11	1.16	1.05	1.13	1.18	0.97
1	0.80	0.83	0.66	1.18	1.27	1.10	1.17	1.18	0.97

Braced bent location. Figure 4.23 shows the complete statistics on the effects of having the braced bent located either on the perimeter of the building or in the building's interior. This also looks at the effects of having greater gravity loads and was only studied in Vancouver. Table 4.18 shows the median statistics. The V_e/V_{de} ratios are equal to 1.0 for exterior and interior bracings.

Looking at the simulated ground motions results in Figure 4.23, there is no significant difference, or tendency, between interior and exterior braced bent locations. However, the historical ground motions indicate slightly higher ratios for interior locations, suggesting that interior braced bents may have a negative effect on the connection demand. Table 4.6 shows SXI buildings to be slightly stiffer when looking at their periods. This is due to the additional base shear coming from the accidental torsion (10%). A higher proportion of the seismic load goes into each brace bents when the distance between the brace bents is decreased while the 10% is always based on the total building width. The interior braced bay locations translate into an increase of 6.7% of the base shear proportion transferred over to a braced bent. An exterior braced bent should translate into lower higher connection force demands, but only if its spectral

design base shear is lower than 80% of the equivalent static base shear. Median ratios under simulated ground motions vary between 1.22 and 1.47 on exterior bracing bents and 1.19 and 1.56 on interior bents. The same ratios for historical ground motions vary between 1.06 and 1.35, and 1.11 and 1.57 for exterior and interior bracing bents, respectively.

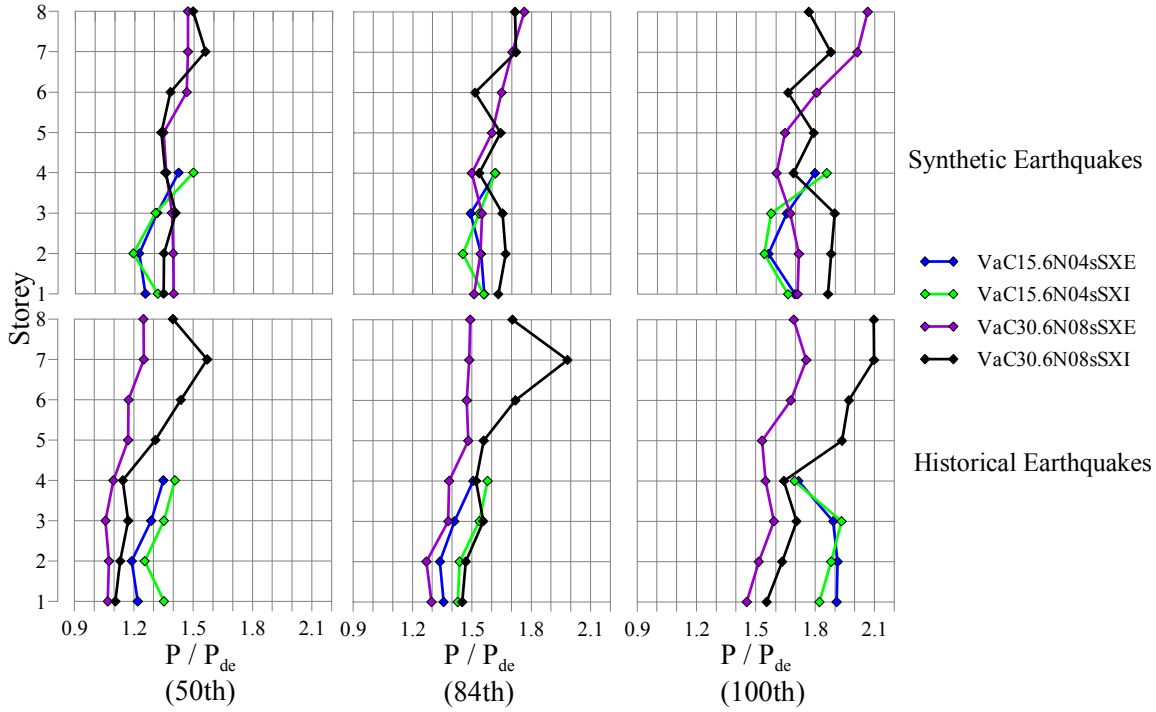

Figure 4.23: P/P_{de} statistics for different braced bent location in Vancouver.

Table 4.18: Median P/P_{de} ratios of different brace bent location effects in Vancouver.

	Synthetic EQs				Historical EQs			
Storey	VaC15.6N04sSXE	VaC15.6N04sSXI	VaC30.6N08sSXE	VaC30.6N08sSXI	VaC15.6N04sSXE	VaC15.6N04sSXI	VaC30.6N08sSXE	VaC30.6N08sSXI
8			1.47	1.50			1.25	1.40
7			1.47	1.56			1.25	1.57
6			1.46	1.38			1.17	1.44
5			1.35	1.33			1.17	1.31
4	1.42	1.50	1.36	1.35	1.35	1.41	1.10	1.14
3	1.31	1.31	1.39	1.41	1.29	1.35	1.06	1.17
2	1.22	1.19	1.39	1.35	1.19	1.25	1.07	1.13
1	1.25	1.32	1.40	1.35	1.22	1.35	1.07	1.11

4.5.1.1. Discussion of Linear Analyses Results

In the linear analyses presented in section 4.5.1 and used to estimate the connection force demand, axial forces considerably higher than the design forces were obtained. Part of this difference can be explained by the fact that a Rayleigh damping equal to 3% of the critical damping was specified in the first two modes while the NBCC 2005 uses spectral accelerations damped to 5%. The Eurocode 8 (ECS 2003) suggests that the difference between these two damping values is an increase of 13% in member forces from analyses with a damping value of 3%. This can account for some of the differences found in section 4.5.1 but does not explain why some median axial forces are sometimes up to 50% greater than the design forces, as shown in Table 4.14.

In an attempt to explain the higher axial loads encountered, several analyses were carried out to examine several parameters concerning the effect of the specified damping on modal and time history analyses. A SAP 2000 (Computer & Structures Inc. 2008) model developed in conjunction with Guilini-Charette, and found in Chapter 3 of

her thesis (Guilini-Charette 2009), was used. This model is equivalent to the VaC15.6N04sSXE model as found in this thesis. A single ground motion was used and Figure 4.24 shows its response spectrum considering 3% and 5% damping as well as the NBCC05 response spectrum (5%). Note that the structure's first two periods of vibration are shown in the same figure. Five analyses were performed and were as follows:

1) Spec – 5%: Spectral analysis using the ground motion's response spectrum considering 5% damping.

2) Spec – 3%: Spectral analysis using the ground motion's response spectrum considering 3% damping.

3) TH – Modal – 3%: Time history analysis using modal superposition considering 3% damping.

4) TH – DI – 3%: Time history analysis using direct integration considering 3% damping.

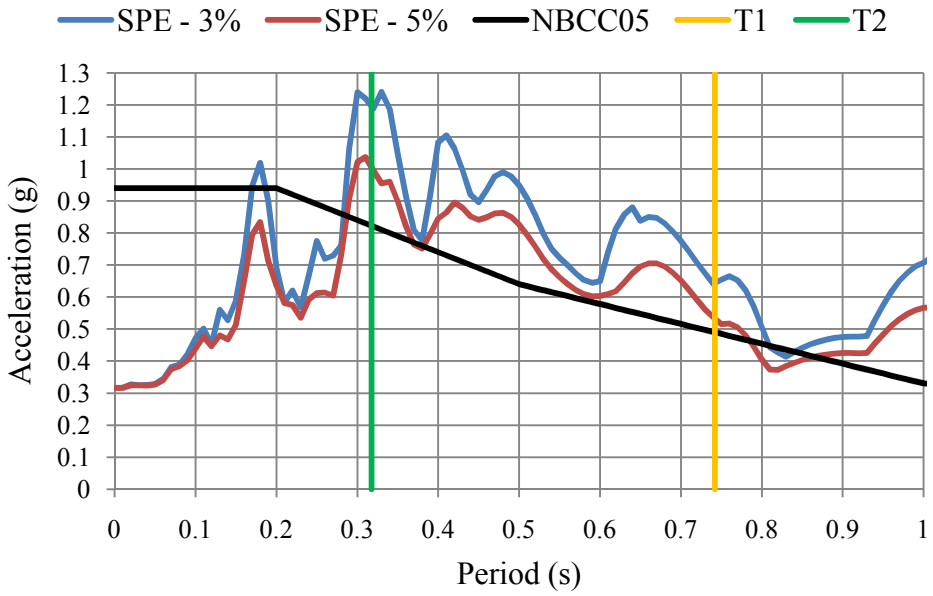

Figure 4.24: Ground motion and NBCC05's response spectra.

The reader is referred to Guilini-Charette's thesis (2009) for a more detailed presentation of the results from the latter analyses. A summary of those results is presented in this section to briefly explain where the high P/P_{de} ratios are coming from.

For each of the analyses enumerated above, Table 4.19 offers percentage differences between the different types of analyses.

Table 4.19: Maximum brace axial load ratios between different analyses.

	Percentage difference			
Storey	SPEC 3% / SPEC 5%	TH DI 3% / TH Modal 3%	TH DI 3% / SPEC 3%	TH-DI 3% / SPEC 5%
1	1.20	1.01	0.98	1.18
2	1.21	0.99	0.98	1.19
3	1.21	0.99	1.00	1.21
4	1.21	1.00	1.20	1.45

The first results column of Table 4.19 shows the spectral analysis with 3% damping yielded brace axial forces approximately 20% greater than the spectral analysis with 5% damping. As mentioned earlier, the Eurocode 8 (ECS 2003) states that this difference can be around 13%. These two analyses showed that this difference can be greater than 13% and somewhere around 20%.

The second results column shows the difference between time history analyses using modal superposition and direct integration. The difference between the two is shown to be negligible in this case.

The third results column shows the difference between a spectral and direct-integration time history analysis using 3% damping. There is very little difference in the first three storeys; a 20% difference is found in the fourth and uppermost storey. This indicates the spectral analysis did not provide a good estimate of the force at the fourth storey. Upon further inspection of the results from the modal time history analysis and as shown in Guilini-Charette's thesis (2009), it was shown the maximum brace axial load from the time history analysis occurred when the brace axial load from the building's second

vibration mode was at its maximum at the same time as the load coming from the first mode; they were also of the same sign. Since the modal combination methods (SRSS, CQC) consider that the maximum loads coming from different modes are not likely to occur at the same time, the spectral analysis underestimated the loads at the uppermost storey. This is the likely explanation for the higher brace axial loads encountered in section 4.5.1 and is consistent with what is shown, for example, in tables 4.13 and 4.14. These showed that the maximum P/P_{de} ratios often occurred at the uppermost storeys.

The fourth results column shows the ratios between the direct integration time history analysis using 3% damping and the spectral analysis using 5% damping. These ratios give a good overview of the results obtained in section 4.5.1.

4.5.2. Nonlinear Analyses – Connection Ductility Demand

The nonlinear analyses results are presented in the form of statistics (50^{th}, 84^{th}, and 100^{th} percentiles) on the total deformations of brace connections. On every floor, connections were modeled at the bottom of both braces and acted as ductile links. The statistics were done on the maximum connection deformation from every storey from all earthquakes along the height of the building. Gravity loads were included in the analyses. In general, the connection ductility demand encountered in this series of analyses will be compared to the maximum connection ductility capacity as discussed in section 4.4.6, which was estimated to be about 31 mm. Results from the analyses correspond to the total connection deformation for the brace, i.e., the sum of the deformation demand on both end connections. As previously discussed, it is assumed that 20% of that deformation will develop at one end and 80% at the opposite end when fracture will occur at the latter. The limit value of 31 mm was established based on this assumption and hence corresponds to the total deformation capacity of the two connections. That value can therefore be directly compared to the analysis results. The 31 mm limit was also used as the connection breaking point in terms of deformation in the nonlinear incremental analyses series, reported in section 4.5.3.

One may expect the deformation demands to exhibit the same trends and relative results as the linear analyses, but this was not necessarily the case. The structures in this analysis series entered their inelastic domain, causing their periods to increase and situate themselves farther to the right on the ground motion's response spectrum. The nonlinear nature of the buildings caused them to exhibit different trends then the linear analyses results.

Standard buildings. Figures 4.25 and 4.26 show the statistics of the connection deformations for both Montreal and Vancouver, respectively. The median deformation statistics are shown in tables Table 4.20 and 4.21 for Montreal and Vancouver, respectively. For Montreal, the V_e/V_{de} ratios are, in increasing order of number of storeys, 0.87, 0.81, 0.83, 0.69, and 0.75. For Vancouver, the V_e/V_{de} ratios are all equal to 1.0.

As can be seen in Figure 4.25, connections in Montreal's standard buildings were never in clear danger of exceeding the 31 mm limit, suggesting that the 15 m height limit need not be applied for these standard buildings with ductile connections in Montreal. Median deformations in Montreal were between 3.7 mm and 7.3 mm. The maximum encountered deformation was just over 21 mm. The situation, however, is more critical in Vancouver. Current design provisions did not provide uniform inelastic deformations along the height of the buildings, especially if a low probability of exceeding the 31 mm is sought. Median deformations were below the 31 mm limit in buildings of 4 storeys or less, while this limit was exceeded in buildings of greater heights, suggesting the 15 m height should be enforced. Overall, median deformations varied between 7.6 mm and 37.0 mm and between 7.1 mm and 33.5 mm for simulated and historical ground motions, respectively. 84^{th} percentile deformation values are significantly above 31 mm as seen in Figure 4.26. From the same figure, buildings with heights greater than 15 m undergo more connection deformations. The higher deformation demands in Vancouver can be explained by the higher V_e/V_{de} ratios, compared to the same ratios being lower than 1.0 in Montreal, which indicated a higher overstrength. On average over the

building heights and for simulated ground motions only, the ratio Vancouver to Montreal for deformations varied between 2.3, 2.0, 3.2, 3.1, and 3.6 for buildings with 2, 4, 6, 8, and 10 storeys, respectively. Connections in Vancouver are therefore subjected to much higher connection deformations than Montreal.

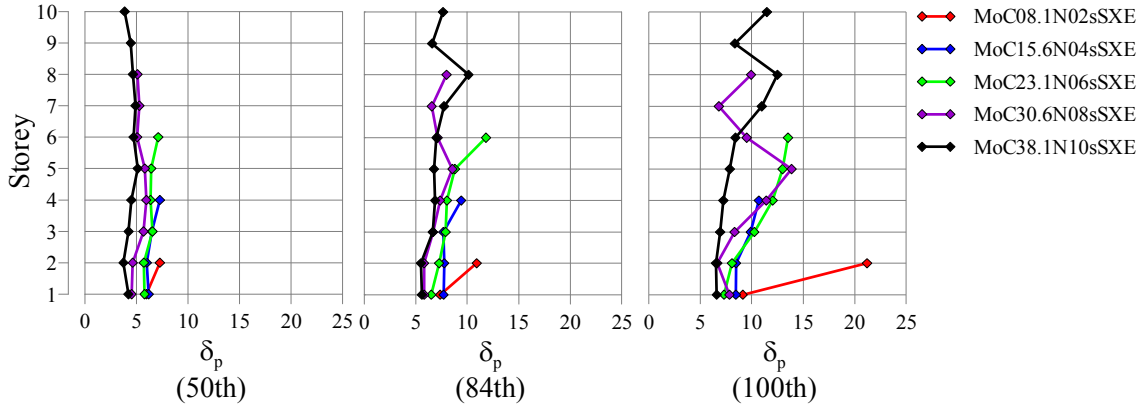

Figure 4.25: Deformation statistics for standard buildings in Montreal under simulated ground motions.

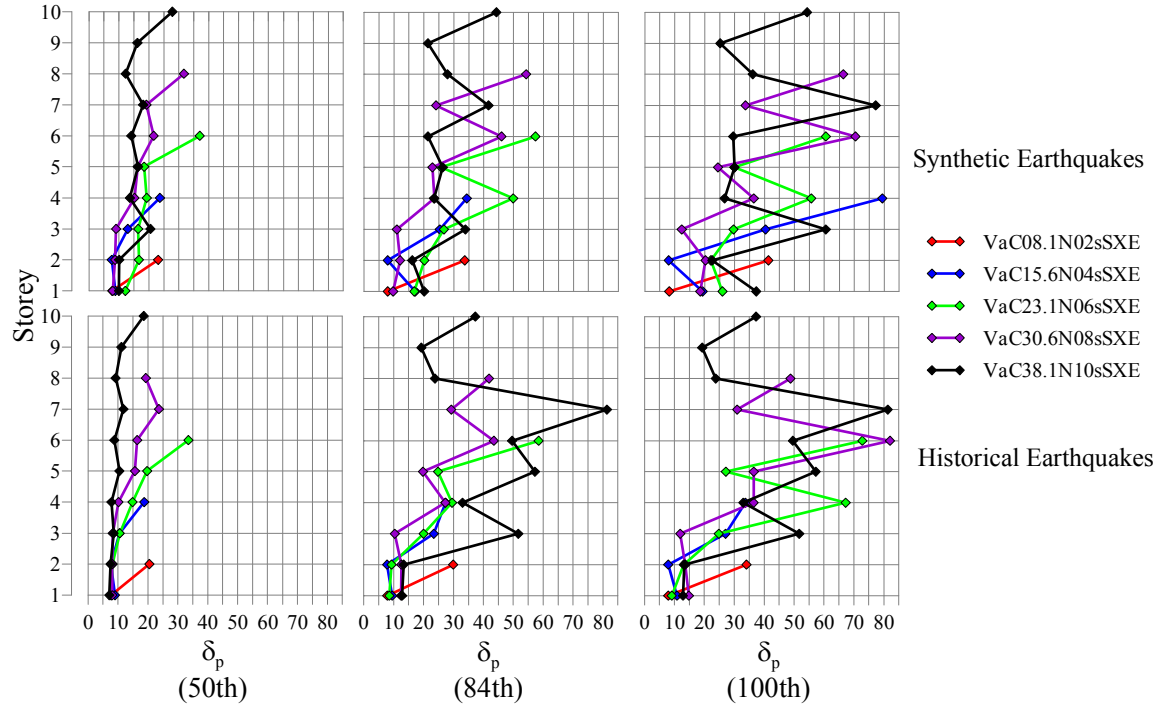

Figure 4.26: Deformation statistics for standard buildings in Vancouver under simulated and historical ground motions.

Table 4.20: Median deformations in Montreal standard buildings.

Storey	MoC08.1N02sSXE	MoC15.6N04sSXE	MoC23.1N06sSXE	MoC30.6N08sSXE	MoC38.1N10sSXE
10					3.8
9					4.4
8				5.1	4.7
7				5.3	4.9
6			7.1	5.1	4.7
5			6.4	5.8	5.1
4		7.3	6.4	6.0	4.5
3		6.5	6.6	5.7	4.2
2	7.3	6.0	5.7	4.6	3.7
1	6.0	6.2	5.8	4.5	4.2

Table 4.21: Median deformations from simulated and synthetic ground motions in Vancouver standards buildings.

	Simulated EQs					Historical EQs				
Storey	VaC08.1N02sSXE	VaC15.6N04sSXE	VaC23.1N06sSXE	VaC30.6N08sSXE	VaC38.1N10sSXE	VaC08.1N02sSXE	VaC15.6N04sSXE	VaC23.1N06sSXE	VaC30.6N08sSXE	VaC38.1N10sSXE
10					27.9					18.6
9					16.2					11.2
8				31.8	12.2				19.3	9.2
7				19.2	18.1				23.7	11.8
6			37.0	21.6	14.1			33.5	16.5	8.8
5			18.4	16.3	16.4			19.7	15.7	10.4
4		23.7	19.3	15.2	13.7		18.8	14.9	10.2	7.8
3		12.9	16.4	9.0	20.5		10.4	10.6	8.2	8.5
2	23.1	7.6	16.7	8.7	10.1	20.4	7.6	8.1	8.1	7.5
1	7.8	8.8	12.1	7.9	10.0	7.8	9.0	7.7	8.1	7.1

Chevrons bracings. Figures 4.27 and 4.28 show the complete deformation statistics on the split-x and chevrons braced structures in Montreal and Vancouver, respectively. Table 4.22 shows the median deformations for the same buildings. In Montreal, the V_e/V_{de} ratios are 0.81 and 0.69 for the split-x and 0.67 and 0.57 for chevrons for the 4- and 8-storey, respectively. In Vancouver, the same ratios are equal to 1.0 for split-x, and 0.95 and 0.89 for 4- and 8-storey chevrons.

There exist little differences between connection deformations of split-x and chevron braced buildings in Montreal. Deformations were kept below the 31 mm limit in Montreal and the median deformations varied between 3.9 mm and 7.3 mm for both types of bracing systems and both the 4- and 8-storey buildings. In Vancouver, the chevron braced buildings seem to have a more uniform distribution of the inelastic deformations along the building height than the split-x braced frames. This is particularly seen at the 84^{th} percentile level in the taller structures. A non-uniform distribution of the connection deformations along the building height can lead to concentrated ductility demands, which is unfavourable to structural elements. Chevron bracings had the general advantage of going through smaller amounts of deformation, which is consistent with the findings of the linear analyses where it was found that connections in chevrons underwent a smaller force demand. As was seen with the force demand in the linear analyses, the median deformations are consistently concentrated at the top level of the Vancouver chevron braced frames, with higher median deformations than the absolute greatest deformation found in its split-x counterpart. This is thought to be due to the smaller columns used. However, at higher probability levels, greater deformation concentrations are observed in the split-x systems. Split-X and chevrons therefore both have their advantages and disadvantages, but based on these observations, one is not more desirable over the other.

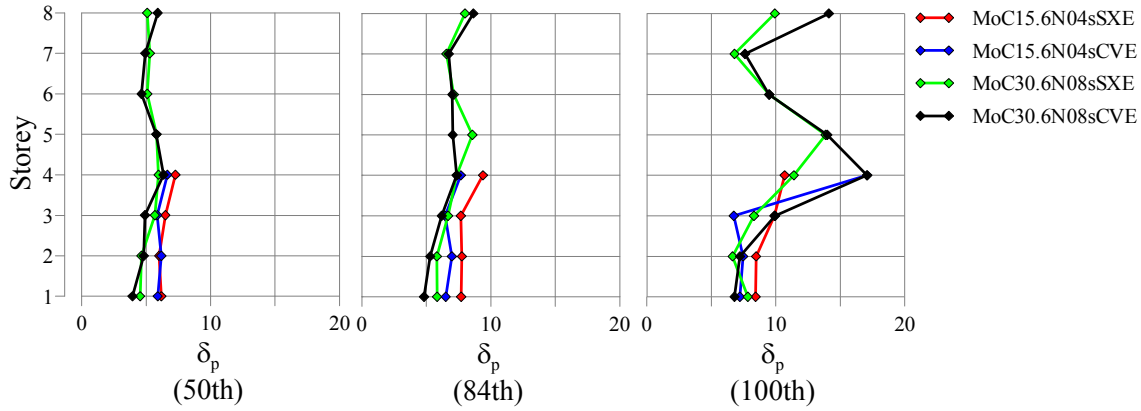

Figure 4.27: Deformation statistics for chevron and split-x bracings in Montreal.

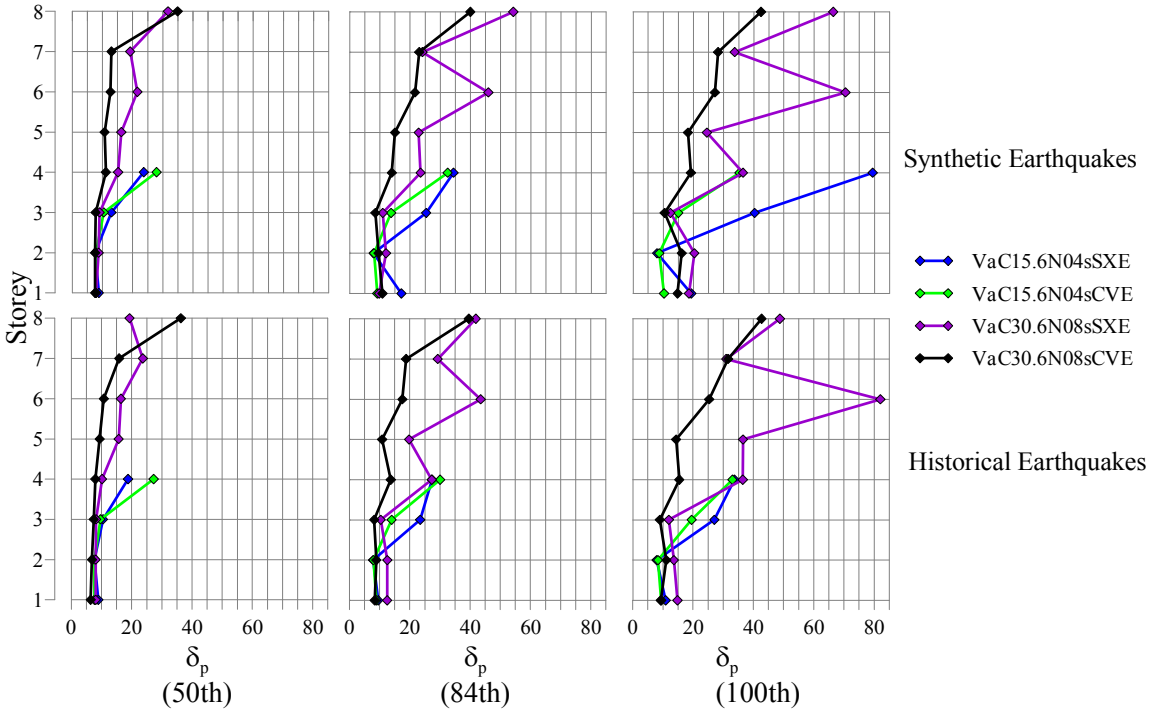

Figure 4.28: Deformations statistics for chevron and split-x bracings in Vancouver under simulated and historical ground motions.

Table 4.22: Median deformations for split-x and chevrons in Montreal and Vancouver.

					Synthetic EQs				Historical EQs			
Storey	MoC15.6N04sSXE	MoC15.6N04sCVE	MoC30.6N08sSXE	MoC30.6N08sCVE	VaC15.6N04sSXE	VaC15.6N04sCVE	VaC30.6N08sSXE	VaC30.6N08sCVE	VaC15.6N04sSXE	VaC15.6N04sCVE	VaC30.6N08sSXE	VaC30.6N08sCVE
8			5.1	5.9			31.7	34.9			19.3	36.3
7			5.3	4.9			19.2	13.0			23.7	15.9
6			5.1	4.6			21.6	12.7			16.5	10.8
5			5.8	5.8			16.3	10.7			15.7	9.4
4	7.3	6.6	6.0	6.3	23.7	28.0	15.2	11.1	18.8	27.3	10.2	8.0
3	6.5	5.9	5.7	4.9	12.9	10.4	9.0	7.7	10.4	9.6	8.2	7.4
2	6.0	6.2	4.6	4.8	7.6	7.9	8.7	7.6	7.6	7.6	8.0	6.9
1	6.2	5.9	4.5	3.9	8.8	7.7	7.9	7.6	9.0	7.6	8.1	6.4

Site classes C and E. Figure 4.29 and Figure 4.30 show the complete statistics for the connection deformations in site classes C and E for Montreal and Vancouver, respectively. Table 4.23 shows the median deformations for both site classes. In Montreal, the V_e/V_{de} ratios are 0.81 and 0.69 for site classes C and 1.0 and 0.88 for site classes E for 4- and 8-storey buildings, respectively. The same ratios are, in Vancouver, equal to 1.0 for site classes C and to 1.0 and 0.97 for site classes E for 4- and 8-storey buildings, respectively.

A site class E has the effect of increasing the connection deformation demand in both Montreal and Vancouver. In Montreal, the differences are mostly seen in the 8-storey building at the median deformations. When a low probability of exceeding the 31 mm is sought, a 15 m height limit would be applicable in Montreal as the 8-storey building underwent important deformations at its fourth storey as shown in Figure 4.29 at the 84th percentile level. However, based on the median deformations as was done when comparing other results, a 15 m height limit is not needed in Montreal for site classes E.

Median deformations for site class E in Montreal varied between 6.7 and 14.0 mm (6.0 and 7.3 mm for C) for 4 storeys and 6.1 and 10.1 mm (4.5 and 6.0 mm for C) for 8 storeys. Under simulated ground motions in Vancouver, these deformations vary between 20.8 and 41.8 mm (7.6 and 23.7 mm for C) for 4 storeys and 16.9 and 65.0 mm (7.9 and 31.7 mm for C) for 8 storeys, while historical ground motions gave deformations between 11.9 and 26.8 mm (7.6 and 18.6 mm for C) for 4 storeys and 8.2 and 36.5 mm (8.0 and 23.7 mm for C) for 8 storeys. In Vancouver, while the 4-storey building on site class C does not have median deformations above the 31 mm limit, the site class E 4-storey building exceeds this limit under simulated ground motions only, even with its median deformations. Four-storey buildings on site class E consistently exceed the deformations seen on a site class C. It is difficult to come to the same conclusion for 8-storey buildings because of their lack of uniform inelastic deformations along their height, but a site class E always induces greater absolute deformations in the latter. Median deformations in Vancouver varied between 16.9 mm and 65.0 mm in both 4- and 8-storey buildings. For site classes E, conventional construction has therefore no restrictions to structures in Montreal but is not suitable for any structures in Vancouver for ductile connections. In order to allow CC Type in Vancouver for structures up to 15 m in height, connections should be detailed to accommodate median deformations of up to 42 mm.

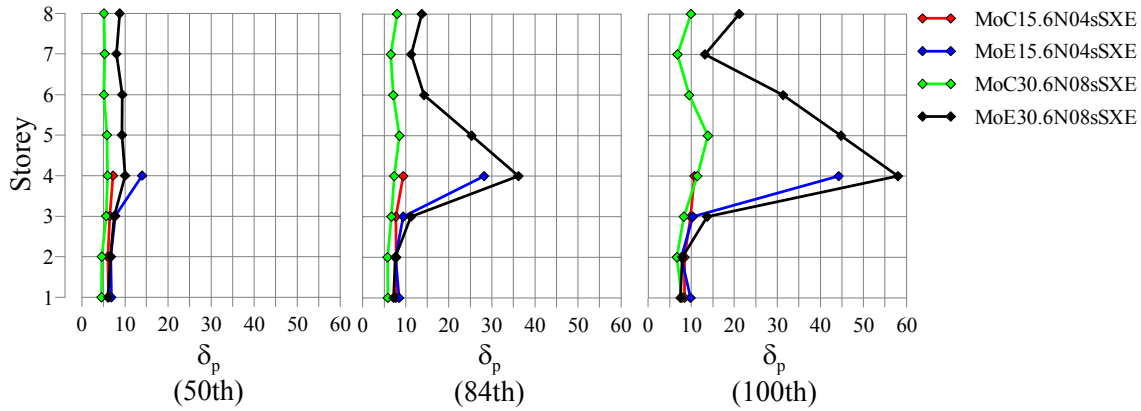

Figure 4.29: Deformations statistics for site classes C and E in Montreal.

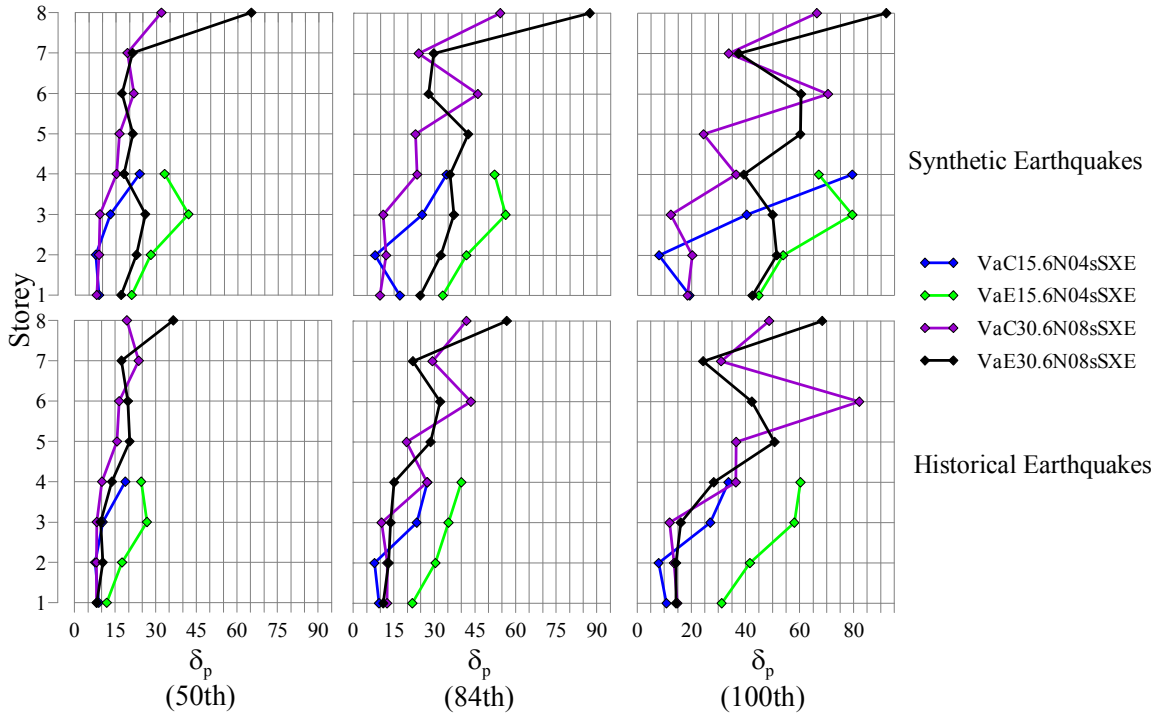

Figure 4.30: Deformations statistics for site classes C and E in Vancouver.

Table 4.23: Median deformations for site classes C and E in Montreal and Vancouver.

					Synthetic EQs				Historical EQs			
Storey	MoC15.6N04sSXE	MoE15.6N04sSXE	MoC30.6N08sSXE	MoE30.6N08sSXE	VaC15.6N04sSXE	VaE15.6N04sSXE	VaC30.6N08sSXE	VaE30.6N08sSXE	VaC15.6N04sSXE	VaE15.6N04sSXE	VaC30.6N08sSXE	VaE30.6N08sSXE
8			5.1	8.7			31.7	65.0			19.3	36.5
7			5.3	8.0			19.2	21.2			23.7	17.4
6			5.1	9.3			21.6	17.1			16.5	19.7
5			5.8	9.3			16.3	21.2			15.7	20.4
4	7.3	14.0	6.0	10.1	23.7	32.9	15.2	17.9	18.8	24.6	10.2	13.8
3	6.5	7.7	5.7	7.5	12.9	41.8	9.0	25.8	10.4	26.8	8.2	9.7
2	6.0	6.7	4.6	6.6	7.6	27.9	8.7	22.6	7.6	17.6	8.0	10.5
1	6.2	6.8	4.5	6.1	8.8	20.8	7.9	16.9	9.0	11.9	8.1	8.2

Storey height effects. Figures 4.31 and 4.32 show, respectively, the complete statistics on the effect of having different storey heights on buildings of equal total height for Montreal and Vancouver. Table 4.24 shows the median deformations for the same buildings. The V_e/V_{de} ratios are equal to 0.73, 0.67, and 0.60 in Montreal and 1.0, 0.95, and 0.85 in Vancouver for 3-, 4-, and 5-storey buildings, respectively.

No important differences exist in Montreal in terms of connection deformations. All deformations are still smaller than the 31 mm limit. The only consistent differences are the slightly smaller deformations in the 5-storey building, which is due to the building's slightly smaller V_e/V_{de} ratio. The median deformations for these three buildings in Montreal vary between 4.2 mm and 7.1 mm. In Vancouver, like Montreal, no significant trend can be observed, except that the 5-storey building has a more uniform distribution of the deformations up to its last storey. It can be noticed that chevrons in Vancouver consistently have the largest deformations at their uppermost storeys. The median deformations for these three buildings vary between 6.9 mm and 32.8 mm for simulated ground motions and 7.2 mm and 24.9 mm for historical ground motions. Even with more storeys but still at the 15 m height limit, the 5-storey building experienced a median connection deformation slightly higher than the 31 mm limit, but only under simulated ground motions. This can serve as an indication that the total building heights governs over the number of storeys when setting restrictions concerning the applicability of conventional construction.

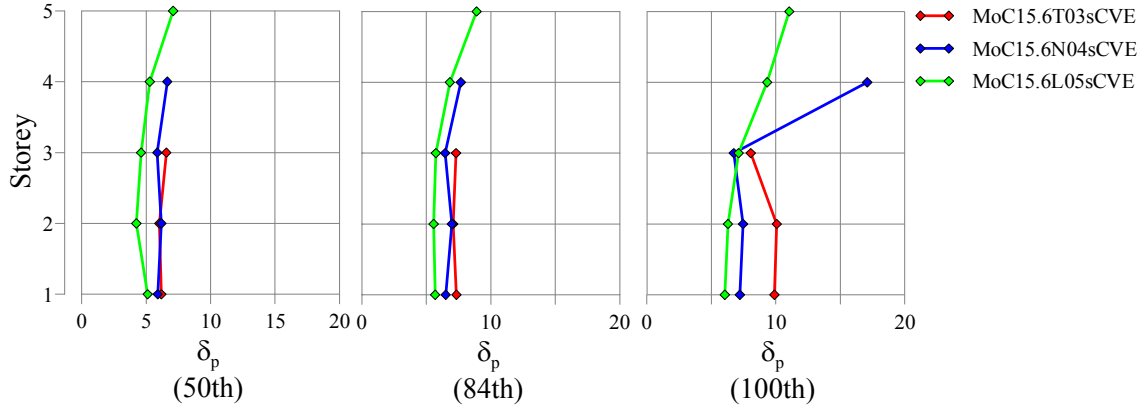

Figure 4.31: Deformation statistics on the storey height effects in Montreal.

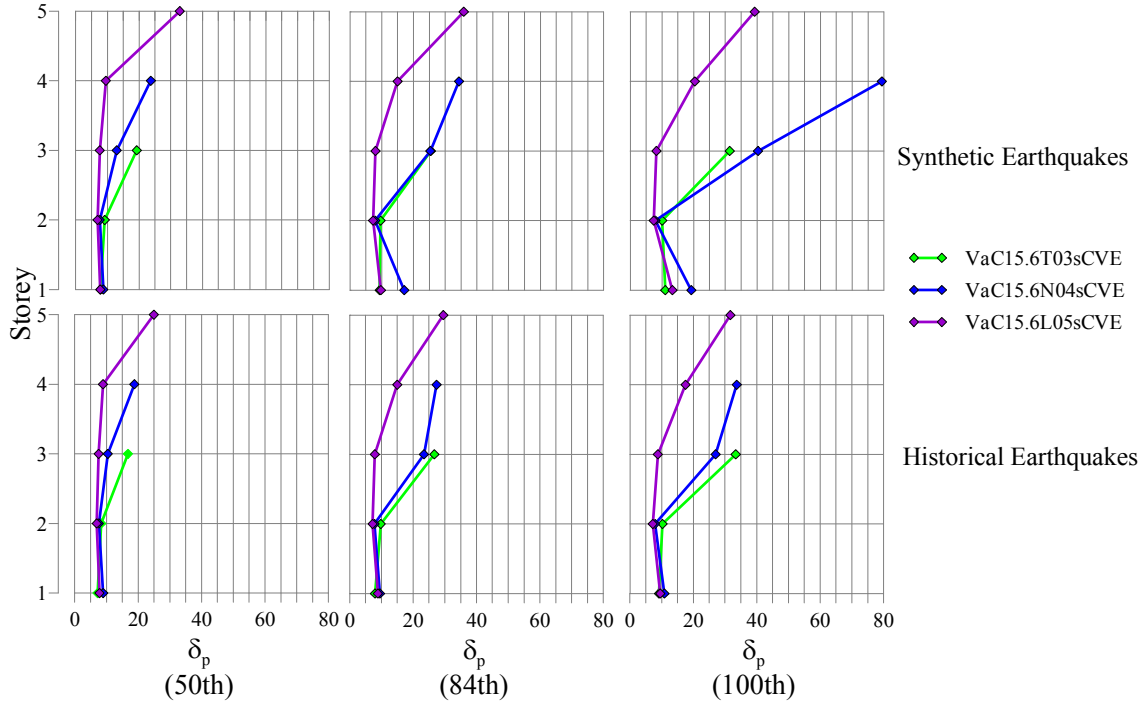

Figure 4.32: Deformation statistics on the storey height effects in Vancouver.

Table 4.24: Median deformations for different storey heights in Montreal and Vancouver.

				Synthetic EQs			Historical EQs		
Storey	MoC15.6N04sCVE	MoC15.6T03sCVE	MoC15.6L05sCVE	VaC15.6N04sCVE	VaC15.6T03sCVE	VaC15.6L05sCVE	VaC15.6N04sCVE	VaC15.6T03sCVE	VaC15.6L05sCVE
5			7.1			32.8			24.9
4	6.6		5.3	28.0		9.5	27.3		8.9
3	5.9	6.6	4.6	10.4	19.3	7.6	9.6	16.8	7.5
2	6.2	6.0	4.2	7.9	9.2	6.9	7.6	8.4	7.0
1	5.9	6.2	5.1	7.7	7.9	7.8	7.6	7.2	7.8

Braced bent location. Figure 4.33 shows the complete statistics on the effect of gravity loads on connection deformation demands, while Table 4.25 provides the median deformations for these same buildings. The V_e/V_{de} ratios are equal to 1.0 for exterior and interior bracings.

As seen in Figure 4.33, especially at the median deformations, no differences exist between braced bents located on the perimeter of the structure and inside the building envelope in terms of median connection deformation demands. It is particularly difficult to draw conclusions on differences between the two at the 84th percentile, as the deformations are not uniformly distributed along the height of the structure.

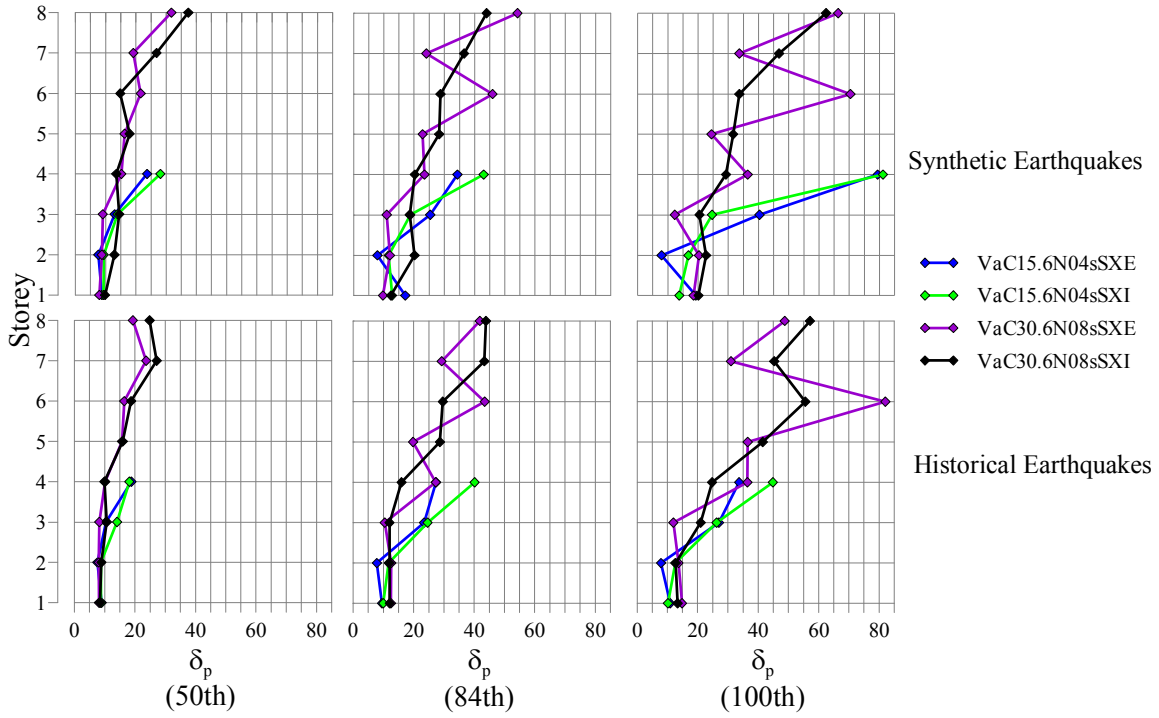

Figure 4.33: Deformation statistics for the effect of brace bent location in Vancouver.

Table 4.25: Median deformations from different braced bent locations in Vancouver.

	Synthetic EQs				Historical EQs			
Storey	VaC15.6N04sSXE	VaC15.6N04sSXI	VaC30.6N08sSXE	VaC30.6N08sSXI	VaC15.6N04sSXE	VaC15.6N04sSXI	VaC30.6N08sSXE	VaC30.6N08sSXI
8			31.7	37.3			19.3	24.8
7			19.2	26.8			23.7	27.2
6			21.6	14.8			16.5	18.7
5			16.3	17.9			15.7	16.0
4	23.7	28.1	15.2	13.5	18.8	18.1	10.2	9.9
3	12.9	13.9	9.0	14.5	10.4	14.1	8.2	10.7
2	7.6	9.4	8.7	12.9	7.6	8.7	8.0	8.9
1	8.8	9.3	7.9	9.7	9.0	8.8	8.1	8.4

4.5.3. Nonlinear Incremental Analyses

Two buildings were chosen to undergo nonlinear incremental analyses according to the specifications of FEMA Report P695, *Quantification of Building Seismic Performance Factors*, as prepared by the Applied Technology Council (ATC 2009). This document will hereinafter be referred to as ATC. As opposed to creating full incremental dynamic analysis (IDA) curves, the ATC recommends finding the earthquake incremental factor at which exactly half of the ground motions of the suite cause structural collapse. In this project, a collapse was defined as the storey drift reaching a value of 10% of the storey height at any level at any given time during an earthquake.

As based on the ATC, the response modification coefficient, R, is evaluated in terms of the acceptability of a calculated collapse margin ratio (CRM). The CMR is the ratio of the ground motion intensity which causes median collapse to the maximum considered earthquake (MCE) as defined by the building code. Both are calculated at the building's design period. The response modification coefficient is not to be mistaken as the ductility factor (R_d) in Canada; it is the equivalent of R_oR_d (1.95 for conventional construction). The acceptability is measured by comparing an adjusted collapse margin ratio (ACMR) to acceptable values, as presented in Table 4.26, that account for the quality of the design requirements, the test data, the analytical models, and the record-to-record variability. The latter four aspects are given ratings, which are described in section 4.5.3.1. The ATC suggests a collapse probability of 10% as acceptable. If the ACMR is large enough to result in a 10% or less chance of probability of collapse, then the R (or R_oR_d) value is acceptable. The ACMR accounts for the ground motions' spectral shape by multiplying the CMR by a spectral shape factor (SSF), equal to 1.06 for both models. The SSF is a function of the building period and period-based ductility and is shown in Table 4.27.

Table 4.26: Acceptable ACMR values based on total system uncertainty

Total System Collapse Uncertainty, β_{TOT}	Collapse Probability				
	5%	10%	15%	20%	25%
0.275	1.57	1.42	1.33	1.26	1.2
0.3	1.64	1.47	1.36	1.29	1.22
0.325	1.71	1.52	1.4	1.31	1.25
0.35	1.78	1.57	1.44	1.34	1.27
0.375	1.85	1.62	1.48	1.37	1.29
0.4	1.93	1.67	1.51	1.4	1.31
0.425	2.01	1.72	1.55	1.43	1.33
0.45	2.1	1.78	1.59	1.46	1.35
0.475	2.18	1.84	1.64	1.49	1.38
0.5	2.28	1.9	1.68	1.52	1.4
0.525	2.37	1.96	1.72	1.56	1.42
0.55	2.47	2.02	1.77	1.59	1.45
0.575	2.57	2.09	1.81	1.62	1.47
0.6	2.68	2.16	1.86	1.66	1.5
0.625	2.8	2.23	1.91	1.69	1.52
0.65	2.91	2.3	1.96	1.73	1.55
0.675	3.04	2.38	2.01	1.76	1.58
0.7	3.16	2.45	2.07	1.8	1.6
0.725	3.3	2.53	2.12	1.84	1.63
0.75	3.43	2.61	2.18	1.88	1.66
0.775	3.58	2.7	2.23	1.92	1.69
0.8	3.73	2.79	2.29	1.96	1.72
0.825	3.88	2.88	2.35	2	1.74
0.85	4.05	2.97	2.41	2.04	1.77
0.875	4.22	3.07	2.48	2.09	1.8
0.9	4.39	3.17	2.54	2.13	1.83
0.925	4.58	3.27	2.61	2.18	1.87
0.95	4.77	3.38	2.68	2.22	1.9

Table 4.27: Spectral shape factors for different periods and period-based ductility

	Period based ductility, m_T			
T (s)	1	1.1	1.5	2
0.5	1.00	1.02	1.04	1.06
0.6	1.00	1.02	1.05	1.07
0.7	1.00	1.03	1.06	1.08
0.8	1.00	1.03	1.06	1.08
0.9	1.00	1.03	1.07	1.09
1	1.00	1.04	1.08	1.1
1.1	1.00	1.04	1.08	1.11
1.2	1.00	1.04	1.09	1.12
1.3	1.00	1.05	1.10	1.13
1.4	1.00	1.05	1.10	1.14
1.5	1.00	1.05	1.11	1.15

The 20 historical ground motions used for incremental analysis are given in section 4.4.8.2, and were increased by increments of 0.5 or 1.0 until more than 10 ground motions caused collapse. From here, all 20 ground motions were given scaling factors, based on judgment and trial and error, which would cause 10 collapses. The same approach was used when performing analyses with the 10 simulated ground motions.

The two buildings chosen for analysis were VaC15.6N04sSXE and VaC15.6L05sCVE. Both these buildings had connection deformation demands at or around the limit of 31 mm. The reasoning was that buildings with higher deformation demands would have a higher probability of collapse; it was therefore decided to study buildings which had connections on the brink of rupturing. Also, taller structures were omitted from the incremental analysis because the 15 m height limit is recommended for Vancouver, as iterated in section 4.6. Also, using two different storey height patterns with the same total height permitted to clarify further what is best to establish restrictions to CC Type structures: the number of stories or the building height. VaC15.6N04sSXE was subjected to both historical and simulated earthquakes, while VaC15.6L05sCVE was subjected only to historical ones. This was done to study any differences between the

uses of either type of ground motion records when performing incremental nonlinear dynamic analyses.

Section 4.5.3 is divided into three sub-sections: one describing the quality ratings used for evaluating the buildings' performances, another presenting the results for historical and simulated ground motions, and a third section presenting observations on the incremental analyses. An example incremental nonlinear dynamic analysis of the VaC15.6N04sSXE model with a single ground motion is provided in APPENDIX IV.

4.5.3.1. Quality Ratings and Uncertainties

The ATC uses a rating system to evaluate the following aspects: design requirements, test data, models, and the record-to-record uncertainty. Each aspect is given two ratings, and the final rating of an aspect is based on the combination of the two ratings. Both models were given the same quality ratings.

Quality Rating of Design Requirements (β_{DR})

Completeness and Robustness: A rating of "high" was used for the completeness and robustness of the design requirements. The ATC suggests this rating for structures completed with mature construction practices, and CC Type structures are one of the most used types of structures in Canada. No special seismic provisions exist for these structures, except for ductile bracing connections, and their design are therefore based on well-established formulas that have long since been studied.

Confidence in Design Requirements: A rating of "medium" was used for the confidence in design requirements with regards to the ductile links. A high confidence is given to the design of all members in a CC Type structure, but the medium rating is chosen because of the lack of in-depth research on ductile connections which are used in these systems. This research project took an initiative at finding ductile connections, but in the author's opinion does not warrant a rating of high. However, due to the relatively simple nature of the bearing failure mode used as an energy dissipater and the reasonable

amount of experimental data obtained in this project, a medium rating was chosen over a low rating.

The combination of the latter "high" and "medium" ratings yielded a β_{DR} of 0.2.

Quality Rating of Test Data (β_{TD})

Completeness and Robustness: A rating of medium was used for the completeness and robustness of the test data. Most of the important testing issues suggested by the ATC were addressed. Among those not addressed are the effect of strain rate and the size effects which could play a role in the response of bearing failures. However, many parameters were studied which justify the medium rating over the low: end distances, bolt spacings, plate thickness, drilled holes, punched holes, and slotted holes. A sufficient amount of tests were performed which all yielded very similar results within each sub-category.

Confidence in Test Results: A rating of medium was used for the confidence in the test results. A high rating is given to test programs with enough data to assess statistical variations. The test program results are not fully contradicted by previous research (supported by research in Alberta), but contradict the maximum bearing stresses suggested by most codes. For these reasons, a medium rating was chosen.

The combination of the latter "medium" and "medium" ratings yielded a β_{TD} of 0.35.

Quality Rating of Models (β_{MDL})

Representation of Collapse Characteristics: A rating of "high" was given to the representation of the collapse characteristics. A large number of building configurations was studied and the buildings used for incremental analysis were strategically chosen based on the results of the ductility demand study performed in the second series of analyses.

Accuracy and Robustness of Models: A rating of "high" was given to the accuracy and robustness of the models used for analyses. These models directly simulated all dominant inelastic effects: rupturing of the bracing connections, buckling of columns and braces, and the effective length of braces. Well established solution algorithms were used.

The combination of the latter "high" and "high" ratings yielded a β_{MDL} of 0.1.

Record-to-Record Uncertainty (β_{RTR})

A record-to-record (RTR) variability of 0.4 is used as a conservative estimate. The ATC recommends this value for systems with significant period elongation. The ATC states that most systems, even those with limited ductility, have significant period elongation and are appropriately evaluated using a β_{RTR} of 0.4 (ATC 2009).

Total Uncertainty

The total uncertainty, β_{TOT}, is calculated using equation 4.14. For both models, the total uncertainty was equal to 0.6.

$$\beta_{TOT} = \sqrt{\beta_{DR}^2 + \beta_{TD}^2 + \beta_{MDL}^2 + \beta_{RTR}^2} \qquad 4.14$$

4.5.3.2. Incremental Analyses Results

Nonlinear incremental dynamic analyses results are given in this section for both VaC15.6N04sSXE and VaC15.6L05sCVE subjected to historical ground motions. VaC15.6N04sSXE had a structural period, T_1, as determined by eigenvalue analysis of 0.73 s, while VaC15.6L05sCVE had a T_1 of 0.93 s. Both had empirical periods, T, of 0.78 s as calculated as $0.05h_n$. Because the NBCC limits the period used to calculate the design base shear to $0.05h_n$, the empirical period (0.78 s) was used as the design period for the 5-storey building, and 0.73 s was used for the 4-storey building. Because of this, the V_e/V_{de} ratios were 1.0 and 0.85 for the 4- and 5-storey buildings, respectively. The

5-storey building therefore has some overstrength and is therefore expected to have a lower probability of collapse than the 4-storey building.

The results from the incremental analysis on both the 4- and 5-storey buildings are shown in Table 4.28. Of special interest in this table are the $\hat{S}_{CT}$ and S_{MT} values; the ratio of the two gives the CMR, the primary parameter used to characterize the collapse safety of the structures. The CMR is the ratio of the median value of the collapse level earthquake to the design ground acceleration from the NBCC uniform hazard spectrum (UHS). Both $\hat{S}_{MT}$ and S_{CT} are calculated at the building's design period, equal to the minimum period between T_1 and T. The CMR ratio is then adjusted to account for the spectral shape with the factor SSF, yielding the ACMR. The ATC provides Table 4.26 to present different levels of confidence against collapse. ACMR values for 5%, 10%, and 15% are provided in Table 4.28, and the probability of collapse is shown at the bottom of the table. The median spectra as well as the NBCC UHS for Vancouver are shown in Figure 4.34.

Table 4.28: Incremental nonlinear analysis results for 4- and 5-storey buildings.

	VaC15.6N04sSXE		VaC15.6L05sCVE
EQ type	Historical	Simulated	Historical
$SF_{col.}$	2.1	2	2.0
T_{des}, (s)	0.73	0.73	0.78
$S_{med}(T_{des})$, (g)	0.505	0.52	0.479
$\hat{S}_{CT}$, (g)	1.061	1.04	0.958
S_{MT}, (g)	0.497	0.497	0.466
CMR	2.13	2.09	2.06
SSF	1.06	1.06	1.06
ACMR	**2.26**	**2.22**	**2.18**
$ACMR_{5\%}$:	2.68	2.68	2.68
$ACMR_{10\%}$:	**2.16**	**2.16**	**2.16**
$ACMR_{15\%}$:	1.86	1.86	1.86
Prob. Of collapse:	Between 5% and 10%	Between 5% and 10%	Between 5% and 10%

For individual buildings, the ATC suggests an acceptable collapse probability of 10% (ATC 2009). As shown, both VaC15.6N04sSXE and VaC15.6L05sCVE have collapse probabilities between 5 and 10%, thus being acceptable. This means the R_oR_d (1.95) used for design is satisfactory. These incremental analyses were performed on buildings close to the 15 m height limit and were found to be just acceptable. For the 4-storey building, the differences between results from the historical and simulated ground motions were very small, with a percent difference in the CMR of less than 2%.

Figure 4.35 shows the partial IDA curves developed for both the 4- and 5-storey building. As shown by these curves, the structures tend to quickly achieve a state of collapse, as evidenced by the gap between the 50th and 84th peak storey drift percentiles and by the lack of gradual softening. Because of this, there is a lack of a warning of imminent structural collapse. All structures showed an initial elastic, or linear, initial region.

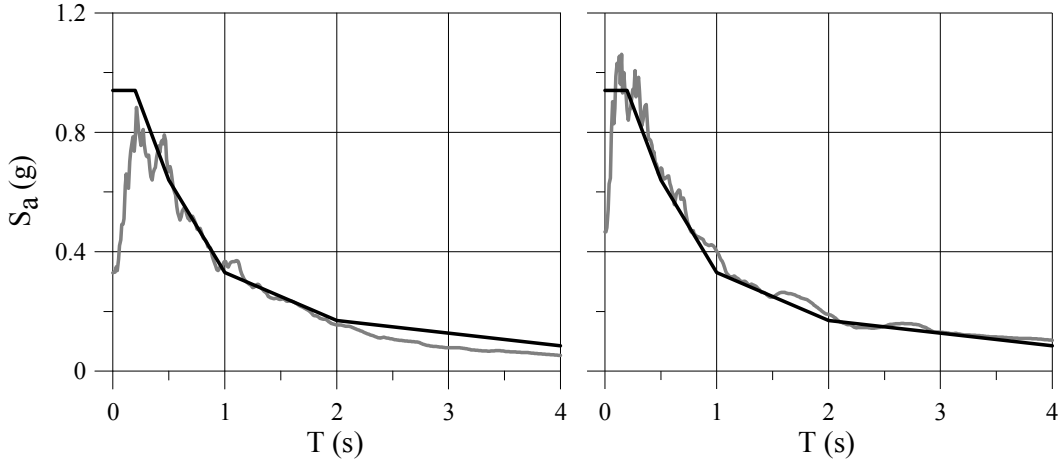

A) Historical ground motions B) Simulated ground motions

Figure 4.34: Median A) historical and B) simulated ground motions spectrum and the NBCC UHS.

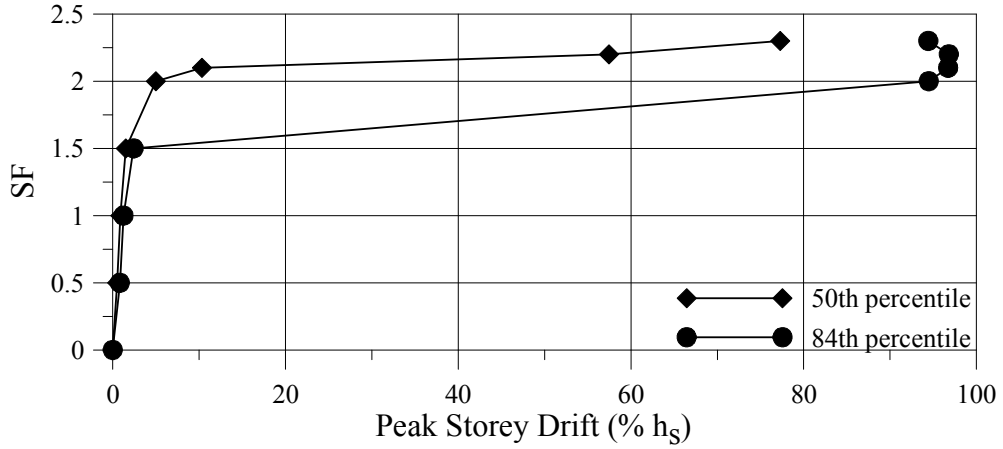

A) VaC15.6N04sSXE - Historical ground motions

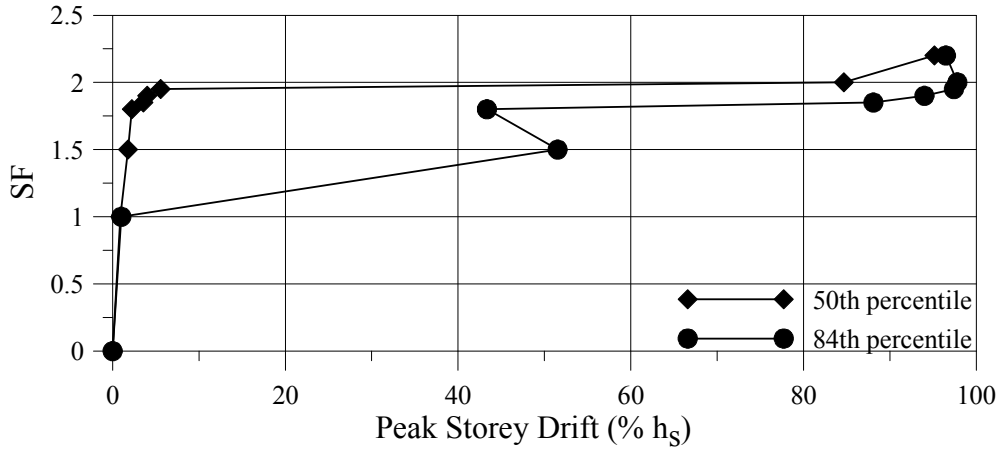

B) VaC15N04sSXE - Simulated ground motions

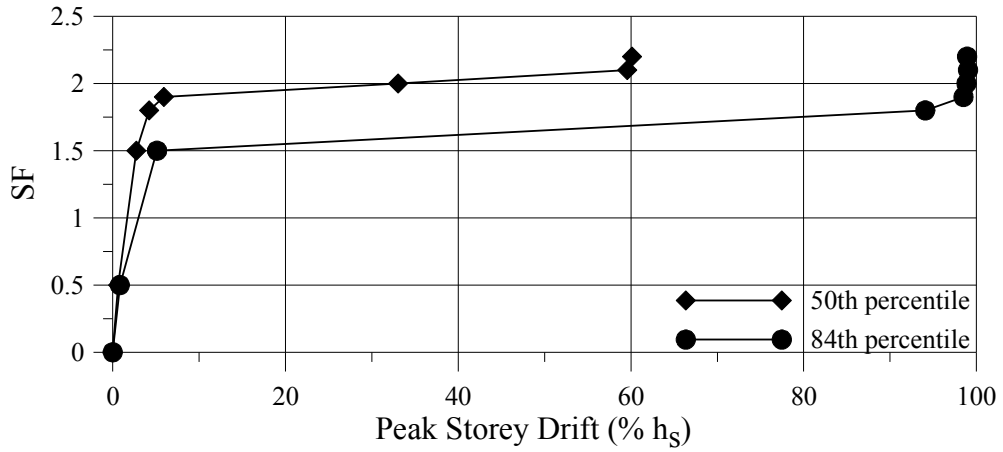

C) VaC15.6L05sCVE

Figure 4.35: Partial IDA curves for VaC15.6N04sSXE under A) historical and B) simulated ground motions and C) VaC15.6L05sCVE under historical ground motions.

4.5.3.3. Remarks on Incremental Results

During the incremental analyses, large connection deformations were obtained, sometimes reaching up to 2000 mm. Evidently, any sort of residual force existing in the connection would be eliminated, as the connection no longer physically exists because the bolts have come entirely out of the gusset plates. Figure 4.36 gives an example of the behaviour of the connections modeled; the first floor connection of the VaC15.6N04sSXE building is shown. As shown, connection models for the incremental analyses used a residual force equal to 10% of the R_oC_f value (maximum load attained in connection). This value was chosen to help convergence in the models.

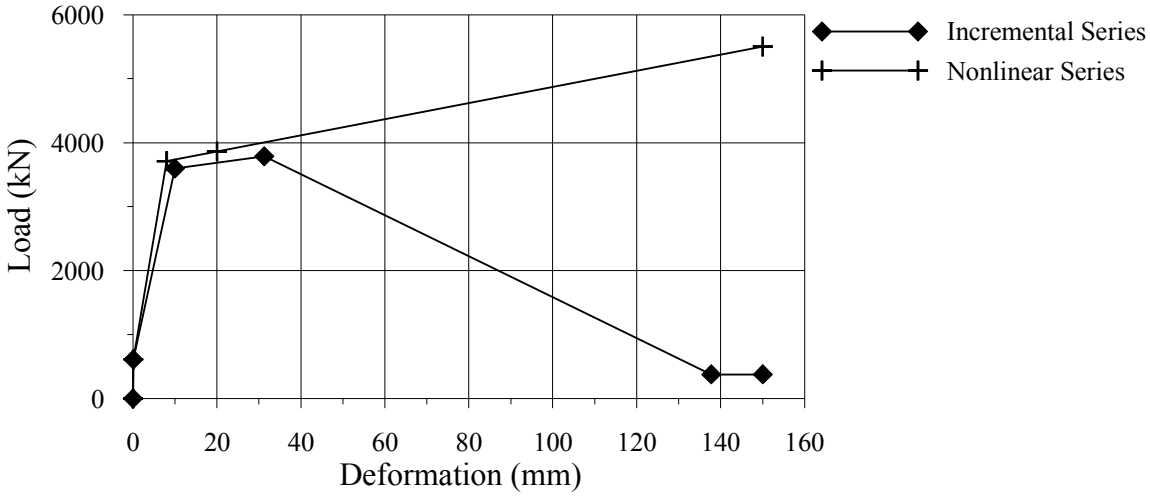

Figure 4.36: Connections modeled in incremental and nonlinear models.

As the critical point in these incremental analyses was the ground motion which causes median collapse, it is interesting to look at the connection deformations in the structure subjected to this ground motion at the incremental scaling factor just before median collapse occurs. For example, the SF_{col} for VaC15.6N04sSXE was 2.1; three ground motions had not caused collapse at a SF of 2.0 but caused collapses at 2.1. By looking at connection deformations at SF equal to 2.0 and determining if these exceeded the length of the connection, one can determine if the SF_{col} is indeed closer to 2.0 or 2.1. Based on the outcome of these observations, it was determined that an additional analysis of the

building at this SF level with close to 0 kN residual forces in connections would be necessary to determine if there was collapse.

Table 4.29 shows the different ground motions that caused median collapse in the 4- and 5-storey buildings for historical ground motions. In the 4-storey structure, the results are from a SF of 2.0 since median collapse occurred at a SF of 2.1. In the 5-storey structure, the results are from a SF of 1.9 since median collapse occurred at a SF of 2.0. Table 4.30 shows the same results, but for VaC15.6N04sSXE subjected to simulated ground motions. In this case, the results are for a SF of 1.95, since median collapse occurred at a SF of 2.0. In both tables, $\delta_{Analysis}$ corresponds to the maximum connection deformation seen in the storey, # Bolts corresponds to the number of bolts in the connection, and the Connection Length corresponds to the maximum deformation before the residual load should drop completely down to zero. The connection length was calculated using bolt spacings of 5d and end distance of 5d. The total number of bolts was divided by two because half the bolts are located on either side of the tubular brace.

Other than at the uppermost storey of the 5-storey building under the first earthquake, connection deformations never exceed the calculated connection length. In the case of the 5-storey building, it was judged unnecessary to redo the analyses for this ground motion with zero residual loads, because the other ground motion was deemed not to have caused collapse and we would therefore still be below the median collapse level. For all three incremental analyses (historical plus simulated), the SF_{inc} values shown in Table 4.28 are therefore acceptable.

Table 4.29: Behaviour of connections of both buildings subjected to historical ground motions preceding the scaling factor causing median collapse

	$\delta_{Analysis}$ (mm)	# Bolts	Connection Length (mm)
VaC15.6N04sSXE - Historical			
EQ #1			
Storey 1	11.6	12	552.5
Storey 2	9.7	10	457.2
Storey 3	22.2	8	362.0
Storey 4	49.0	4	171.5
EQ #2			
Storey 1	327.4	12	552.5
Storey 2	10.6	10	457.2
Storey 3	32.8	8	362.0
Storey 4	21.1	4	171.5
EQ #3			
Storey 1	15.9	12	552.5
Storey 2	9.8	10	457.2
Storey 3	40.9	8	362.0
Storey 4	38.2	4	171.5
VaC15.6L05sCVE - Historical			
EQ #1			
Storey 1	14.8	12	552.5
Storey 2	9.3	10	457.2
Storey 3	13.7	8	362.0
Storey 4	18.3	8	362.0
Storey 5	239.6	4	171.5
EQ #2			
Storey 1	327.4	12	552.5
Storey 2	29.4	10	457.2
Storey 3	32.8	8	362.0
Storey 4	21.1	8	362.0
Storey 5	16.0	4	171.5

Table 4.30: Behaviour of connections of VaC15.6N04sSXE subjected to simulated ground motions preceding the scaling factor causing median collapse

	$\delta_{Analysis}$ (mm)	# Bolts	Connection Length (mm)
VaC15.6N04sSXE - Simulated			
EQ #1			
Storey 1	464.1	12	552.5
Storey 2	15.0	10	457.2
Storey 3	9.3	8	362.0
Storey 4	23.2	4	171.5
EQ #2			
Storey 1	19.7	12	552.5
Storey 2	10.9	10	457.2
Storey 3	45.9	8	362.0
Storey 4	32.4	4	171.5

4.5.4. Column Axial Force Demand

In this section, the column axial force demands between the three different series of analyses is examined. Three models were looked at: VaC15.6N04sSXE, VaC15.6L05sCVE, and VaC30.6N08sSXE. The 4- and 5-storey structures had results available from the three analysis series, while the 8-storey building had results available from only the linear and nonlinear analysis series. Results taken from the incremental analyses were from a SF value of 1.0.

This will provide a look at the effect of using ductile connections versus non-ductile ones. CSA S16-01 requires the connection design loads to be amplified by a factor of 1.5 (R_d) when using non-ductile connections. The building is then expected to have more of a linear response. It is interesting to look at what is happening to the rest of the structure (i.e. the columns) when non-ductile connections are used.

As a mean of evaluating the column axial load, the ratio C_f/C_u was studied for the three latter buildings. From each analysis series, the ten common historical ground motions

were kept and the peak column axial force, C_f, at every storey was determined. Statistics were then performed at every level on the ten C_f values available and are presented in this section. The C_f values include the gravity loads. C_u corresponds to the expected buckling capacity of the column (ϕ=1 and R_y=1.1), as calculated using clause 13.3.1 of CSA (2001). A ratio C_f/C_u greater than 1.0 means the column is overloaded and on the verge of buckling.

It is important to note the top storey column in the chevron-braced, 5-storey building does not see any seismic load as the load from the brace is transmitted immediately to the lower level. Its C_f/C_u ratios are therefore equal to 0 at the top level. The C_f/C_u statistics for the three subject buildings are provided in Figure 4.37. Results from the three series of analysis are shown. Only the linear and nonlinear results are available for the 8-storey structure, as no incremental analysis was performed.

It is also important to note that connections in the nonlinear models (series 2 and 3) had connections with assigned overstrength equal to 1.3, or R_o. Practicing engineers could readily choose to design their ductile bracing connections for higher seismic design forces, or with an overstrength greater than the one chosen in this project. This would translate into higher column demands as the ductile connections would be able to transfer even greater forces to the columns. The columns demands shown in this section can therefore be taken as the minimal demands, should the connection designer design the connection to exactly the seismic force calculated with R_oR_d equal to 1.95.

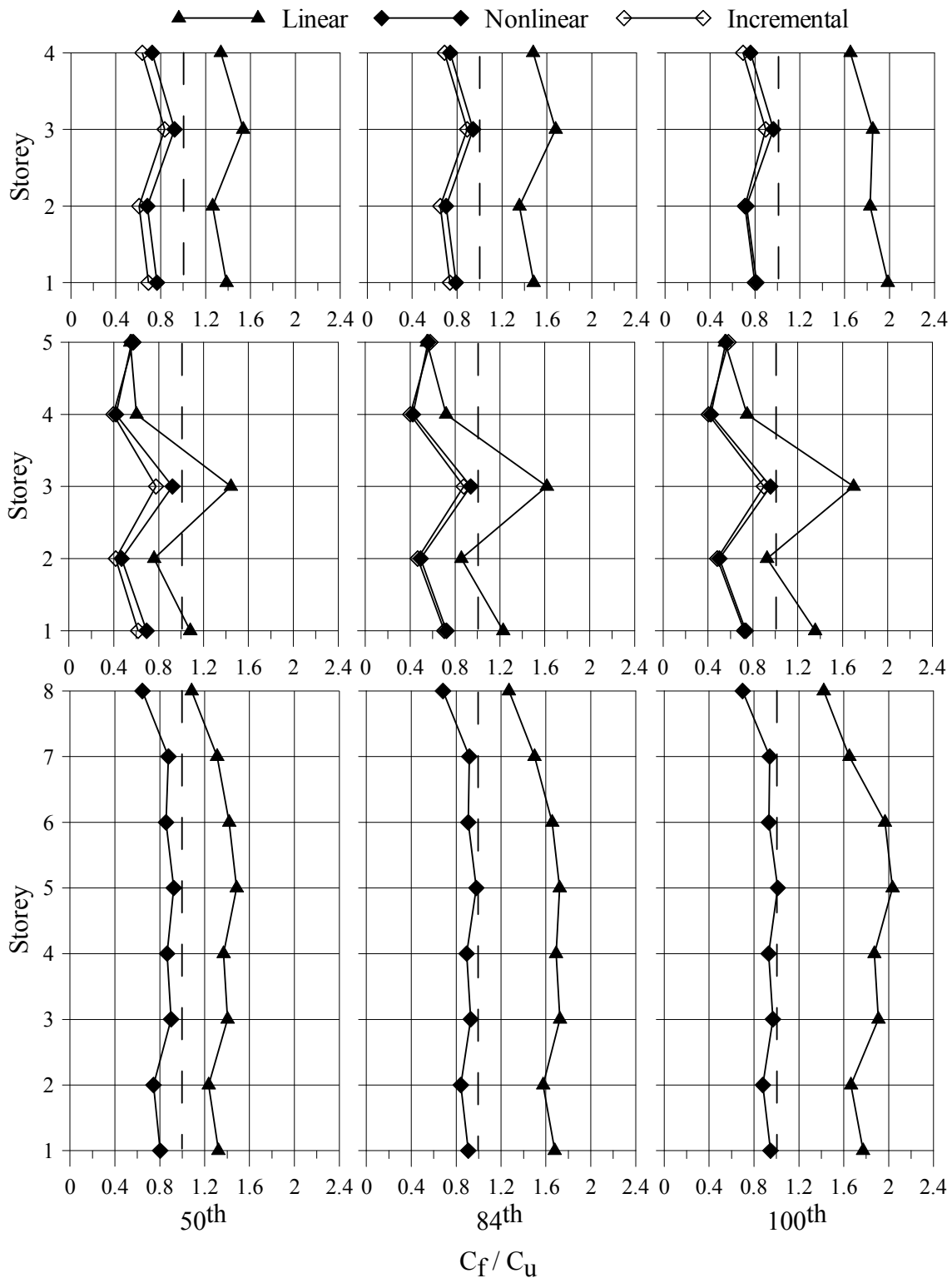

Figure 4.37: Statistics on C_f/C_u ratios for the three buildings studied.

The benefits of using ductile connections are evident in Figure 4.37. With no special seismic detailing or provisions used for members in conventional construction, there exists a strong possibility of overloading the columns when using non-ductile connections and introducing fatigue failures in members. Buildings with ductile connections consistently had a C_f/C_u ratio at or below 1.0, for all levels of probability. At the median level, buildings with non-ductile connections often exceeded a C_f/C_u of 1.0. The slight differences between the C_f/C_u ratio of the nonlinear and incremental analyses is due to the differences in modeling the connections, as shown in Figure 4.36. Connections in nonlinear analysis were not able to break off and their forces were therefore allowed to reach, theoretically, any level.

4.6. Summary / Conclusions

A summary of the observations and conclusions made based on the analytical results is offered in this section in point form.

Connection Force Demand

- Standard buildings in Montreal showed that the connection force demand was excessive for buildings with heights greater than 15 m. In Vancouver, all standard buildings had excessive force demands. On average over the building heights, the P/P_{de} ratios in Vancouver were 1.3 to 1.5 times greater than Montreal. To avoid any heights limits, connections would have to be designed for seismic forces corresponding to R_oR_d of 0.8 and 0.65 for Montreal and Vancouver, respectively.

- For chevrons in Montreal, the P/P_{de} ratios were below 1.0 for all buildings because of their seismic overstrength (smaller V_e/V_{de} ratios). In Vancouver, the same chevron-braced buildings had excessive force demands. Should they be allowed to be used for structures up to 30.1 m, the connections would need to be designed for seismic forces corresponding to R_oR_d of 0.65.

- In Montreal and Vancouver, buildings located on a site class E had P/P_{de} ratios greater than 1.0. To allow CC Type structures on site class E for heights up to 30.8 m in Montreal and 15 m in Vancouver, the connection seismic design forces should be calculated with R_oR_d of 0.76 and 0.65 in Montreal and Vancouver, respectively.

- For different storey height patterns and different brace bent locations (interior or exterior), no trends were observed. However, comparisons between buildings of equal height but with a different number of storeys showed no significant differences, suggesting that a building's height is a more suitable parameter when restricting the application of CC Type CBFs.

Connection Ductility Demand

- In Montreal, deformations were always below 31 mm. In Vancouver, deformations were 2.0 to 3.6 times higher than those of Montreal. For heights greater than 15 m in Vancouver, deformations were higher than 31 mm. For standard CC Type structures to be used in Vancouver, the connections would have to be detailed to accommodate deformations of approximately 40 mm.

- Compared to their Split-X equivalents, chevron-braced buildings generally underwent smaller connection deformations. In Montréal, deformations were kept below the 31 mm limit. In Vancouver, deformations reached up to 28 and 35 mm for the 4- and 8-storey buildings, respectively. The maximum deformations were consistently at the top levels of the chevrons.

- On site class E in Montreal, deformations climbed to 14 mm for the 30.1 m 8-storey building. In Vancouver, the deformations reached 42 mm and 65 mm in the 4- and 8-storey buildings, respectively. On average, connection deformations in structures on site class E were 1.5 and 2.0 times higher than site class C in Montreal and Vancouver, respectively. In Vancouver, unless the deformations

can be accommodated for, it appears CC Type structures are not adequate for site class E.

- Deformations do not seem to vary between buildings of the same height but of different number of storeys, nor for different locations of the brace bent (interior or exterior).

Incremental Dynamic Analyses

- Both the 4- and 5-storey buildings had collapse probabilities between 5% and 10%, considered acceptable.

- The two buildings studied had total heights of 15.6 m, just above the 15 m NBCC 05 limit. This result suggests that buildings with 15.6 m or less would provide adequate protection against collapse, on the condition that ductile connections are used, the building is located on site class C, and that the building has Split-X or chevron braces. It would be important to verify, in the future, structures with different parameters, such as non-ductile connections, a site class E, and greater heights.

Column Axial Load Demands

- The study on the column axial load demands showed that ductile connections had the effect of greatly reducing the demand on columns compared to non-ductile connections.

- Based on median statistics, the column demands decreased on average by factors of 2.0, 1.6, and 1.6 for the 4-, 5-, and 8-storey buildings.

Chapter 5. CONCLUSIONS / RECOMMENDATIONS

5.1. Conclusions

The main objectives of this research project were to:

- Evaluate the ductility capacity of typical vertical bracing member connections. This was done in two separate experimental phases. The first phase consisted of testing five connection failure modes under monotonic loading and choosing a failure mode having the most potential to be used as a ductile connection in conventional construction. The second phase consisted of optimizing the ductility capacity of the connection failure mode chosen in the first phase by studying the effect of changing the connection parameters. The second phase used monotonic and cyclic loading.

- Study the seismic behaviour of buildings of the conventional construction category through detailed finite element modeling using the OpenSees software. The main objective of this analytical phase was to re-evaluate the 15 m height limit imposed on CC Type CBF structures by the NBCC 05 and perhaps make this height limit a function of different building parameters: type of connections used (ductile or non-ductile) and the soil type (class C or E), among others. This analytical phase was separated into three series of analyses where twenty-four buildings of different configurations were used. The first was used to determine the connection force demand when non-ductile connections are used. The second was to determine the connection ductility demand when ductile connections are used. The third was to determine the probability of collapse of two structures using ductile connections through incremental analyses. Results for three buildings were compiled and the effect of using ductile versus non-ductile connections on the column axial force demand was examined.

The following results were obtained during the first experimental phase:

- For parallel fillet weld failing in shear, there was an average ultimate deformation of 7.3 mm.
- For gusset plates failing under bolt bearing, there was an average ultimate deformation of 22.7 mm.
- For angles failing in their net areas, there was an average ultimate deformation of 16.0 mm.
- For a bolt failing under shear, its average ultimate deformation was 15.7 mm.
- For angles failing in shear and tension block failure, there was an average ultimate deformation of 15.5 mm.

It is important to note all these deformations include deformations at both ends of the specimens, which had two identical connections at either ends. Based on these results, it was determined to use gusset plates failing under bolt bearing as the ductile connection failure mode of choice, as it provided the most ductility.

The following conclusions were drawn from the second experimental phase:

- Bolt end distances of 5d and bolt spacings of 6d (5d6d) provided the most deformation capacity at rupture with a deformation of 47 and 34 mm under monotonic and cyclic loading, respectively. The 4d5d specimens underwent 41 and 25 mm and the 2d5d specimens underwent 42 and 23.5 mm under monotonic and cyclic loading, respectively. Specimens failing under pure bolt bearing failure underwent significantly higher bearing stresses than the $3F_u$ limit used in CSA-S16. For cyclic tests, the four 4d5d specimens had ultimate bearing stresses of approximately $4F_u$ while the 5d6d specimens were close to $4.7F_u$. Because of the unexpectedly high bearing stresses encountered in specimens 5d6d, it is recommended to use bolt spacings of 4d5d.

- The differences between punched and drilled bolt holes were minimal in terms of deformation at rupture. However, it was shown that plates with punched holes tend to develop transverse fractures even when undergoing bearing failures. This is believed to be due to micro-cracks developing in the immediate vicinity of the bolt hole during the hole punching process. It is therefore recommended to use drilled holes.

- Short-slotted holes had slightly lower ultimate loads and were less stiff than standard round holes. They do not provide any clear benefits and it is therefore recommended to use standard round holes.

Based on the above, it is recommended to use a bolt end distance of 4d and a bolt spacing of 5d with round, drilled holes.

Following the experimental phase, the analytical phase was performed and examined the seismic behaviour of buildings of the conventional construction category when using non-ductile and ductile vertical bracing connections. A ductile connection's ductility demand was compared to the deformation capacity of experimental specimen BRD4D5D's deformation capacity under cyclic loading, equal to 31 mm when accounting for deformations at either end of the brace member. The following observations and conclusions were made with respect to the non-ductile connections, ductile connections, the nonlinear incremental analyses, and the column axial load demands.

Connection Force Demand

- Standard buildings in Montreal showed that the connection force demand was excessive for buildings with heights greater than 15 m. In Vancouver, all standard buildings had excessive force demands. On average over the building heights, the P/P_{de} ratios in Vancouver were 1.3 to 1.5 times greater than Montreal. To avoid any heights limits, connections would have to be designed

for seismic forces corresponding to R_oR_d of 0.8 and 0.65 for Montreal and Vancouver, respectively.

- For chevrons in Montreal, the P/P_{de} ratios were below 1.0 for all buildings because of their seismic overstrength (smaller V_e/V_{de} ratios). In Vancouver, the same chevron-braced buildings had excessive force demands. Should they be allowed to be used for structures up to 30.1 m, the connections would need to be designed for seismic forces corresponding to R_oR_d of 0.65.

- In Montreal and Vancouver, buildings located on a site class E had P/P_{de} ratios greater than 1.0. To allow CC Type structures on site class E for heights up to 30.8 m in Montreal and 15 m in Vancouver, the connection seismic design forces should be calculated with R_oR_d of 0.76 and 0.65 in Montreal and Vancouver, respectively.

- For different storey height patterns and different brace bent locations (interior or exterior), no trends were observed. However, comparisons between buildings of equal height but with a different number of storeys showed no significant differences, suggesting that a building's height is a more suitable parameter when restricting the application of CC Type CBFs.

Connection Ductility Demand

- In Montreal, deformations were always below 31 mm. In Vancouver, deformations were 2.0 to 3.6 times higher than those of Montreal. For heights greater than 15 m in Vancouver, deformations were higher than 31 mm. For standard CC Type structures to be used in Vancouver, the connections would have to be detailed to accommodate deformations of approximately 40 mm.

- Compared to their Split-X equivalents, chevron-braced buildings generally underwent smaller connection deformations. In Montréal, deformations were kept below the 31 mm limit. In Vancouver, deformations reached up to 28 and

35 mm for the 4- and 8-storey buildings, respectively. The maximum deformations were consistently at the top levels of the chevrons.

- On site class E in Montreal, deformations climbed to 14 mm for the 30.1 m 8-storey building. À Vancouver, the deformations reached 42 mm and 65 mm in the 4- and 8-storey buildings, respectively. On average, connection deformations in structures on site class E were 1.5 and 2.0 times higher than site class C in Montreal and Vancouver, respectively. In Vancouver, unless the deformations can be accommodated for, it appears CC Type structures are not adequate for site class E.

- Deformations do not seem to vary between buildings of the same height but of different number of storeys, nor for different locations of the brace bent (interior or exterior).

Incremental Dynamic Analyses

- Both the 4- and 5-storey buildings had collapse probabilities between 5% and 10%, considered acceptable.

- The two buildings studied had total heights of 15.6 m, just above the 15 m NBCC 05 limit. This result suggests that buildings with 15.6 m or less would provide adequate protection against collapse, on the condition that ductile connections are used, the building is located on site class C, and that the building has Split-X or chevron braces. It would be important to verify, in the future, structures with different parameters, such as non-ductile connections, a site class E, and greater heights.

Column Axial Load Demands

- The study on the column axial load demands showed that ductile connections had the effect of greatly reducing the demand on columns compared to non-ductile connections.

- Based on median statistics, the column demands decreased on average by factors of 2.0, 1.6, and 1.6 for the 4-, 5-, and 8-storey buildings.

5.2. Recommendations

The following is a list of recommendations for future work:

- Additional research should be performed on bolt bearing failures to determine the ultimate bearing stresses that can be sustained by gusset plates. The width of the gusset plate at the bolt holes could be studied, as the amount of material to the sides of the bolt hole most likely provides constraints on the plate material and may play an important role on the maximum bearing stresses attainable.

- Due to the ductile nature of bearing failures, the effect of designing bearing failures with $4F_u$ as the maximum bearing stress on the serviceability of the structure should be studied. It is possible that connections may not be allowed to be designed to this level as this could cause serviceability issues.

- The study showed that site class E has the effect of increasing the connection force demands and deformations. Limited to ductile connections and buildings of 15 m or less in Montreal for site class E, CC Type buildings are greatly restricted. A detailed look at CC Type structures is warranted, particularly with an emphasis on the interaction between the ground and structure.

- The analyses showed that structures on a site class C in Montreal offered good behaviour, regardless of whether ductile or non-ductile connections are used. The maximum height of the buildings was 38.1 m for “standard” buildings and 30.1 m when other parameters were looked at. It would be beneficial to study even taller structures and ensure that no other limit is needed.

- It was shown that the P/P_{de} ratios were often highest at the uppermost storeys, indicating the spectral analyses poorly predicted the brace axial forces at the

uppermost storeys. This should be considered and studied closely in future studies.

REFERENCES

AALBERG, A. and LARSEN, P. K., "The Effect of Steel Strength and Ductility on Bearing Failure of Bolted Connections," in *3rd European Conference Steel Structures* Coimbra, Portugal, 2002, pp. pp. 869-878.

AISC, "ANSI/AISC 360-05 Specifications for Structural Steel Buildings," 13th ed Chicago, IL., 2005.

AISC, "Seismic Provisions for Structural Steel Buildings, Including Supplement No. 1," Chicago, IL., 2005.

ATC, "Quantification of Building Seismic Performance Factors," Report No. ATC-P695, Applied Technology Council, Redwood City, California 2009.

ATKINSON, G. M., "Earthquake time histories compatible with the 2005 National building code of Canada uniform hazard spectrum," *Canadian Journal of Civil Engineering,* vol. 36, pp. 991-1000, 2009.

BERNAL, D., "Amplification Factors For Inelastic Dynamic P- Delta Effects In Eeartquake Analysis," *Earthquake Engineering & Structural Dynamics,* vol. 15, pp. 635-651, 1987.

CAI, Q. and DRIVER, R. G., "End Tear-Out Failures of Bolted Tension Members," in *Structural Engineering Report 278* Edmonton, AL: Department of Civil and Environmental Engineering, University of Alberta, 2008.

CAI, Q. and DRIVER, R. G., "End Tear-Out Failures of Bolted Tension Members," Department of Civil and Environmental Engineering, University of Alberta, Edmonton, AL 2008.

CARTER, C., E-mail correspondence ed, R. Tremblay, Ed., July 27, 2009.

CHESSON, J. E. and MUNSE, W. H., "Behavior of riveted connections in truss-type members," *American Society of Civil Engineers -- Proceedings -- Journal of the Structural Division,* vol. 83, p. 61, 1957.

COMPUTER & STRUCTURES INC., C., "SAP2000 - Integrated Software for Structural Analysis and Design, Version 12 (Computer Program)," Berkeley, CA: CSI, 2008.

CSA, "CAN/CSA-S16.1 Limits States Design of Steel Construction, Including S16S1-05 Supplement," 9th ed Willowdale, Ont.: Canadian Standards Association, 2001.

CSA, "CAN/CSA-S16 DRAFT STANDARD: Limit States Design of Steel Construction," 9th ed Willowdale, Ont.: Canadian Standards Association, 2009.

DRIVER, R. G., GRONDIN, G. Y., and KULAK, G. L., "Unified block shear equation for achieving consistent reliability," *Journal of Constructional Steel Research,* vol. 62, pp. 210-222, 2006.

ECS, "Design of structures for earthquake resistance," in *Eurocode 8, 1998,* Brussels, Belgium: European Committee for Standardization, 2003.

FRANK, K. H. and YURA, J. A., "An Experimental Study of Bolted Shear Connections," Office of Research and Development, Federal Highway Administration, U.S. Department of Transportation, Washington, D.C. December 1981.

GUILINI-CHARETTE, K., "Effets des mouvements sismiques sur les structures en acier de la catégorie des constructions conventionnelles," in *Département des Génies Civil, Géologique et des Mines*. vol. M.Sc.E. Montreal, QC: École Polytechnique de Montréal, 2009.

GUPTA, A. and KRAWINKLER, H., "Seismic Demand Evaluation for Performance of Steel Moment Resisting Frame Structures. Report No. 132," in *John A. blume Earthquake Eng. Research Center, Dept. of Civil and Env. Eng.* Stanford, CA: Standord University, 1999.

HINES, E. M. and GRYNIUK, M. C., "Preliminary Results: Collapse Performance of Low-Ductility Chevron Braced Steel Frames in Moderate Seismic Regions," 2006.

HUMAR, J., MAHGOUB, M., and GHORBANIE-ASL, M., "Effect of second-order forces on seismic response," *Canadian Journal of Civil Engineering,* vol. 33, pp. 692-706, 2006.

IWANKIW, N. and SCHLAFLY, T., "Effect of Hole-Making on the Strength of Double Lap Joints," vol. V 19, pp. 170-178, 1982.

IZVERNARI, C., "The Seismic Behaviour of Steel Braces with Large Sections," in *Département des Génies Civil, Géologique et des Mines*. vol. M.Sc.E. Montreal, QC: École Polytechnique de Montréal, 2007.

JONES, J., "Effect of bearing ratio on static strength of riveted joints," *American Society of Civil Engineers -- Proceedings -- Journal of the Structural Division,* vol. 82, pp. 10-13, 1957.

KIM, B. S., "The Effect of End Distance on the Bearing Strength of Bolted Connections." vol. M. Sc. Eng. Austin, TX.: University of Texas at Austin, 1996.

KIM, H. J. and YURA, J. A., "Effect of ultimate-to-yield ratio on the bearing strength of bolted connections," *Journal of Constructional Steel Research,* vol. 49, pp. 255-269, 1999.

KULAK, G. L., FISHER, J. W., and STRUIK, J. H. A., *Guide to Design Criteria for Bolted and Riveted Joints*, 2nd ed. New York: Wiley, 1987.

LACERTE, M. and TREMBLAY, R., "Making use of brace overstrength to improve the seismic response of multistorey split-X concentrically braced steel frames," *Canadian Journal of Civil Engineering,* vol. 33, pp. 1005-1021, 2006.

LEWIS, B. E. and ZWERNEMAN, F. J., "Edge Distance, Spacing, and Bearing in Bolted Connections," School of Civil and Environmental Engineering, Oklahoma State University, Oklahoma, OK 1996.

LIN, M. L., TSAI, K. C., HSIAO, P. C., and TSAI, C. Y., "Compressive behaviour of buckling-restrained brace gusset connections," in *The First International Conference on Advances in Experimental Structural Engineer AESE,* Nagoya, Japan, July 19-21, 2005.

LIU, J. and ASTANEH-ASL, A., "Cyclic testing of simple connections including effects of slab," *Journal of structural engineering New York, N.Y.,* vol. 126, pp. 32-39, 2000.

MCKENNA, F. and FENVES, G. L., "Open System for Earthquake Engineering Simulation (OpenSees)," Pacific Earthquake Engineering Research Center (PEER), University of California, Berkeley, CA., 2004.

MITCHELL, D., TREMBLAY, R., KARACABEYLI, E., PAULTRE, P., SAATCIOGLU, M., and ANDERSON, D. L., "Seismic force modification factors for the proposed 2005 edition of the National Building Code of Canada," *Canadian Journal of Civil Engineering,* vol. 30, pp. 308-327, 2003.

MUIR, L. S., "Designing for ductile performance of bolted seismic connections to axially loaded members," *Engineering Journal,* vol. 44, pp. 35-39, 2007.

MULLIN, D. T. and CHENG, J. J. R., "Ductile Gusset Plates - Tests and Analyses," in *Proc. 2004 Pacific Structural Steel Conference* Long Beach, California, 2004.

MULLIN, D. T. and CHENG, J. J. R., "Response of Seismically Loaded Low Rise Steel CBF Structures with Inelastic Gusset Plate Connections," in *Proc. 2004 Pacific Structural Steel Conference* Long Beach, California, 2004.

NAST, T., GRONDIN, G. Y., and CHENG, J. J. R., "An Analytical Study of the Cyclic Behaviour of Steel Gusset Plate Connections," in *Structural Engineering Report 229* Edmonton, AL: Department of Civil and Environmental Engineering, University of Alberta, 1999.

NBCC, "National Building Code of Canada 2005," 12th ed, O. National Research Council of Canada, ON., Ed. Ottawa, ON., 2005.

OWENS, G. W., DRIVER, P. J., and KRIGE, G. J., "Punched holes in structural steelwork," *Journal of Constructional Steel Research,* vol. 1, pp. 34-47, 1981.

PERRY, W. C., "The Bearing Strength of Bolted Connections," in *Faculty of Graduate School*. vol. M. Sc. E. Austin, TX: University of Texas at Austin, 1981.

RABINOVITCH, J. S. and CHENG, J. J. R., "Cyclic Behaviour of Steel Gusset Plate Connections," in *Structural Engineering Report 191* Edmonton, AL: Department of Civil and Environmental Engineering, University of Alberta, 1993.

REDWOOD, R. G., LU, F., BOUCHARD, G., and PAULTRE, P., "Seismic response of concentrically braced steel frames," *Canadian Journal of Civil Engineering,* vol. 18, pp. 1062-1077, 1991.

THORNTON, W. A., "BRACING CONNECTIONS FOR HEAVY CONSTRUCTION," *Engineering Journal,* vol. 21, pp. 139-148, 1984.

TREMBLAY, R., "Cost Effective Seismic Design of Braced Steel Frames Using CSA-S16-01 (and CSA-S16S1-05) and NBCC 2005," in *North American Steel Construction Conference*, PowerPoint Presentation, CISC website: http://quebec.cisc-icca.ca/Library/pdf/NASCC05_CBFcourseRTremblay050406.pdf, 2005.

TREMBLAY, R. and BOUATAY, N., "Loading Protocols for the Seismic Testing of Ductile Bracing Members in Concentrically Braced Steel Frames," in *12th European Conference on Earthquake Engineering*. vol. no. 480 London, UK, 2002.

TREMBLAY, R., EERI, M., and ATKINSON, G. M., "Comparative study of the inelastic seismic demand of eastern and western Canadian sites," *Earthquake Spectra,* vol. 17, pp. 333-358, 2001.

VASARHELYI, D. D., BEANO, S. Y., MADISON, R. B., LU, Z. A., and VASISHTH, U. C., "Effects of fabrication techniques on bolted joints," *American Society of Civil Engineers Proceedings, Journal of the Structural Division,* vol. 85, pp. 71-116, 1959.

WALBRIDGE, S. S., GRONDIN, G. Y., and CHENG, J. J. R., "An Analysis of the Cyclic Behaviour of Steel Gusset Plate Connections," in *Structural Engineering Report 225* Edmonton, AL: Department of Civil and Environmental Engineering, University of Alberta, 1998.

WALBRIDGE, S. S., GRONDIN, G. Y., and CHENG, J. J. R., "Gusset plate connections under monotonic and cyclic loading," *Canadian Journal of Civil Engineering,* vol. 32, pp. 981-995, 2005.

WALLIN, L., "Punching Holes: Expereimental Tests of the Strength of Punched Holes, translated from Swedish by Stromberg, J.," 1975.

WHITMORE, R. E., "Experimental investigation of stresses in Gusset plates," University of Tennessee -- Engineering Experiment Station -- Bulletin 1952.

APPENDIX I.

Experimental Phase I Specimens

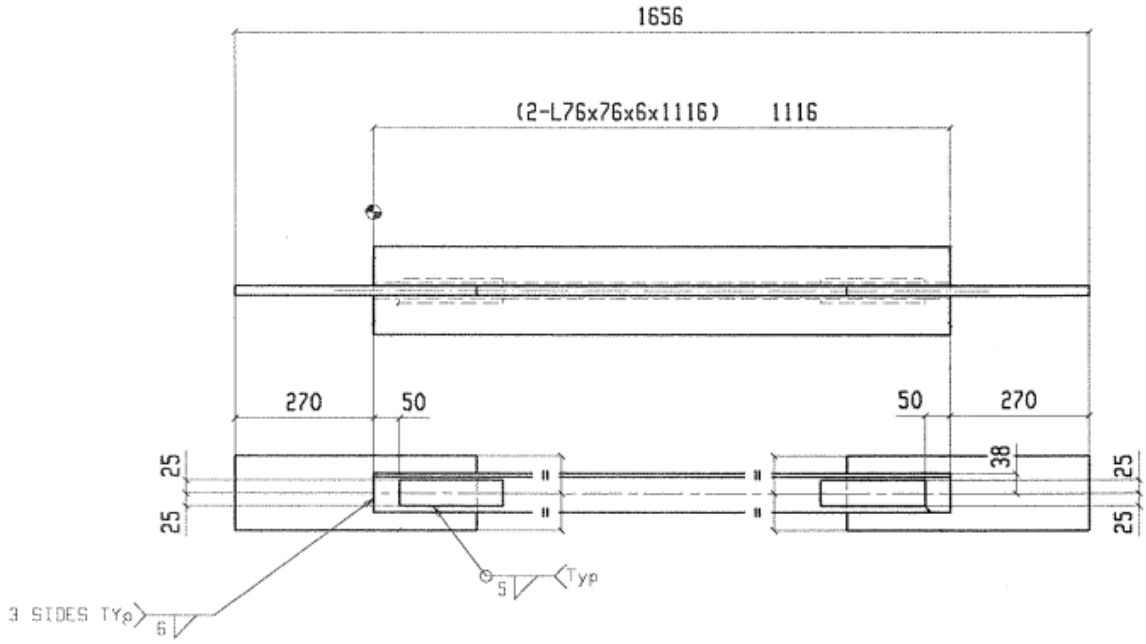

Figure I.1: Specimen D01X (yielding of angles).

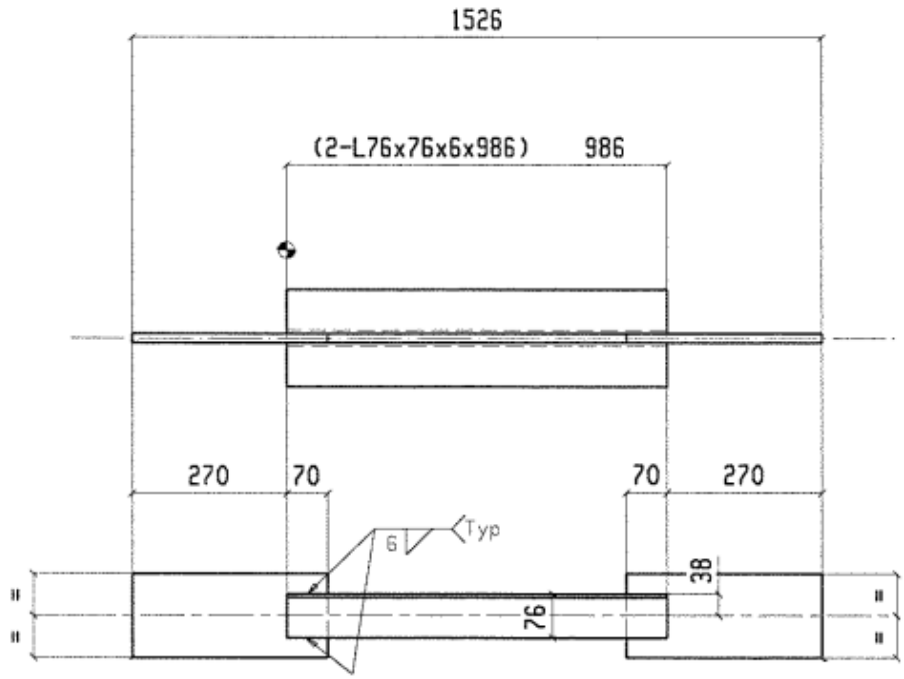

Figure I.2: Specimen D02X (parallel welds fracture).

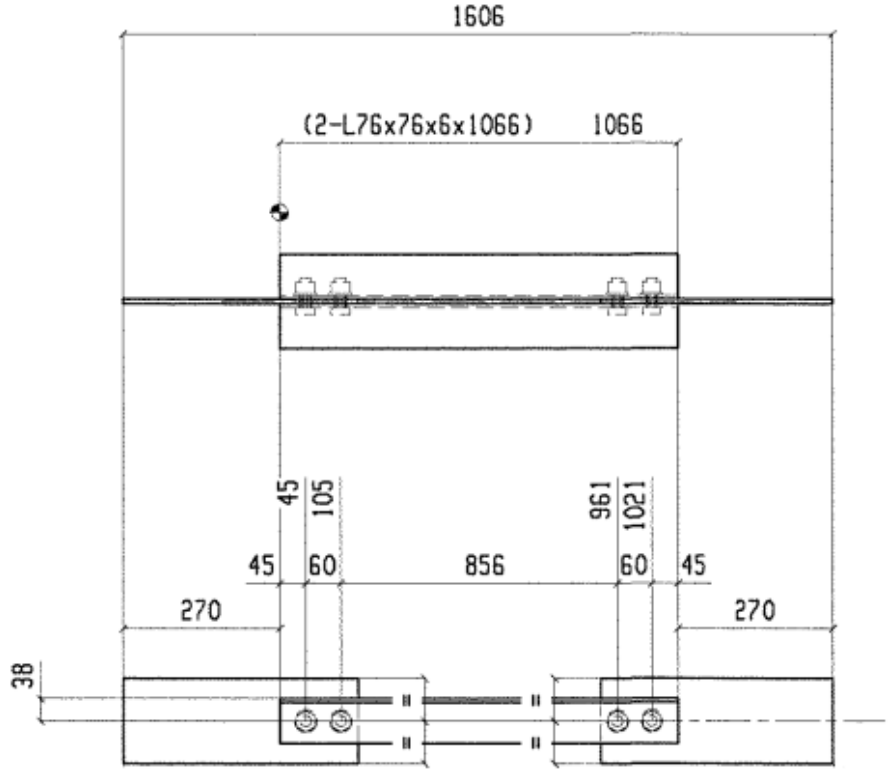

Figure I.3: Specimen D03X (bolt bearing failure of gusset plate).

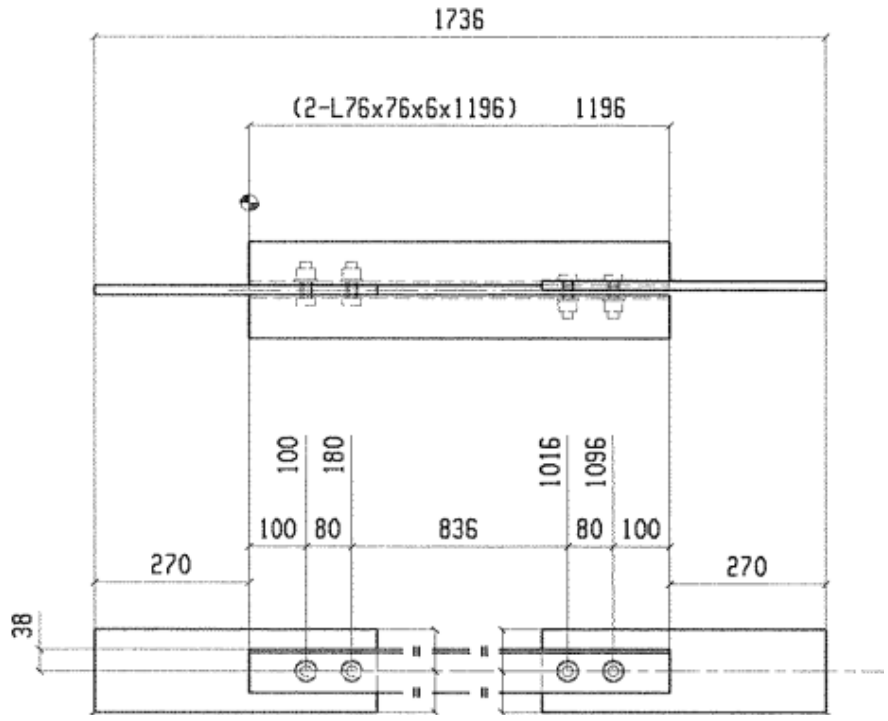

Figure I.4: Specimen D04X and D14X (net area rupture of angles).

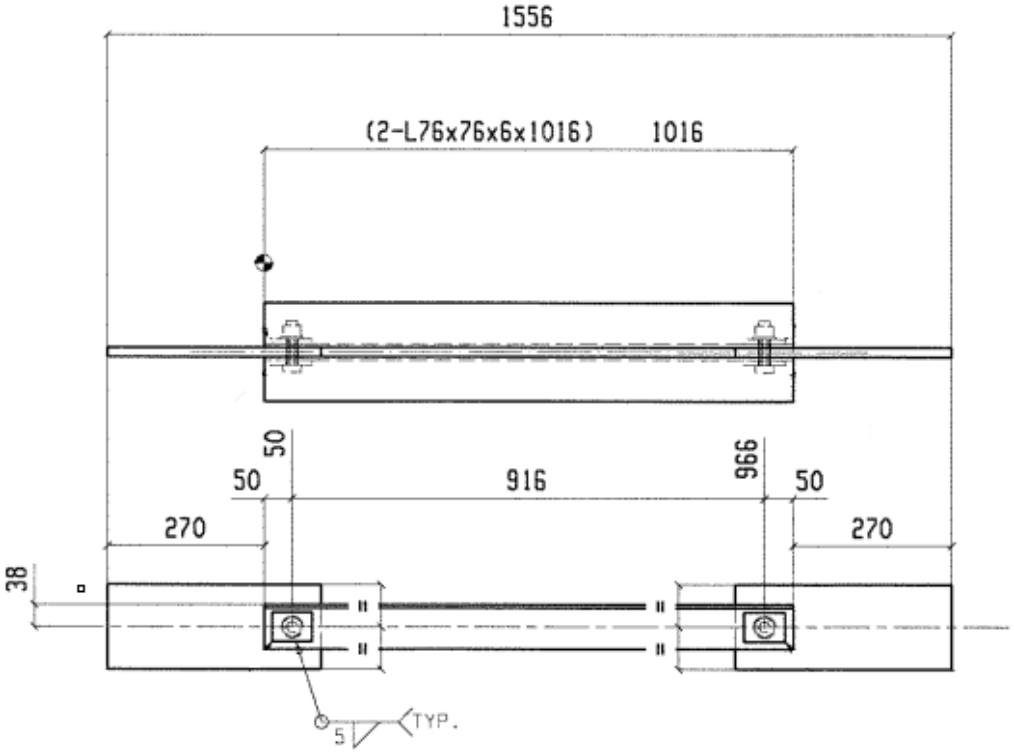

Figure I.5: Specimen D05X (bolt shear rupture).

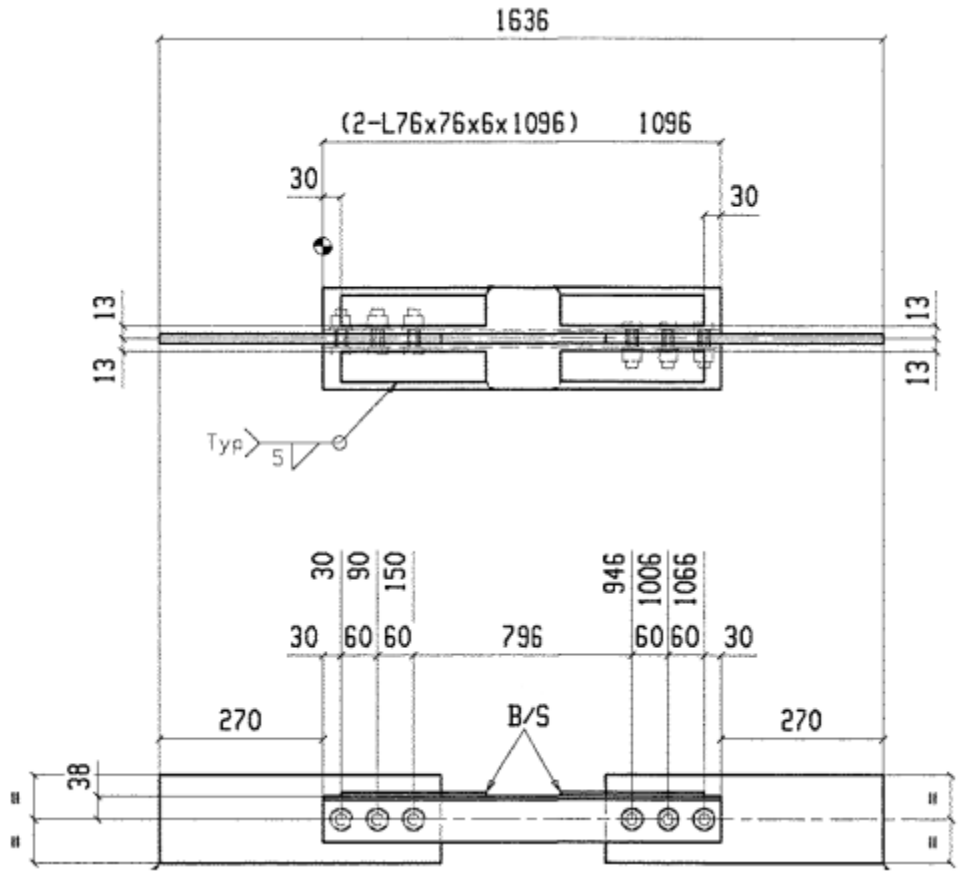

Figure I.6: Specimen D06X (shear and tension block failure of angles).

APPENDIX II.

Validation of the OpenSees Model

Before proceeding with the analyses, the linear and nonlinear 4-storey model with Split-X bracing model was tested and validated. The following key points were looked at:

- Axial brace load.
- Comparison of the ductile link force and the brace force.
- The column loads.

To validate the model, a transient analysis was performed as described in section 4.4.7. The Loma Prieta 1989 earthquake, a 7.0 magnitude earthquake registered 54 km from its epicentre, was used and is shown in Figure II.1.

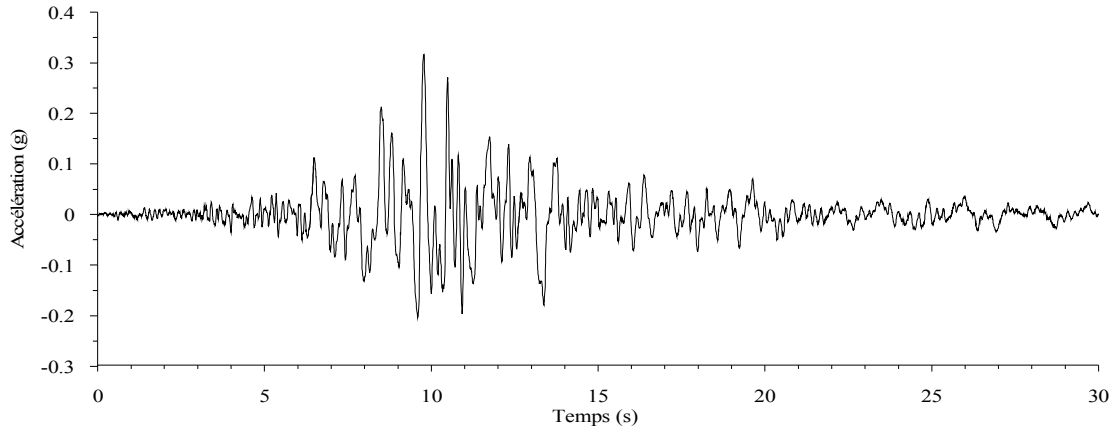

Figure II.1:Loma Priea 1989 ground motion used for validating the OpenSees model.

First, the equilibrium between the brace and the ductile link's internal axial load was confirmed. An example of this equilibrium is shown in Figure II.2. One can see the equal but opposite in sign load values between the left and right braces, and the superimposed internal axial loads from the rigid link, the ductile link, and the first brace element. There is good agreement in terms of the axial loads between the connection

and brace elements. Figure II.3 through Figure II.5 show the same results as those of Figure II.2 for storeys two through four, but for the left brace only.

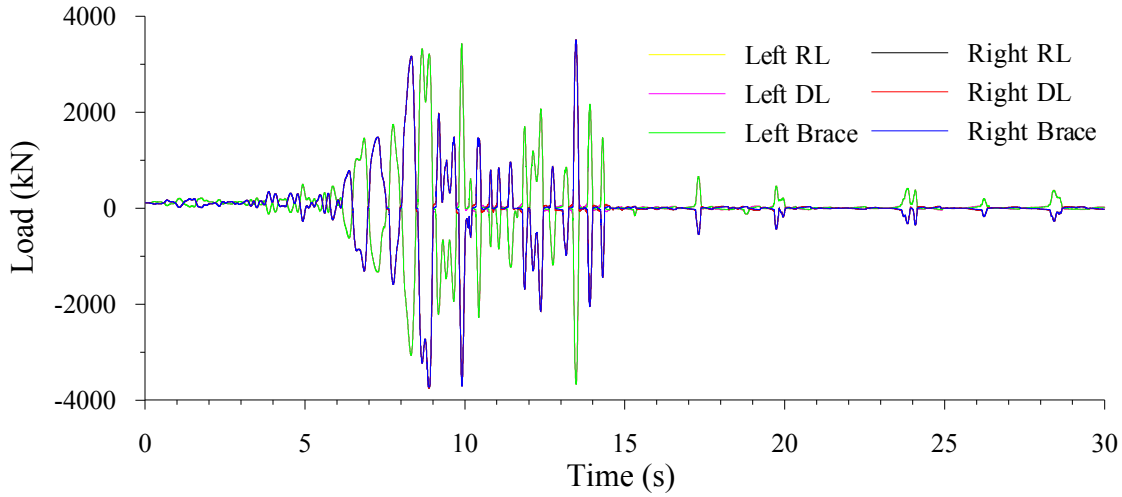

Figure II.2: Internal axial load found in brace and connection elements in left and right brace of the first storey.

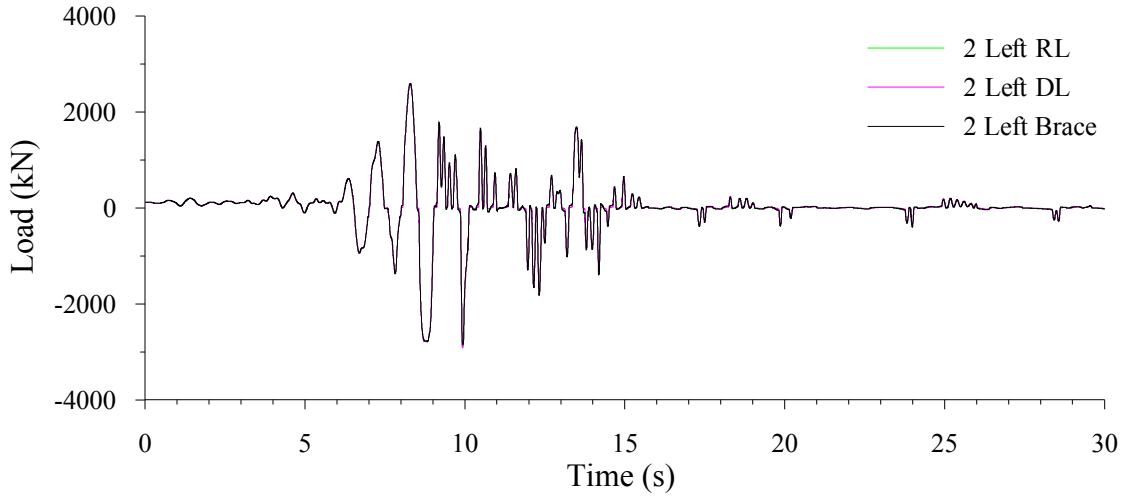

Figure II.3: Nonlinear axial forces comparison between rigid link, ductile link, and brace element left brace of the second storey.

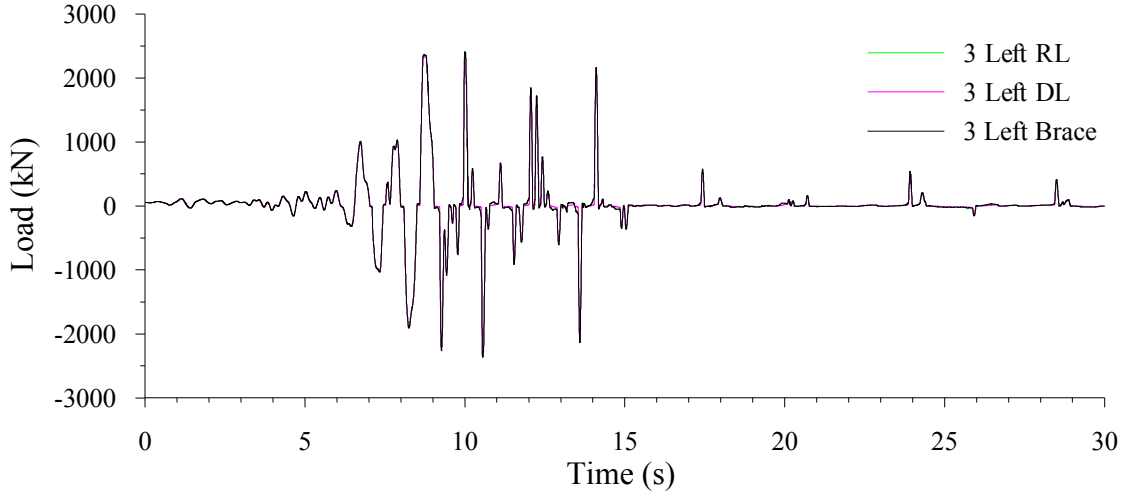

Figure II.4: Nonlinear axial forces comparison between rigid link, ductile link, and brace element left brace of the third storey.

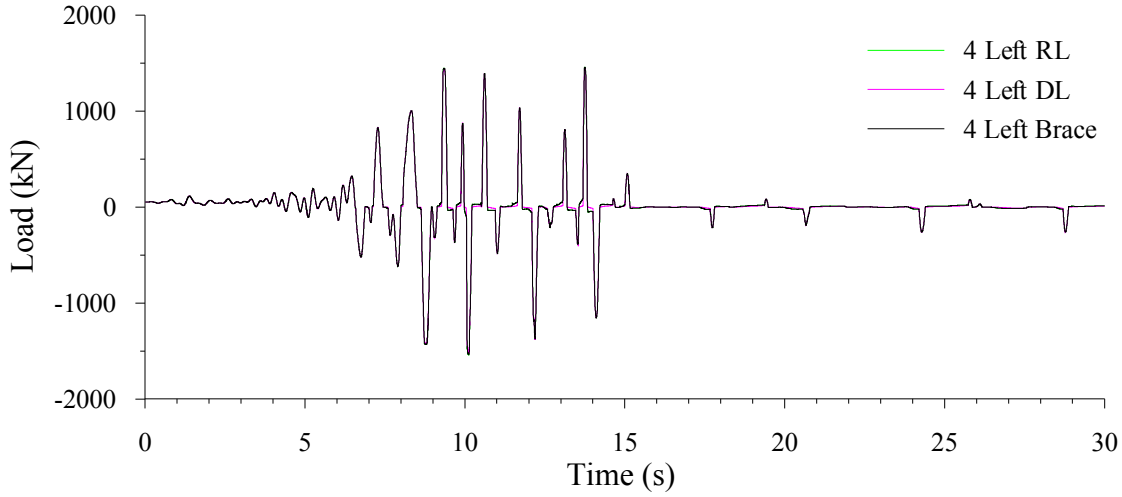

Figure II.5: Nonlinear axial forces comparison between rigid link, ductile link, and brace element left brace of the fourth storey.

From the last three figures, we can see that the forces between the rigid link, the ductile link, and the first brace element are the same as they are practically superimposed. Very slight differences can be seen due to the nature of the solution algorithm used for convergence; these slight differences, however, are considered negligible. The sections where the forces are null represent instances in the connection where the bolts have

come out of bearing against the gusset plate and are travelling inside the "newly slotted" hole.

Figures Figure II.6 and II.7 show the brace axial loads for the linear and nonlinear models, respectively. We notice the nonlinear forces are reduced by a factor close to R_d, 1.5, because of the presence of the ductile links. There was therefore obvious yielding in the ductile links place at the bottom end of every brace.

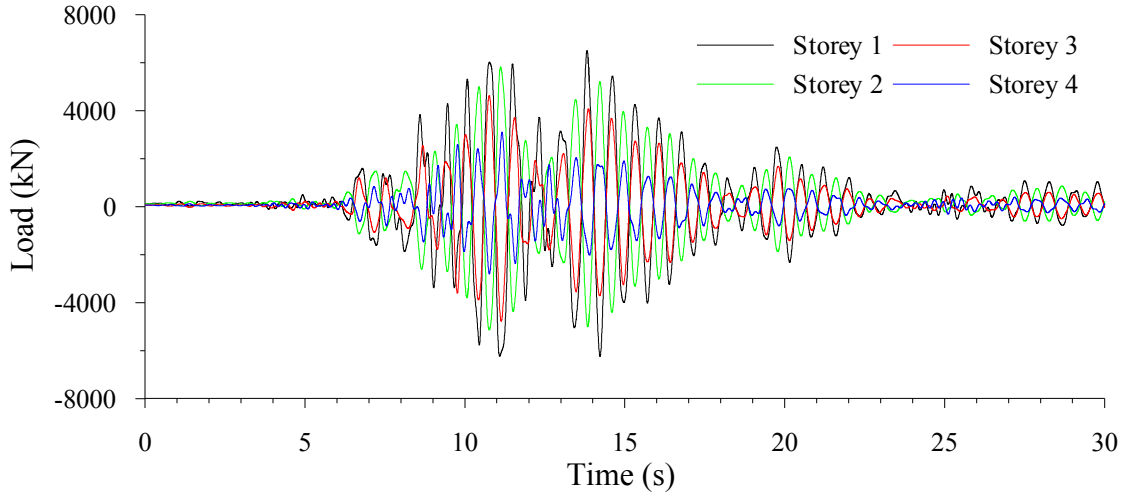

Figure II.6: Brace axial load from the linear analysis.

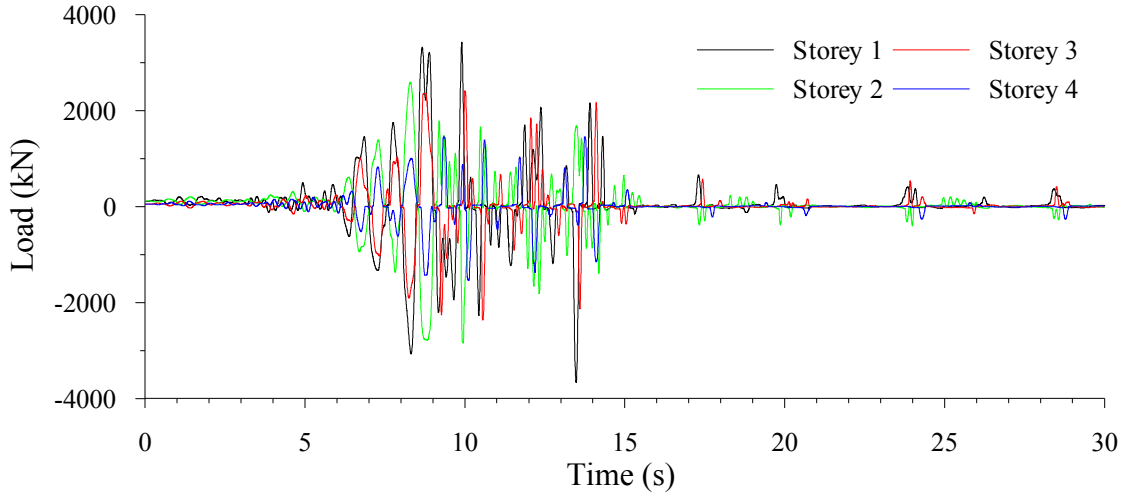

Figure II.7: Brace axial load from the nonlinear analysis.

Figures Figure II.8 and II.9 show the hysteretic behaviour of the same ductile links and again demonstrates they behave under the desired manner. These two plots confirm that the ductile links perform both linearly and nonlinearly for their respective analyses. The nonlinear ductile link hysteretic results follow the behaviour explained in section 4.4.5.

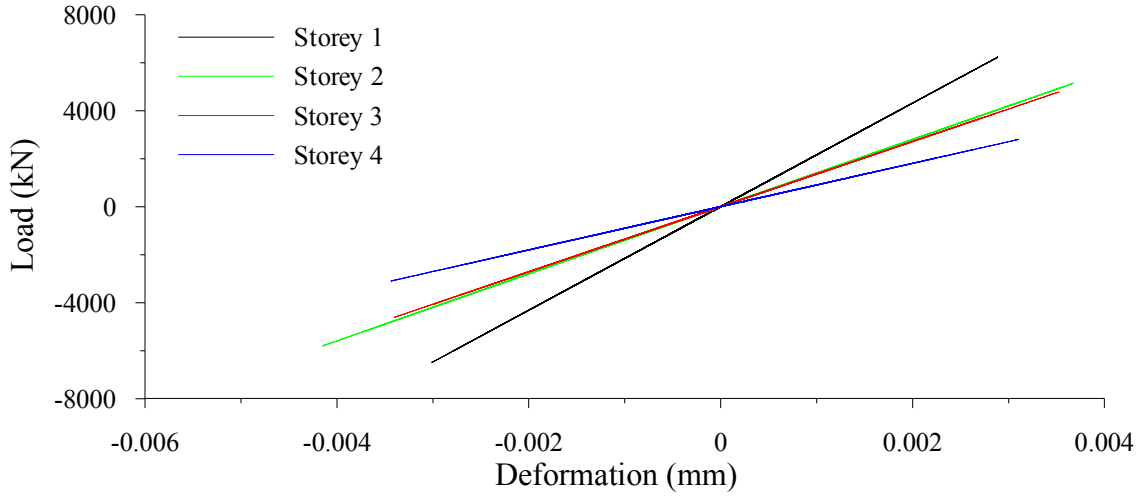

Figure II.8: Hysteretic behaviour of ductile links in linear model.

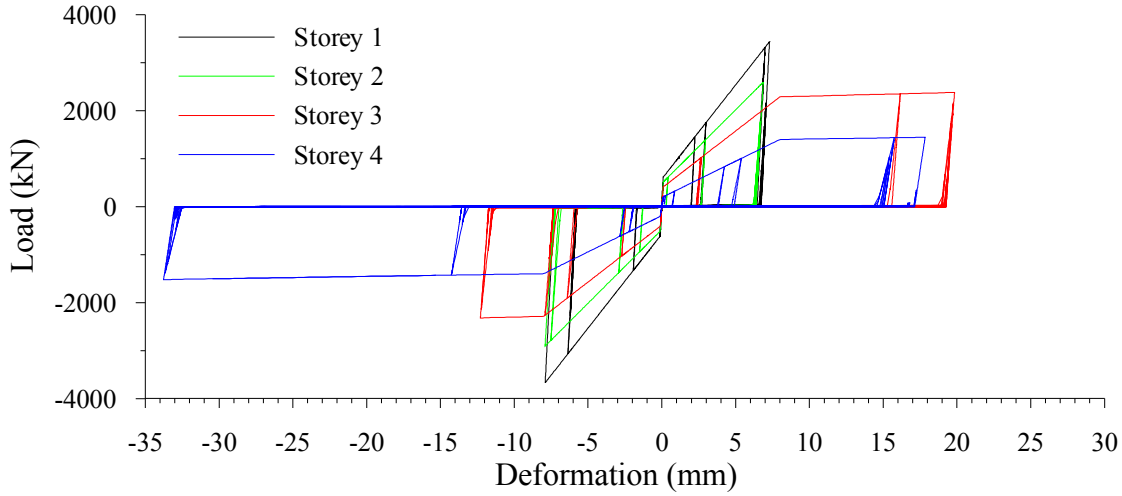

Figure II.9: Hysteretic behaviour of ductile links in nonlinear model.

Figures Figure II.10 and II.11 show a comparison between the column base force and the sum of the vertical load coming from the braces and the gravity loads for,

respectively, linear and nonlinear models. Figure II.12 shows the column base force of the linear and nonlinear model.

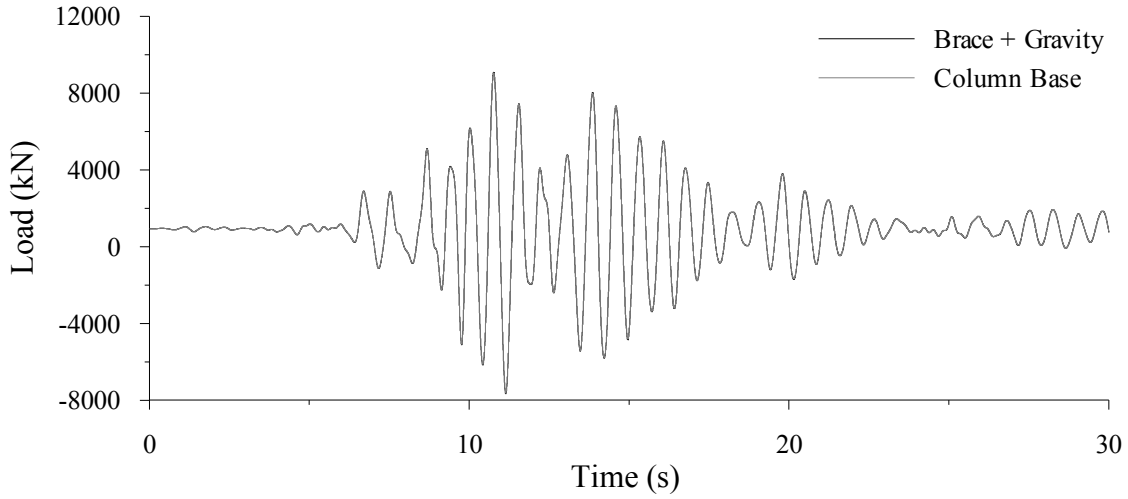

Figure II.10: Axial load at base of column and sum of vertical loads coming from braces and gravity loads in linear model.

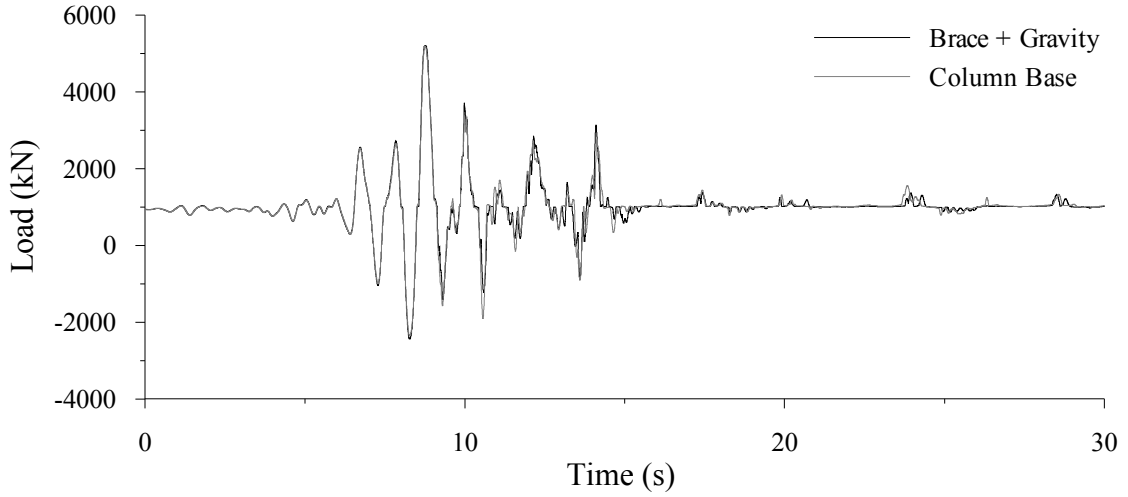

Figure II.11: Axial load at base of column and sum of vertical loads coming from braces and gravity loads in nonlinear model.

From the last two figures, we see the linear model offers two superimposed curves while the nonlinear models has two curves very similar to one another. They are both considered acceptable. From Figure II.12, we see a significant reduction in the column axial loads.

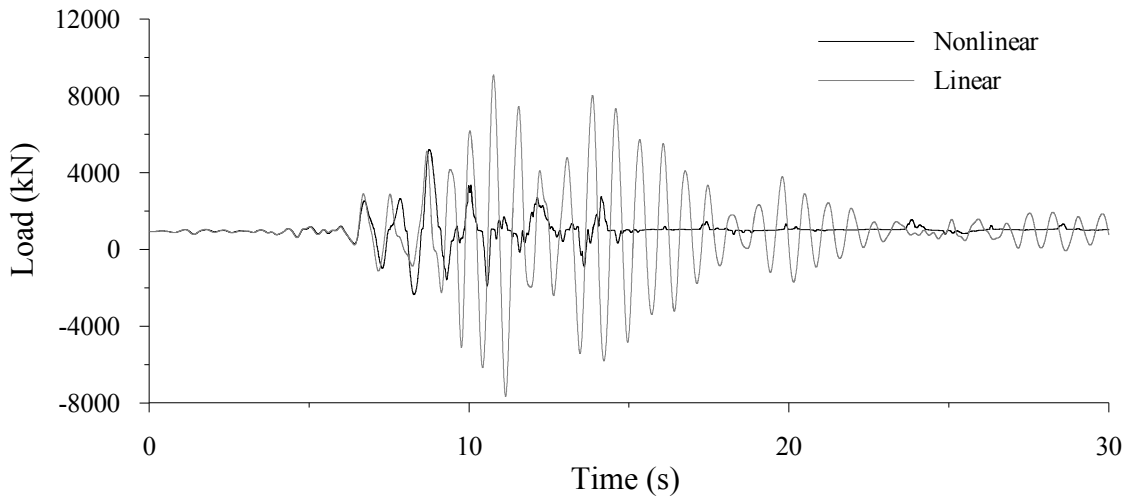

Figure II.12: Column base axial load for both linear and nonlinear models.

APPENDIX III.

Ground Motions Used for Dynamic Analyses

Table III.1: Montreal simulated ground motions for site classes C and E

Event	M_W	R (km)	Component (°)	PGA (g)	SF
Site Class C					
Synthetic (trial 2)	6.0	20	0	0.60	1.0
Synthetic (trial 2)	6.0	20	315	0.35	1.0
Synthetic (trial 3)	6.0	10	90	0.29	1.0
Synthetic (trial 3)	6.0	10	45	0.56	1.0
Synthetic (trial 3)	6.0	10	315	0.36	1.0
Synthetic (trial 3)	6.0	10	225	0.56	1.0
Synthetic (trial 1)	7.0	40	0	0.28	1.0
Synthetic (trial 1)	7.0	30	315	0.47	1.0
Synthetic (trial 3)	7.0	40	0	0.33	1.0
Synthetic (trial 3)	7.0	40	135	0.26	1.0
Site Class E					
Synthetic (trial 2)	6.0	20	0	0.51	1.0
Synthetic (trial 3)	6.0	10	45	0.42	1.0
Synthetic (trial 1)	7.0	30	225	0.40	1.0
Synthetic (trial 1)	7.0	40	225	0.52	1.0
Synthetic (trial 1)	7.0	40	135	0.53	1.0
Synthetic (trial 2)	7.0	30	0	0.35	1.0
Synthetic (trial 3)	7.0	50	90	0.33	1.0
Synthetic (trial 3)	7.0	30	225	0.36	1.0
Synthetic (trial 3)	7.0	30	135	0.28	1.0
Synthetic (trial 3)	7.0	40	135	0.23	1.0

Table III.2: Vancouver simulated and historical ground motions for site class C

Event	M_W	R (km)	Station	Comp. (^{o})	PGA (g)	SF
Synthetic (trial 3)	6.5	10		225	0.50	1.0
Synthetic (trial 3)	6.5	20		90	0.50	1.0
Synthetic (trial 2)	7.5	20		315	0.39	1.0
Synthetic (trial 3)	7.5	20		270	0.56	1.0
Synthetic (trial 3)	7.5	20		180	0.55	1.0
Synthetic (trial 3)	7.5	20		135	0.41	1.0
Synthetic (trial 2)	7.5	30		45	0.73	1.0
Synthetic (trial 2)	7.5	30		315	0.28	1.0
Synthetic (trial 2)	7.5	30		180	0.44	1.0
Synthetic (trial 3)	7.5	50		225	0.35	1.0
1994-01-17 Northridge	6.7	44	Castaic, Old Ridge Rd	90	0.57	0.6
1994-01-17 Northridge	6.7	30	Santa Monica City Hall	360	0.37	1.1
1994-01-17 Northridge	6.7	34	Los Angeles Baldwin Hills	360	0.17	1.8
1971-02-09 San Fernando	6.6	31	Castaic, Old Ridge Rd	291	0.27	1.4
1994-01-17 Northridge	6.7	26	Pacific Palisades Sunset	280	0.20	2.0
1992-04-25 Cape Mendocino	7.0	52	Eureka - Myrtle & West	90	0.18	1.6
1989-10-18 Loma Prieta	7.0	54	Stanford Univ.	360	0.29	1.1
1989-10-18 Loma Prieta	7.0	100	Presidio	90	0.20	1.4
1949-04-13 West.Wash.	7.1	76	Olympia, Test Lab	86	0.28	1.5
1992-06-28 Landers	7.3	93	Barstow	90	0.14	2.3

Table III.3: Vancouver simulated and historical ground motions for site class E

Event	M_W	R (km)	Station	Comp. (^{o})	PGA (g)	SF
Synthetic (trial 3)	6.5	10		225	0.54	1.0
Synthetic (trial 3)	6.5	20		135	0.90	1.0
Synthetic (trial 1)	7.5	20		45	0.44	1.0
Synthetic (trial 1)	7.5	30		315	0.61	1.0
Synthetic (trial 1)	7.5	50		315	0.46	1.0
Synthetic (trial 1)	7.5	20		135	0.56	1.0
Synthetic (trial 2)	7.5	50		45	0.33	1.0
Synthetic (trial 2)	7.5	20		135	1.15	1.0
Synthetic (trial 3)	7.5	20		270	0.68	1.0
Synthetic (trial 3)	7.5	30		90	0.91	1.0
1979-10-15 Imperial Valley	6.5	31	El Centro Array #11	140	0.37	1.3
1979-10-16 Imperial Valley	6.5	31	El Centro Array #12	230	0.37	1.5
1979-10-15 Imperial Valey	6.5	30	El Centro Array #3	140	0.26	1.5
1987-11-24 Superstition Hills	6.5	37	El Centro Imp. Co.Cent	0	0.29	1.6
1987-11-24 Superstition Hills	6.5	21	Westmorland Fire Sta	90	0.21	2.8
1987-11-25 Superstition Hills	6.5	21	Westmorland Fire Sta	180	0.21	1.6
1989-10-18 Loma Prieta	6.9	66	Redwood City APEEL 2	43	0.25	1.0
1989-10-19 Loma Prieta	6.9	66	Redwood City APEEL 2	133	0.25	1.7
1989-10-18 Loma Prieta	6.9	66	Foster City APEEL 1	0	0.29	1.8
1989-10-18 Loma Prieta	6.9	66	Foster City APEEL 2	90	0.29	1.0
1989-10-18 Loma Prieta	6.9	99	Treasure Island	0	0.13	2.9
1989-10-18 Loma Prieta	6.9	99	Treasure Island	90	0.13	1.7

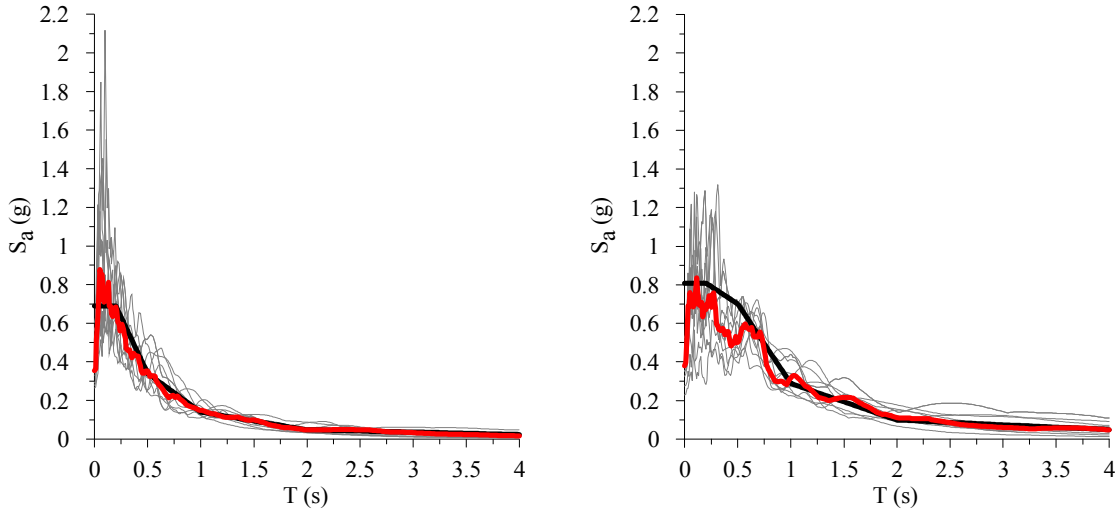

A) Site Class C B) Site Class E

Figure III.1: Design spectrum and ten ground motions with their spectrums for A) site class C and B) site class E.

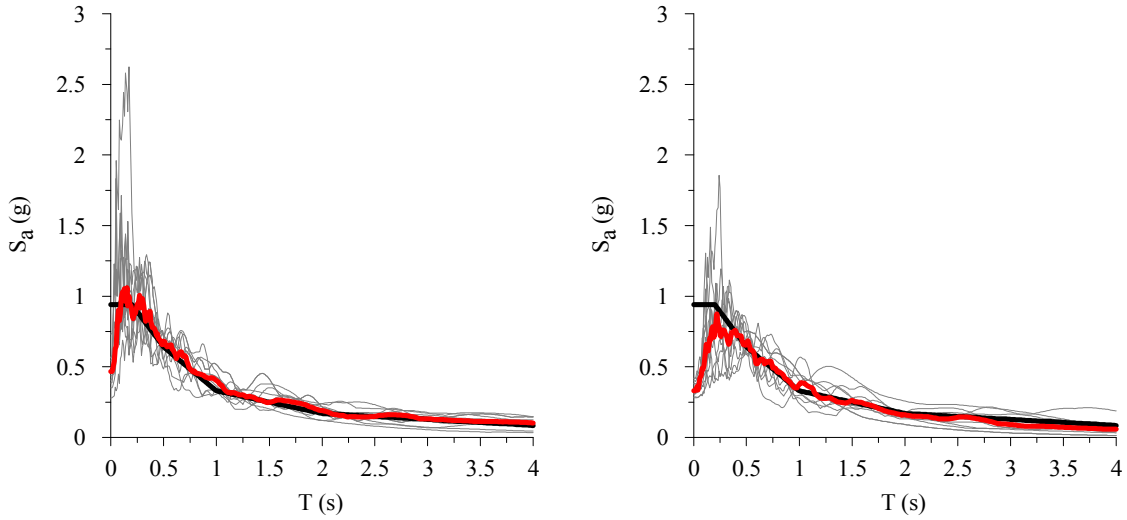

A) Simulated, site class C. B) Historical, site class C

Figure III.2: Simulated and historical ground motions for Vancouver on site class C, with the median and design spectrum shown.

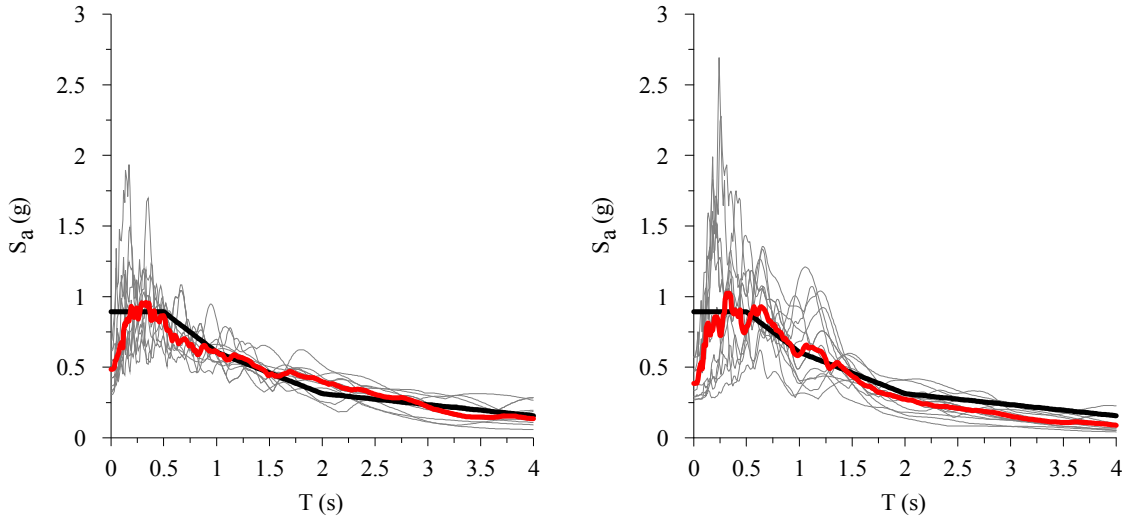

A) Simulated, site class E. B) Historical, site class E

Figure III.3: Simulated and historical ground motions for Vancouver on site class E, with the median and design spectrum shown.

Table III.4: Vancouver historical ground motions used for incremental analyses

Event	M_W	R (km)	Station	Comp. (^{o})	PGA (g)	SF
1979-10-15 Imperial Valley	6.5	25	Cerro Prieto	147	0.18	2.0
1992-06-28 Landers	7.3	14	Joshua Tree	0	0.25	0.9
1992-06-28 Landers	7.3	44	Lucerne	260	0.72	0.7
1979-10-15 Imperial Valley	6.5	49	Parachute Test Site	315	0.17	2.9
1999-10-16 Hector Mine	7.1	27	Hector	90	0.31	0.8
1984-04-24 Morgan Hill	6.2	17	Gilroy Array #6	90	0.34	0.9
1989-10-18 Loma Prieta	6.9	29	Gilroy - Gavilan Coll.	67	0.33	1.2
1952-07-21 Kern County	7.4	43	Taft Lincoln School	111	0.17	1.8
1987-11-24 Superstition Hills	6.5	16	Parachute Test Site	315	0.49	0.8
1979-10-15 Imperial Valley	6.5	12	Casa Flores	0	0.36	1.6
1994-01-17 Northridge	6.7	44	Castaic, Old Ridge Rd	90	0.57	0.6
1994-01-17 Northridge	6.7	30	Santa Monica City Hall	360	0.37	1.1
1994-01-17 Northridge	6.7	34	Los Angeles Baldwin Hills	360	0.17	1.8
1971-02-09 San Fernando	6.6	31	Castaic, Old Ridge Rd	291	0.27	1.4
1994-01-17 Northridge	6.7	26	Pacific Palisades Sunset	280	0.20	2.0
1992-04-25 Cape Mendocino	7.0	52	Eureka - Myrtle & West	90	0.18	1.6
1989-10-18 Loma Prieta	7.0	54	Stanford Univ.	360	0.29	1.1
1989-10-18 Loma Prieta	7.0	100	Presidio	90	0.20	1.4
1949-04-13 West.Wash.	7.1	76	Olympia, Test Lab	86	0.28	1.5
1992-06-28 Landers	7.3	93	Barstow	90	0.14	2.3

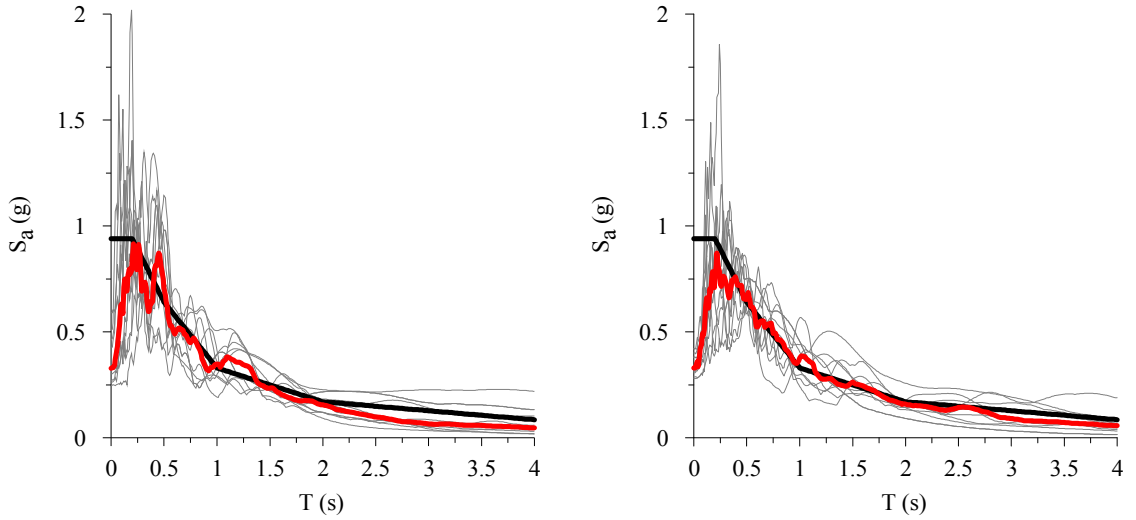

A) Ten additional records.

B) Ten previous records as used in previous analyses series.

Figure III.4: Historical ground motions used for incremental analyses

APPENDIX IV.

Example Incremental Analysis on 4-Storey Building with a Single Ground Motion

APPENDIX IV gives an example incremental dynamic analysis on building VaC15.6N04sSXE using a single ground motion. The June 28, 1992 Landers earthquake is used. This earthquake has a peak ground acceleration of 0.135g with a magnitude of 7.3 and was amplified by 2.3 to match the NBCC UHS. The time history is shown in Figure IV.1 and its spectrum is showed in Figure IV.2 along with the NBCC uniform hazard spectrum (UHS). The spectrum accelerations at the building first period of vibration of the OpenSees model are also shown. From the time history, we see that much of the earthquake intensity is found between 15 and 20 seconds, with a second burst of energy between 25 and 30 seconds. A 10% storey drift at any instant will again be used as an indicator that dynamic instability and collapse has occurred.

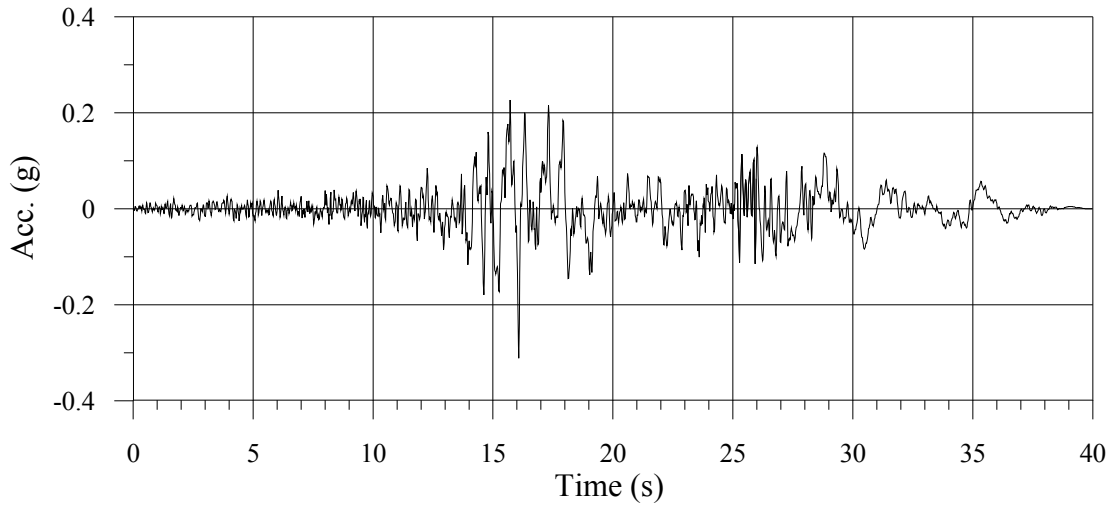

Figure IV.1: 1992 Landers ground motion

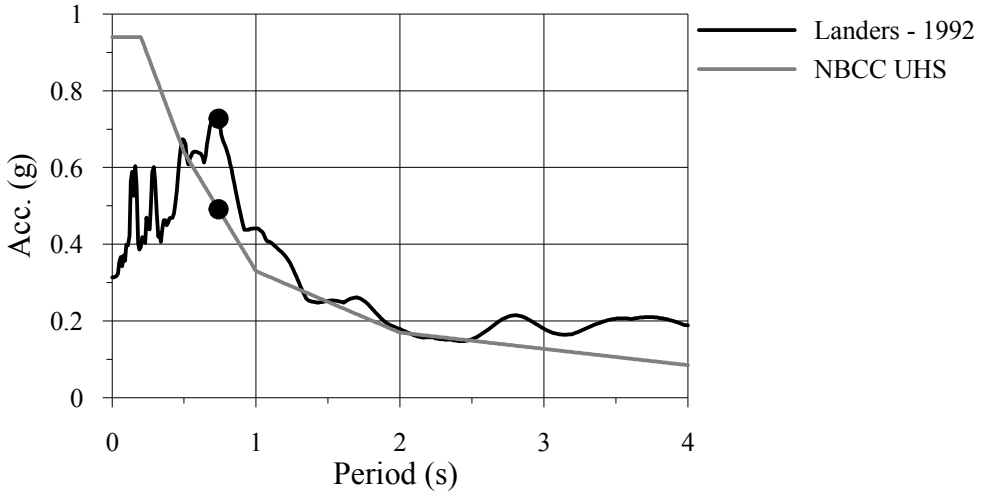

Figure IV.2: 1992 Landers response spectrum and NBCC UHS

As shown in Figure IV.2, the Landers earthquake is expected to be quite a damaging earthquake with respect to the NBCC's uniform hazard spectrum at the building's period. The ground motion's response spectrum remains above the UHS until a period of just below 1.3 s. Unless the building experiences an important period elongation because of inelastic behaviour, it will remain subjected to spectral accelerations greater than the UHS. Because of this, the 4-storey building was not able to reach the incremental scaling factor of 2.1 that caused the median collapse in the suite of 20 ground motions. Rather, building collapse was observed at a scaling factor of 1.7 under the Landers 1992 earthquake.

Figure IV.3 shows the partial incremental dynamic analysis curve (IDA) obtained for the VaC15.6N04sSXE model subjected to the Landers earthquake. As explained in section 4.5.3, the ATC does not call for the use of a complete IDA curve as only the incremental scaling factor causing median collapse of the building is needed. Therefore, only scaling factors of us to 1.7, the factor causing collapse, is shown in Figure IV.3. As was the tendency in the suite of ground motions, collapse occurred very quickly and without much warning, since by the lack of a gradual softening of the curve.

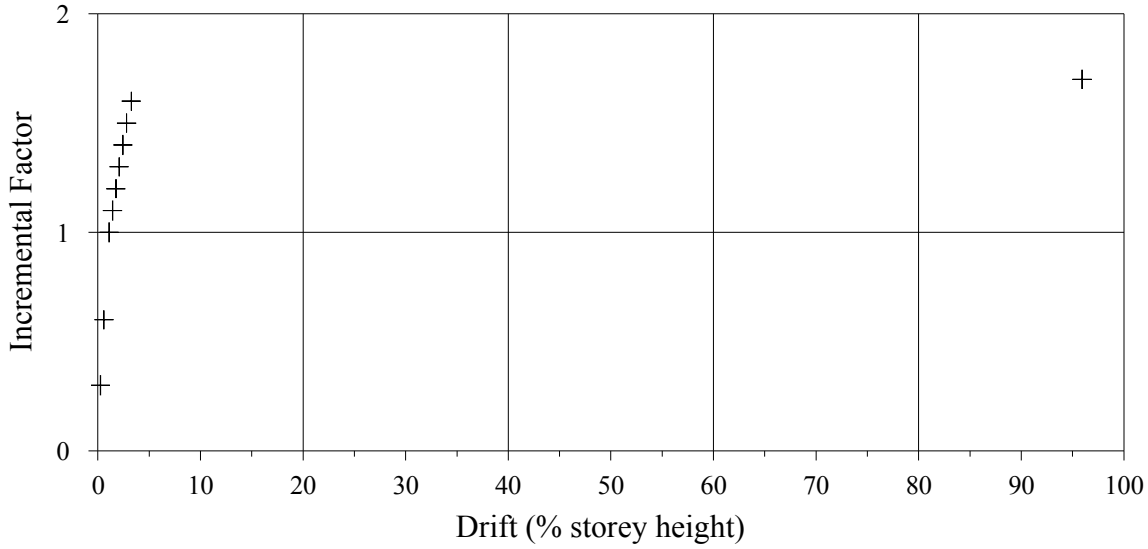

Figure IV.3: Partial incremental dynamic analysis curve

Figure IV.4 shows the storey drifts at every scaling factor, with the x-axis broken in order to better show the lower scaling factors. Again, we see that collapse happens very quickly between factors 1.6 and 1.7, considering that storey drifts at 1.6 were at most 3.3%. Storey drifts for levels 3 and 4 are not shown in the figure because they fall between 5 and 80% storey drifts.

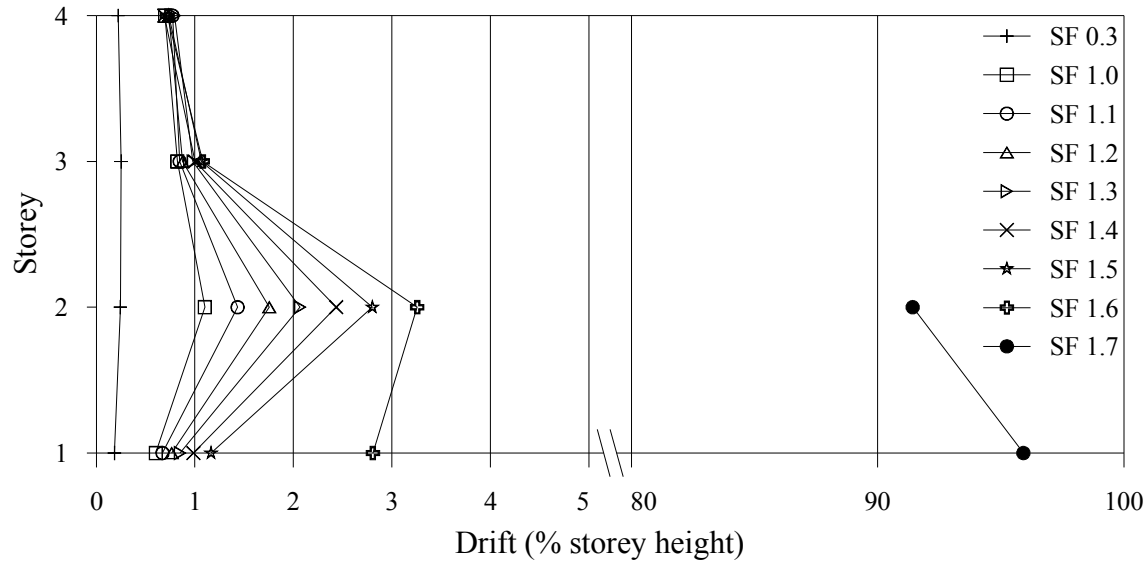

Figure IV.4: Building storey drifts at every scaling factor

It is interesting to take a closer look at what is happening in the brace connection at a scaling factor of 1.7. Shown in Figure IV.6 through Figure IV.13 are the connection hystereses at every level for both the right and left side brace connections at every 5 seconds. To complement this, Figure IV.5 shows the building storey drifts at the same time intervals; notice the different x-axis scaling used for different times.

Nothing unusual happens before 15 seconds into the earthquake. Between 15 and 20 seconds, the bottom right brace connection breaks off and is at its residual force, as shown in Figure IV.9. This is consistent with the concentration of energy between 15 and 20 seconds as seen in Figure IV.1. From Figure IV.5, we see the storey drifts after 20 seconds reach up to 4%.

The state of the connections does not aggravate in the next five seconds. However, after 30 seconds, the right connection at the first floor reaches deformations of up to 950 mm and the storey drift increases accordingly up to 17%. Again, this is consistent with the second burst of energy seen between 25 and 30 seconds in Figure IV.1. The ground shaking seen between 30 and 35 seconds is enough to cause the left connection on the second floor to rupture and cause the storey drift to reach 84% at the first level after 35 seconds. Further elongation of the connections continued until the end of the earthquake at 40 seconds. Storey drifts reach up to 96% and 90% at the first and second storeys, respectively.

This is essentially what is happening to the structures subjected to incremental dynamic analysis in section 4.5.3. In section 4.5.3.3, it is brought the attention of the reader than the connections are modeled with a residual force equal to 10% of the maximum encountered connection force. It was shown that for the three series of incremental analyses performed (two historical and one simulated), it was not necessary to redo any of the analyses with a smaller residual force if, and only if, the connection deformation exceeded the connection length at the scaling factor preceding that of the scaling factor caused the median collapse. For this 4-storey structure which is subjected to a single

earthquake, the state of its connections at times 20 s, 30 s, and 40 s when the ground motion is amplified by 1.6 is given in Figure IV.14 through Figure IV.16.

Base on the number of bolts with end distances of 4d and spacings of 5d, the connection lengths from storeys 1 through 4, respectively, are 553 mm, 457 mm, 362 mm, and 172 mm. As we can tell from the connection hystereses shown in the respective figures, the maximum connection deformation was just below 150 mm at the right brace connection of the first floor. This is well below the connection length of 553 mm and it is therefore considered reasonable to have the 10% residual force even after these deformations.

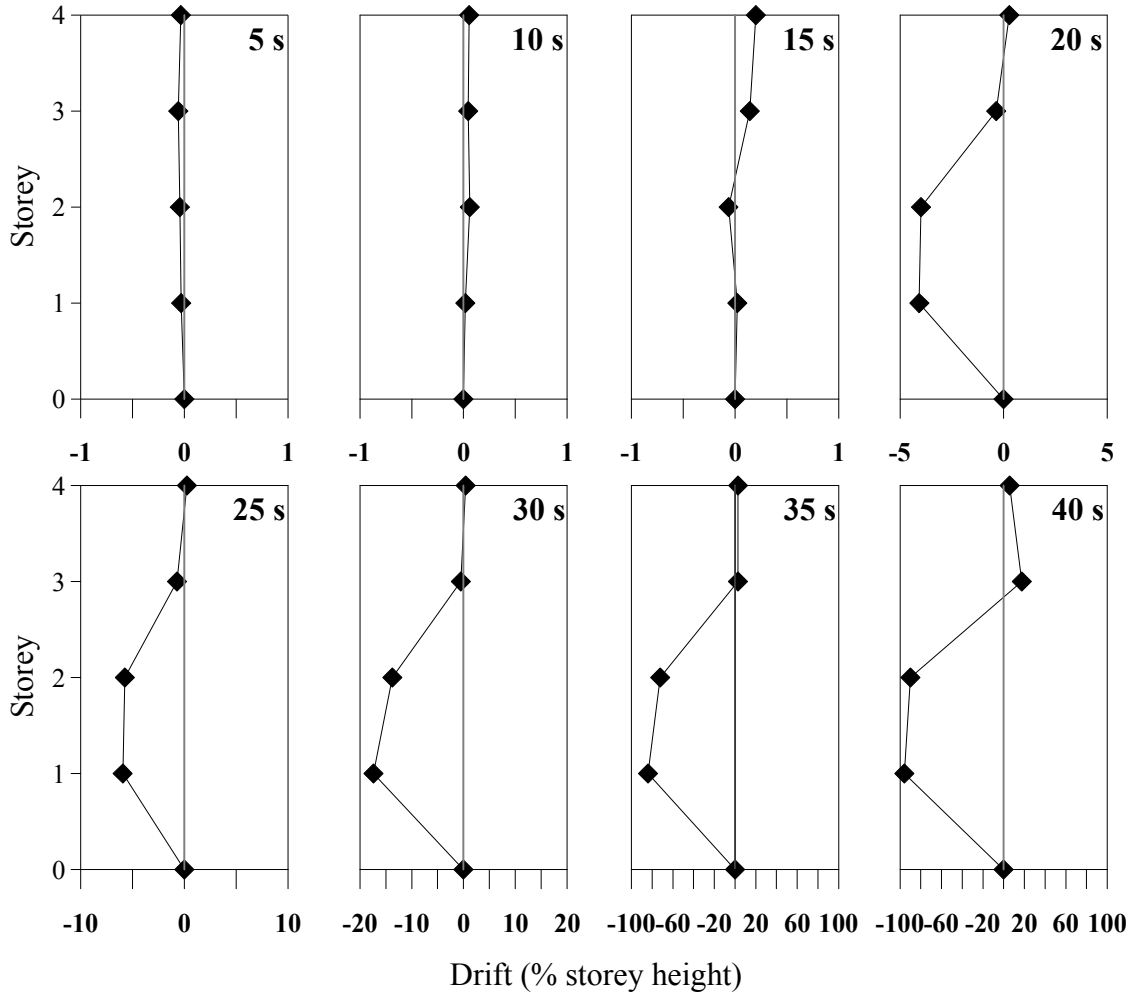

Figure IV.5: Storey drifts at every 5 seconds

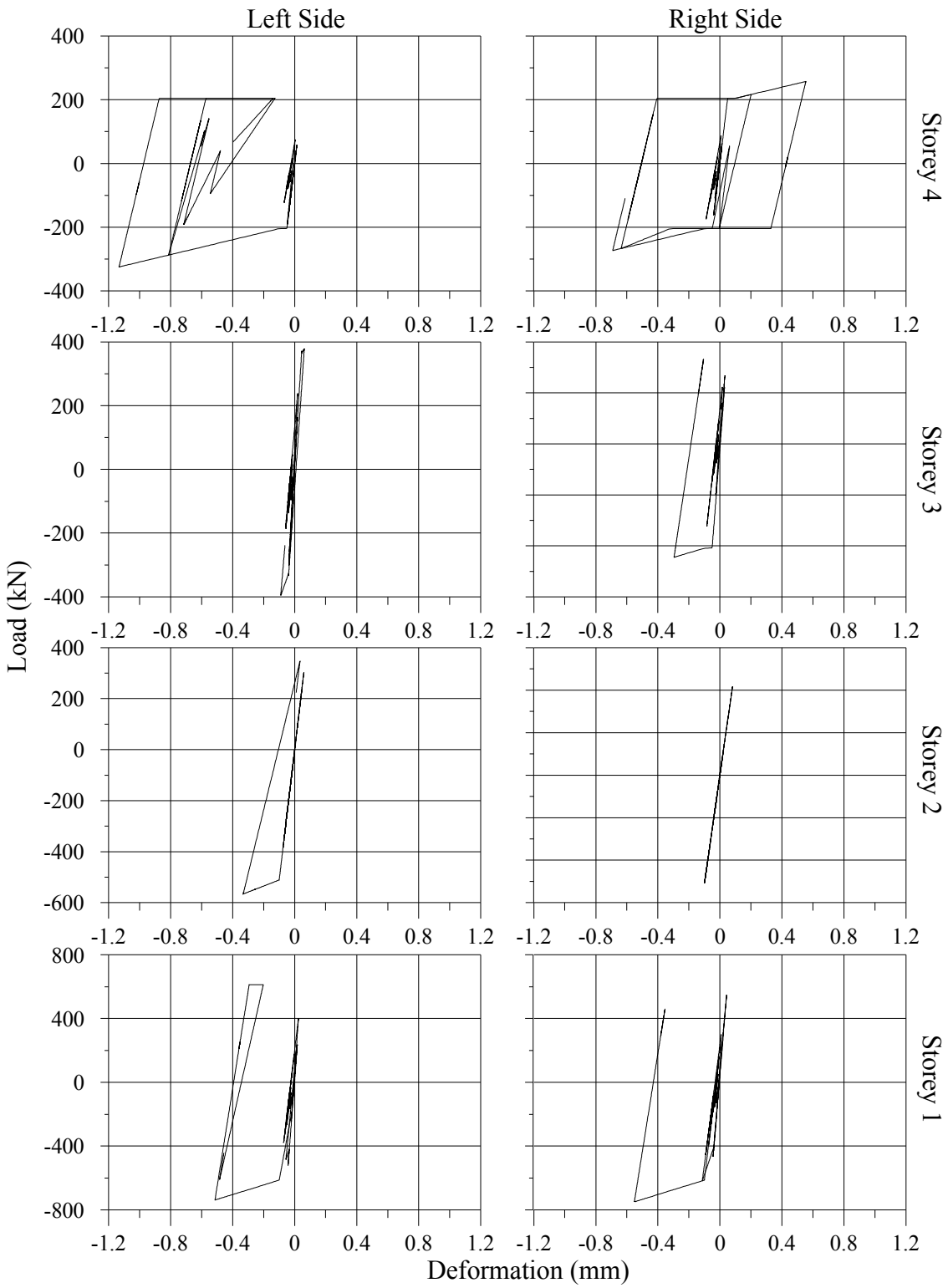

Figure IV.6: Connections at 5 s with SF equal to 1.7.

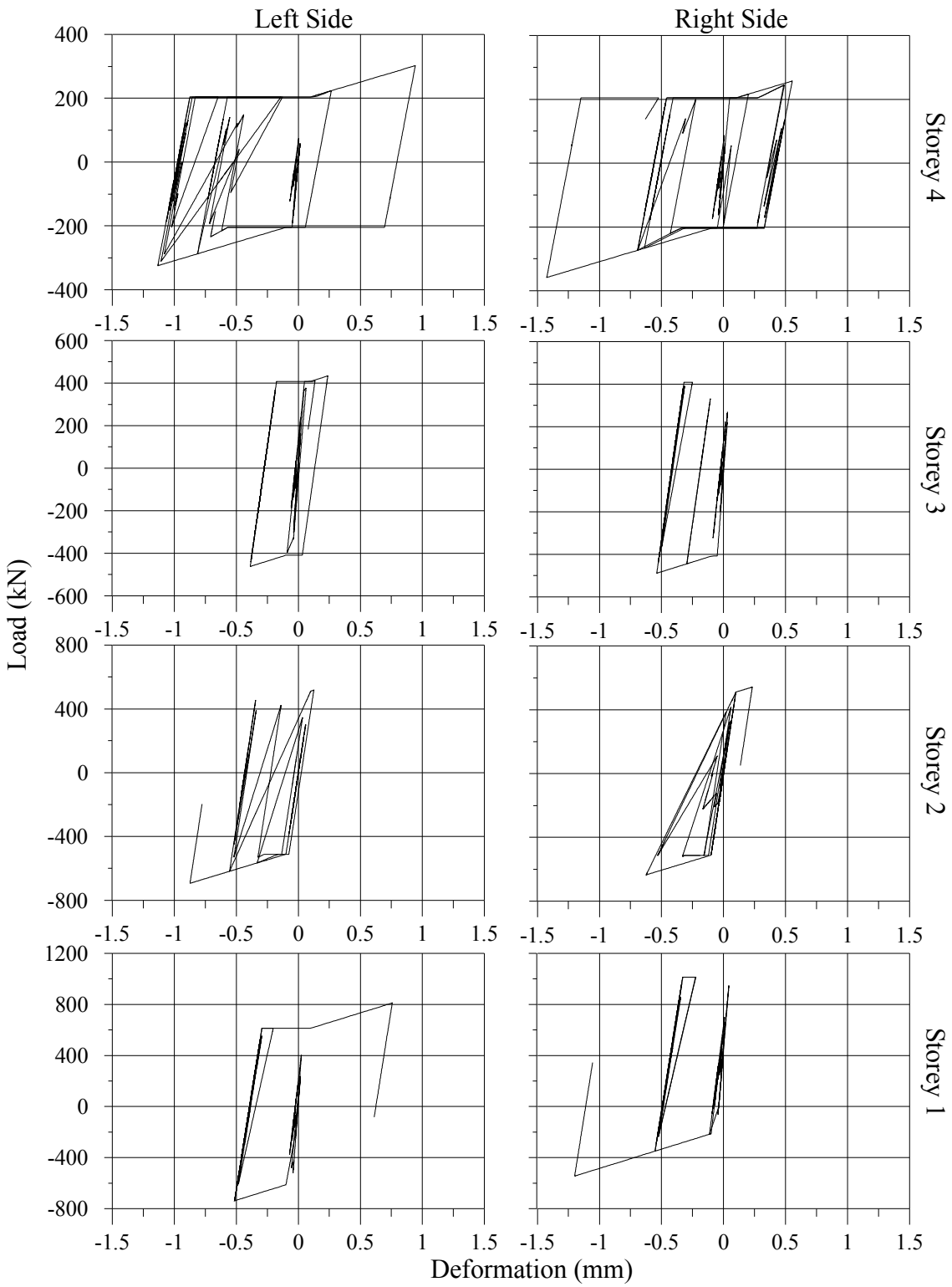

Figure IV.7: Connections at 10 s with SF equal to 1.7.

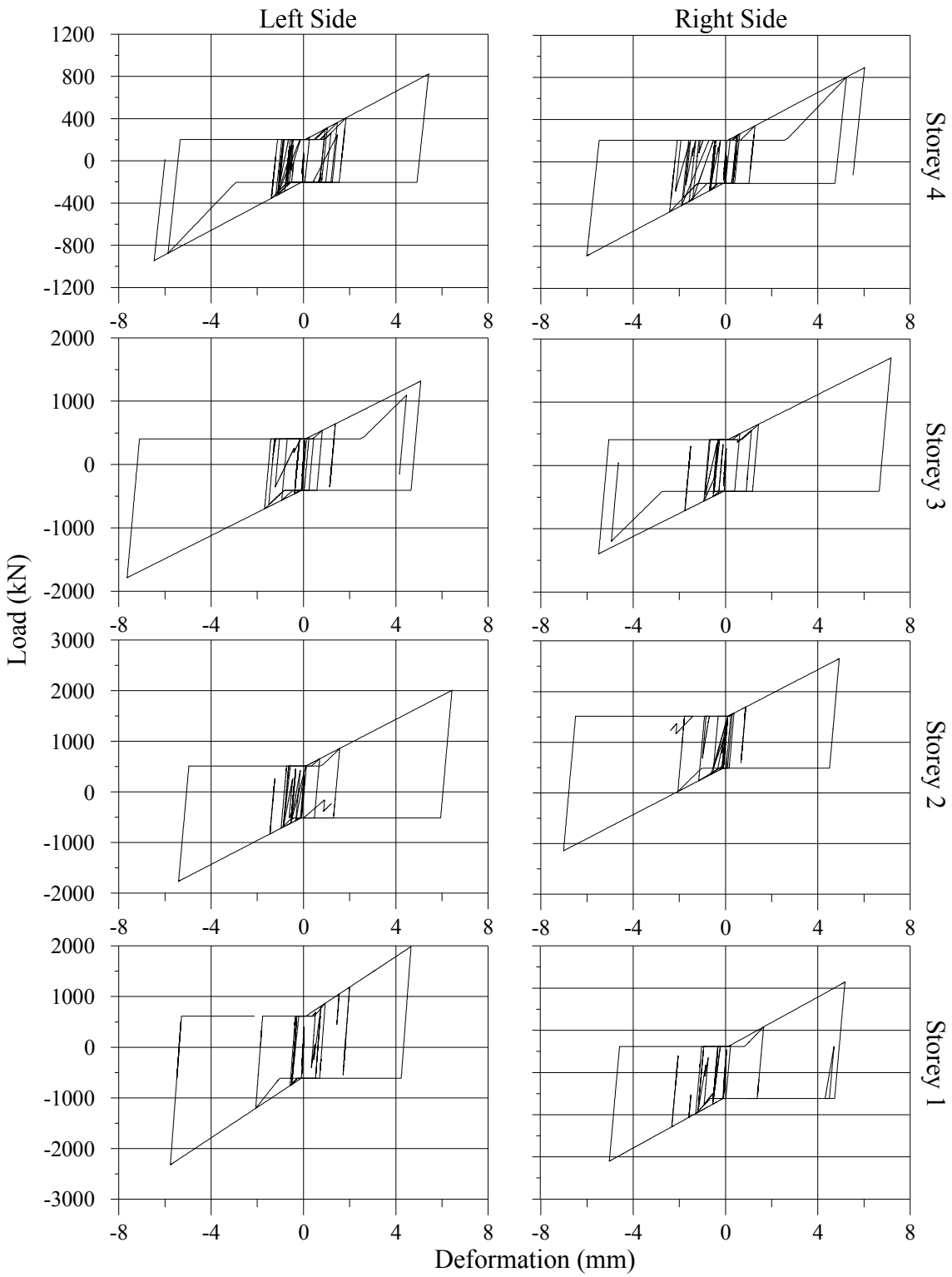

Figure IV.8: Connections at 15 s with SF equal to 1.7.

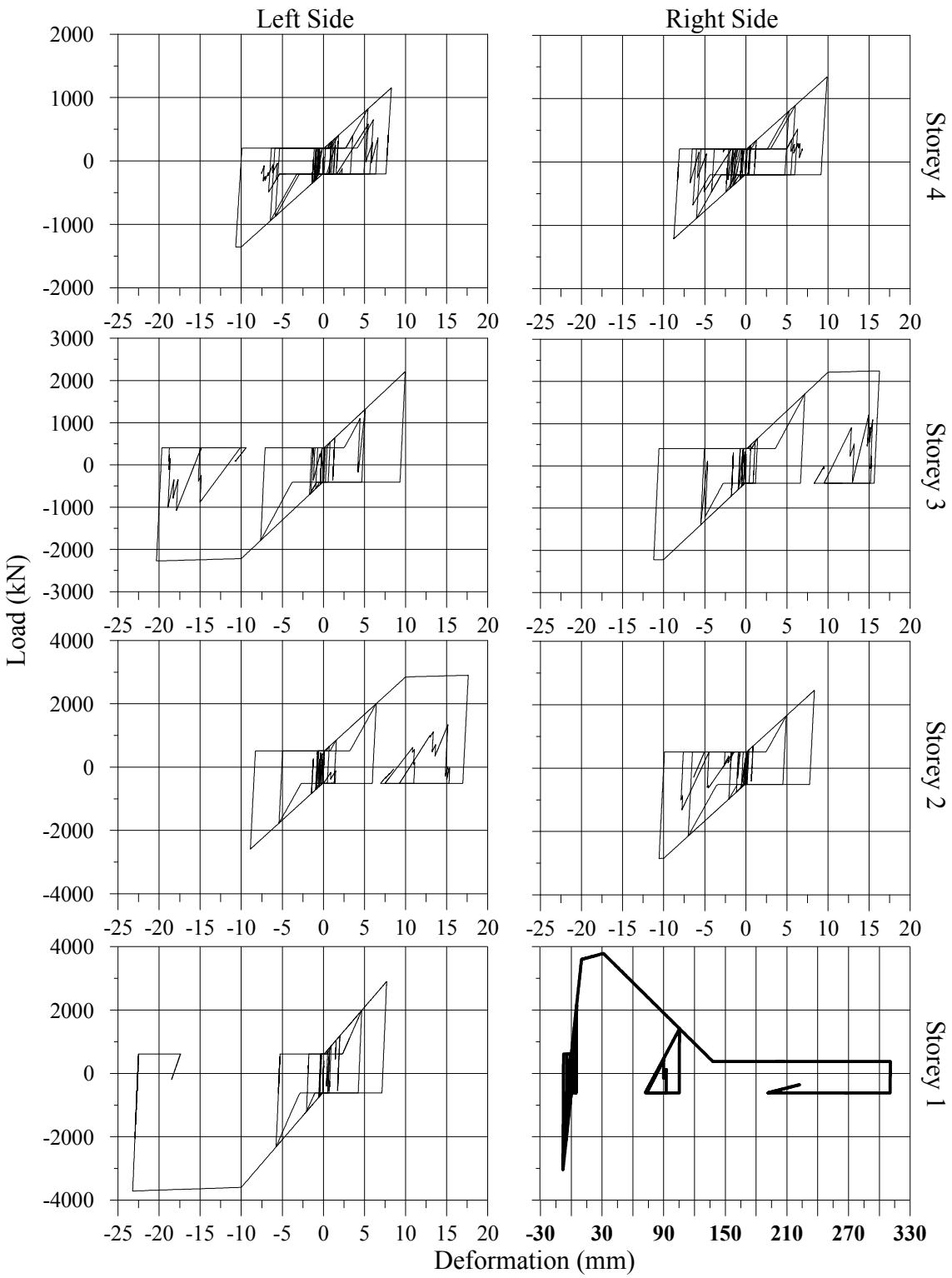

Figure IV.9: Connections at 20 s with SF equal to 1.7.

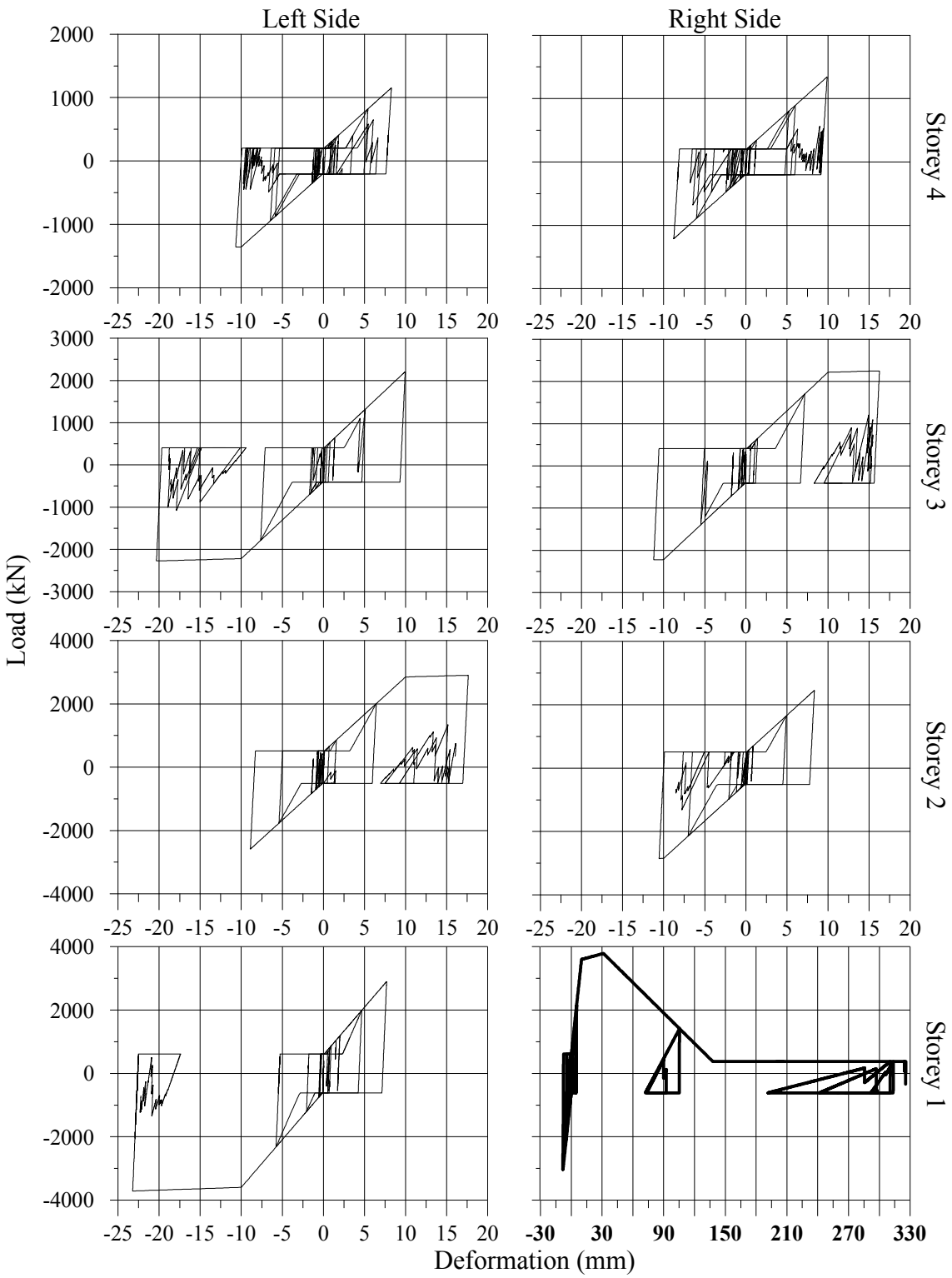

Figure IV.10: Connections at 25 s with SF equal to 1.7.

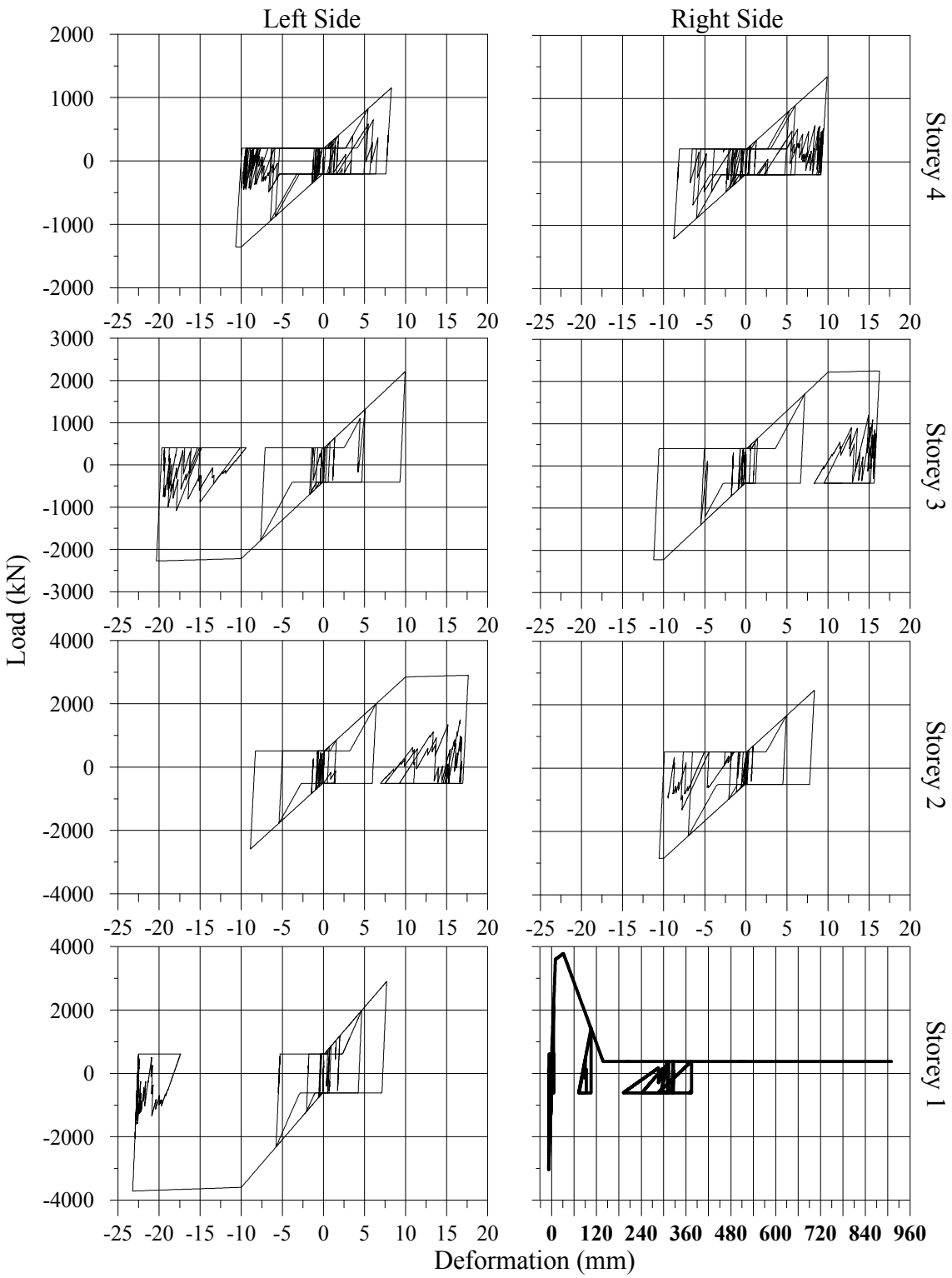

Figure IV.11: Connections at 30 s with SF equal to 1.7.

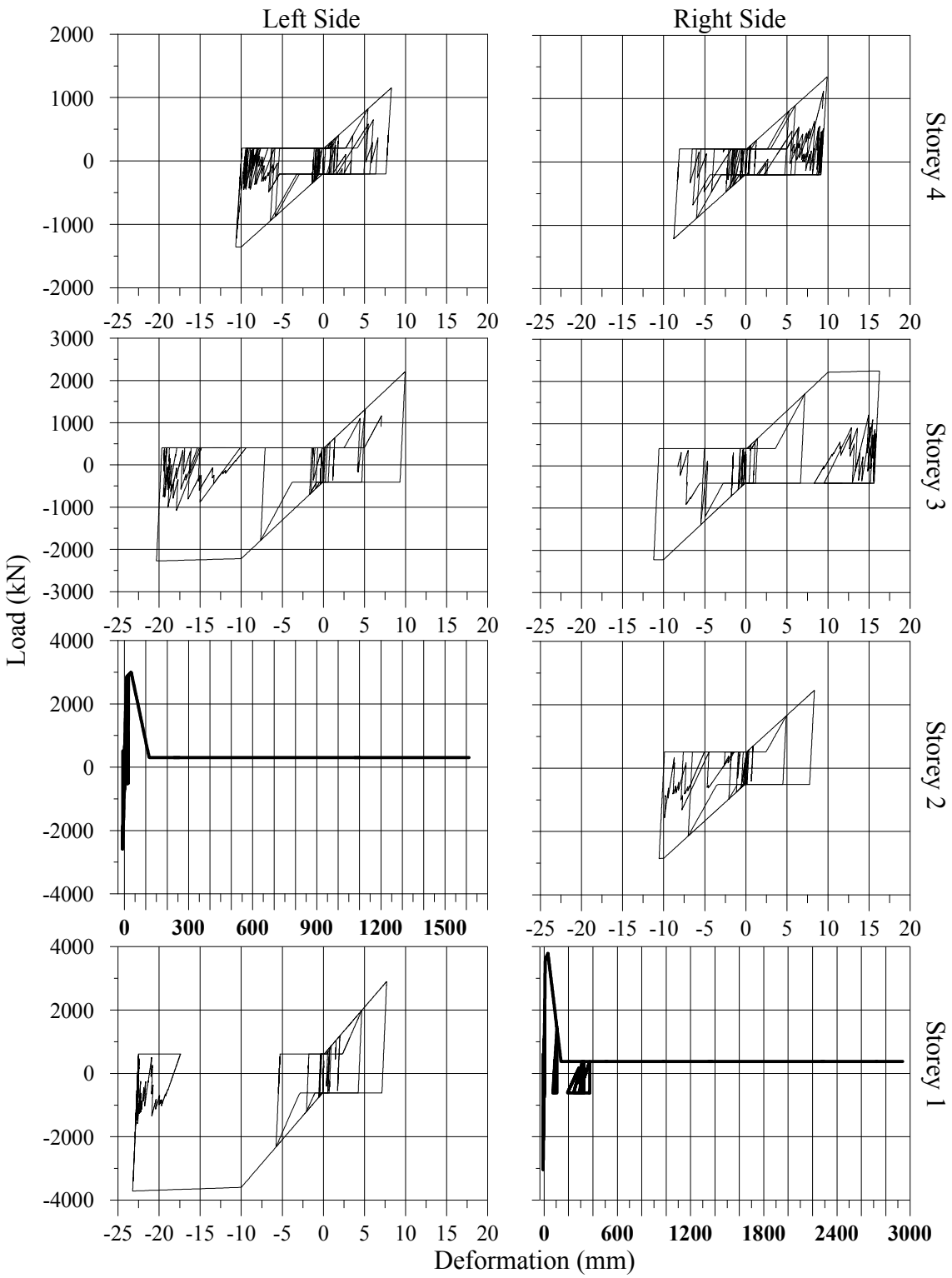

Figure IV.12: Connections at 35 s with SF equal to 1.7.

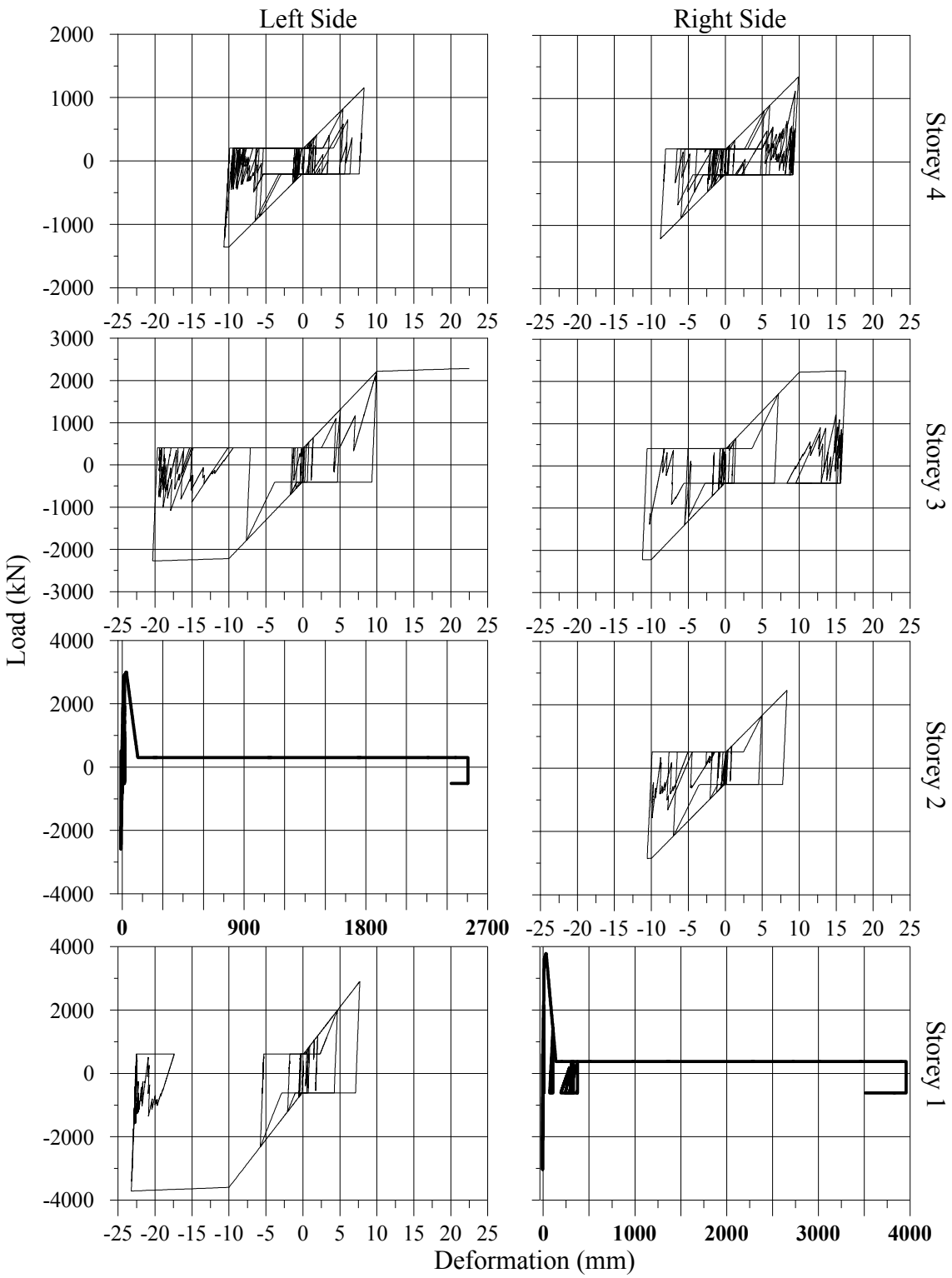

Figure IV.13: Connections at 40 s with SF equal to 1.7

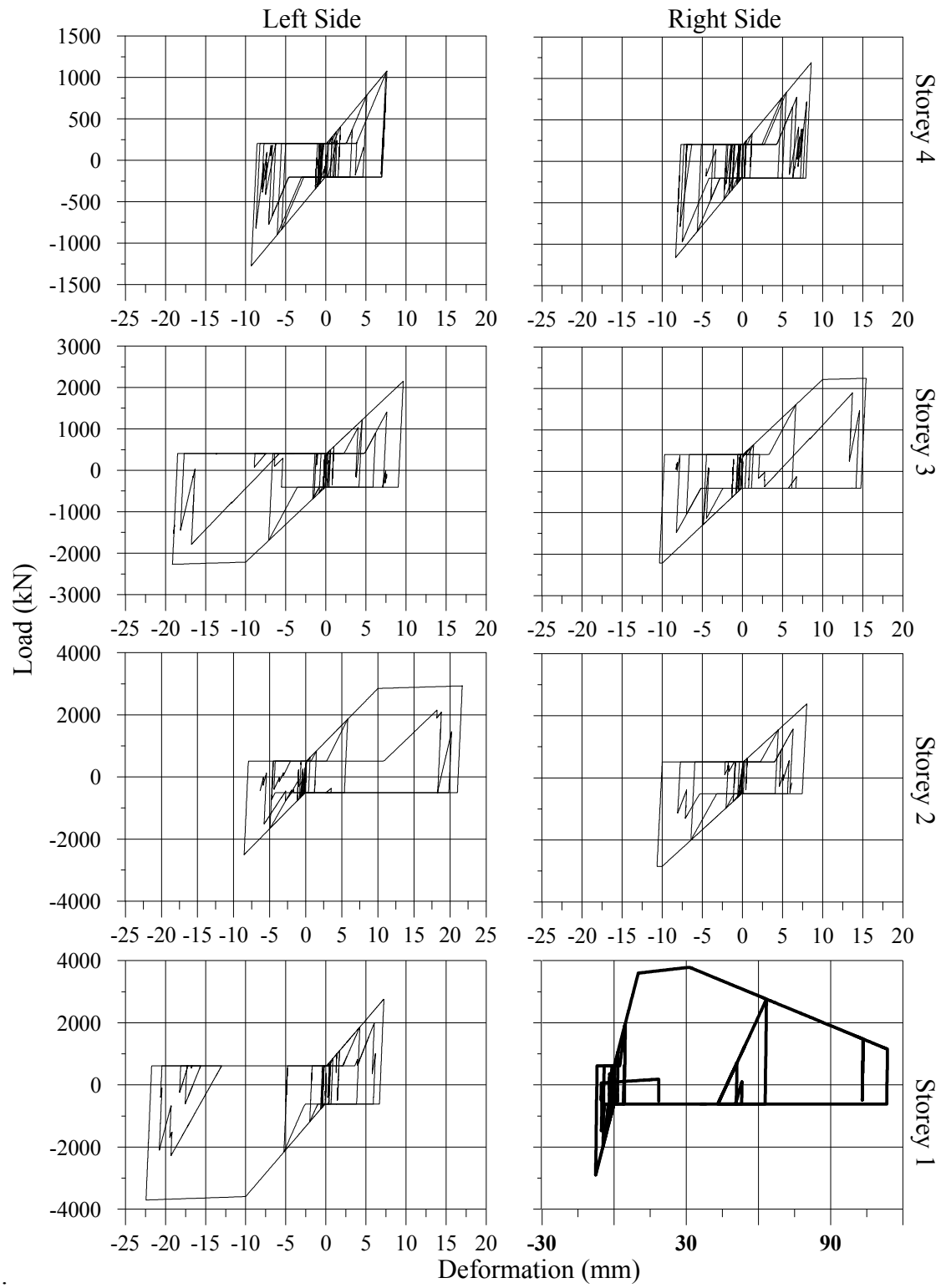

Figure IV.14: Connections at 20 s for scaling factor 1.6

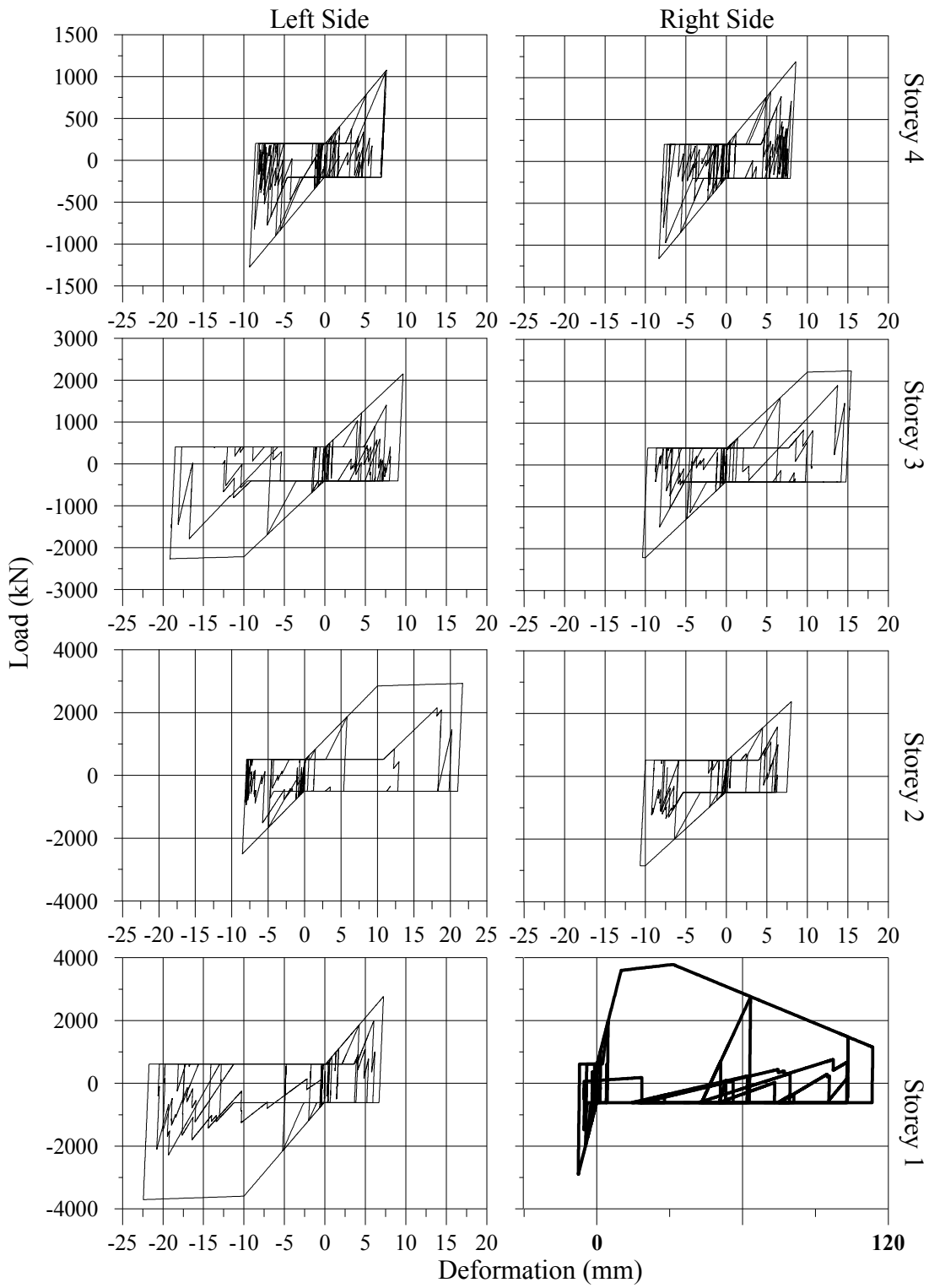

Figure IV.15: Connections at 30 s for scaling factor 1.6

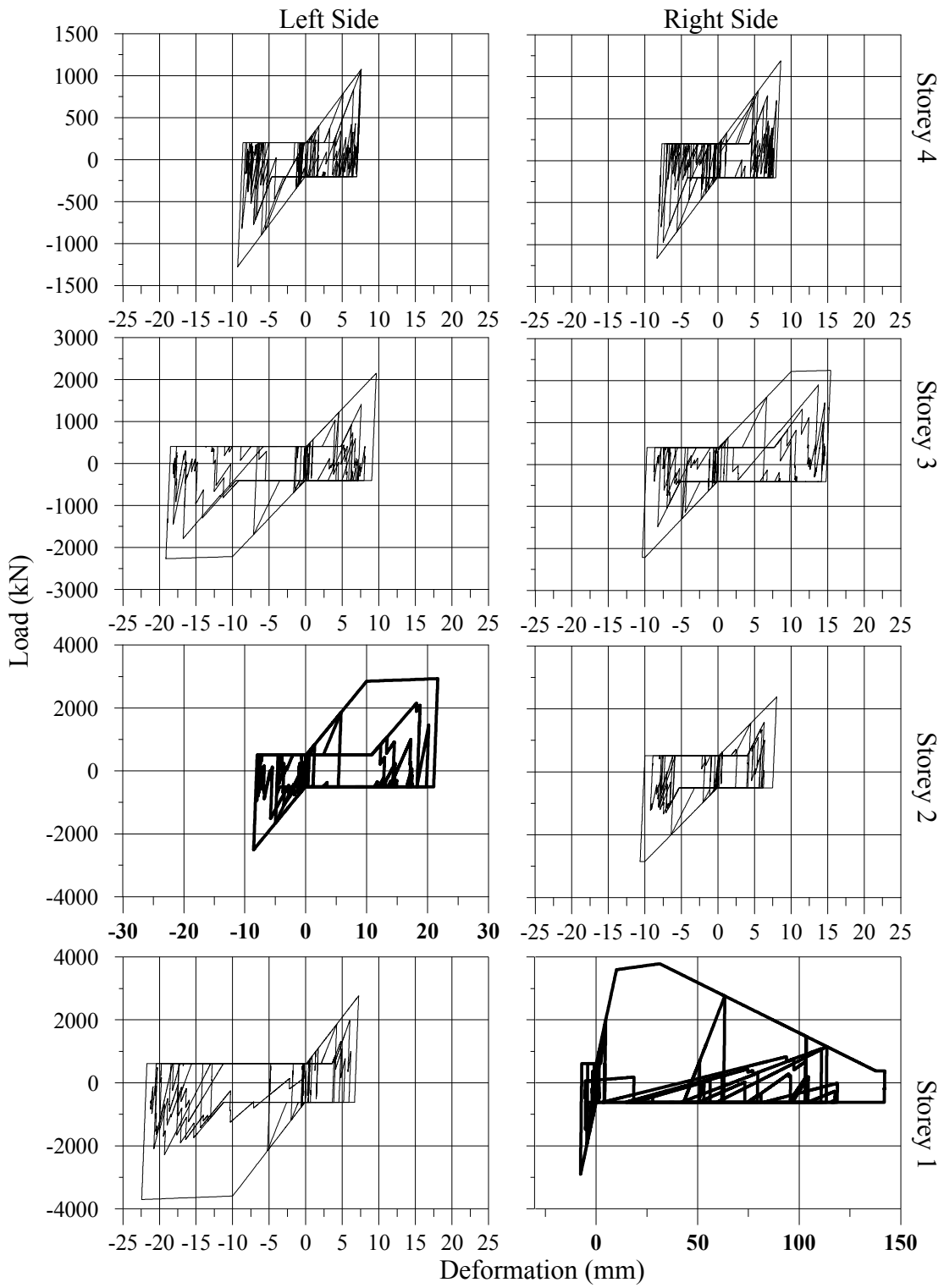

Figure IV.16: Connections at 40 s for scaling factor 1.6